

**POLYANILINE BASED NANOCOMPOSITES AS
ADSORBENTS AND PHOTOCATALYSTS IN THE
REMOVAL OF ORGANIC DYES**

SYED SHAHABUDDIN

**FACULTY OF SCIENCE
UNIVERSITY OF MALAYA
KUALA LUMPUR**

2016

**POLYANILINE BASED NANOCOMPOSITES AS
ADSORBENTS AND PHOTOCATALYSTS IN THE
REMOVAL OF ORGANIC DYES**

SYED SHAHABUDDIN

**THESIS SUBMITTED IN FULFILMENT OF THE
REQUIREMENTS FOR THE DEGREE OF
DOCTOR OF PHILOSOPHY**

**FACULTY OF SCIENCE
UNIVERSITY OF MALAYA
KUALA LUMPUR**

2016

UNIVERSITY OF MALAYA

ORIGINAL LITERARY WORK DECLARATION

Name of Candidate: **Syed Shahabuddin**

Registration/Matric No: **SHC130038**

Name of Degree: **Doctor of Philosophy (Ph.D.)**

Title of Thesis: **POLYANILINE BASED NANOCOMPOSITES AS ADSORBENTS AND PHOTOCATALYSTS IN THE REMOVAL OF ORGANIC DYES**

Field of Study: Polymer Chemistry

I do solemnly and sincerely declare that:

- (1) I am the sole author/writer of this Work;
- (2) This Work is original;
- (3) Any use of any work in which copyright exists was done by way of fair dealing and for permitted purposes and any excerpt or extract from, or reference to or reproduction of any copyright work has been disclosed expressly and sufficiently and the title of the Work and its authorship have been acknowledged in this Work;
- (4) I do not have any actual knowledge nor do I ought reasonably to know that the making of this work constitutes an infringement of any copyright work;
- (5) I hereby assign all and every rights in the copyright to this Work to the University of Malaya ("UM"), who henceforth shall be owner of the copyright in this Work and that any reproduction or use in any form or by any means whatsoever is prohibited without the written consent of UM having been first had and obtained;
- (6) I am fully aware that if in the course of making this Work I have infringed any copyright whether intentionally or otherwise, I may be subject to legal action or any other action as may be determined by UM.

Candidate's Signature

Date:

Subscribed and solemnly declared before,

Witness's Signature

Date:

Name: Dr. Norazilawati Muhamad Sarih

Designation: Senior Lecturer

ABSTRACT

Polyaniline (PANI), due to the delocalization of electrons in a continuously overlapped π -conjugated electron system, has been most intensively investigated conjugated conductive polymer. In recent years, enhancing the properties of PANI for its viable commercial applications by incorporating with metal oxides such as in our case, cobalt oxide (Co_3O_4) and strontium titanate (SrTiO_3), as well as organic material such as chitosan and graphene, has been the focus of research to explore its multifunctional abilities such as photocatalysis and adsorption. With the aim to obtain some PANIs based nanocomposites with controlled morphology, enhanced specific surface area and electronic properties, various synthetic pathways have been designed and carried out. This work describes the synthesis of Co_3O_4 nanocube-doped polyaniline nanocomposites via in situ oxidative polymerization. It was established that Co_3O_4 nanocube plays an important role in enhancing the surface morphology of PANI and thereby increasing the effective surface area of nanocomposite. The nanocomposite demonstrated enhanced removal of carcinogenic methyl orange (MO) dye (99%) from aqueous solution as compared to bare PANI. Furthermore, PANI was successfully grafted with chitosan to synthesis chitosan-grafted-polyaniline copolymer (ChGP) and Co_3O_4 nanocube-doped ChGP nanocomposites via oxidative-radical copolymerization for the photocatalytic degradation of methylene blue (MB) dye. Here chitosan acts as flexible matrix which enhances the adsorption of MB (which otherwise shows no affinity towards PANI due to its cationic nature) and the result exhibits enhanced photocatalytic degradation of MB (88%) within 180 minutes upon ultraviolet (UV) light illumination. Alternatively, wide band gap SrTiO_3 nanocubes were synthesized through hydrothermal technique and incorporated into PANI matrix via the in situ oxidative polymerization for the photocatalytic degradation of MB dye under visible light. It has been established that upon irradiation under visible light SrTiO_3 produces electrons and holes which were trapped in the vacant HOMO orbitals of PANI thereby creating efficient charge separation and mineralizing MB very efficiently (97%) within a short duration of time (90 minutes). Finally, PANI, graphene oxide and SrTiO_3 nanocubes comprising ternary nanocomposites were synthesized for the effective removal of cationic and anionic dyes from waste water. Here PANI was synthesized in the presence of graphene oxide and then decorated with SrTiO_3 nanocubes via the in situ oxidative polymerization technique where the synthesized nanocomposites were capable of removing MB in 10 minutes and MO in 30 minutes; within a very short duration of time. The photocatalysis and adsorption performance of the newly synthesized nanocomposites reveal that these materials are highly beneficial in designing efficient water treatment systems by harvesting energy from the UV light or natural sunlight and the adsorption phenomenon. It is worth mentioning that all the nanocomposites were synthesized for the first time by the mentioned techniques.

ABSTRAK

Polianilina (PANI) dengan kehadiran petaksetempatan elektron dalam sistem bertindih π berkonjugat elektron yang berterusan, menjadikan polimer berkonjugat ini yang paling intensif dikaji. Sejak kebelakangan ini, peningkatan sifat-sifat PANI untuk aplikasi komersial yang berdaya maju dengan penggabungan oksida logam seperti kobalt oksida (Co_3O_4) dan strontium titanat (SrTiO_3), serta bahan organik seperti kitosan dan grafena telah menjadi tumpuan penyelidikan untuk meneroka kebolehan kepelbagai fungsi. Dengan matlamat untuk mendapatkan beberapa nanokomposit polianilina dengan berasaskan morfologi terkawal, meningkatkan kawasan permukaan tertentu dan ciri-ciri elektronik, pelbagai laluan sintetik telah direka dan dijalankan. Kerja ini menerangkan sintesis nanokomposit polianilina Co_3O_4 nanokuib-terdop melalui pempolimeran oksidatif in situ. Didapati bahawa Co_3O_4 nanokuib memainkan peranan penting dalam meningkatkan morfologi permukaan PANI dan dengan itu meningkatkan kawasan permukaan yang berkesan kepada nanokomposit. Nanokomposit tersebut menunjukkan penyingkiran yang berkesan pewarna berkarsinogenik metil jingga (MO) (99%) daripada larutan akueus berbanding PANI asal. Tambahan pula, PANI telah berjaya dicantumkan dengan kitosan untuk sintesis kopolimer kitosan-polianilina (ChGP) dan nanokomposit Co_3O_4 nanokuib-terdop ChGP melalui pengkopolimeran oksidatif radikal untuk degradasi fotopemangkin pewarna metilena biru (MB). Di sini kitosan bertindak sebagai matriks fleksibel yang meningkatkan penjerapan MB (jika sebaliknya pewarna tersebut tidak akan menunjukkan tarikan terhadap PANI kerana sifat kationiknya) dan meningkatkan degradasi fotopemangkin MB (88%) dalam tempoh 180 minit di bawah pencahayaan sinar ultra ungu (UV). Sebagai alternatif, nanokuib SrTiO_3 yang mempunyai jurang jalur yang lebar telah disintesis melalui teknik hidroterma dan dimasukkan ke dalam matriks polianilina melalui pempolimeran oksidatif in situ untuk degradasi fotopemangkin MB di bawah cahaya matahari. Telah ditetapkan bahawa apabila penyinaran di bawah cahaya matahari, SrTiO_3 menghasilkan elektron dan lubang-lubang yang terperangkap dalam orbital HOMO PANI yang kosong, dengan itu mewujudkan pemisahan caj yang cekap dan pemineralan MB yang sangat efisien (97%) dalam tempoh singkat (90 minit). Akhir sekali, nanokomposit yang terdiri daripada PANI, grafena oksida dan SrTiO_3 nanokuib telah disintesis untuk penyingkiran berkesan bagi suatu pewarna kationik dan pewarna anionik daripada air sisa. Di sini PANI telah disintesis dengan kehadiran grafena oksida dan kemudian ditambah dengan nanokuib SrTiO_3 melalui teknik pempolimeran oksidatif in situ yang mana nanokomposit yang disintesis mampu menyingkirkan MB dalam tempoh 10 minit dan MO dalam tempoh 30 minit secara serentak dalam tempoh yang sangat singkat. Dengan potensi fotopemangkinan dan penjerapan oleh nanokomposit yang baru disintesis mendedahkan bahawa bahan-bahan ini sangat bermanfaat dalam mereka-bentuk sistem rawatan air yang cekap dengan penggunaan tenaga daripada cahaya UV atau cahaya semulajadi matahari dan fenomena penjerapan. Ia adalah penting untuk dinyatakan bahawa semua nanokomposit telah disintesis buat kali pertama dengan teknik yang telah dinyatakan.

ACKNOWLEDGEMENTS

In the name of Allah, the Most Gracious and the Most Merciful. All praises to Allah (Subhanahu Wa Taalaa) for the strength and His blessing for granting me the capability to complete this thesis. This appearance of this thesis in its present form is due to the assistance and guidance of several people. I would therefore like to offer my earnest thanks to all of them.

Firstly, I would like to express my sincere gratitude to my advisor Dr Norazilawati Muhamad Sarih for the continuous support of my PhD study and related research, for her patience with me, her critical review which allowed me to enhance the quality of my research writings, motivation, and immense knowledge. Her guidance helped me in all the time of research and writing of this thesis. I could not have imagined having a better advisor and mentor for my PhD study. I likewise express my earnest gratitude to my co-supervisor Associate Professor Sharifah Mohamad for her unlimited moral and intellectual help during the entire tenure of my research, her motivational sessions to boost up my work and providing support in preparation of various manuscripts for publications. I would like to extend my gratitude to Dr. Juan Joon Ching and Dr. Huang Nay Ming for their treasured support with analytical measurements instruments and sharing the laboratory facilities which were crucial for the success of my PhD work.

I have many thanks for friends, my lab mates and my colleagues; Fatem Hamime Ismail, Siti Nor Atika Bahrin, Shehu Habibu, Shahid Mehmood, Syed Tawab Shah, Nouman Arshid, Eraj Humayun Mirza and all those who supported me knowing or unknowingly. I thankfully acknowledge the funding sources, High Impact Research (HIR) grant, Fundamental Research Grant Scheme (FRGS) and Post Graduate Research Fund under IPPP that made my PhD work possible.

Finally, my sincere gratitude goes to my deceased father for his hard work, undemanding love, innumerable sacrifices and unconditional support throughout my life. It is possible for me to complete my studies and fulfil his dream because of his sacrifices which he made to achieve this degree. Last but not least, I feel honoured and deeply indebted for the support, encouragement, sacrifices, patience and prayers of my loving mother, sisters, brothers and my dearest Rashmin Khanam, which made it possible to accomplish this task. To those who indirectly contributed in this research, your kindness means a lot to me and could not be revealed in the words.

DEDICATION

I dedicate this thesis to the departed souls of my loving father and sister.

May Allah grant them Jannat-ul—Fidaous (Ameen)

University of Malaya

TABLE OF CONTENTS

ABSTRACT	III
ABSTRAK.....	IV
ACKNOWLEDGEMENTS.....	V
DEDICATION	VI
TABLE OF CONTENTS.....	VII
LIST OF FIGURES	XIII
LIST OF TABLES	XVIII
LIST OF SYMBOLS AND ABBREVIATIONS.....	XIX
LIST OF APPENDICES.....	XXI
CHAPTER 1: INTRODUCTION.....	1
1.1 Background of Research.....	1
1.2 Aims and Objectives of Research.....	3
1.3 Hypothesis.....	5
1.4 Outlines of Thesis.....	7
CHAPTER 2: LITERATURE REVIEW	8
2.1 Conducting Polymers.....	8
2.1.1 History of Conducting Polymers	8
2.1.2 Doping of Polymers	10
2.1.3 Intrinsic and Extrinsic Conducting Polymers.....	12
2.1.4 Band Structure of Conducting Polymers: Solitons, Polarons and Bipolarons	13
2.2 Polyaniline:.....	17
2.2.1 Synthesis of Polyaniline.....	20
2.2.1.1 Chemical Polymerization of Aniline.....	20
2.2.1.2 Electrochemical Polymerization of Aniline	21
2.2.2 Mechanism of Polymerization.....	22

2.2.3	Concept of Polyaniline Doping	26
2.2.4	Properties of Polyaniline	28
2.2.4.1	Conductivity	28
2.2.4.2	Solubility and Processibility	30
2.3	Metal Oxides Nanoparticles	31
2.3.1	Synthesis of Metal Oxide Nanoparticle	32
2.3.1.1	Chemical Method.....	33
(a)	<i>Co-precipitation Method</i>	33
(b)	<i>Sol-gel Method</i>	33
(c)	<i>Microemulsion Method</i>	34
(d)	<i>Hydrothermal or Solvothermal Method</i>	34
(e)	<i>Template Method</i>	35
2.3.1.2	Physical Method.....	35
(a)	<i>Mechanical Attrition</i>	35
(b)	<i>Mechanochemical Synthesis</i>	36
(c)	<i>Chemical Vapour Deposition (CVD) and Chemical Vapour Condensation (CVC)</i>	37
(d)	<i>Laser Ablation</i>	38
2.3.2	Properties of Metal Oxides	38
2.3.2.1	Surface Properties	38
2.3.2.2	Electrical Properties	40
2.3.2.3	Optical Properties.....	41
2.3.2.4	Other Properties	42
2.4	Chitosan	42
2.4.1	Chitin and Chitosan	42
2.4.2	Applications of Chitosan Based Composites in Adsorption of Pollutants.....	44
2.5	Graphene and Graphene Oxide	46
2.5.1	Graphene	46
2.5.2	Graphene Oxide	47
2.5.3	Synthesis of Graphene Oxide	49
2.5.4	Properties of Graphene Oxide	50
2.5.4.1	Structure Properties	50
2.5.4.2	Dispersibility.....	52

2.6	Polyaniline Based Nanocomposites.....	52
2.6.1	Synthesis of Polyaniline Nanocomposites	53
2.6.1.1	Chemical In-Situ Polymerization.....	53
2.6.1.2	Physical Blending/Mixing	54
2.6.2	Application of Polyaniline Based Nanocomposites	55
2.6.2.1	Adsorption of Toxic Pollutants.....	55
2.6.2.2	Photocatalysis	57
2.6.2.3	Other Applications	59

CHAPTER 3: SYNTHESIS AND CHARACTERIZATION OF CO₃O₄ NANOCUBE-DOPED POLYANILINE NANOCOMPOSITES WITH ENHANCED METHYL ORANGE ADSORPTION FROM AQUEOUS SOLUTION 60

3.1	Introduction	60
3.2	Experimental Section.....	64
3.2.1	Materials.....	64
3.2.2	Synthesis Methodology.....	64
3.2.2.1	Synthesis of CO ₃ O ₄ Nanocubes	64
3.2.2.2	Preparation of Polyaniline (PANI).....	65
3.2.2.3	Preparation of PANI- CO ₃ O ₄ Nanocomposite.....	65
3.2.3	Characterisation Techniques	65
3.2.4	Dye Adsorption Study.....	66
3.3	Results and Discussion	67
3.3.1	Characterization.....	67
3.3.1.1	Morphological Analysis of Nanocomposites.....	67
3.3.1.2	Thermal Analysis	72
3.3.1.3	XRD Analysis	74
3.3.1.4	BET Analysis	76
3.3.1.5	FTIR Analysis	77
3.3.2	Adsorption Studies.....	79
3.3.2.1	Adsorption of MO	79
3.3.2.2	Effect of Adsorbent Dosage.....	87
3.3.2.3	Effect of Time	88
3.3.2.4	Effect of pH	88
3.3.2.5	Effect of NaCl Concentration	90

3.3.2.6	Reusability Studies.....	91
3.4	Conclusion.....	92
CHAPTER 4: SYNTHESIS OF CHITOSAN-GRAFTED-POLYANILINE/CO₃O₄ NANOCUBE NANOCOMPOSITE AND ITS PHOTOCATALYTIC ACTIVITY TOWARD METHYLENE BLUE DYE DEGRADATION		
94		
4.1	Introduction.....	94
4.2	Experimental Section.....	97
4.2.1	Materials.....	97
4.2.2	Synthesis Methodology.....	97
4.2.2.1	Synthesis of Co ₃ O ₄ Nanocubes.....	97
4.2.2.2	Preparation of Polyaniline (PANI).....	98
4.2.2.3	Preparation of Chitosan-Grafted Polyaniline (ChGP).....	98
4.2.2.4	Preparation of the ChGP-Co ₃ O ₄ Nanocomposite.....	99
4.2.3	Characterisation Techniques	100
4.2.4	Measurement of Photocatalytic Activities	100
4.3	Results and Discussion	101
4.3.1	Characterization.....	101
4.3.1.1	Morphological Analysis of Nanocomposites.....	101
4.3.1.2	Thermal Analysis	105
4.3.1.3	XRD Analysis	107
4.3.1.4	XPS Analysis	109
4.3.1.5	UV-Vis Analysis	111
4.3.1.6	FTIR Analysis.....	112
4.3.2	Photodegradation Studies.....	114
4.3.2.1	Photocatalytic Degradation of MB Under UV Illumination.....	114
4.3.2.2	Comparison of Photocatalytic Efficiencies	120
4.3.2.3	Reproducibility of the photocatalysts.....	121
4.4	Conclusions	123
CHAPTER 5: SRTIO₃ NANOCUBE-DOPED POLYANILINE NANOCOMPOSITES WITH ENHANCED PHOTOCATALYTIC DEGRADATION OF METHYLENE BLUE UNDER VISIBLE LIGHT		
124		
5.1	Introduction	124

5.2	Experimental Section.....	128
5.2.1	Materials.....	128
5.2.2	Synthesis Methodology.....	128
5.2.2.1	Synthesis of SrTiO ₃ Nanocubes.....	128
5.2.2.2	Preparation of Polyaniline (PANI).....	129
5.2.2.3	Preparation of PANI-SrTiO ₃ Nanocomposite.....	129
5.2.3	Characterisation Techniques	130
5.2.4	Measurement of Photocatalytic Activities	131
5.3	Result and Discussion.....	132
5.3.1	Characterization.....	132
5.3.1.1	Morphological Analysis of Nanocomposites.....	132
5.3.1.2	Thermal Analysis	135
5.3.1.3	XRD Analysis	137
5.3.1.4	BET Analysis.....	139
5.3.1.5	UV-Vis Analysis	141
5.3.1.6	FTIR Analysis.....	142
5.3.2	Photodegradation Studies	144
5.3.2.1	Photocatalytic Degradation of MB Under UV Illumination.....	144
5.3.2.2	Comparison of Photocatalytic Efficiencies	149
5.4	Conclusions	149
 CHAPTER 6: SYNTHESIS OF POLYANILINE COATED GRAPHENE OXIDE @ SRTIO₃ NANOCUBE NANOCOMPOSITES FOR ENHANCED REMOVAL OF CARCINOGENIC DYES FROM AQUEOUS SOLUTION 150		
6.1	Introduction.....	150
6.2	Experimental Section.....	154
6.2.1	Materials.....	154
6.2.2	Synthesis Methodology.....	154
6.2.2.1	Synthesis of Graphene oxide (GO)	154
6.2.2.2	Synthesis of SrTiO ₃ Nanocubes.....	155
6.2.2.3	Synthesis of Polyaniline (PANI).....	155
6.2.2.4	Synthesis of PANI coated GO (GOPSr-0)	155
6.2.2.5	Synthesis of SrTiO ₃ Nancocubes-doped PANI Coated GO (GOPSr).....	156

6.2.3	Characterisation Techniques	157
6.2.4	Dye adsorption study	157
6.3	Results and Discussion	158
6.3.1	Synthesis	158
6.3.2	Characterization.....	159
6.3.2.1	Morphological Analysis of Nanocomposites.....	159
6.3.2.2	FTIR Analysis.....	163
6.3.2.3	XRD Analysis	165
6.3.3	Adsorption Studies.....	167
6.3.3.1	Adsorption Analysis of MB and MO	167
6.3.3.2	Effect of Adsorbent Dosage.....	171
6.3.3.3	Effect of Contact Time	172
6.3.3.4	Effect of pH	173
6.3.3.5	Effect of NaCl Concentration	174
6.3.3.6	Reusability Studies.....	175
6.3.4	Proposed Mechanism	177
6.4	Conclusion.....	179
	CHAPTER 7: CONCLUSION AND FUTURE WORK.....	180
	REFERENCES	184
	APPENDIX A Supplementary data	208
	LIST OF PUBLICATIONS AND PAPERS PRESENTED.....	213

LIST OF FIGURES

Figure 1.1: (a) Number of papers per year on polyaniline and (b) Number of citations per year on Polyaniline. The data was extracted on February 2, 2016 from the Institute of Scientific Information (ISI) database via Polyaniline as a keyword that appeared in topic	2
Figure 2.1: Atomic arrangements in (a) Polyacetylene (b) Graphite (c) Diamond	12
Figure 2.2: Most common examples of intrinsically conducting polymers.....	13
Figure 2.3: A schematic representation of energy gaps in (a) metals, (b) insulators (c) semiconductors	14
Figure 2.4: Leucoemeraldine Base	18
Figure 2.5: Pernigraniline Base	19
Figure 2.6: Emeraldine Base	19
Figure 2.7: Mechanism for the formation of anilinium radical cation and its resonant structures	23
Figure 2.8: Mechanism for the formation anilinium cation dimer and corresponding radical cation	24
Figure 2.9: Plausible mechanism for polyaniline formation	25
Figure 2.10: Side reaction during polyaniline polymerization.....	26
Figure 2.11: Acid doping in polyaniline	27
Figure 2.12: The polysemiquinone radical cationic form of polyaniline.....	28
Figure 2.13: Chemical structure of chitosan and chitin	44
Figure 2.14: Structure of C-containing molecules.....	46
Figure 2.15: Preparation of graphene oxide (GO).....	50
Figure 2.16: Some of the proposed graphene oxide structure.....	51
Figure 3.1: FESEM micrographs of (a and b) Co_3O_4 , (c) PANI, and (d) PANI- Co_4	68
Figure 3.2: TEM image of Co_3O_4 nanocubes.....	69
Figure 3.3: TEM image of PANI- Co_4 nanocomposite	69

Figure 3.4: (a) FESEM image and (b) EDX elemental mapping of PANI-Co4 nanocomposite on a Si wafer for the following elements: (c) C, (d) N, (e) Co and (f) Cl	71
Figure 3.5: EDX spectrum of PANI-Co4 nanocomposite	72
Figure 3.6: TGA patterns of Co ₃ O ₄ , PANI and PANI-Co4	74
Figure 3.7: XRD patterns of Co ₃ O ₄ , PANI and PANI-Co4	75
Figure 3.8: Nitrogen adsorption–desorption isotherms (BET) of PANI, PANI-Co4 and PANI-Co8 nanocomposites	77
Figure 3.9: FTIR spectrum of Co ₃ O ₄ , PANI and PANI-Co4	78
Figure 3.10: (a) Adsorption rate of MO at different time intervals and (b) Percentage removal of MO in the presence of various adsorbents. {initial MO concentration: 50 mg l ⁻¹ ; amount of adsorbent: 0.5mg ml ⁻¹ ; pH 7 at room temperature}	81
Figure 3.11: UV-vis absorption spectra of MO aqueous solution at different times in the presence of (a) PANI, (b) PANI-Co2, (c) PANI-Co4 and (d) PANI-Co8. {initial MO concentration: 50 mg l ⁻¹ ; amount of adsorbent: 0.5mg ml ⁻¹ ; pH 7 at room temperature}	82
Figure 3.12: Dissociation of methyl orange dye in aqueous solution.....	83
Figure 3.13: Pseudo-first-order kinetic plots for the removal of MO by (a) PANI, (b) PANI-Co2, (c) PANI-Co4 and (d) PANI-Co8. {initial MO concentration: 50 mg l ⁻¹ ; amount of adsorbent: 0.5mg ml ⁻¹ ; pH 7 at room temperature}	85
Figure 3.14: Pseudo-second-order kinetic plots for the removal of MO by(a) PANI, (b) PANI-Co2, (c) PANI-Co4 and (d) PANI-Co8. {initial MO concentration: 50 mg l ⁻¹ ; amount of adsorbent: 0.5mg ml ⁻¹ ; pH 7 at room temperature}	86
Figure 3.15: Effect of adsorbent dosage on percentage removal of MO in presence of PANI-Co4 at different time intervals {initial MO concentration: 50 mg l ⁻¹ ; pH 7 at room temperature}	87
Figure 3.16: Effect of time on percentage removal of MO in presence of PANI-Co4 {initial MO concentration: 50 mg l ⁻¹ ; amount of adsorbent: 2 mg ml ⁻¹ ; pH 7 at room temperature}	88
Figure 3.17: Effect of pH on percentage removal of MO in presence of PANI-Co4 {initial MO concentration: 50 mg l ⁻¹ ; amount of adsorbent: 2mg ml ⁻¹ ; time: 45 min; at room temperature}	90

Figure 3.18: Effect of NaCl concentration on percentage removal of MO in presence of PANI-Co ₄ {initial MO concentration: 50 mg l ⁻¹ ; amount of adsorbent: 2mg ml ⁻¹ ; time: 45 min; pH: 7; at room temperature}	91
Figure 3.19: Reproducibility cycles of PANI-Co ₄ {initial MO concentration: 50 mg l ⁻¹ ; amount of adsorbent: 2 mg ml ⁻¹ ; time: 45 min; pH: 7; at room temperature}	92
Figure 4.1: Reaction pathway for the synthesis of chitosan-grafted-polyaniline copolymer	99
Figure 4.2: FESEM micrographs of (a and b) Co ₃ O ₄ , (c) PANI, (d) chitosan, (e) ChGP (f) ChGPCo ₂ and continue.....	102
Figure 4.3: (a) FESEM image and (b) EDX elemental mapping of ChGPCo ₂ nanocomposite on a Si wafer for the following elements: (c) C, (d) N, (e) Co and (f) O	104
Figure 4.4: EDX spectrum of ChGPCo ₂ nanocomposite	105
Figure 4.5: TGA thermogram analysis of PANI, chitosan, Co ₃ O ₄ and nanocomposites	107
Figure 4.6: XRD patterns of Co ₃ O ₄ , PANI and chitosan.....	108
Figure 4.7: XRD patterns of ChGP, ChGPCo ₁ , ChGPCo ₂ and ChGPCo ₄	109
Figure 4.8: XP spectra of ChGPCo ₂ (a) Survey scan. The symbol * represents the Auger peaks; for Co(LMV), Co(LMM) and O(KLL) (b) C 1s core level and (c) Co 2p core level	110
Figure 4.9: UV-Visible spectra of (a) chitosan, (b) Co ₃ O ₄ , (c) PANI and (d) ChGPCo ₂	112
Figure 4.10: FTIR spectrum of (a) Co ₃ O ₄ , (b) PANI, (c) chitosan and (d) ChGPCo ₂ .	113
Figure 4.11: (a) Adsorption–desorption equilibrium rate of MB under dark conditions versus time in the presence of various photocatalysts (b) Photodegradation rate of MB at different time intervals in the presence of various photocatalysts.....	115
Figure 4.12: (a) Percentage degradation of MB in the presence of various photocatalysts (b) UV-vis absorption spectra of MB aqueous solution at different times in the presence of ChGPCo ₂ as a photocatalyst	116
Figure 4.13: Proposed mechanism for the photocatalytic degradation of MB under UV irradiation	119

Figure 4.14: Schematic illustration for the formation of advanced oxidation species in Co_3O_4 -doped chitosan-grafted-polyaniline hybrid photocatalyst.....	120
Figure 4.15: Reproducibility of ChGPCo2. (The symbol D represent dark adsorption whereas R represents repeated cycle)	122
Figure 5.1: FESEM micrographs of (a) PANI, (b and c) SrTiO_3 and (d) P-Sr500.....	133
Figure 5.2: TEM image of SrTiO_3 nanocubes. The inset highlights the SAED pattern of SrTiO_3	133
Figure 5.3: (a) FESEM image and (b) EDX elemental mapping of P-Sr500 nanocomposite on a Si wafer for the following elements: (c) C, (d) O, (e) N, (f) Sr and (g) Ti.....	134
Figure 5.4: EDX spectrum of P-Sr500 nanocomposite	135
Figure 5.5: TGA thermogram analysis of PANI, SrTiO_3 and P-Sr500 nanocomposite	137
Figure 5.6: XRD patterns of PANI, SrTiO_3 , and P-Sr500 nanocomposite	139
Figure 5.7: Nitrogen adsorption–desorption isotherms (BET) of P-Sr500 nanocomposite	140
Figure 5.8: BJH pore-size distribution of P-Sr500 nanocomposite.....	141
Figure 5.9: UV-Visible spectra of (a) SrTiO_3 , (b) PANI (c) P-Sr250, (d) P-Sr500 and (e) P-Sr750 nanocomposite	142
Figure 5.10 FTIR spectrum of (a) SrTiO_3 , (b) PANI, (c) P-Sr250, (d) P-Sr500 and (e) P-Sr750 nanocomposite.....	143
Figure 5.11 (a) Adsorption–desorption equilibrium rate of MB under dark conditions versus time in the presence of various photocatalysts (b) UV-vis absorption spectra of MB aqueous solution at 60-minute dark adsorption–desorption equilibrium.....	145
Figure 5.12: (a) Photodegradation rate of MB at different time intervals in the presence of various photocatalysts. (b) Percentage degradation of MB in the presence of various photocatalysts	146
Figure 5.13: UV-vis absorption spectra of MB aqueous solution at different times in the presence of (a) PANI, (b) P-Sr250, (c) P-Sr500 and (d) P-Sr750 nanocomposite	147
Figure 6.1: Reaction pathway for the synthesis of PANI coated GO nanocomposite (a) doped with SrTiO_3 and (b) without SrTiO_3	156

Figure 6.2: FESEM micrographs of (a) PANI, (b) GO, (c) SrTiO ₃ nanocubes, (d) TEM of SrTiO ₃ (e) GOPSr-0, (f) GOPSr-2 nanocomposite and (d) TEM image of SrTiO ₃ nanocubes	161
Figure 6.3: (a) FESEM image and (b) EDX elemental mapping of GOPSr-2 nanocomposite on a Si wafer for the following elements: (c) C, (d) O, (e) Cl, (f) N, (g) Sr and (h) Ti.....	163
Figure 6.4: FTIR spectrum of (a) PANI, (b) GO, (c) SrTiO ₃ , (d) GOPSr-0 and (e) GOPSr-5	165
Figure 6.5: XRD pattern of PANI, GO, SrTiO ₃ , and GOPSr-2.....	167
Figure 6.6: UV-vis absorption spectra of MB aqueous in the presence of various adsorbents and (b) Percentage removal of MB in the presence of various adsorbents. {initial MB concentration: 20 mg l ⁻¹ ; amount of adsorbent: 0.5mg m ⁻¹ ; pH 7; time: 30 minutes; at room temperature}	168
Figure 6.7: UV-vis absorption spectra of MO aqueous in the presence of various adsorbents and (b) Percentage removal of MO in the presence of various adsorbents. {initial MO concentration: 20 mg l ⁻¹ ; amount of adsorbent: 0.5mg ml ⁻¹ ; pH 7; time: 30 minutes; at room temperature}	169
Figure 6.8: Effect of adsorbent dosage on percentage removal of (a) MB and (b) MO in presence of GOPSr-2. {initial MB and MO concentration: 20 mg l ⁻¹ ; pH 7; time: 30 minutes at room temperature}	172
Figure 6.9: Effect of pH on percentage removal of (a) MB and (b) MO in presence of GOPSr-2. {initial MB and MO concentration: 20 mg l ⁻¹ ; amount of adsorbent (MB): 0.5mg ml ⁻¹ , (MO) :2mg ml ⁻¹ ; time: 30 minutes at room temperature}	173
Figure 6.10: Effect of time on percentage removal of (a) MB and (b) MO in presence of GOPSr-2. {initial MB and MO concentration: 20 mg l ⁻¹ ; amount of adsorbent (MB): 0.5mg ml ⁻¹ , (MO) :2mg ml ⁻¹ ; pH(MB): 9.5 (MO): 7; at room temperature}	174
Figure 6.11: Effect of NaCl conc. on percentage removal of MB and MO in presence of GOPSr-2. {initial MB and MO concentration: 20 mg l ⁻¹ ; amount of adsorbent (MB): 0.5mg ml ⁻¹ , (MO) :2mg ml ⁻¹ ; pH(MB): 9.5 (MO): 7; at room temperature}	175
Figure 6.12: Reproducibility cycles of GOPSr-2 for MB and MO adsorption {initial MB and MO concentration: 20 mg l ⁻¹ ; amount of adsorbent (MB): 0.5mg ml ⁻¹ , (MO) :2mg ml ⁻¹ ; pH(MB): 9.5 (MO): 7; at room temperature}	177
Figure 6.13: Proposed mechanism for the adsorption of MB and MO on the surface of GOPSr-2.....	178

LIST OF TABLES

Table 2.1: A list of conductive polymers and their abbreviations (Ateh et al., 2006; Balint et al., 2014).....	9
Table 2.2: Physical (solid state) and chemical terms of the defects present in conducting polymers.....	16
Table 2.3: Effect of size on surface area of cube.....	39
Table 3.1: TGA summary of Co_3O_4 , PANI and PANI- Co_4	73
Table 3.2: Kinetic parameters for MO adsorption ^a	86
Table 4.1: TGA summary of Co_3O_4 , Chitosan, PANI, ChGP, ChGPCo1, ChGPCo2 and ChGPCo4.	106
Table 4.2: Comparison of photocatalytic efficiencies.....	121
Table 4.3: Percent of MB dye dark adsorption and photodecomposition.....	122
Table 5.1: Yield and % PANI loading in various nanocomposites.	130
Table 5.2: TGA summary of SrTi_3 , PANI and PSr-500.	136
Table 5.3: Comparative study of the photocatalytic efficiencies of the different photocatalysts.....	147

LIST OF SYMBOLS AND ABBREVIATIONS

AOP	:	Advanced oxidation process
AOS	:	Active oxidative species
APS	:	Ammonium persulfate
BET	:	Brunauer-Emmett-Teller
BJH	:	Barrett-Joyner-Halenda
CB	:	Conduction band
ChGP	:	Chitosan-grafted-polyaniline
CVC	:	Chemical Vapour Condensation
CVD	:	Chemical Vapour Deposition
DSSC	:	Dye-sensitized solar cells
EDX	:	Energy Dispersive X-ray spectroscopy
E_g	:	Band gap
e.g.	:	exempli gratia
et al	:	et alia
etc.	:	et cetra
eV	:	electron volt
FESEM	:	Field emission scanning electron microscopy
FRGS	:	Fundamental Research Grant Scheme
FTIR	:	Fourier Transform Infrared spectroscopy
GIC	:	Graphite intercalation compound
GO	:	Graphene oxide
HIR	:	High Impact Research
HOMO	:	Highest occupied molecular orbitals
ISI	:	Institute of Scientific Information

IUPAC	:	International Union of Pure and Applied Chemistry
KeV	:	Kilo electron Volt
LUMO	:	Lowest unoccupied molecular orbital
MB	:	Methylene blue
MBC	:	Modified ball clay
mmol	:	milli mole
mL	:	milli liter
MO	:	Methyl orange
MWCNT	:	Multi walled carbon nanotubes
OH	:	Hydroxyl
PLA	:	Pulsed laser ablation
SAED	:	Selected area electron diffraction
TEM	:	Transmission electron microscopy
TGA	:	Thermogravimetry analysis
UM	:	University of Malaya
UV/Vis	:	Ultra violet/ visible
VB	:	Valence band
WAXD	:	Wide-angle X-ray diffraction
XPS	:	X-ray photoelectron spectroscopy
XRD	:	X-ray diffraction

LIST OF APPENDICES

Figure A- 1 FESEM images of (a) PANI homopolymer and (b) P-Sr750.....	208
Figure A- 2 TEM image of P-Sr500	208
Figure A- 3 XRD patterns of P-Sr250 and P-Sr750	209
Figure A- 4 Nitrogen adsorption–desorption isotherms (BET) of SrTiO ₃ nanocomposite	209
Figure A- 5 Proposed mechanism for the photocatalytic degradation of MB under UV irradiation	210
Figure A- 6 FESEM images of (a) and (b) GOPSr-2 nanocomposite at different magnifications	211
Figure A- 7 TEM images GOPSr-2 nanocomposite at different magnifications.	211
Figure A- 8 EDX spectrum of GOPSr-2 nanocomposite.....	212

CHAPTER 1: INTRODUCTION

1.1 Background of Research

Conductive polymers comprise of the organic macromolecules which are able to conduct electricity and mimic metals by possessing mobile electrons as the charge carriers. These polymers might exhibit semiconductivity or metal like conductivity in some case. Conductive polymers are usually non-thermoplastic in nature and belongs to the class of organic material. Polyaniline (PANI), an intrinsically conducting polymers (ICPs) which belongs to the semi-flexible rod polymer family, was discovered around 150 years ago but gain massive scientific consideration only since the early 1980s. Polyaniline exhibits a wide varieties of applications in the field of photocatalysis (Ameen et al., 2011; Min et al., 2007; Shahabuddin et al., 2015a; Wang et al., 2007; Xiong et al., 2012; Xiong et al., 2013), sensor (Feng et al., 2006; JX Huang et al., 2003; Liu et al., 2004; McQuade et al., 2000; Virji et al., 2004), adsorption (Javadian et al., 2014; Tang et al., 2014; Yan et al., 2015), solar cells (Ahdulrazzaq et al., 2015; Dinari et al., 2016; Yang et al., 2015) etc. Polyaniline has been extensively studied conducting polymer as revealed by the published papers and citation data obtained from Web of Science (Figure1.1).

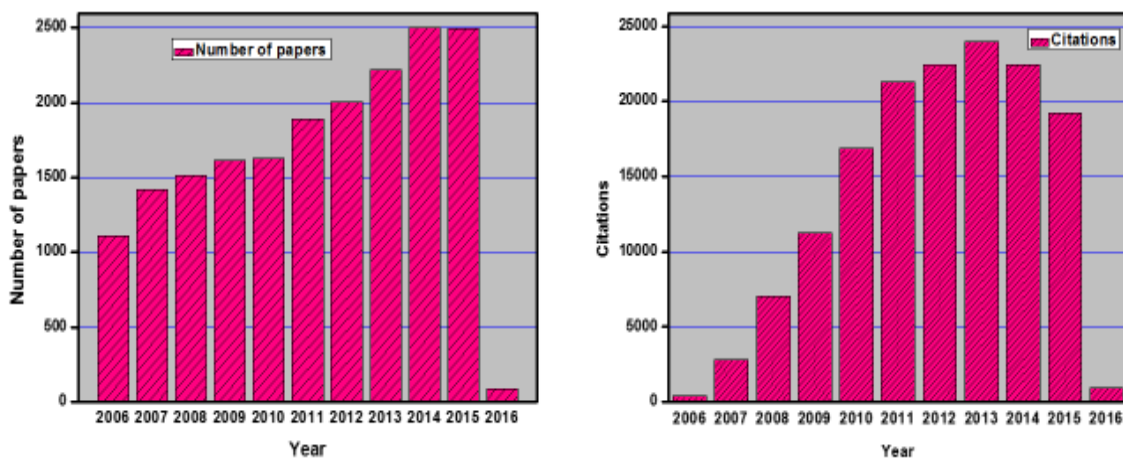


Figure 1.1: (a) Number of papers per year on polyaniline and (b) Number of citations per year on Polyaniline. The data was extracted on February 2, 2016 from the Institute of Scientific Information (ISI) database via Polyaniline as a keyword that appeared in topic

Polyaniline suffers a major drawback such as its infusibility, very low solubility in most of the existing solvents, inferior conductivity compared to that of metals, processability, hygroscopicity and structural instability. To enhance the properties of polyaniline various researches had synthesized different types of composites of polyaniline with metals, metal oxides, carbon nanotubes, graphene etc. where the synthesized nanocomposites exhibited enhanced physical and physiochemical properties. The synthesis, characterization, and application of electronically conducting PANI-nanocomposite systems continues to be the centre of research activity in electro-polymer chemistry. The major reasons for this immense scientific interest may be considered due to the rational keenness of researchers, which emphasises on understanding the mechanism of these systems specially focusing on the charge transfer processes that arises during redox reactions of conducting polymeric materials and secondly due to the wide variety of promising applications of these nanocomposite materials such as photocatalysis, adsorption, energy storage, electrochemistry, bioelectrochemistry, electroanalysis, sensors, electronic devices, microwave screening and corrosion protection, etc.

In recent years, polyaniline-based nanocomposites have been extensively studied and explored for numerous applications. Dumping of organic waste such as dyes, phenols and other organic matter is a serious environmental concern as these organic pollutants are non-biodegradable. Adsorption and photocatalysis are extensively used for efficient treatment of organic pollutants since they are facile and cost-effective techniques. Polyaniline has a wide band gap which falls within the range of semiconductors and the band gap can be effectively tuned via chemical modifications of the polymeric backbone by doping with wide band gap metal oxides thereby making it a suitable candidate for photocatalysis. Additionally, the conductive form of polyaniline through its extended π -conjugated system and positively charged backbone can efficiently adsorb anionic organic pollutants through ionic interaction and hydrogen bonding. Removal of these organic pollutants from aquatic bodies has been an active area of research where polyaniline based nanocomposite materials have efficiently been utilised as adsorbents and photocatalysts to remove and degrade toxic organic pollutants. Thus modified polyaniline nanocomposites are the promising candidates for the environmental problem.

1.2 Aims and Objectives of Research

As stated above, the significant photochemical, physicochemical and electrochemical properties of polyaniline make it a suitable candidate to be used as a matrix for the synthesis of nanocomposites intended for various applications. It has been established that doping of polyaniline with wide band gap semiconducting metal oxides not only enhanced the performance of PANI and metal oxides but also exhibits added unique properties as a result of interaction between the HOMO-LUMO of PANI and d-orbital electrons of metal oxides. The nanoparticles act as impurities which suppresses the

growth of crystalline PANI thereby increasing the effective surface area for enhanced adsorption applications. Designing facile, economic, environmentally stable and non-hazardous synthetic pathways for preparing PANI based nanocomposite materials is an important and challenging task. The performance of the nanocomposites is significantly affected by the band gap, morphology, size and distribution of nanoparticles in the polymeric matrix, which are crucial parameters to be controlled effectively.

With the purpose of achieving the above stated objectives, we designed and accomplished the following researches:

- 1) Synthesis of Co_3O_4 nanocube-doped polyaniline nanocomposites via in-situ oxidative polymerization technique using ammonium persulfate (APS) as an oxidant in acidic medium. The resultant nanocomposite material can be used as an adsorbent material for effective removal of carcinogenic and highly concentrated methyl orange dye from aqueous solution within a short duration of time.
- 2) Synthesis of chitosan-grafted-polyaniline copolymer (ChGP) and Co_3O_4 nanocube-doped chitosan-grafted-polyaniline copolymer nanocomposites through oxidative-radical copolymerization technique using ammonium persulfate in acidic medium. The adsorption capacity of the nanocomposites could be enhanced by incorporation flexible polymeric matrix using chitosan. The resultant nanocomposites can be investigated for photocatalytic degradation of methylene blue (MB) under ultraviolet (UV) light irradiation.

- 3) Synthesis of polyaniline-based nanocomposites doped with SrTiO₃ nanocubes synthesized via the in-situ oxidative polymerization technique using ammonium persulfate (APS) as an oxidant in acidic medium. The effective surface area of the synthesized nanocomposite could be enhanced by varying the proportion of nanoparticles in polymer matrix. The resultant nanocomposites could be explored for photocatalytic degradation of methylene blue (MB) under natural sunlight irradiation.
- 4) Synthesis of SrTiO₃ nanocube decorated polyaniline-graphene oxide nanocomposites via the in-situ oxidative polymerization technique using ammonium persulfate (APS) as an oxidant in acidic medium. The resultant nanocomposites can be used as adsorbent material for the efficient removal of carcinogenic, cationic as well as anionic dyes from the aqueous solutions.

1.3 Hypothesis

Before performing the experiments, some of the following hypotheses were taken into account:

- a) Oxidative polymerization approach for the synthesis of conductive polyaniline and its nanocomposites with various organic and inorganic substances is a very fascinating approach owing to its facile nature, less time consuming and environmental friendly. Additionally, it was established that polyaniline can be easily doped with various metal oxides and organic substance by simple in-situ polymerization method which can lead to the enhancement and development of some novel properties of nanocomposites for wide variety of application.

- b) Co_3O_4 have attracted the attention of researchers due to simplistic synthetic methodologies, excellent catalytic properties, and diverse morphologies. Nanoparticles of Co_3O_4 possess very high effective surface area and a band gap of 1.6 eV. Co_3O_4 nanoparticles may act as impurities that retard the growth of the crystalline polyaniline which can thereby leads in the enhancement of the effective surface area of the nanocomposites material. The d-orbital conducting band of Co_3O_4 can undergoes chemical bond interaction with LUMO of PANI upon UV irradiation and electrons can be injected from the conduction band of Co_3O_4 to LUMO of PANI since band gap of PANI (2.8 eV) is higher than Co_3O_4 . These electronic interactions might create effective charge separation leading to the formation of active oxidative species (AOS) which can degrade organic pollutants.
- c) SrTiO_3 is a wide band gap metal oxide with a value of 3.3 eV. Polyaniline doped with SrTiO_3 may lead to the formation of nanocomposite where electron can absorb energy in visible region of spectrum and transfer electron from metal oxide to polyaniline empty conduction bands. This might result in efficient charge separation and prevent recombination of electrons and holes more effectively thereby forming AOS and degrading organic pollutant.
- d) Polyaniline in conductive emeraldine salt form possess a positively charged backbone which can be utilised to adsorbent anionic pollutants from aqueous. This adsorption efficiency can be further enhanced by doping with metal oxides nanoparticles which retards crystalline growth of PANI thereby increasing effective surface area. Graphene oxide possess high amount of negative charge and lots of epoxy and hydroxyl functional groups on its surface which could easily adsorb cationic pollutants on its surface. The composite material comprising PANI and graphene oxide can be effectively

utilized for removal of anionic as well as cationic pollutants by simple adsorption process.

1.4 Outlines of Thesis

The thesis was written in seven chapters. Chapter one presents the background of study, aim and objectives of research, and hypothesis. Chapter two comprises of a literature review on conductive polymers, polyaniline, metal oxide nanoparticles, graphene and graphene oxide, polyaniline-based nanocomposites and applications of polyaniline-based nanocomposite. Chapter three, four, five and six deals with experimental details and result and discussion involving different type of nanocomposites and their applications:

- i. Synthesis and characterization of Co_3O_4 nanocube-doped polyaniline nanocomposite with enhanced methyl orange adsorption from aqueous solution.
- ii. Synthesis of chitosan grafted-polyaniline/ Co_3O_4 nanocube nanocomposites and their photocatalytic activity toward methylene blue dye degradation.
- iii. SrTiO_3 nanocube-doped polyaniline nanocomposites with enhanced photocatalytic degradation of methylene blue under visible light.
- iv. Synthesis of polyaniline coated graphene oxide doped with SrTiO_3 nanocube nanocomposites for enhanced removal of carcinogenic dyes from aqueous solution.

Chapter seven provides conclusion of the thesis and the proposed future work.

CHAPTER 2: LITERATURE REVIEW

2.1 Conducting Polymers

2.1.1 History of Conducting Polymers

Polymers, since long period of time, were believed to be and used as insulator materials. Moreover, any electrical conductivity was usually considered as an unwanted phenomenon in polymers which was believed to be due to loosely bound ions (Inzelt, 2012a). However, this concept was discarded after the discovery of conductive polymeric materials. Conductive polymers are the organic macromolecules which have the ability to conduct electricity and imitate metals by having mobile electrons responsible for carrying charge. These polymers may show semiconductivity or their conductivity may be comparable to the metals in some case. Unlike traditional polymers, conductive polymers are non-thermoplastic in nature but belongs to the class of organic material. Although these polymers exhibit higher electrical conductivities but they lack important properties of conventional polymers such as mechanical strength, melt property, elasticity etc. These polymers possess the properties of metals such as capability to conduct electricity along with flexibility in processing and facile synthetic methodologies (Ateh et al., 2006). They were first produced several decades ago (Shirakawa et al., 1977) and until today, more or less 25 conductive polymer systems have been discovered so far (Ateh et al., 2006; Balint et al., 2014). Table 2.1 provides some of the conductive polymeric systems which have been reported till date (Balint et al., 2014; Kirchmeyer et al., 2005; Kumar et al., 1998; Rupprecht, 1999; Wan, 2008).

Table 2.1: A list of conductive polymers and their abbreviations (Ateh et al., 2006; Balint et al., 2014)

Conductive Polymer	Abbreviation
Polypyrrole	(PPy)
Polyaniline	PANI
Poly(3,4-ethylenedioxythiophene)	PEDT, PEDOT
Polythiophene	PTh
Polythiophene-vinylene	PTh-V
Poly(2,5-thienylenevinylene)	PTV
Poly(3-alkylthiophene)	PAT
Poly(p-phenylene)	PPP
Poly-p-phenylene-sulphide	PPS
Poly(p-phenylenevinylene)	PPV
Poly(p-phenylene-terephthalamide)	PPTA
Polyacetylene	PAC
Poly(isothianaphthene)	PITN
Poly(α -naphthylamine)	PNA
Polyazulene	PAZ
Polyfuran	PFu
Polybutadiene	PBD
Poly(3-octylthiophene-3-methylthiophene)	POTMT
Poly(p-phenylene-terephthalamide)	PPTA

The immense attraction towards conducting polymers began around 1970s when a group of three prominent scientists, Alan J. Heeger, Alan G. MacDiarmid, and Hideki Shirakawa observed that the conductivity of a normally semiconductive polymer,

polyacetylene, increased to 10 million-fold upon partial oxidation in presence of iodine vapours (Shirakawa et al., 1977; Zhou et al., 2009). This discovery was a breakthrough in the field of conductive polymers and Shirakawa et al received the Nobel Prize in Chemistry in 2000 “for the discovery and development of electronically conductive polymers” (Chiang, 1978; Chiang et al., 1977; Heeger, 2001; Ito et al., 1974; MacDiarmid, 2001; Shirakawa, 2001; Shirakawa et al., 1977). Thus, the synthesis, characterization, and application of conducting and electrochemically active polymeric systems emerged as an innovative branch of research activity in materials chemistry. There are nevertheless two foremost causes for the passionate research interest in conductive polymers. Firstly, is the rational interest of researchers, which concentrates on understanding the nature of these systems, specifically on the mechanism regarding charge transfer pathways that takes place during redox reactions of conducting polymeric materials. Secondly, the eclectic array of encouraging applications of conductive polymers such as energy storage, electronic devices electroanalysis, sensors, corrosion protection, bioelectrochemistry, electrocatalysis, photoelectrochemistry, etc. Thus, conducting polymers continues to fascinate the attraction of researchers owing to their unique properties and are explored worldwide for the benefit of mankind.

2.1.2 Doping of Polymers

The electrical property of a material is anisotropic, that is, direction dependent. For instance, diamond, graphite and polyacetylene constitutes three simple carbon compounds which may be regarded as three, two and one dimensional form of carbonaceous material (Heeger et al., 2000). While diamond and graphite are the allotropes of carbon, polyacetylene contains hydrogen atom bonded to each carbon atom along its chain length (Figure 2.1). Due the presence of sigma bonds and highly

symmetrical structure, diamond possess isotropic properties and is an insulator. On the other hand, graphite and acetylene contain mobile electrons in their π conjugation system and becomes highly anisotropic upon doping behaving like metallic conductor. Thus concept of doping is an important aspect in conduction polymers which differentiate intrinsically conducting polymers (ICPs) from all other types of polymers (Yilmaz, 2007).

Basically conductive polymeric material may exist in two forms, namely, non-doped conducting polymers (non-conductive form) and doped-conductive polymers (conductive form). In the non-doped state, the organic conducting polymer behaves as semiconductors or insulators (Tourillon et al., 1986). The phenomenon to convert non-conductive state of polymer backbone into π –conjugated charged conductive chains is usually termed as “doping”. The electrical, magnetical, optical and structural properties of a conductive polymer changes comprehensively by doping the neutral form of polymer with a small quantity of dopant material ($\approx 10\%$). The electrical conductivity of the doped conductive polymers is enhanced by multiple degree of magnitude as compared with the undoped polymer. It is important to note that the chemical nature of the polymeric backbone do not change upon doping and it is purely a reversible process where undoping can be achieved easily by chemical treatment of conductive polymer. Conductivity in the polymeric chains can easily be controlled between insulating/semiconducting and conductive states by adjusting the amount of dopant molecules. This provides an efficient tool for tuning the properties of conductive polymers for a wide variety of applications under various conditions. Doping of conductive polymers can be achieved by redox doping also known as p-doping or via partial reduction doping commonly known as n-doping (MacDiarmid et al., 1989). Doping usually alters the number of electrons associated with the polymeric backbone and dramatically changes the conductive properties of polymer materials.

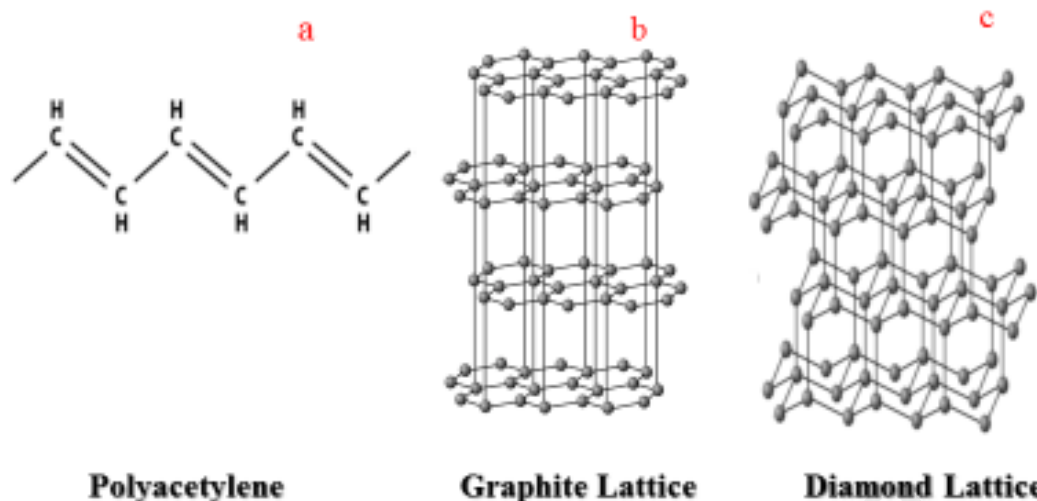


Figure 2.1: Atomic arrangements in (a) Polyacetylene (b) Graphite (c) Diamond

2.1.3 Intrinsic and Extrinsic Conducting Polymers

The concept of intrinsically and extrinsically doped semiconductors in solid state chemistry is totally different with the concept in conductive polymers. According to the definition intrinsic semiconductors are the materials which exhibits semiconductivity without doping whereas extrinsic semiconductors are referred to the materials which show semiconductivity upon external doping agents. On the contrary, doped polymers are often termed as intrinsically conducting polymers (ICPs) whereas the polymers which attains conductivity upon mixing with conductive materials such as metal particles, stainless steel fibres, carbon black etc. are termed as extrinsically conducting polymers. In conductive polymers it is ICPs which are more important as they possess unique electrochemical properties by doping with small amount of dopants. ICPs, also termed as synthetic metals, belong to the family of organic polymers which demonstrates the properties of conventional polymers such as rheological properties, mechanical strength and processibility along with distinctive electronic, electric, optical and magnetic properties of metals. They thus appear to be an amalgamated systems imitating metals in one aspect and conventional polymers in other aspects. Some of the ICPs are listed below in Figure 2.2

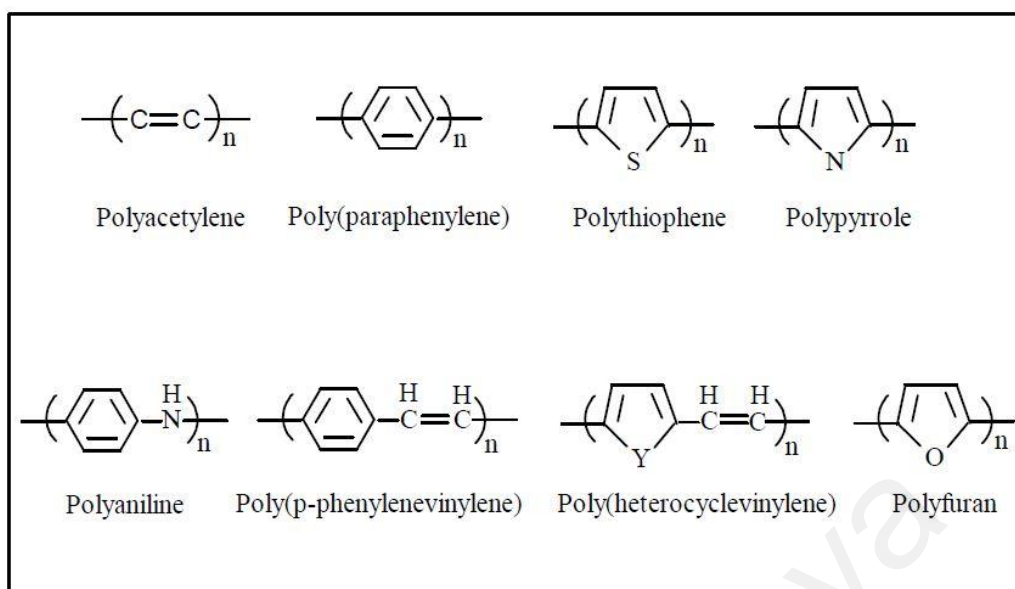


Figure 2.2: Most common examples of intrinsically conducting polymers

ICPs consist of extended π -bonded systems and are non-conductive in undoped state. One of the main requisition to achieve conductivity in ICPs is the open shell electronic configuration which can be attained through oxidation or reduction of the non-conducting polymeric chains containing extended π -conjugated systems in their backbone. Where oxidation prompts the partial emptying of formerly filled bands, reduction phenomenon initiates the partial filling of formerly empty bands. This partial filling or emptying of the bands leads to the formation of p- and n-type conductive polymeric systems (Wynne et al., 1982).

2.1.4 Band Structure of Conducting Polymers: Solitons, Polarons and Bipolarons

The electrical properties of the semiconducting materials, according to the band theory (Harrison, 1979), are generally determined via their electronic band structures where electrons move within distinct energy levels known as bands. Similar to the electronic structures of inorganic semiconductor materials, conducting polymers possess bonding and antibonding π molecular orbitals generating energy bands. The occupied π -bonding

molecular band is called as valence band or highest occupied molecular orbitals (HOMO), whereas the empty π^* -antibonding molecular band is called as conduction band or lowest unoccupied molecular orbitals (LUMO). The energy difference between the valence and conduction band is referred to as band gap. In order to jump from valence band to conduction band, electrons must have extra energy which is the measure of electrical conductivity of the material. In order to conduct electricity, the bands should be partially filled, since neither full nor empty bands can conduct electricity. Metals, for instance, exhibits high degree of conductivity due to the presence of partially filled energy bands (Figure 2.3). The energy bands of conventional polymers are either completely empty or completely full having a wide energy gap, thereby making them insulators. On the contrary, conjugated polymers possess lower band gaps (Figure 2.3) and doping can alter their electronic band structures either by adding electrons to conduction band (n-doping) or removing electrons from valence band (p-doping) resulting in the formation of new bands (Dai, 2004).

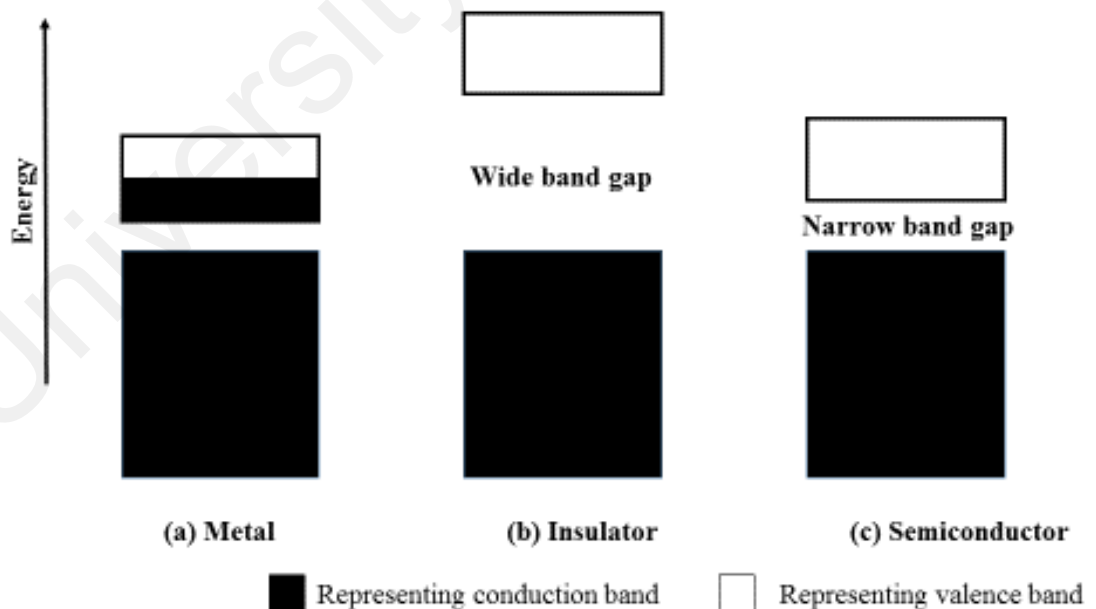


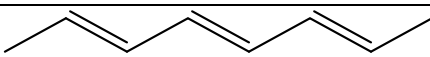

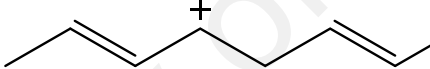
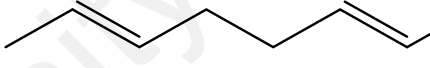
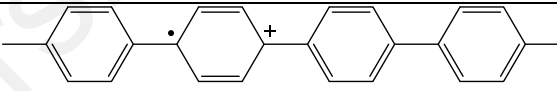
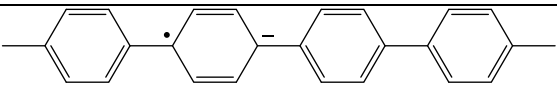
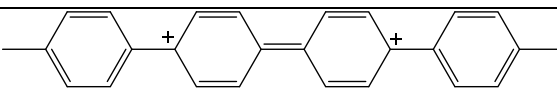
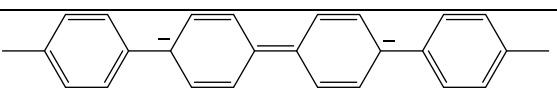
Figure 2.3: A schematic representation of energy gaps in (a) metals, (b) insulators (c) semiconductors

The band structure of conjugated polymers such as *trans*-polyacetylene possess degenerate ground state (equivalent energy states) as the energy of the molecule remains same irrespective of the position of double bond. This leads to the formation of a new band in the middle of valence and conduction band when the number of electrons in the π -conjugate system is altered. Oxidation of the π -conjugate system i.e. removal of electron from valence shell (p-doping), leads in the formation of an empty band, a 'positive soliton' band within the band gap whereas addition of electron to the conduction band or reduction of π -conjugate system (n-doping) leads to the formation of filled band, a 'negative soliton' within the band gap (MacDiarmid et al., 1991a). Formation of solitons does not occur in conjugated polymers having non-degenerate ground states, for example, polyaniline, polypyrrole and polythiophene upon alteration in number of electrons in their π -conjugate systems (Bredas et al., 1985). In such types of conductive polymers, the p-doping (removal of electrons) results in the formation of 'positive polaron' where as n-doping (addition of electrons) leads in the formation of 'negative polaron'. Dimerization of two polarons leads to the formation of bipolarons band structures. Formation of polarons or bipolarons depends upon the extent of doping. At different doping levels a conductive polymer may exist as polaron or bipolaron. The concentration of solitons, polarons, and bipolarons rises with the doping level. New energy bands with overlapped valence and conduction bands are formed at elevated doping levels as the localized solitons, polarons or bipolarons overlapped near the dopant ions. This leads to the enhancement in the electrical conductivity of the conductive polymer.

In addition to the charged solitons, neutral solitons might be present in the π -conjugated system of undoped conducting polymers such as polyacetylene. Distortions caused by the rotation around the single C-C bond in the structure of polymer chain results

in the formation of neutral solitons (Chien, 1984). These distortions are caused by the bending and twisting of the molecular chains causing disruptions of the π -conjugated systems of polyacetylene. All these defects present in the band structures of conducting polymers are responsible for their unique electronic properties. Some of the defects are shown in Table 2.2.

Table 2.2: Physical (solid state) and chemical terms of the defects present in conducting polymers

Physical terms	Chemical terms	
Non-doped state		Undisturbed conjugation
Neutral soliton		Free radical
Positive soliton		Carbocation
Negative soliton		Carbanion
Positive polaron		Radical cation
Negative polaron		Radical anion
Positive bipolaron		Carbocation
Negative bipolaron		Carbodianion

2.2 Polyaniline:

In the beginning of 19th century, aniline was prepared from the residual coal tar in gas industries which later played an important role in the development of basic organic chemistry and found immense use in chemical industries. Initially, aniline was used to prepare synthetic dyes which were used as substitutes to for the dyes obtained from natural resources. Later, discovery of selective toxicity of aniline compounds by P. Erlich open the new era of pharmaceutical industries (Inzelt, 2012a). It was Dr. Henry Letheby, a physician by profession and an elite member in the Board of Health, London, who developed keen interest in aniline as it was the major cause of poisoning of industrial workers at that time. He discovered a bluish green precipitate during electrolysis of aniline at anode, which tends to become colourless upon reduction and retains its bluish green colour upon reoxidation (Letheby, 1862). The same phenomenon was observed by Runge (Inzelt, 2012b) and Fritzsche (Fritzsche, 1840), during oxidation of aniline in acidic environment. Runge, due to the formation of bluish-green compound, proposed the name kyanol (meaning blue in Greek) or Blauöl (after German word for blue). Later, Fritzsche proposed name 'aniline' which become the accepted name till date. Since the discovery of 'aniline black' by Fritzsche (Fritzsche, 1840) numerous researchers become interested in oxidation of aniline owing to its unique properties. It was found out that aniline compounds exist in four different kind of oxidation states which were named as emeraldine series (Green et al., 1910; Willstätter et al., 1909). Yasui et al. proposed the reaction pathway for the electrooxidation at a carbon electrode for aniline in 1935 (Yasui, 1935). Autocatalytic nature of electrooxidation of aniline was later suggested by Khomutov and Gorbachev in 1950 (Inzelt, 2011). Electrooxidation mechanism of aniline was reinvestigated by Mohilner, Adams, and Argersinger in 1962 using aqueous sulfuric acid solution at a platinum electrode (Mohilner et al., 1962). While research on understanding the mechanism of electrochemical oxidation of aniline continues (Breitenbach et al.,

1973; Dunsch, 1975), the term 'polyaniline' was normally accepted (Breitenbach et al., 1973).

Polyaniline has become as one of the most important class of conducting polymers with large number of review article being reported by various researchers (Armes et al., 1988; MacDiarmid et al., 1989; Pron et al., 1988) in past decade. The investigations for enhancing the quality and quantity of polyaniline yields have been reported by numerous group of scholars (Cao et al., 1989; Leng et al., 1992; Oh et al., 1993). A large numbers of polyaniline derivatives can be prepared via substitution on aromatic ring or at N atoms in polymeric chain. One of the unique feature of polyaniline is the doping of polymer chain with protonic acids to make it conductive in nature. The properties of polyaniline can be can be modified by controlling the type and amount of dopant acids. Polyaniline usually exist in three different oxidation states which can be isolated (MacDiarmid et al., 1991b) and are completely interchangeable. They are the leucoemeraldine oxidation state, the emeraldine oxidation state, and the pernigraniline oxidation state. Moreover, other oxidation states of polyaniline are obtained as a result of physical mixture of these three oxidation states.

(i) Leucoemeraldine base: This form of non-doped polyaniline is fully reduced and non-conductive. The polymer chains comprise of exclusively reduced units as presented below:

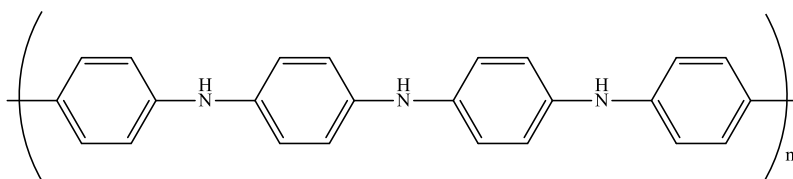


Figure 2.4: Leucoemeraldine Base

(ii) Pernigraniline base: This form of non-doped polyaniline is fully oxidised and non-conductive. The polymer chains comprise of exclusively oxidized units as presented below:

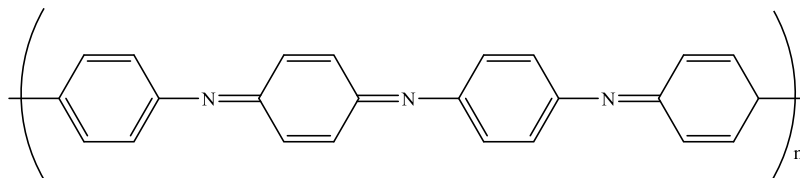


Figure 2.5: Pernigraniline Base

(iii) Emeraldine base: This is the intermediate oxidation state of non-doped polyaniline. The polymer chains are composed of equivalent amount of alternating reduced base and oxidized base units as presented below:

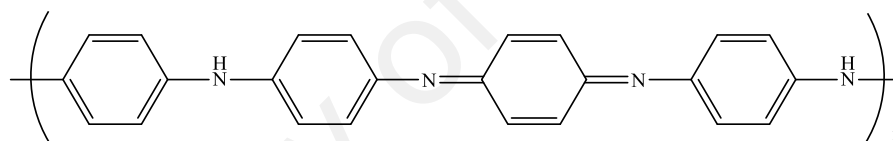


Figure 2.6: Emeraldine Base

Volumetric titration techniques using TiCl_3 can be employed for accurate determination of the oxidation states of polyaniline (Mattoso et al., 1994). Besides, various spectroscopic approaches for instance, Raman, FT-IR, and UV-Vis can be exploited to obtain qualitative data regarding the oxidation state of polyaniline (Banerjee et al., 1995).

2.2.1 Synthesis of Polyaniline

2.2.1.1 Chemical Polymerization of Aniline

Polyaniline can be synthesized chemically by oxidative polymerization of aniline in acidic environment to get conductive form of polyaniline. Several polymerization techniques, such as solution, suspension, precipitation, emulsion, dispersion, microsuspension, microemulsion, miniemulsion, reverse micelle and inverse polymerizations, have been utilized for the synthesis of conductive polyaniline. However, oxidative polymerization using various oxidizing agents in solution polymerization is the most common, facile, less time consuming and economic technique for the synthesis of polyaniline. Different oxidizing agents have been employed by various researchers, such as ammonium peroxydisulfate (MacDiarmid et al., 1987a; Willstätter et al., 1909), hydrogen peroxide, ferric chloride (Yasuda et al., 1993), ceric nitrate and sulfate (Hand et al., 1974, 1978), for achieving the efficient polymerization of aniline.

Chemical oxidative polymerization of aniline is a simple chemical approach where the synthesis is based on simultaneous mixing of aqueous aniline solution prepared in acidic media and ammonium peroxydisulfate solution at ambient temperature, followed by filtration of polyaniline precipitates and drying. The effective polymerization of aniline monomer is attained only in acidic medium where it exists as anilinium cation (Stejskal et al., 2002). A wide variety of organic and inorganic acids with varying concentrations have been employed in the synthesis of polyaniline which provide polymer with different solubility, conductivity and stability (Nalwa, 1997). For better conductivity using simple techniques, hydrochloric acid in equimolar proportion to aniline and using ammonium peroxydisulfate as initiator with molar ratio 1:1.25 with respect to aniline, have been reported in technical report published by International Union of Pure and Applied

Chemistry (IUPAC) (Stejskal et al., 2002). The polymerization takes place at room temperature completes within 10 minutes whereas requires approximately 1 hour at 0-2 °C (Stejskal et al., 2002; Sulimenko et al., 2001).

2.2.1.2 Electrochemical Polymerization of Aniline

Currently, electrochemical polymerization of aniline is exploited as an advanced technique due to many advantages. Electrochemical polymerization proved to be a better procedure of aniline polymerization as it provides a tranquil control over initiation and termination steps during the course of polymerization. Besides, electrochemical polymerization is considered to be technologically potent technique as the reactions are much cleaner as compared to chemical synthesis and the polymer synthesized is considered to be in a significantly pure form as it does not required addition of other chemicals such as surfactant, oxidant, and so on (Bhadra et al., 2009). Moreover, as compared to chemical polymerization, it is considered more environmental friendly owing to limited use of chemicals.

Electrochemical approaches are frequently employed for the polymerization of aniline under various conditions such as at constant potential, at constant current, at potential scanning, at potential sweeping and so on. Electrochemical polymerization of aniline is carried out using two-electrode system where the electrodes are dipped in the electrolytic solution of monomer. A specific current (in case of constant current) is passed through the solution which results in the formation of polyaniline film on the surface of electrode. At constant potential, aniline is polymerized in form of powder which is feebly deposited on the electrode (Diaz et al., 1980). An even polyaniline film is produced via electro-

oxidation of aniline monomer, through constant cycling amid the predetermined potentials, which adheres firmly on the surface of electrode (Genies et al., 1985a; Genies et al., 1985b). The synthesized thin polyaniline films can either be oxidized or reduced for better control of conductivity (Bhadra et al., 2008a). By using this technique, thick polyaniline films may also be produced which can later be peeled off from the surface of electrode. Using templates in electrochemical polymerization, fine nanowires can also be obtained in good yield (Diaz et al., 1980). Usually, electro-oxidation of aniline is commonly carried out using inert electrode. However, many researchers have reported metals such as Cu (Mengoli et al., 1981), Au (Paul et al., 1985), Fe (Camalet et al., 1998; DeBerry, 1985), graphite (Bhadra et al., 2007b), stainless steel (Hussain et al., 2003; Iroh et al., 2003) and vitreous carbon (Hand et al., 1974, 1978), besides normal platinum and ITO electrodes.

2.2.2 Mechanism of Polymerization

The most comprehensive mechanism for the polymerization of aniline was proposed by Wei et al. (Wei et al., 1990a; Wei et al., 1994; Wei et al., 1990b; Wei et al., 1989) based upon the kinetics investigations of the oxidative polymerization of aniline. As per their investigations, dimerization of aniline monomer by oxidation is the slowest step in the polymerization of process. This is due to the fact that oxidation potential of aniline monomer is comparatively higher than those of the dimer molecules. Once dimers are formed upon oxidation, they instantly oxidized and react with aniline molecules through electrophilic aromatic substitution reaction leading to the formation of trimers and tetramers. This process is continuously repeated until the presence of monomer which results in the formation of polyaniline.

The general mechanism of polymerization of polyaniline assumed to follow same steps no matter whether it is polymerized using chemical or electrochemical techniques. In both scenario, the polymerization course follows the following fundamental steps:

- a. Initiation: The initiation begins with the formation of radical anilinium cation by an electron transfer to aniline nitrogen atom as shown in Figure 2.7 The anilinium radical cation stabilises itself through various resonating structures where the radical is localized over entire benzene ring. Due to the absence of steric hindrance and substituent inductive effect, structure (c) is the most reactive resonance form of radical anilinium cation.

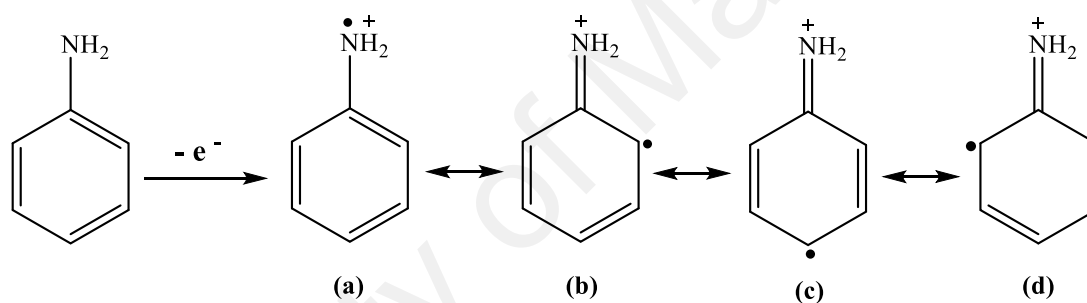


Figure 2.7: Mechanism for the formation of anilinium radical cation and its resonant structures

- b. Propagation: Head-to-tail reaction between the anilinium radical cation and its resonance form in acidic environment results in dimerization reaction. The dimers immediately oxidized to form dimerized radical cation as shown in Figure 2.8

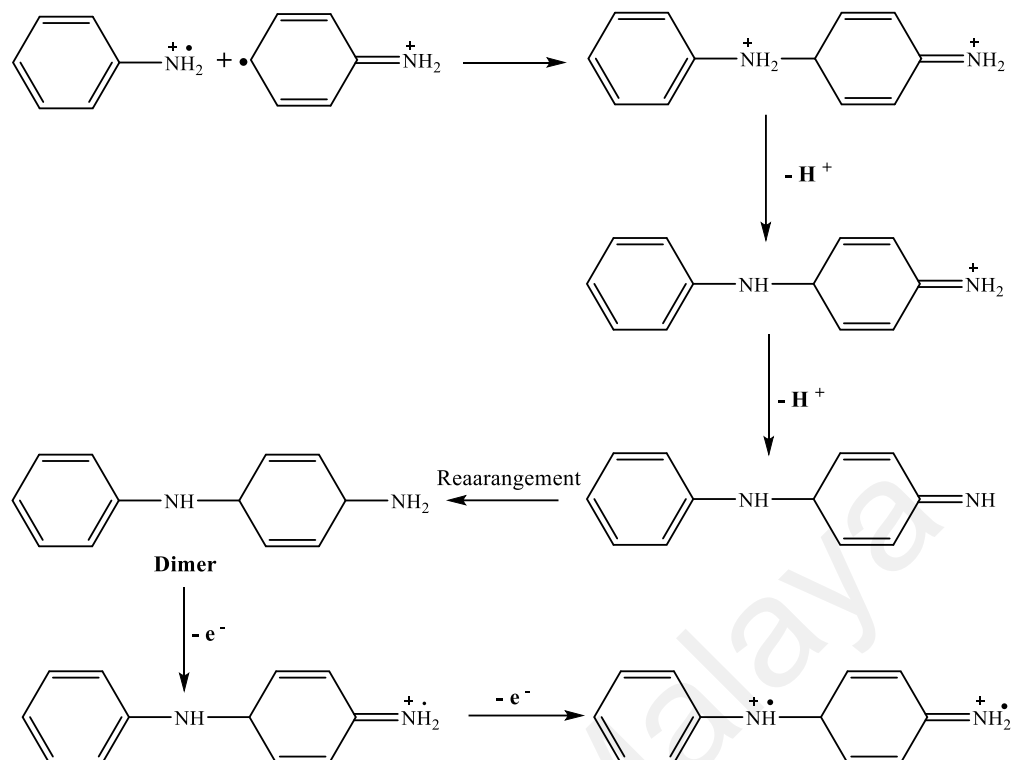


Figure 2.8: Mechanism for the formation anilinium cation dimer and corresponding radical cation

- c. Formation of polyaniline: In the next step, the dimers form of radical cations may react with anilinium cation radical or dimer cation radical to form a trimer or a tetramer, respectively, through electrophilic aromatic substitution reaction as shown in Figure 2.9 The repetitions of the above steps, finally leads to the formation of polyaniline chains.

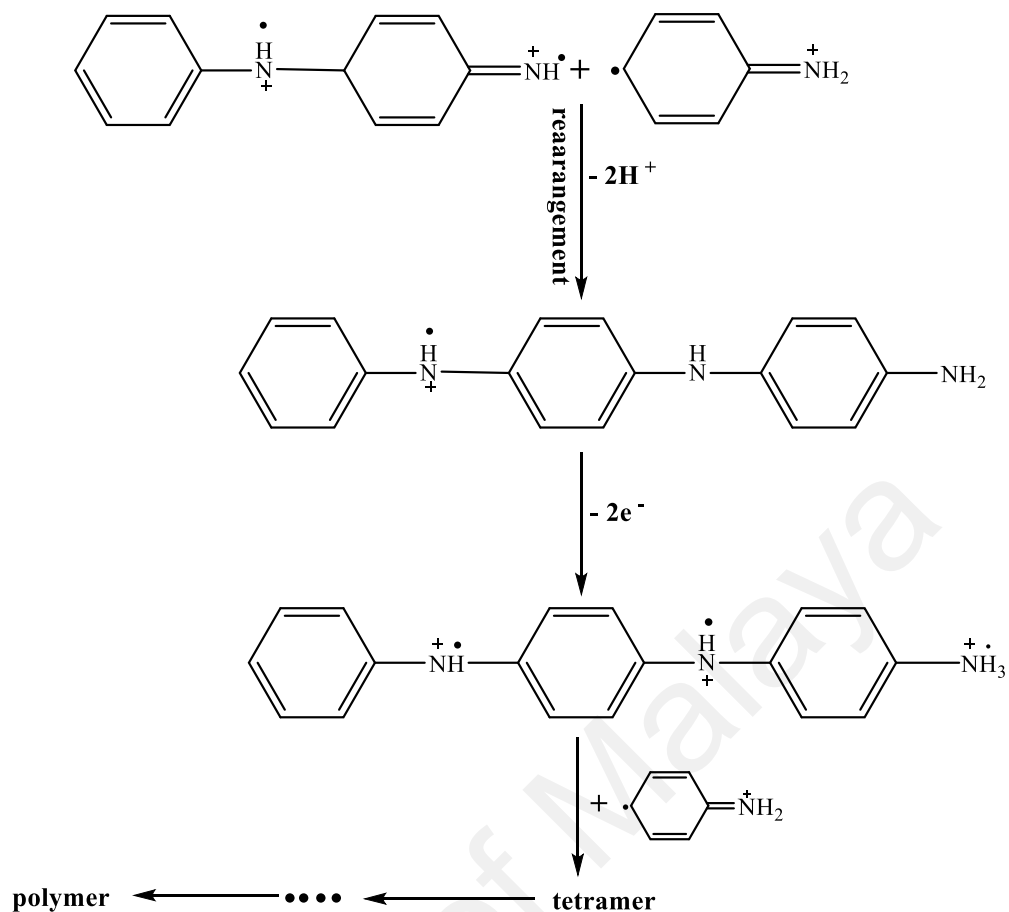


Figure 2.9: Plausible mechanism for polyaniline formation

Besides the above mentioned steps, some unavoidable side reactions also take place during the polymerization of aniline (Figure 2.10) comprising of:

- Coupling of aniline with its oligomers in “ortho” position;
- Substitution of chlorine in aromatic ring (in systems with HCl and LiCl or NaCl);
- formation of benzidine groups through “tail to tail” coupling;
- formation of N=N bonds;
- formation of N-C_{Ar} grafting bridges between chains;
- polymer hydrolysis (=O and -OH groups).

All these reactions are considered as chain defects which results in the formation of unwanted side products.

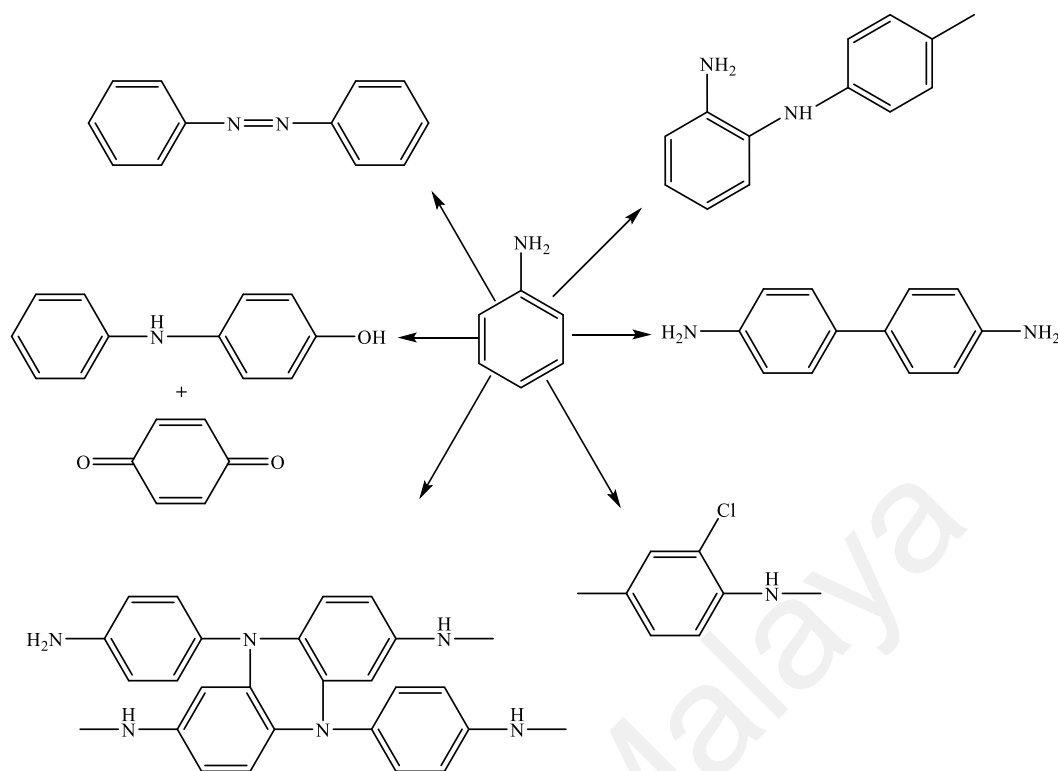


Figure 2.10: Side reaction during polyaniline polymerization

2.2.3 Concept of Polyaniline Doping

The conception of doping is the distinctive, significant, subject which differentiates conducting polymer from all other conventional polymers. The concept of doping in conductive polymers is phenomenological. It does not simply indicate the participation of any particular mechanism or method. In the conducting polymer arena, a chemical dopant is an agent, a moderately slight amount of which significantly alters the electronic, optical, magnetic, and/or structural properties of the conductive polymer and is supplemented by an enormous rise in conductivity. The two well-established forms of doping in the field of conducting polymers are (MacDiarmid et al., 1995):

(a) Redox doping” where an oxidizing agent removes or a reducing agent add electrons from the polymer backbone e.g. p- or n-doping of $(\text{CH})_x$ and

(b) acid/base doping also called as protonic doping, where the total electrons linked with the polymer chain stay unaltered. This type of doping is usually referred to as primary doping where the intrinsic properties of the polymer remain unaltered by doping.

Polyaniline, at molecular level, can exist in three distinct oxidation states namely, leucoemeraldine oxidation state, the emeraldine oxidation state, and the pernigraniline oxidation state. Amongst all the three oxidation states of polyaniline, only the emeraldine oxidation state can undergo non-redox or acid doping phenomena and get transformed into a highly conductive form. The imine nitrogen atoms in polyaniline can be protonated either fully or partially to yield the corresponding emeraldine salt. The extent of protonation in polyaniline is governed by the pH of aqueous dopant acid. The doping of emeraldine base form of polyaniline using dopant acid becomes the first example of the “doping” of an organic polymer into the highly conducting metallic form through the charge transfer route where the total electrons associated with the polymer remained unaltered through the course of doping (Angelopoulos et al., 1988). The process of doping emeraldine base by treating it with aqueous protonic acids is as depicted below in Figure 2.11

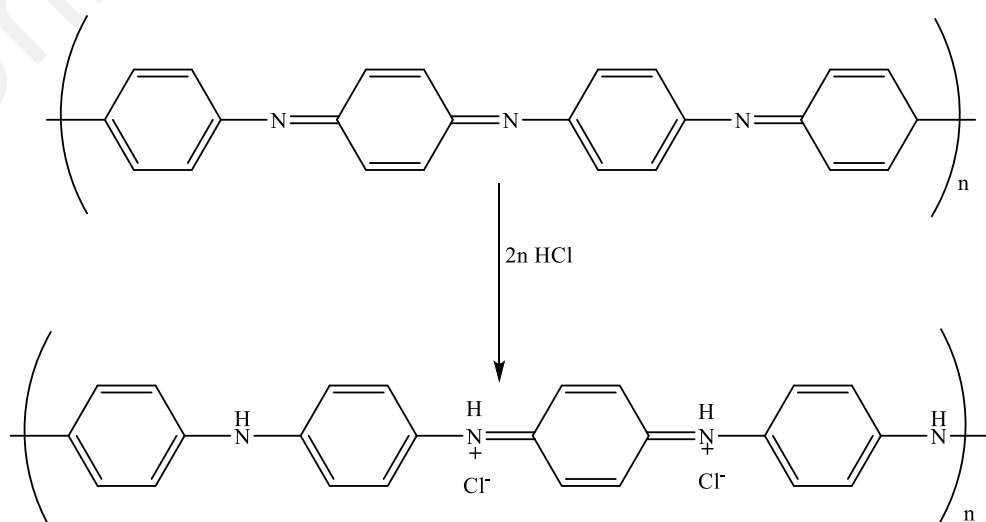


Figure 2.11: Acid doping in polyaniline

As compared with the conductivity of undoped polyaniline, the conductivity increase to 10 orders of magnitude in doped polyaniline ($\approx 1-5$ S/cm; 4 probe; compressed powder pellet). If the emeraldine base form of polyaniline is doped completely i.e., 100 percent protonation of imine nitrogen atoms, the polymer must exist in bipolaron state and essentially be diamagnetic in nature. However, widespread investigations on the magnetic behaviour of conductive emeraldine form of polyaniline revealed that it exists as a strongly paramagnetic material with a linear increase in Pauli's magnetic susceptibility with increased degree of protonation (Epstein et al., 1987). These studies illustrated that doped polyaniline exist as stable polysemiquinone radical cation containing two separated polarons units in its resonance structure (Angelopoulos et al., 1987), as shown in Figure 2.12 below:

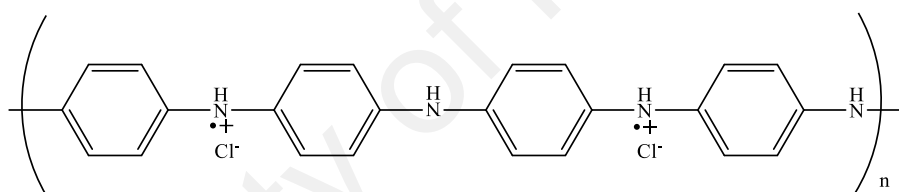


Figure 2.12: The polysemiquinone radical cationic form of polyaniline

Moreover, it is obvious from the structure that alternate resonance form also exists where the charge and spin can be transferred to neighbouring nitrogen atoms, thereby suggesting that the band structure of the doped polyaniline is expected to have a half-filled lower polaron band.

2.2.4 Properties of Polyaniline

2.2.4.1 Conductivity

The electrical conductivity (σ) of any material is directly proportional to:

- a. the charge carried by each carrier atom or molecule (e)
- b. the density of charge carriers (n)
- c. and the mobility of each carrier (μ)

$$(\sigma) = e n \mu \text{ (Bhadra et al., 2009)} \quad (3.1)$$

Where e is the unit electrostatic charge.

The concentration of the carrier units, their mobility and type of carrier for a semiconducting material can be estimated using the Hall Effect measurements. According to Hall Effect calculations, for n-type semiconductors (negative charge carriers) the Hall voltage is positive whereas for the p-type semiconductors (positive charge carriers) the Hall voltage is negative. The investigations on polyaniline revealed that majority of charge carriers in polymer chains are holes, thereby specifying that polyaniline is a p-type semiconductor (Beier et al., 1992; Fukushima et al., 1998; Ramadin et al., 1998). This semi-conductivity in polyaniline is due to the presence of delocalized π -conjugate system. The π -bonding molecular orbitals constitutes the valence band whereas the π^* -antibonding molecular orbitals produces the conduction band. The energy difference between the valence and conduction band forms the energy band gap. This energy gap is responsible for the electronic and optical properties of polyaniline. The band gap for polyaniline can be calculated by using UV-Vis spectroscopy (Bhadra et al., 2008a; Bhadra et al., 2009).

The significant features which effect the conductivity of polyaniline are: molecular weight of polyaniline, percentage of crystallinity and inter chain separation, degree of oxidation, type of dopant and percentage of doping (Bhadra et al., 2008a; Bhadra et al., 2007a; Bhadra et al., 2007b; Bhadra et al., 2006).

2.2.4.2 Solubility and Processibility

One of the major limitation of polyaniline is its solubility. Majority of the polymerization methods for synthesis of polyaniline yields powders and films which are insoluble in water and most of the common solvents. Water and/or polar solvent soluble polyaniline is most often related to the type of dopant utilized during synthesis process.

Currently, much scientific interest is attracted toward the synthesis of soluble derivatives of polyaniline to increase its processibility. One of the technique to increase the solubility and processibility of polyaniline, is the introduction of alkyl substituents in the polymer chains of doped and undoped polyaniline which has enhanced the solubility to greater extent (Bhadra et al., 2008b; Chevalier et al., 1992; Nguyen et al., 1994). However, the existence of these alky substituents on the polyaniline chains results in the decrease in electrical conductivity (Bhadra et al., 2008b). Doping of polyaniline with functionalized proton acids is alternative way to increase the processibility and solubility. Cao et al. synthesized water soluble polyaniline which was doped with dodecylbenzenesulfonic acid (DBSA), which acts as doping agents as well as substituent for polyaniline (Cao et al., 1992). On the other hand, another alternate method to obtain processable and soluble polyaniline, is to prepare it in colloidal system. Numerous efforts have been carried out to prepare polyaniline via colloidal polymer surfactants (Armes et al., 1990). Additional dopants namely, 4,4-bis(4-hydroxy phenyl)-valeric acid, 1,2-benzene dicarboxylic acid, 4-sulfo-, 1,2-bis(2--ethylhexyl) ester (DEHEPSA) with dichloroacetate acid (DCAA) or difluorochloroacetic acid (DFCAA) as solvent dibutyl naphthalene sulfonic acid (DBNSA) have been effectively explored in the synthesis of a soluble polyaniline (Bhadra et al., 2009; Stan et al., 2015). Hence,

processibility and solubility of polyaniline can be enhanced by careful selection of dopant acid and substituent alkyl group.

2.3 Metal Oxides Nanoparticles

In modern era of chemistry, physics, material science, biotechnology and so on, metal oxides play a significant role and has been the centre of attraction by scientific world (Henrich et al., 1994; Noguera, 1996; Rodriguez et al., 2007). Elemental metal has the tendency to form diverse varieties of oxide compounds. These compounds may exhibit a diverse range of structural geometries along with unique electronic properties. They might demonstrate metallic, semiconducting or insulating properties. Metals oxides have been applied in wide varieties of application including, catalysis, sensors, coating materials, fuel cells, piezoelectric devices, microelectronic circuits, photocatalysis and so on (Fernández - García et al., 2011). In the emergent arena of nanotechnology, an objective is to synthesis nanoarrays and nanostructures having distinctive properties as compared to the bulk or single particle species. Metal oxide nanoparticles reveals exclusive physical and chemical properties owing to their restricted size and a higher density of corner or edge surface sites. The particle size in any material is usually effects structural, characteristics such as symmetry of lattice and cell parameters. The decrease in particle size is associated with the decrease in the surface free energy of the material which changes its thermodynamic stability drastically as compared to the bulk material. As a result, nanomaterials exhibit enhanced mechanical and structural stability as compared to the bulk material (Chen, 2002).

Recently, scientific investigations comprising nanoparticles and nanoscale materials has created an excessive amount of curiosity from researchers and engineers of almost all disciplines. This attention has been caused due to the investigations that a large number of physical properties comprising surface reactivities, optical and magnetic properties, melting points specific heats and so on, are size-dependent. These properties, which are considered to be size-dependent, are extensively said to be the outcome of the higher ratio of surface area as compared to bulk atoms along with the associating state they epitomize between atomic and bulk materials. Materials in nanoscale range, mainly metal oxides, might be considered as they neither belong to atomic size species which are characterized by distinct molecular orbitals, nor as bulk materials which possess electronic band structures, but relatively by size-reliant widened energy states. Since metal oxides own prominent significance industrially, therefore, it is necessary to have an extensive understanding of their properties as small clusters to bulk materials. Even though, these nanoscale metal oxides are of great importance to researchers of various disciplines, approaches for their synthesis and applications are largely the focus of chemists (Interrante et al., 1997).

2.3.1 Synthesis of Metal Oxide Nanoparticle

The principal necessity of any innovative research in the field of nano metal oxides is the preparation of the material. The designing of an efficient method for the synthesis of metal oxide nanoparticles, is a present-day challenge. The synthetic methodologies for metal oxide nanoparticles can be subdivided into following categories:

2.3.1.1 Chemical Method

Chemical method for the synthesis of metal oxide nanoparticles is referred to as bottom-up approach where the nanoparticle synthesis is achieved by the chemical reduction of metal salts, electrochemical procedures or from the metastable organometallic compounds by their precisely controlled decomposition. Numerous kinds of stabilizers such as surfactants, donor ligands, polymeric compounds etc. are employed for controlling the growth of initially synthesized nanoparticles and restraining them from agglomeration. The important types of chemical method for the synthesis of metal oxide nanoparticles are discussed as follows:

(a) Co-precipitation Method

Co-precipitation method is one of the oldest technique for the synthesis of nanoscale material. This technique comprises of dissolution of a precursor which are usually metal salts such as metal chlorides, nitrides etc. in solvent (can be water) to precipitate the oxo-form of metal hydroxide by using a base. However, chemical homogeneity and control over size of particles is often difficult to achieve. Nevertheless, by using stabilizers such as surfactants, sonochemical techniques etc. appears to be unique and practical options to control the resultant morphologies (Chen, 2002; Fernández - García et al., 2011).

(b) Sol-gel Method

This is a facile and unique method for the synthesis of metal oxide nanoparticle through the formation of gels. In this process metal oxides are synthesized through hydrolysis of precursor materials which are normally the alcoholic solutions of metal alkoxide. The hydrolysis results in the formation of corresponding oxo-hydroxides. These

molecules then undergo condensation by removing water molecule which leads in the formation of metal hydroxide network. The hydroxyl moieties polymerize via condensation and transform into the dense and porous gel like material. Upon drying under appropriate conditions followed by calcination results the ultrafine, porous nano metal oxides (Interrante et al., 1997).

(c) *Microemulsion Method*

This process is based on the formation of micelles or reverse micelles structures which acts as nano-cavities for the synthesising nano scale materials. Microemulsion technique through the formation of direct micelles or reverse micelles creates micro or nano-reaction vessels in the presence of ternary mixture of surfactant, water and oil in the reaction medium. Metal oxides precursors solution in water will undergoes precipitation as oxo-hydroxides which is monodispersed in nature due to the presence of surfactant molecules. Controlled sizes metal oxides nanoparticles can be synthesized using this technique (Uskoković et al., 2005).

(d) *Hydrothermal or Solvothermal Method*

This technique utilizes high pressure and high temperature by using steel autoclave. Here, metal salts or precursors are decomposed at elevated temperatures by boiling their solutions in an inert atmosphere or using high steam pressures using steel autoclaves. To control the particle size and to prevent agglomeration, an appropriate surfactant agent is commonly added to the reaction medium. Hydrothermal technique provides very fine control over the structural morphology of the nanoparticles where differed shapes namely

cubic, spherical, tubes, fibres etc. can be achieved by careful control over physical parameters such as temperature, pressure etc.

(e) Template Method

Amongst numerous synthetic route for the synthesis of controlled sized metal oxide nanoparticles, the templates technique is one of the encouraging approaches to prepare nanoscale metal oxides. In templates based nanoparticles synthesis, porous materials comprising of uniform void spaces are utilized as a host to trap nanoparticles as a guest. Template methods are commonly used in some of the prior stated approaches and specifically applies two types of templates, soft-templates (surfactants) and hard-templates (porous solid materials such as silica or carbon).

2.3.1.2 Physical Method

Physical method is also generally known as top-down approach for the synthesis of nanoscale material. In this approach the bulk material is transformed into nanomaterial by using physical forces such as milling, grinding, vapour phase deposition etc. Some of the important physical approaches for the synthesis of nano-materials is as discussed below:

(a) Mechanical Attrition

One of the important physical method for the synthesis of nanoparticles is mechanical attrition or mechanical milling of bulk material to convert it into low dimensional materials. This technique yields nanoparticles by using milling equipments which are

categorised as “low energy milling” and “high energy milling” based upon the material to be transformed into nano-materials. The main goal of milling technique is the reduction of particle size and merging of particles in new phases. In contrast to the several procedures cited above, mechanical attrition leads to the formation of nanostructures through the structural decomposition of cruder grained structures instead of cluster assembly as a result of mechanical deformation. The ball milling and rod milling systems has attained ample consideration as a potent tool for the production of numerous advanced materials. Mechanical attrition is a distinctive technique which can be carried out at room temperature. The procedure of mechanical attrition has been performed on both, high energy mills, vibratory type mill, centrifugal type mill, and low energy tumbling mill.

Some of the important milling techniques includes attrition ball mill, planetary ball mill, vibrating ball mill, low energy tumbling mill and high energy ball mill.

(b) *Mechanochemical Synthesis*

One of the recent approach for the synthesis of nano-materials is mechanochemistry which is the combination of mechanical and chemical phenomenon. The combination of mechanical and chemical process on molecular level which includes mechanical action along with the chemical phenomena on the mechanically stressed materials have paved way to a unique methodology for facile synthesis of nanoparticles (Rajput, 2015). This technique varies with the standard mechanical attrition approach which utilizes inert atmosphere leading to the temperate breakage of powder particle and ultimately forming the nanosized grains within micron-sized particles. In mechanochemical process, during the ball milling process, a standard solid state displacement reaction takes place which

eventually results in nanoscale particle ranging up to 5 nm in size trapped within the bigger by-product phase particles (Lue, 2007). The mechanochemical synthesis procedure has been explored previously for the synthesis of wide variety of nanoparticles such as Ag, Co, Cr, Cu etc., along with other nanomaterials for instance metal oxides and sulphides (Rajput, 2015). In this technique, particle size of the material can be controlled by tuning factors such as volume fraction of the by-product phase made through milling, time duration of milling, energy of milling collision, ball-to-powder mass ratio, ball size, temperature, and the usage of method control agents.

(c) Chemical Vapour Deposition (CVD) and Chemical Vapour Condensation (CVC)

Chemical vapour deposition (CVD) is a renowned technique where a solid material is deposited on a pre-heated surface of a substrate through a chemical reaction from the vapour or gas phase. This process need an appropriate amount of activation energy to initiate nanoparticle synthesis which can be supplied through numerous ways. In thermal CVD, activation energy to initiate the reaction is provided by elevated temperature (up to 900 °C). In case of plasma CVD, the reaction is triggered by plasma at temperatures range of 300 and 700 °C. In laser equipped CVD technique, pyrolysis of bulk solid takes place upon the adsorption of heat from laser thermal energy which eventually leads to nanoscale material synthesis. In photo-laser equipped CVD, the ultra violet radiation induces the chemical reaction which has adequate amount of photon energy to breakdown the chemical bond in the reactant molecules. Alternative method termed as chemical vapour condensation (CVC) was established in Germany in 1994. It comprises pyrolysis, under the reduced pressure atmosphere, of the vapours of metal-organic precursors. Nanoparticles of metal oxides such as ZrO_2 , Y_2O_3 and nano-whiskers have been synthesized by exploiting CVC method (Chang et al., 1994; Rajput, 2015).

(d) Laser Ablation

Among the physical methods of nanoparticle synthesis, pulsed laser ablation (PLA) is an efficient synthetic technique due to its capability to yield nanoparticles with a narrow size distribution. As per the principles of gas dynamics, the PLA method can be divided into two main processes: (i) evaporation of the aimed solid material and (ii) hydrodynamic expansion of the ablated product in the ambient gas.

The formation of the nanoparticles in PLA technique proceed through the following stages: (i) the atomic vapours of the solid produced due to laser ablation began to supersaturate and homogeneous nucleation of the atoms takes place and (ii) growth of the nanoparticles where the nuclei start to grow by capturing atoms on their surfaces and transforming into nano-scale particles (Han et al., 2002).

2.3.2 Properties of Metal Oxides

2.3.2.1 Surface Properties

The physical and chemical properties on any material mainly depends upon its surface properties regardless of its bulk or nanoscale nature. Surfaces execute various purposes such as they maintain things in or out; they permit the movement of energy or a material through an interface; they can either initiate or terminate a chemical reaction, like in the case of catalysts. When a bulk solid or material is further segmented into the nano-regime materials, the total collective surface area is significantly enhanced although the total volume remains the same. As a consequence, the surface-to-volume ratio of the material is increased manifolds as compared with the bulk parent material. For instance consider

a cube of size 1 meter and see the effect of decreasing its size by cutting in smaller and smaller cubes as shown in Table 2.3 (Fiiipponi et al., 2012).

Table 2.3: Effect of size on surface area of cube

Dimension of cubic side	No. of cubes	Total effective surface area
1 m	1	6 m ²
0.1 m	1 000	60 m ²
0.01 m = 1 cm	10 ⁶ (1 million)	600 m ²
0.001 m = 1 mm	10 ⁹ (1 billion)	6 000 m ²
10 ⁻⁹ m = 1 nm	10 ²⁷	6 x 10 ⁹ = 6 000 km ²

In any material, the properties are usually determined by the chemical groups present on the surface of that substance. Important material properties such as reactivity, adhesion, catalytic behaviour, electrical resistivity and gas adsorption or storage exclusively rest on the nature of the interface of material. Nano-scale metal oxides possess substantial amount of atoms present at their surfaces, which have a significant and major effects on surface related properties such as physical adsorption of various compounds, catalysis reaction including photocatalysis, sensor and detection reactions and so on. The presence of large number of atoms at the surface of the nanoparticles of metal oxides effects physical properties such as melting point, boiling point, morphology and chemical nature. For instance, the melting point of nano-metal oxides will be lower as compared to the bulk metal oxides since the surface atoms are easier to remove as compared to bulk atoms, thereby decreasing the amount of energy required to overcome the intermolecular forces of attraction holding the atoms, thus decreasing the melting point.

Thus surface properties of metal oxides are changed drastically upon converting them into nano-sized materials which can be exploited in various areas of scientific research.

2.3.2.2 Electrical Properties

Electrical property of metal oxides is one of the important parameters which can be explored in numerous applications including photocatalysis studies, sensors applications and so on. Metal oxides can exhibit ionic or mixed ionic conductivity and has been proved experimentally that this property is significantly size dependent which can be tailored by controlling nanostructures of metal oxides (Fiiipponi et al., 2012). As per the Boltzmann statistics, the number of electronic charge carriers in metal oxide depends upon the fundamental band energy gap. The electronic conduction in metal oxides, based upon charge carrier, is stated to as n- or p-type, respectively, for electrons or holes. The number of charge carriers, that is, free electrons or holes, can be significantly enhanced by introducing non-stoichiometry which can easily be balanced by less mobile oxygen/cation vacancies present in metal oxides. Similar to the hopping-type conduction due to the electrons and holes, ionic conduction can also take place in the metal oxides where the respective ions can move from site to site by hopping within the crystal lattice due to thermal activation in accordance with the modified Fick's second law (Fiiipponi et al., 2012).

The behaviour of the charge carriers in polycrystalline oxides is greatly influenced by the size since conductivity runs parallel to the surface properties of materials. The strain at the particle boundaries and total surface energy, which contributes in electrostatic potential of metal oxides, are significantly altered at nano-scale as compared with bulk

material. The distribution of the charge carriers or defects within the crystal lattice of metal oxide also undergoes momentous modifications from bulk materials to nano-materials, since nanoparticles contains charge carries over the entire material as a result of the shielded electrostatic potential reduction at surface layers of nanosized materials (Rodriguez et al., 2007). As an outcome of these nanoscale derived effects, it is a renowned fact that metal oxides in nano-scale displays enhanced conductivity which could be many order of magnitude larger than the analogous bulk or micro-crystalline metal oxides, and is attributed to a noteworthy augmentation of the electronic contribution.

2.3.2.3 Optical Properties

The optical properties of a material are due to the interaction between the light and the matter. One of the important fundamental property of metal oxides is the optical conductivity which can be calculated experimentally via reflectivity and absorption analysis. It is a well-known fact that reflectivity is, undoubtedly, a size-dependent property as scattering phenomenon can be considerably change when the size of metal oxides particles fall within or out of the wavelength range of photon (Scott et al., 2001). Owing to quantum-size internment, light absorption usually becomes both discrete-like and size-dependent. For nano-metal oxides, the transitions between discrete or quantized electron and hole results in the development of both linear (one exciton per particle) and non-linear optical (multiple excitons) properties. Thus, nano-sized metal oxides proved to be promising materials for novel optical properties which can be applied in diverse scientific areas of research.

2.3.2.4 Other Properties

Besides the above discussed properties, metal oxides exhibit distinctive chemical, mechanical, catalytic and adsorption properties. Metal oxide nanoparticles have been extensively employed for industrial applications in the field of catalysis as active compositions or as supports materials. Metal oxides possess photocatalytic abilities which can be exploited to solve present day energy crises. In 1972, Fujishima and Honda first reported the photocatalytic splitting of water using TiO_2 , which was the initial photocatalyst appropriate for water splitting and the commencement of a new field of modern heterogeneous photocatalysis. Currently, metal oxide nanoparticles owing to large surface to volume ratio and enhanced surface binding properties have been employed as adsorbent to remove environmental pollutants. Metal oxide nanoparticles exhibit stability towards radioactive radiations, thermal and mechanical changes and are exploited for the irreversible, selective and efficient removal of large amounts of pollutants from contaminated water.

Thus metal oxide in nanoscale have demonstrated unique and distinctive properties and have been applied extensively in the field of chemical, nuclear-energy, pharmaceutical, food, bioengineering, dairy, water treatment, and electronic industries.

2.4 Chitosan

2.4.1 Chitin and Chitosan

Chitin, a naturally mucopolysaccharide, is found abundantly in nature as the structural component within the exoskeleton of crustaceans, insects as well as in cell walls of some fungi. Chitin is mainly composed of 2-acetamido-2-deoxy- β -d-glucose through a β (1 \rightarrow 4)

linkage, characteristic of natural occurring chitin. Chitin is biodegradable and can be easily degraded by naturally occurring enzyme, chitinase. Despite of the presence of nitrogen atom in its structure, chitin is biocompatible with exceptionally low immunogenicity. Like cellulose, chitin is also highly insoluble material and exhibits chemical inertness. Chitin acts as structural polysaccharide, which is white, rigid, inelastic and nitrogenous macromolecule and was considered to be the key source of surface pollution in coastal regions (Rinaudo, 2006).

Chitosan is synthesized commercially through deacetylation of chitin and can be considered as N-deacetylated derivative of chitin. However, complete N-deacetylation of chitin is difficult to achieve and a precise nomenclature between chitin and chitosan, with respect to the degree of N-deacetylation, has not been defined yet (Muzzarelli, 1973; Zikakis, 2012). The extent of deacetylation of chitin can be determined by various spectroscopic techniques such as NMR, FT-IR etc. and the degree of deacetylation in commercial grade chitosan ranges from 60 to 100%. A simple technique is used for the synthesis of chitosan employing excess of sodium hydroxide as a reagent in water as a solvent. Figure 2.13 illustrates the structure of chitin and chitosan (Rinaudo, 2006). Chitin and chitosan are explored widely in scientific research due to the presence of high nitrogen percentage (6.89%), biodegradability, non-toxicity, biocompatibility, adsorption and cheaper cost (Muzzarelli, 1973; Rinaudo, 2006) despite having certain limitations of reactivity and processibility (Amass et al., 1998; Ilium, 1998).

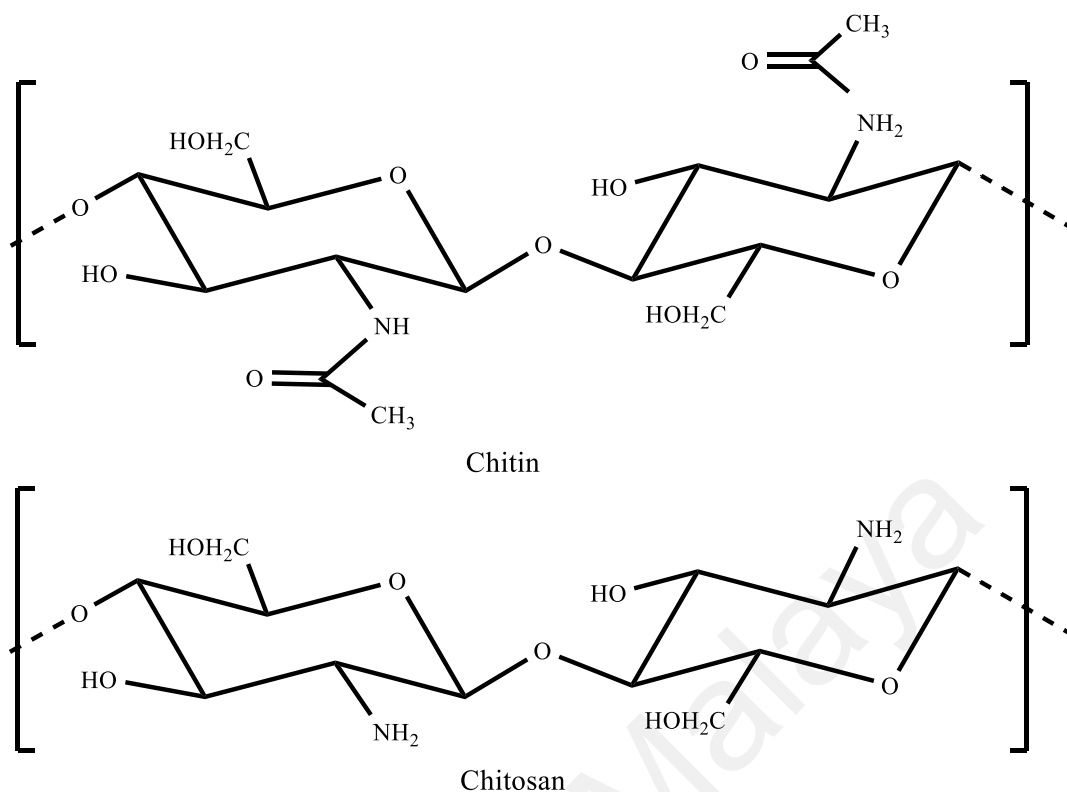


Figure 2.13: Chemical structure of chitosan and chitin

2.4.2 Applications of Chitosan Based Composites in Adsorption of Pollutants

In the area of removal of hazardous pollutants through adsorption, chitosan is considered to be the most potent and promising biomaterial which has been utilized in various applications. Due to the presence of hydroxyl and amino groups in the chain of chitosan, it can adsorb pollutants such as heavy metals, dyes, pesticides, herbicides etc. via physical interactions such as hydrogen bonding, Van de Waal's attraction etc. These functional groups present in chitosan can be further modified and utilized for various applications (Kyzas et al., 2015).

The removal of heavy metals from waste water using chitosan based composites was first described by the research work of Muzzarelli in 1969 (Muzzarelli et al., 1969). Since

then chitosan based adsorbents have been widely reported for decontamination of polluted water. The composite comprising of chitosan and modified ball clay (MBC) has been reported by Auta and Hameed for batch and fixed-bed absorption of methylene blue dye. The composites were synthesized by dissolving chitosan in acetic acid and subsequently adding MBC followed by dropping in NaOH to form composite beads. It was found to be an excellent adsorbent which efficiently remove methylene blue from aqueous solution (Auta et al., 2014). Fan et al. prepared magnetic nanocomposite comprising of chitosan/ β -cyclodextrin and demonstrated the successful removal of methylene blue dye from aqueous solution with higher adsorption efficiencies (Fan et al., 2012). Elwakeel et al. illustrates the synthesis of chitosan and glutaraldehyde based resin by chemical modification which was achieved by treatment with NH_4OH and epichlorohydrine. The prepared resin was then utilized for the removal of cationic dye, BBR250 from aqueous solution (Elwakeel et al., 2012). Chitosan grafted poly(methyl methacrylate) composite was reported by Jiang et al. where chitosan was functionalised by glycidyl methacrylate and then copolymerized with methyl methacrylate to obtain composite material. This composite material was successfully employed as efficient adsorbent for the removal of anionic dye, RB19 from waste water (Jiang et al., 2014). Chitosan-modified magnetic graphitized multi-walled carbon nanotubes (CS-m-GMCNTs) nanocomposites were synthesized by Zhu et al. The synthesized nanocomposites exhibited enhanced surface area and were efficiently utilized as adsorbent for the removal of congo red dye from aqueous media (Zhu et al., 2013).

Thus chitosan can be efficiently utilized in the synthesis of different kind of nanocomposites for the remediation of waste water as it possesses unique structure and functional groups for enhancing the adsorption of organic and inorganic pollutants.

2.5 Graphene and Graphene Oxide

2.5.1 Graphene

Graphene is a two-dimensional material which is one of the allotropes of carbon. It comprises of single-atom thick, two dimensional, planer monolayer of carbon atoms which are arranged in a honeycomb like lattice arrangement having C-C bond length of about 0.142 nm. All the carbons in graphene are sp^2 hybridized and are the building units of many graphitic materials including graphite, carbon nanotubes and fullerene as shown in Figure 2.14

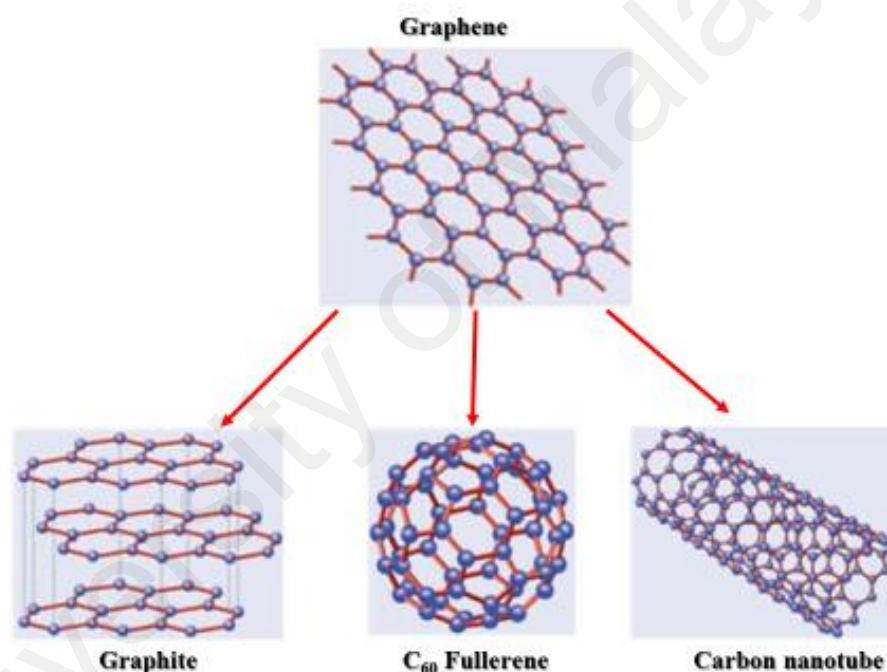


Figure 2.14: Structure of C-containing molecules

Graphite comprises of stacked layers of graphene sheets with the interplanar distance of 0.3 nm which are stabilized by weak van der Waals forces. Buckminsterfullerene is formed by graphene sheets folded to form sphere including some pentagonal and hexagonal rings into the lattice structure whereas carbon nanotubes are visualized as cylindrical rolls of graphene (Dinadayalane et al., 2012). Graphene possess electrons which act as relatively massless particles are responsible for unusual properties like the

absence of localization and anomalous quantum Hall effect (Dinadayalane et al., 2012). Graphene has revealed diverse fascinating properties such as extremely high electron mobility at ambient temperature, extraordinary thermal conductivity and higher mechanical properties with Young's modulus of 1 TPa. Owing to the utmost significance in scientific world, the Nobel Prize in Physics 2010 was bestowed to Andre Geim and Konstantin Novoselov "for ground breaking experiments regarding the two-dimensional material graphene". Graphene has been exploited in almost every field of science including physics, chemistry, biology, biotechnology and so on. Some of the potential applications of graphene includes:

- Single molecule gas detection
- Transparent conducting electrodes
- Biological sensor material
- Energy storage devices such as supercapacitors
- Energy conversion devices such as fuel cells
- Lithium ion batteries
- Semiconducting devices such as transistors

2.5.2 Graphene Oxide

One of the economical method for the synthesis of graphene-based single sheets, is chemical method which involves the chemical conversion of graphite to graphene oxide, with a considerable amount of yield. Graphite flakes are usually oxidized in the presence of concentrated acids such as sulphuric acid or nitric acid and potassium permanganate into graphite oxide as reported by Hummers (Hummers Jr et al., 1958). As compared with the pristine graphite, the carbon planes of graphite oxide bear excessive amount of oxygenated functional groups comprising of hydroxyl and epoxy groups. In addition to

the presence of these groups at sp^3 hybridized carbon on the basal plane, graphite oxide also possess carbonyl and carboxyl groups situated at the edges of the sheets on sp^2 hybridized carbon. Due to the presence of the functional groups graphite oxide becomes highly hydrophilic which can be easily exfoliated through sonication in water yielding a stable, single layered graphene oxide dispersion. Even though, graphite oxide and graphene oxide possess analogous chemical properties including surface functional groups, but these have different structural properties. Graphene oxide is actually a single layer planar material which is obtained by the exfoliation of graphite oxide. Adequately dilute colloidal suspension of graphene oxide synthesized via sonication are usually homogeneous and clear with indefinitely stability. Graphene is highly conductive material due to the presence of long-range sp^2 hybridized bonding network whereas graphene oxide is usually insulator or semiconductor due to the interruption of sp^2 bonding network by the oxygen-comprising groups. However, the conductivity of graphene oxide can be enhanced via reinstating the sp^2 bonding network in the graphitic lattices by reducing the oxygen containing functionalities. This process is called as reduction and the product formed is termed as reduced-graphene oxide or chemically modified graphene.

The conductivity of GO can be returned by removing oxygen-containing groups and restoring the sp^2 bonding network in the process named reduction. The complete exclusion of oxygen-containing functional groups has not been attained yet, leading to the formation of lower electrically conductive reduced-graphene oxide as compared to the pristine graphene. A wide variety of methods have been developed to reduce graphene oxide such as chemical reduction method by using reducing agents, electrochemical reduction method, thermal annealing reduction method and so on.

2.5.3 Synthesis of Graphene Oxide

One of the most convenient and reliable techniques for the synthesis of graphene oxide was developed by Hummer in 1958 as a safe, fast and efficient method from graphite flakes (Hummers Jr et al., 1958). Prior to Hummer's method, graphene oxide synthesis was a time-consuming and hazardous process. After observing the health hazard possessed by the workers, William S. Hummers and Richard E. Offeman designed an innovative alternate method. Their method involved the addition of graphite flakes into the concentrated acids solution along with sodium nitrate and potassium permanganate. They also limited the temperature to 98 °C in order to avoid the risk of explosion as it occurred in previous methods. According to their procedure, 100 g of graphite and 50 g of sodium nitrate were added to the solution of concentrated sulphuric acid at 66 °C followed by cooling to 0 °C. Later, 300 g of potassium permanganate was then added under continuous stirring followed by incremental addition of water. The final solution comprises about 0.5% of solids which was then purified to remove the impurities and dehydrated with phosphorus pentoxide.

Thus, the method for the preparation of graphene oxide can be summarized in two major steps:

- (i) First, oxidation of graphite powder to obtain graphite oxide which, due to the presence of oxygen-containing hydroxyl and epoxide groups across the basal planes of graphite oxide and carbonyl and carboxyl groups situated at the edges of lattice, can be easily dispersed in water.
- (ii) Second, the exfoliation of the bulk graphite oxide sheets through to obtain colloidal dispersions of mono, bi or few-layers commonly known as graphene oxide.

This is illustrated by the following Figure 2.15 (Li et al., 2014):

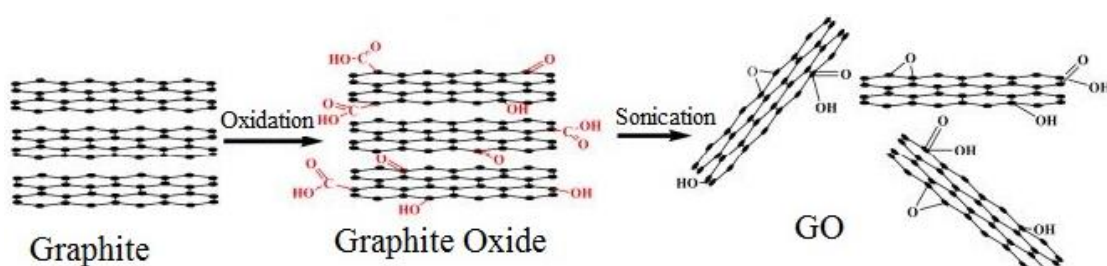


Figure 2.15: Preparation of graphene oxide (GO)

Many modifications in Hummer's method have been reported by various researchers and many new techniques such "Modified Hummers method", "improved Hummers method" and so on, have been proposed and are commonly used for the synthesis of graphene oxide (Li et al., 2014).

2.5.4 Properties of Graphene Oxide

2.5.4.1 Structure Properties

Keeping apart the effective oxidative mechanism, the defined graphene oxide structure has been the topic of significant argument over the years, and until today no explicit model exists. The complexity of the structure of graphene oxide may be owing to various reasons such as:

- Absence of accurate analytical techniques for the characterization of this kind of materials
- Complex nature of material due to its amorphous nature which vary from sample to sample
- Nonstoichiometric atomic composition or berthollide character

Even though, due to the above reasons it is difficult to comprehend the structure of graphene oxide, sensible efforts have been made by various scientists to understand the structure. According to the earliest structural models, graphene oxide was proposed to be made up of regular lattices having repeated distinct units as depicted in Figure 2.16 (Dreyer et al., 2010).

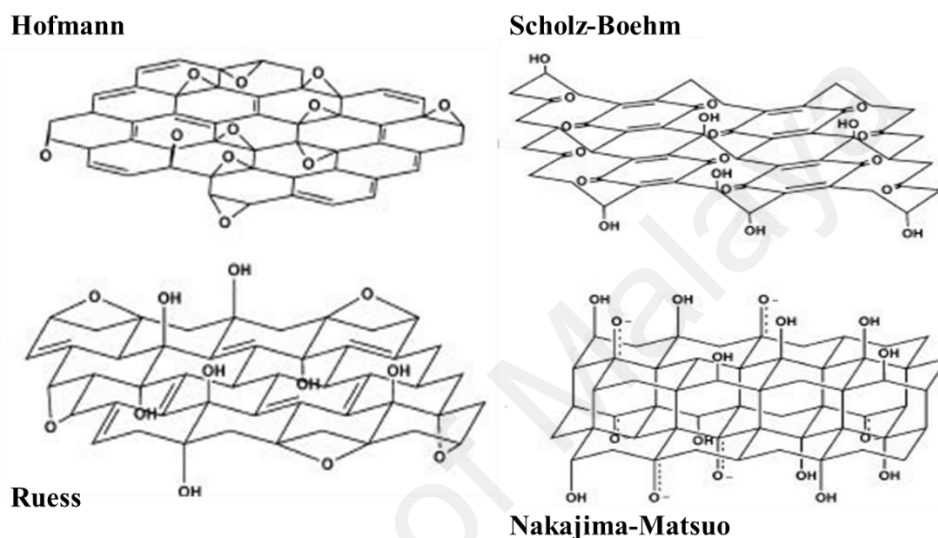


Figure 2.16: Some of the proposed graphene oxide structure

In the structure proposed by Hofmann and Holst's, the basal planes of graphite contain epoxy groups with overall molecular formula of C_2O . The structure proposed by Ruess in 1946 integrated hydroxyl groups into the basal plane, thereby introducing the hydrogen content in graphene oxide. Later, Scholz and Boehm, revised the stereochemistry of this model and changed it to ridged carbon layers comprising interchangeably linked ribbons of quinoidal structure and opened cyclohexane rings having chair conformation. According to them there was no proof for the occurrence of neither epoxy nor ether in the graphene oxide structure. Nakajima and coworkers have proposed one of the useful model proposing that the lattice framework of graphene oxide is similar to poly(dicarbon monoFluoride), $(C_2F)_n$, resulting in the formation of graphite intercalation compound (GIC) (Dreyer et al., 2010).

2.5.4.2 Dispersibility

Graphite oxide is easily exfoliated in water, due to its superior hydrophilicity, and presence of excessive oxygenated functional groups, forming stable dispersion in water by exfoliation of aggregated sheets. This homogeneous dispersion comprises monolayer sheets which are commonly referred to as graphene oxide sheets. The most common solvent for dispersing graphene oxide is water and few other polar solvents. There are basically two methods to disperse graphene oxide in water namely sonication and mechanical stirring. Sonication appears to be most common technique to preparing graphene oxide from bulk graphitic oxide but may also generates structural defects and reduces the size of graphene oxide sheets (Dreyer et al., 2010). Usually, the concentration of graphene oxide in water is maintained at about 1–4 mg/ml. These dispersions may also form in various other solvents such as ethylene glycol, N-methylpyrrolidine, N,N-dimethylformamide (DMF) and tetrahydrofuran. Therefore, graphene oxide is supposed to be amphiphilic in nature with more hydrophilic edges and core more hydrophobic and can behave like a surfactant.

2.6 Polyaniline Based Nanocomposites

Nanocomposites belongs to the category of composite materials where at least one of the phases possess nanoscale dimensions. Nanocomposite materials have appeared as appropriate substitutes to tackle the precincts of micro-composites and monolithics materials. Nanomaterials still faces challenges of controlling the stoichiometry and elemental composition during their preparation in nano-phase. These materials are rightfully described as ‘21st century materials’ in the opinion of owning design distinctiveness and unique properties combinations which are not found in conventional composite materials. Conducting polyaniline based nanocomposite materials have been

explored comprehensively and unique properties such as controlled morphology, electrical conductivity, processability etc. had been enhanced for various viable application.

2.6.1 Synthesis of Polyaniline Nanocomposites

Polyaniline based nanocomposites are prepared usually through the chemical route, whereas electrochemical synthesis has also been explored in certain cases.

2.6.1.1 Chemical In-Situ Polymerization

In-situ polymerization of aniline monomer in the presence of various additives or materials such as nanoparticles, carbon nanotubes, metal, polymers etc. is considered to be a useful methodology for synthesis of unique nanocomposites. In-situ polymerization offers more homogenised mixing of components which is not achieved by mechanical or physical blending due to incompatibility of different components. Various review articles for describing the mechanism and benefits of in-situ polymerization of polyaniline with other components have been reported which has highlighted this process in detail. This method comprises of following approaches:

- In one approach, aniline monomer and the doping or host components are mixed physically. This mixture of monomer and other components is then added to the oxidant solution and allowed to polymerize. The resultant material is then collected by filtration and dried to obtained composite material.
- In another approach for the synthesis of composite material, the additive component or nanomaterial is mixed or dispersed with the oxidant forming a

solution or dispersion. This dispersion or mixture is then to the acidic solution of aniline leading to the formation of conducting nanocomposites material.

In both approaches the general idea remains the same, that is, polymerization of aniline monomer in finally dispersed nanomaterial which results in the formation uniformly amalgamated composite material. The morphology, size, porosity etc. can be controlled by varying several parameters such as temperature, dopant acid, acidic strength, amount of additive components, and ratio of monomer to oxidant. Optimization of all these parameters is an essential requirement for the synthesis of nanocomposites with unique morphologies and properties.

2.6.1.2 Physical Blending/Mixing

One of the simplistic approach for the synthesis of polyaniline nanocomposite material is the physical mixing or blending of additive components such as nanoparticles carbon nanotubes, metal, polymers etc. with pre-synthesized polyaniline polymer. Blending technique sometimes appears to be more appropriate technique where the production is required on large scale such as industrial production. Blending technique can be:

- Solution blending: where the additive components and/or polymer can be dissolved in some solvents and mixed together to form a homogeneous composite blend.
- Dry blending: dry blends are often prepared by mechanically blending the polyaniline powder with additive components using a mixer.

2.6.2 Application of Polyaniline Based Nanocomposites

2.6.2.1 Adsorption of Toxic Pollutants

The adsorption process has been established as an effective procedure with enhanced efficiency and capability to remove toxic waste pollutants on a large scale besides having other benefits such as recovery, and recycling of adsorbents (Ali et al., 2006; Anand et al., 1998; Pud et al., 2003). Numerous types of adsorbents, such as activated carbon (Chen et al., 2010), natural and synthetic polymers (Hu et al., 2010), MWCNT (Ma et al., 2012) etc. have been employed as adsorbents for the removal of toxic waste pollutants from wastewater. Polyaniline based nanocomposites had been extensively employed as low cost adsorbent material for the removal of wide variety of pollutants ranging from heavy metals, dyes and other toxic industrial effluents. Polyaniline due to the presence of conjugated π -bonds and nitrogen containing imine group ($-N=$) and amine group ($-N<$) have a tendency to adsorb a wide variety of compounds due to various physical phenomenon such as electrostatic attraction, hydrogen bonding, π - π interactions. These properties of polyaniline have been enhanced by developing unique nanocomposites material by integrating various components such as metal oxides, MWCNT, chitosan, graphene etc., in the matrix of polyaniline and have been exploited as efficient adsorbent materials.

Ayad et al. reported the synthesis of polyaniline nanotubes as an adsorbent material for the efficient removal of cationic dyes from waste water. They demonstrated that nanotubes of polyaniline can be proficiently exploited as an efficient adsorbent for the removal of carcinogenic methylene blue dye from aqueous solution (Ayad et al., 2010). Mostafa et al. reported the synthesis of novel hybrid nanocomposites based on immobilizing copper and silver over polyaniline-grafted amino-modified chitosan. They

illustrated that the synthesized nanocomposite can be utilized for the treatment of meat waste water which possess a grave danger to aquatic life (Mostafa et al., 2014). Shao et al. illustrated the synthesis of polyaniline (PANI)/multi-walled carbon nanotubes (MWCNT) nanocomposites and reported their efficient utilization as adsorbent material for the removal of Pb(II) ions from waste water (Shao et al., 2012). Li et al. reported the synthesis of polyaniline/humic acid composite material. They investigated the synthesized material for the adsorption of heavy metals from waste water. They found out that polyaniline/humic composite material exhibits enhanced adsorption efficiency for Hg(II) and Cr(VI) ions and can be used as an adsorbent material for their effective removal (Li et al., 2011). Ahmad et al. reported the synthesis of polyaniline/iron oxide nanocomposites via facile in situ polymerization technique. They demonstrated that the synthesized nanocomposites can be efficiently utilized in effective removal of amido black 10B (AB10B) dye from aqueous solutions (Ahmad et al., 2010). Karthik et al. described the synthesis of cross linked-chitosan-grafted-polyaniline composite material and demonstrated its application as an adsorbent for the enhanced removal of Cr(VI) ions from waste waters (Karthik et al., 2014). Najim et al. reported the synthesis of polyaniline nanofiber based nanocomposites with natural silica, fibre glass, and poly(ethylene terephthalate) powder from waste bottles. They demonstrated that the nanocomposites exhibited potential for removal of Cr(VI) and phosphate by adsorption phenomenon and can be applied for waste water treatment (Najim et al., 2014). Gupta et al. reported the facile synthesis of polyaniline/polystyrene composites and illustrated that these composites can be utilized as adsorbents materials to the detoxification of waste water by removing heavy metal pollutants such as Hg(II) ions (Gupta et al., 2004). Besides these a wide variety of novel adsorbent material based on polyaniline nanocomposite have been synthesized and demonstrated for efficient removal of toxic pollutants from waste water by researchers from all corners of the world. Thus polyaniline based nanocomposites can

be efficiently employed as low cost adsorbent materials to tackle the present day issue of environmental pollution.

2.6.2.2 Photocatalysis

Among the varied variety of approaches to degrade hazardous waste materials, especially organic compounds, to less toxic or less harmful materials, photocatalysis has emerged as one of the most encouraging techniques because it exemplifies a tranquil method of exploiting the energy of either natural sunlight or artificial illumination, such as ultraviolet light, microwaves, etc (Riaz et al., 2014; Shahabuddin et al., 2015b; Zhou et al., 2015). During last few decades, heterogeneous photocatalysis had been investigated vastly especially for confronting energy crisis and environmental remediation. Some of the extensively explored arena in photocatalysis includes water splitting by harnessing solar energy, purification of air and treatment of waste water containing toxic pollutants (Riaz et al., 2015a). Polyaniline, due to its notable physical and chemical properties such as thermal stability, high conductivity, easy preparation procedure, better processability, low cost and wide variety of applications, is one of the vastly investigated conducting polymers amid all the conducting polymers. Additionally, polyaniline is an efficient electron donors and good hole transporter upon visible-light excitation. In combined state with a wide band gap semiconductors polyaniline can transfer the electrons generated upon visible-light irradiation to the conduction band of semiconductor such as TiO_2 since the lowest unoccupied molecular orbital (LUMO) level of PANI is energetically higher than the conduction band (CB) edge of TiO_2 (F Wang et al., 2010). As a consequence, substantial amount of interfacial charge transfer occurs and recombination of electron-hole pair is considerably reduced which could provide a significant photoresponse in solar light range of spectrum. This development will benefit the application of the

photocatalysis under sunlight. Therefore, polyaniline has been doped with large numbers of semiconducting material for preparation of novel photocatalysts for degrading harmful pollutants.

Kant et al. prepared polyaniline nanocomposites with $\text{Fe}_{0.01}\text{Ni}_{0.01}\text{Zn}_{0.98}\text{O}$ nanoparticles (FNZPs) through chemical in situ free radical polymerization. These nanocomposites exhibited sunlight induces photocatalytic activity for the degradation of methylene blue dye. The degradation efficiency achieved was 98.55% within 2 hours (Kant et al., 2013). Eskizeybek et al. reported the synthesis of polyaniline/ZnO nanocomposite through simplistic in situ chemical oxidative polymerization. They applied the synthesized nanocomposite for the photocatalytic degradation of methylene blue and malachite green dyes in aqueous medium both under natural sunlight as well as UV light irradiation. They demonstrated that upon addition of ZnO nanoparticles in polyaniline matrix, photocatalytic efficiency was greatly increased and 99% degradation efficiency was achieved (Eskizeybek et al., 2012). Pandiselvi et al. reported the synthesis of chitosan–polyaniline (CPA) and chitosan– polyaniline/ZnO nanocomposites with different weight ratio of ZnO for the degradation of reactive orange 16 dye. The maximum degradation efficiency achieved was 99% with nanocomposites having 2.5 wt% of Zn salt (Kannusamy et al., 2013). Olad et al. developed polyaniline nanocomposites doped with nanoparticles of zinc oxide (ZnO) through in situ oxidative polymerization technique. They obtained polyaniline core-shell nanocomposites which were efficiently employed as photocatalyst to degrade methylene blue dye under natural visible light as well as UV illumination. As per their investigations, methylene blue degradation was found to 28% under UV irradiation and 82% under visible light irradiation (Olad et al., 2012). Tadjarodi et al. prepared polyaniline/CdO nanocomposite using aqueous diethylene glycol solution

as reaction medium via in situ oxidative polymerization method. These nanocomposites demonstrated enhanced photocatalytic activity for the degradation of methylene blue and malachite green dyes under sunlight illumination. The degradation efficiency of these nanocomposites were found to be approximately 99% (Tadjarodi et al., 2013). Zhang et al. reported the synthesis of novel PdSeCdS modified by polyaniline nanocomposites by sonochemical procedure. The synthesized photocatalysts had depicted excellent photocatalytic phenomenon for evolution of hydrogen gas without any noble metal and demonstrated enhanced anti-photocorrosion as compared to bare polyaniline or PdSeCdS (Zhang et al., 2012). Su et al. reported the enhanced thermoelectric and photosensitive properties in polyaniline nanocomposites doped with TiO₂ nanotube. These nanocomposites demonstrated enhanced light garnering properties by the low-energy photon absorption in the red and infrared range without any substantial recombination of the charge carriers (Su et al., 2012). The photocatalytic degradation of pollutants by polyaniline based nanocomposites have been systematically reviewed which has shown the importance of polyaniline based nanocomposites in potential environmental application (Riaz et al., 2015a, 2015b).

2.6.2.3 Other Applications

Besides adsorption and photocatalysis, polyaniline based nanocomposites have been widely applied in the field of sensors, coatings, batteries, solar cells and so on. These nanocomposites are still widely explored and utilized in all areas of science including biotechnology, chemistry, physics and so on.

**CHAPTER 3: SYNTHESIS AND CHARACTERIZATION OF Co_3O_4
NANOCUBE-DOPED POLYANILINE NANOCOMPOSITES WITH
ENHANCED METHYL ORANGE ADSORPTION FROM AQUEOUS
SOLUTION¹**

3.1 Introduction

Water pollution, due to the rapid industrialization over the past few decades, possess a serious threat to the environment and have attracted considerable attention worldwide. The organic dyes from the effluents discharged from textile and food industries are major sources of environmental pollution since these dyes are non-biodegradable (Raffainer et al., 2001), decreases the penetration of sunlight into the water bodies affecting photosynthesis in the aquatic habitat (Gupta, 2009), potentially carcinogenic and toxic to human beings (McCann et al., 1976). Around 10–15% of the dyes are dumped into the environment globally after their usage in the dyeing industries (Moussavi et al., 2009) which contributes around 17-20% of the total industrial water pollution as per the World Bank estimate (Chan et al., 2011; Huang et al., 2014). Sodium 4-((4-dimethylamino)phenyldiazenyl)benzenesulfonate, generally known as methyl orange (MO), is a synthetic dye with a complex chemical structure due to which it is impervious to biodegradation and very stable to light and oxidation. (Aksu, 2005). The wide range techniques had been developed to treat dye wastewater such as coagulation/flocculation (Papić et al., 2004), photocatalysis (Shahabuddin et al., 2016b; Shahabuddin et al., 2015a), biological treatment (Gonzalez - Gutierrez et al., 2009), and adsorption (Guo et

¹ This chapter has been published in RSC Advance. *RSC Adv.*, 2016, **6**, 43388–43400 (Q1, Impact Factor: 3.84)

al., 2011; Haldorai et al., 2014; Mahto et al., 2015). The adsorption method has been demonstrated to be an effective procedure with enhanced efficiency and capability to remove dyes on a large scale besides having other benefits such as recovery, and recycling of adsorbents (Ali et al., 2006; Gil et al., 2011; Sadeghi - Kiakhani et al., 2013). Numerous types of adsorbents, such as activated carbon (Chen et al., 2010), natural and synthetic polymers (Hu et al., 2010), MWCNT (Ma et al., 2012) etc. have been employed to remove dyes from wastewater.

Currently, conducting polymers continue to attain a considerable amount of interest at academics and industrial level. Due to the delocalization of electrons in a continuously overlapped π -conjugated electron system, conjugated polymers possess interesting electronic and optoelectronic properties. Numerous conducting polymers such as polythiophene, polyacetylene, polypyrrole, polyphenylene and polyaniline have been extensively explored in multidisciplinary scientific research areas such as sensors (Bairi et al., 2015) batteries (Sengodu et al., 2015), electronics, thermoelectric, electromagnetic, electro-luminescence, and electromechanical applications (Bhadra et al., 2009; Hu et al., 2015; Shih et al., 2015). Polyaniline (PANI), amongst all the electrically conducting polymers, has been most intensively investigated conducting polymer due to its tranquil synthesis, low cost, good environmental stability, enhanced thermal stability, distinctive electrochemical performance, and wide variety of applications (Riaz et al., 2015a). Recently, PANI has been explored as a low cost adsorbent material due to the presence of available active sites with shorter diffusion chain length, better suspension ability, low-dimensional systems and comparatively large surface area. Due to the presence of nitrogen containing protonic ammine groups in the polymeric backbone, PANI have the tendency to bind with heavy metals such as Hg, Cr, Cu, Pb, As etc. as well as toxic anionic

contaminants through electrostatic attraction (Ahmad Rafiqi et al., 2015). Even though exhibiting notable adsorption property, PANI as an adsorbent, could be limited by the lower adsorption efficiencies and limited surface area due to crystalline nature of polymeric chains. Active surface area plays a crucial role in enhancing the adsorption capacity which can be achieved by polymerising PANI in the presence of different metal oxide nanoparticles, as its morphology is greatly influenced by the presence of metal oxide nanoparticles. It is an eminent fact that the properties of a material and its applications are significantly influenced by its morphology which plays a key role in modifying the properties of the material. Hence, various morphologies of polyaniline and its nanocomposites including nanowires (Liang et al., 2002), nanofibers (J Huang et al., 2003), nanospheres (Guo et al., 2011) and nanosheets (Zhang et al., 2009; Zhou et al., 2008) have been widely explored. PANI and its nanocomposites have been investigated by various researchers as an efficient adsorbent for the removal of dyes and other organic pollutants from waste water and they continue to be the promising candidate for the environmental application (Guo et al., 2011; Krika et al., 2015; Mahanta et al., 2008; Mahto et al., 2015) .

Inorganic metal oxides possess potential applications in water treatment, photoluminescence (Talapin et al., 2009), photovoltaics (Clifford et al., 2011; Gong et al., 2012), photochromism (Kazuma et al., 2012; Matsubara et al., 2007) and photo degradation (Huang et al., 2014; Shahabuddin et al., 2015b) due to their high surface area, low production and regeneration costs, significant photochemical, physicochemical and electrochemical properties. Nano metal oxides have fascinated the consideration of researchers for the treatment of dye wastewater owing to their greater degradation efficacy, excellent physical and chemical properties and low toxicity. Various metal

oxides including mixed oxide of cobalt-nickel (Chowdhury et al., 2010), TiO_2 (Khataee et al., 2010), Fe_3O_4 (Zhang et al., 2011), Co_3O_4 (Nassar et al., 2012) etc. have been employed as an adsorbent for removal of dyes from aqueous solution. Cobalt oxide (Co_3O_4), a magnetic p-type semiconductor, is an important class of inorganic metal oxide which belongs to normal spinel structure based on a cubic close packing array of oxide ions. Spinel cobalt oxide (Co_3O_4) nanomaterials have been widely explored recently as they possess facile synthetic methodologies, excellent catalytic properties, and diverse morphologies (Jiao et al., 2010). Thus Co_3O_4 appears to be a promising candidate for various applications, including fuel cells, lithium ion batteries, photocatalysis, artificial photosynthesis, gas sensors, etc., due to its eclectic abundance and economic cost (Hu et al., 2008; Jiao et al., 2009; Li et al., 2005; Shahid et al., 2014).

Herein, the present investigation highlights the Co_3O_4 nanocube-doped polyaniline nanocomposites synthesized via in situ oxidative polymerization for the adsorption of anionic dye (methyl orange). Co_3O_4 nanocubes were synthesized using the simplistic hydrothermal technique and integrated into the polymer matrix during polymerization which had greatly enhanced the effective surface area of polymeric material and aided in efficient removal of methyl orange dye from aqueous solution. Conductive emeraldine form of polyaniline, due to the presence of nitrogen containing functionalities (imine group $-\text{N}=\text{}$ and amine group $-\text{N}<$), get positively charged in aqueous solution and establishes intensive electrostatic attraction between nanocomposite and the anionic methyl orange. The adsorptive capacity for the removal of MO was investigated spectrophotometrically with different wt% of Co_3O_4 contents, and the optimised Co_3O_4 content for enhanced performance was found to be 4 wt% with respect to aniline, with enhanced adsorption capacity. Facile synthesis, cost-effectiveness and high degree of

adsorption of methyl orange make these Co_3O_4 nanocube-doped polyaniline nanocomposites potential adsorbent material for waste water treatment.

3.2 Experimental Section

3.2.1 Materials

Aniline (Fluka, $\geq 99\%$) was distilled under reduced pressure and stored in the dark before use. Ammonium peroxydisulfate, APS (Merck, $\geq 99\%$); Cobalt acetate tetrahydrate (Sigma Aldrich, 99.8%); Hydrochloric Acid, HCl (Merck, 37%); Methanol (Merck, 99.9%); and ammonia solution (R & M, 25%) were used as received without further purification. All of the reagents that were involved in the experiments were of analytical grade. Deionised water was used throughout the entire study.

3.2.2 Synthesis Methodology

3.2.2.1 Synthesis of Co_3O_4 Nanocubes

A recently reported typical hydrothermal technique was utilised for the synthesis of cobalt oxide nanocubes (Shahid et al., 2014). The calculated amount of $\text{Co}(\text{CH}_3\text{COO})_2 \cdot 4\text{H}_2\text{O}$ (83 mM) was dissolved in DI water under constant stirring to obtain a homogenous solution. To this solution, 15 ml of 6% ammonia solution was added dropwise at a rate of one drop per second with vigorous stirring. After two hour of stirring, 75 ml of the reaction mixture was transferred to a 100 mL Teflon-lined stainless steel autoclave and subjected to hydrothermal treatment at 180°C for 12 hr. The obtained precipitate of Co_3O_4 nanocubes were then washed thoroughly with DI water and ethanol several times and dried in a vacuum oven at 60°C for 24 hours.

3.2.2.2 Preparation of Polyaniline (PANI)

Polyaniline was synthesized by the oxidative polymerization of distilled aniline that was dissolved in aqueous HCl (1 M), using ammonium persulfate (APS) as an oxidant. Aniline (0.0215 mol) was dissolved in 30 ml of an aqueous solution of HCl (1 M), and APS (0.0268 mol) was dissolved in 35 ml HCl (1 M). The oxidant solution was then added slowly to the aniline solution with continuous stirring at 25°C. The reaction mixture was stirred continuously for two hours. The reaction mixture was then filtered and washed with HCl (0.5 M) until the filtrate became colourless and subsequently with DI water until the filtrate became neutral. The obtained polymer was dried in a vacuum oven at 60°C overnight. The green colour of the obtained polymer indicated the formation of conductive polyaniline emeraldine salt.

3.2.2.3 Preparation of PANI- Co₃O₄ Nanocomposite

Cobalt oxide nanocube-doped polyaniline nanocomposites were prepared with different wt% of Co₃O₄ (2, 4, and 8 wt% w.r.t. aniline). Co₃O₄ nanocubes were dispersed in DI water by sonication and added dropwise to aniline solution in HCl with vigorous stirring. The resulting mixture was sonicated for a few minutes until it became uniform. The work-up procedure was the same as described in the previous section. The obtained nanocomposites were labelled as PANI-Co2, PANI-Co4 and PANI-Co8 indicating 2%, 4%, and 8% Co₃O₄ nanocubes, respectively.

3.2.3 Characterisation Techniques

The surface morphological and elemental analysis of the synthesized products were conducted using a JEOL JSM-7600F field emission scanning electron microscope

operated at 10 kV. The size and shape of the obtained Co_3O_4 nanocubes were studied using a JEOL JEM-2100F high-resolution transmission electron microscope. Thermal stability investigations were carried out using Perkin Elmer TGA6 under an N_2 atmosphere at a heating rate of $10^\circ\text{C}/\text{min}$. Then, 10 mg of dried sample was loaded inside the alumina crucible, and the weight changes were monitored from 35°C to 900°C . X-ray diffraction (XRD) patterns were recorded using an Empyrean X-ray diffractometer from $2\theta = 10^\circ$ to 90° using $\text{Cu K}\alpha$ radiations ($\lambda = 1.5418 \text{ \AA}$) at a scan rate of 0.02 sec^{-1} . Brunauer-Emmett-Teller (BET) analysis were carried out using Micromeritics ASAP2020 surface area analyzer. Fourier transform infrared (FT-IR) spectra of the powdered samples were recorded using a Perkin Elmer RX1 FT-IR ATR spectrometer in the range of $400\text{--}4000 \text{ cm}^{-1}$ using spectral-grade KBr pellets.

3.2.4 Dye Adsorption Study

The adsorption studies were carried out using MO, an anionic dye, as a model dye in the water phase to investigate the adsorption capacity of nanocomposites. The dye adsorption experiments were conducted at room temperature in a set of Erlenmeyer flasks by batch process to study the outcome of different parameters such as type of adsorbent (PANI, PANI-Co2, PANI-Co4 and PANI-Co8), time (0–120 min), initial pH (2–10) and effect of NaCl concentration (10–50 g/L). In general, 50 mg of the MO dye was dissolved in 1 L of distilled water and the solution pH was adjusted by adding HCl (0.1N) or NaOH (0.1N). 0.050 g of adsorbent was added in 100 ml dye solution and was kept on shaker with constant shaking at 180 rpm. Then, 3 ml of the dye suspension was withdrawn at a regular time interval and centrifuged. The UV-visible absorption spectra of the supernatant solution were analysed using a UV-visible spectrometer (Thermo Scientific Evolution) in 1 cm quartz cuvettes to monitor the characteristic absorption peak of MO.

The percentage dye removal from the aqueous solution was determined according to the following equation(Mahto et al., 2015):

$$\text{Percentage of dye removal, \%R} = \{(C_0 - C_t)/C_0\} \times 100 \quad (3.1)$$

where C_0 is the initial concentration of the MO (mg/L) and C_t is the concentration of MO (mg/L) at time t .

The amount of MO adsorbed per unit mass of adsorbent at equilibrium (adsorption capacity), q_e (mg/g), was calculated using the equation(Guo et al., 2011; Krika et al., 2015; Mahto et al., 2015):

$$q_e = \{(C_0 - C_e)/W\} \times V \quad (3.2)$$

where C_0 is the initial concentration of MO (mg/L), C_e is the equilibrium concentration of MO (mg/L) in solution, m is the mass of adsorbent (g) and V is the volume of the solution (L).

3.3 Results and Discussion

3.3.1 Characterization

3.3.1.1 Morphological Analysis of Nanocomposites

Morphologies of synthesized cobalt oxide nanocubes, PANI and PANI-Co₄ nanocomposite were investigated by FESEM and SEM techniques. Figure 3.1 (a) and (b) illustrate the morphology of the cobalt oxide nanocubes at different magnifications. These images clearly demonstrate the formation of cube-shaped cobalt oxide nanoparticles with an approximately uniform particle size. Additionally, TEM analysis was carried out to further confirm the formation of cubic shaped cobalt oxide. Figure 3.2 reveals the TEM micrograph of cobalt oxide nanoparticles which clearly specify the formation of the cubic

cobalt oxide particles in the nano range, confirming the formation of cobalt oxide nanocubes. Figure 3.1 (c) represents the morphology of PANI which clearly specifies that PANI is largely composed of irregular flakes-like structure which is the characteristic of PANI. Figure 3.1(d) demonstrates Co_3O_4 nanocube-doped polyaniline nanocomposite material, PANI-Co4, revealing the formation of granular polymeric network. As evident from the Figure 3.1 (d), the irregular flake-like morphology of PANI transformed into much segregated granular flakes which enhances the specific surface area suggesting that Co_3O_4 nanocube plays an important role in transforming the morphology of polymeric chains in the nanocomposite. Figure 3.3 represents the TEM image of PANI-Co4 where Co_3O_4 nanoparticles can be seen embedded into the polymeric matrix (marked with arrows).

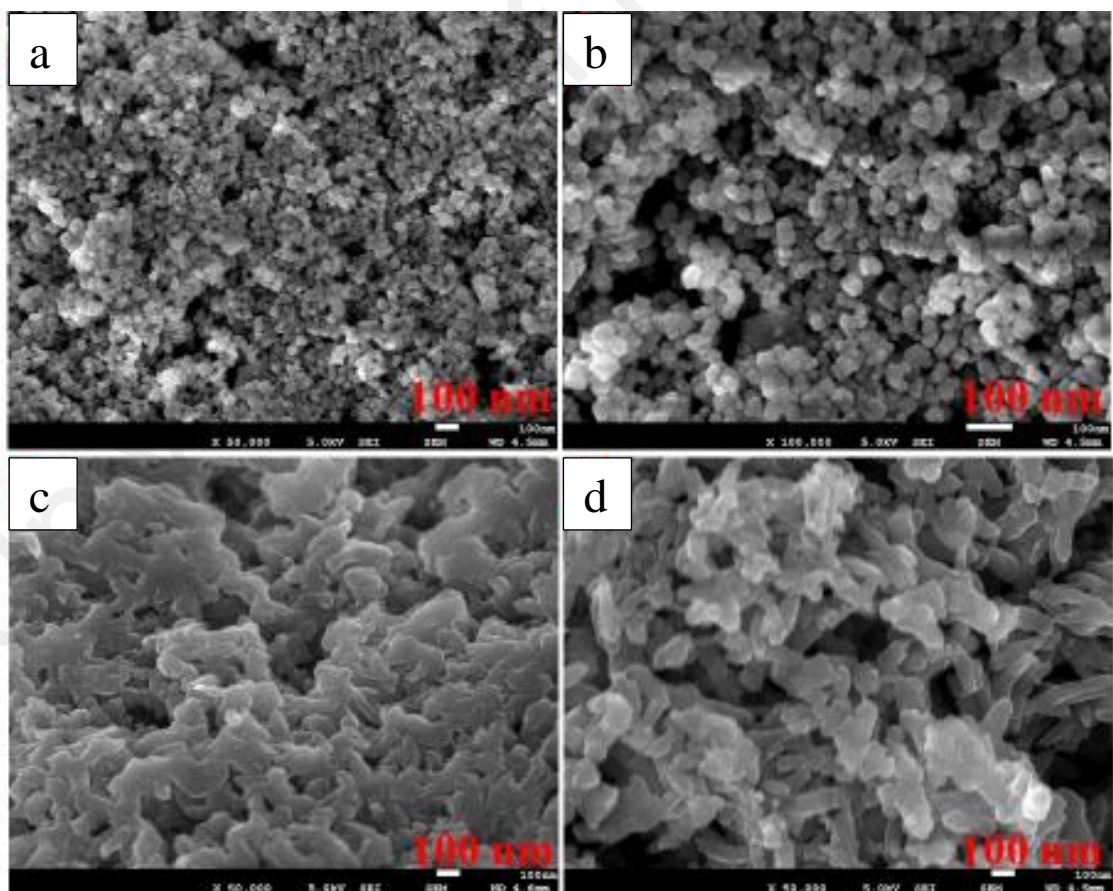


Figure 3.1: FESEM micrographs of (a and b) Co_3O_4 , (c) PANI, and (d) PANI-Co4

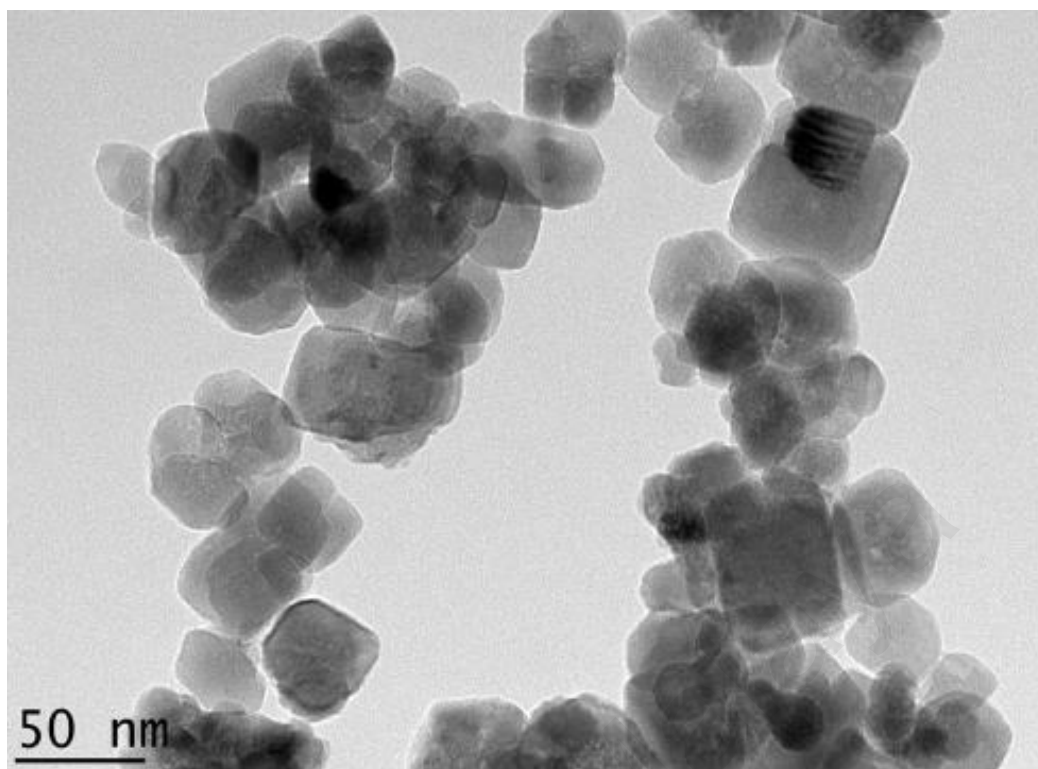


Figure 3.2: TEM image of Co₃O₄ nanocubes

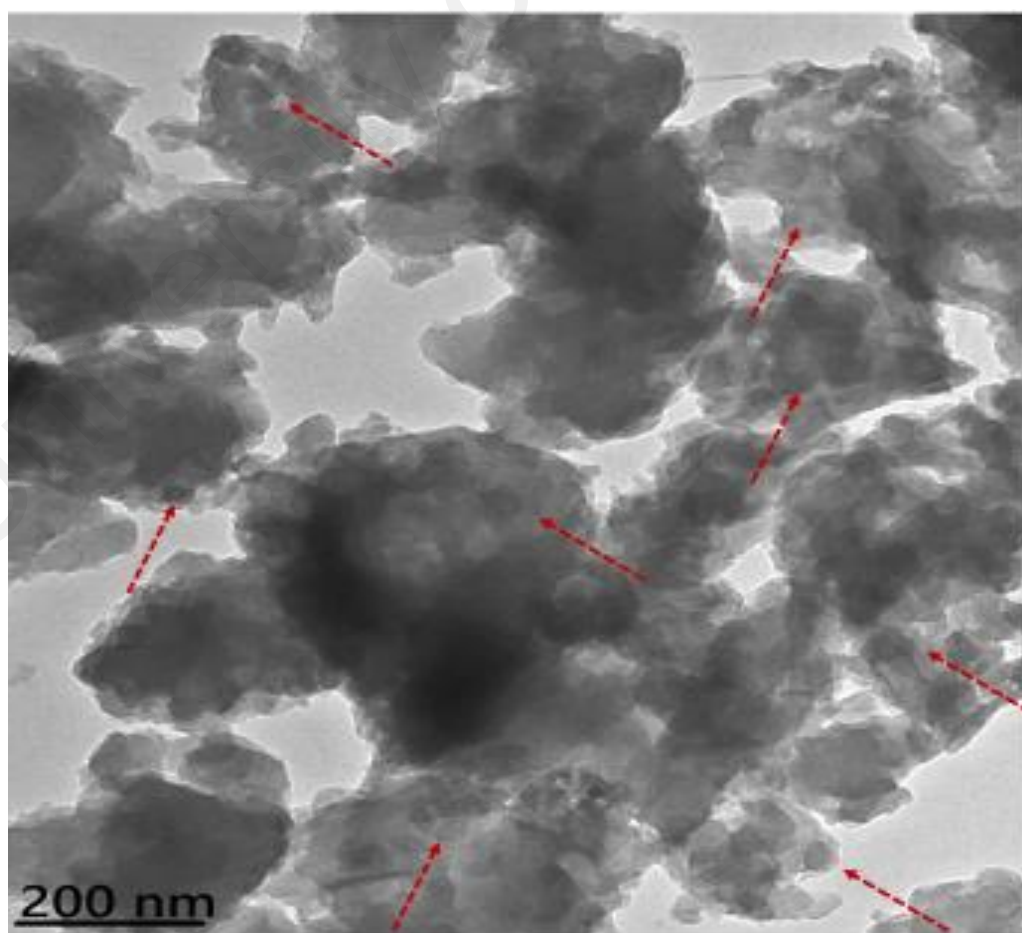


Figure 3.3: TEM image of PANI-Co₄ nanocomposite

As evident from the SEM analysis of PANI-Co4 in Figure 3.3, Co₃O₄ nanocubes in nanocomposite seems to be wrapped inside the matrix of PANI. In order to detect the distribution of Co₃O₄ nanocubes in the matrix of PANI homopolymer, it is suitable to detect the presence of elemental components in nanocomposites through the suitable techniques. Thus, FESEM-EDX and FESEM-mapping appear to be suitable means to demonstrate the doping of cobalt oxide nanocubes in the matrix of polyaniline. Figure 3.4 illustrates the mapping result of nanocomposite with 4% cobalt oxide nanocubes (PANI-Co4). The results clearly reveal the uniform presence of cobalt oxide in the nanocomposite material along with carbon, nitrogen and chlorine. An elemental analysis (Figure 3.5) shows the presence of cobalt, which further confirms the formation of cobalt oxide nanocube-doped polyaniline nanocomposites.

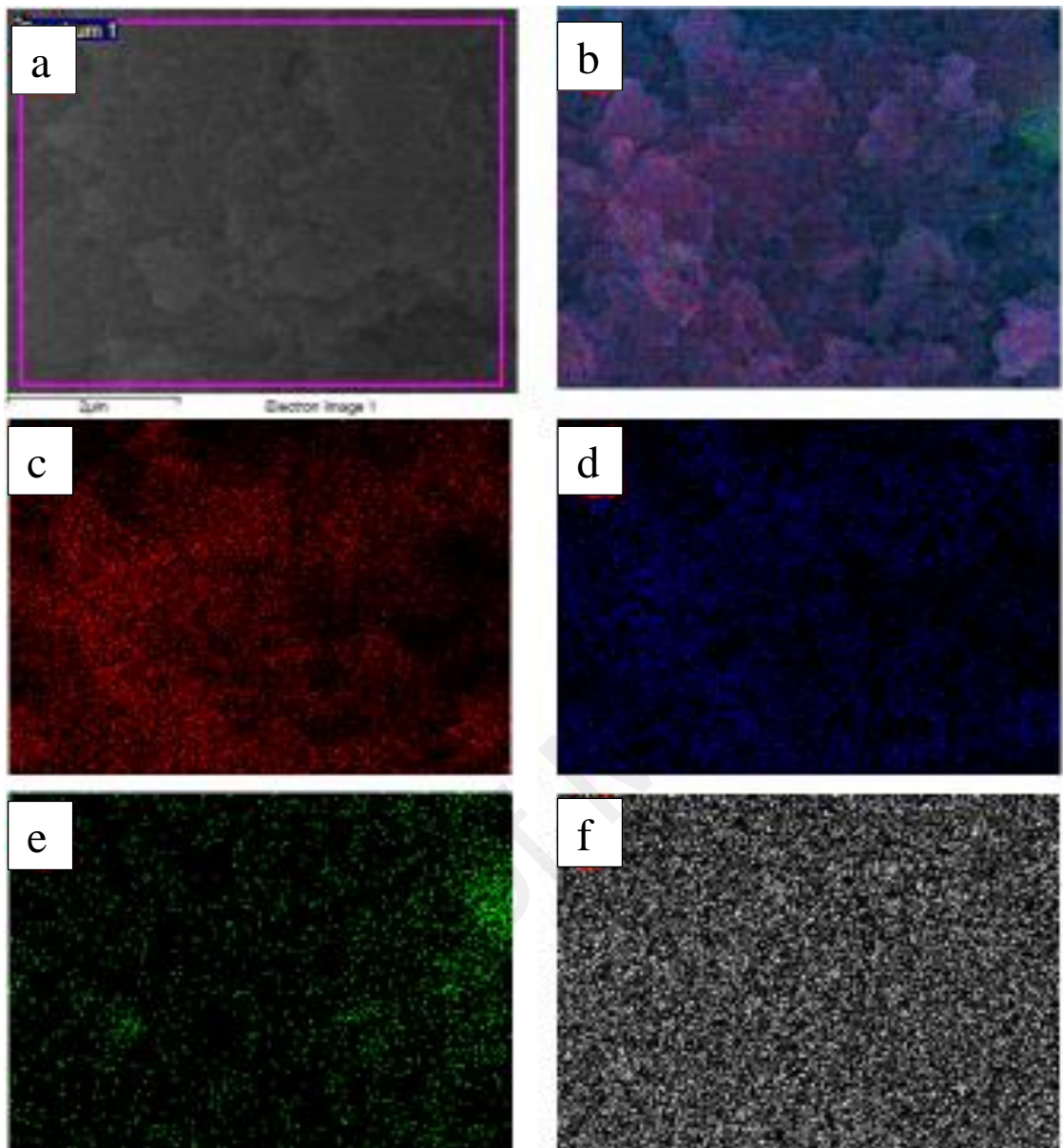


Figure 3.4: (a) FESEM image and (b) EDX elemental mapping of PANI-Co4 nanocomposite on a Si wafer for the following elements: (c) C, (d) N, (e) Co and (f) Cl

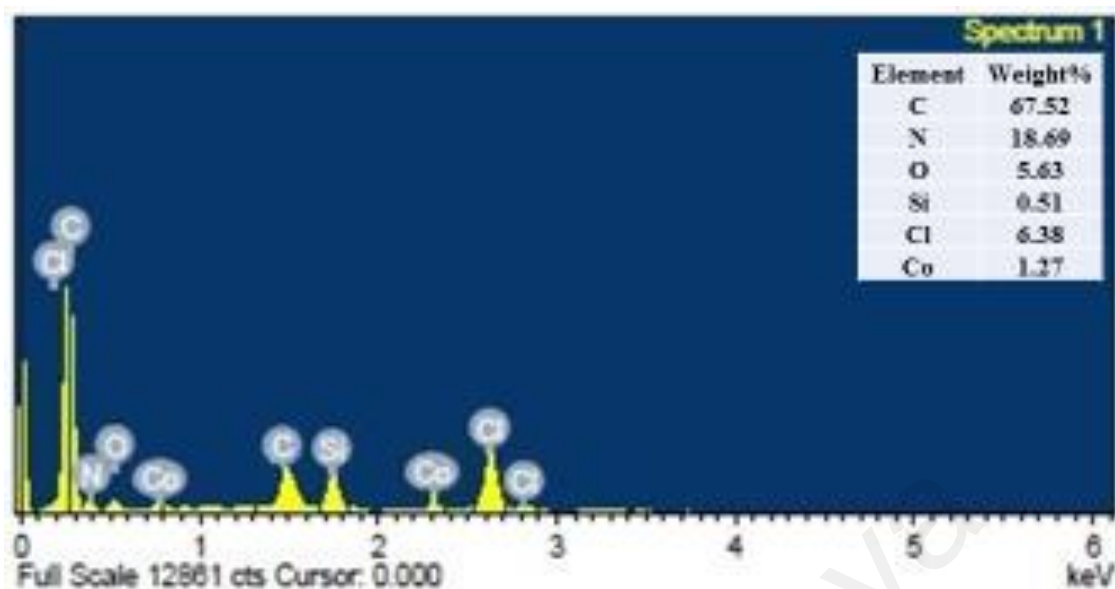


Figure 3.5: EDX spectrum of PANI-Co4 nanocomposite

3.3.1.2 Thermal Analysis

Figure 3.6 represents the thermal analysis of cobalt oxide nanocubes synthesized via hydrothermal method, PANI homopolymer and Co_3O_4 nanocube-doped polyaniline nanocomposite (PANI-Co4), performed under a nitrogen atmosphere by heating samples from 30°C to 900°C with a ramp rate of $10^\circ\text{C}/\text{min}$. As apparent from the TGA thermogram of Co_3O_4 , the first weight loss occurred between the temperature ranging from $50\text{-}150^\circ\text{C}$, which may be accredited to the dehydration of the absorbed moisture. Thermal decomposition of Co_3O_4 takes place as per the following equation (Abu-Zied et al., 2009; Makhoulouf et al., 2012):



where Co_3O_4 started to release oxygen with no further prominent changes being observed in the TGA curve of Co_3O_4 and total weight loss for a temperature range $35\text{-}900^\circ\text{C}$ was found out to be $< 10\%$. Thermal analysis of PANI homopolymer clearly reveals three major weight losses for a temperature range of $35\text{-}900^\circ\text{C}$. The first weight loss occurred from $40\text{-}120^\circ\text{C}$, which may be attributed to the loss of adsorbed moisture,

the decomposition of impurities and the decomposition of unreacted monomers. The second major weight loss is obvious from 120-260°C which might be ascribed to the loss of the dopant ions (HCl) and the final weight loss appeared from 260 to 900°C which is certainly due to the decomposition of polymeric chains (Mostafaei et al., 2012). Thermal stability of Co₃O₄ nanocube-doped polyaniline nanocomposite (PANI-Co₄) has been enhanced to a greater extent as revealed by the TGA analysis of nanocomposite due to the presence of thermally stable pure Co₃O₄ nanocubes in the nanocomposite material. At the end of the experiment at 900°C, approximately 9% of PANI-Co₄ persisted as residue thereby demonstrating higher degree of stability as compared to PANI homopolymer. The major thermal events are summarised in table 3.1.

Table 3.1: TGA summary of Co₃O₄, PANI and PANI-Co₄.

Material	Initial Temp. (°C)	End Temp. (°C)	Percentage of Residue (%)	Major thermal events
Co ₃ O ₄	30	900	92%	<ul style="list-style-type: none"> a) 50-150 °C (dehydration of the absorbed moisture). b) 150-900 °C (Thermal decomposition of Co₃O₄).
PANI	30	900	0.5%	<ul style="list-style-type: none"> a) 40-120°C (loss of adsorbed moisture, the decomposition of impurities and the unreacted monomer). b) 120-260°C (loss of dopant, HCl). c) 260-900°C (decomposition of polymeric chains).
PANI-Co ₄	30	900	9%	<ul style="list-style-type: none"> a) Same as for PANI homopolymer.

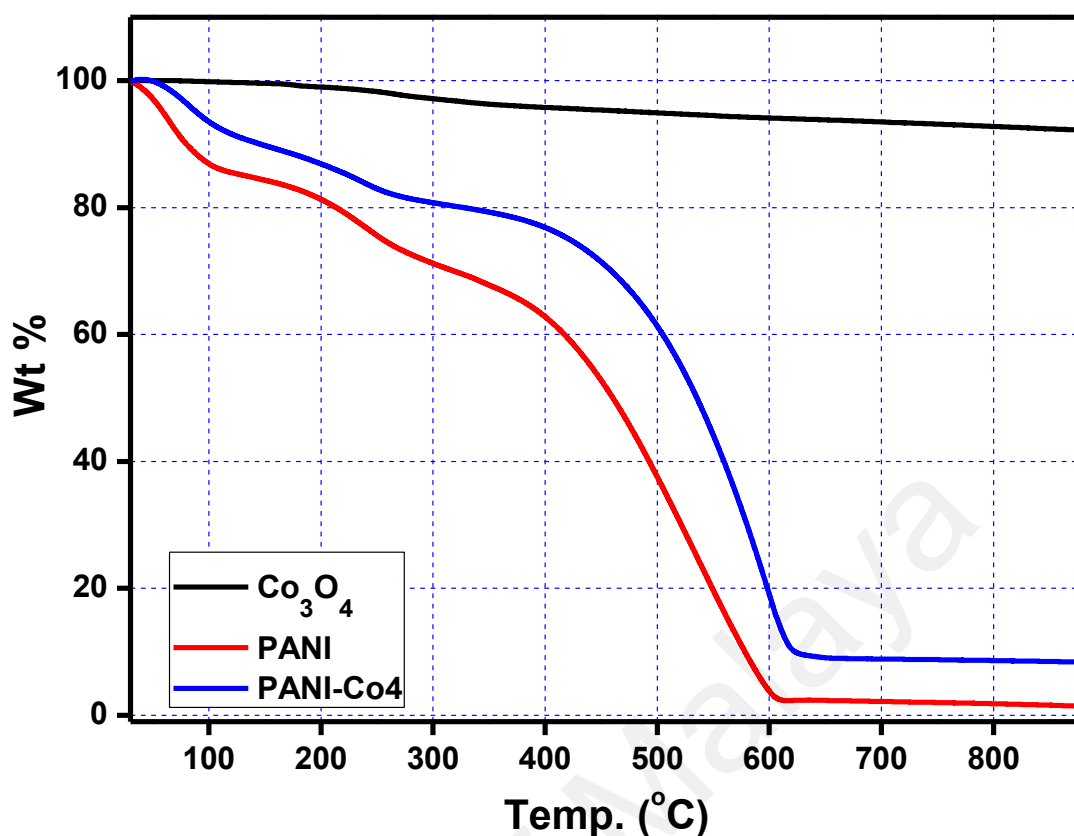


Figure 3.6: TGA patterns of Co_3O_4 , PANI and PANI-Co4

3.3.1.3 XRD Analysis

Figure 3.7 exhibits the typical room temperature XRD spectra of hydrothermally synthesized cobalt oxide nanocubes, PANI and Co_3O_4 nanocube-doped polyaniline nanocomposite (PANI-Co4). Co_3O_4 nanocubes indicated good crystallinity with diffraction peaks appearing at the 2θ value of 31.34, 36.87, 44.84, 55.82, 59.36 and 65.28, which correspond to (220), (311), (400), (422), (511) and (440) planes of face centered cubic (fcc) Co_3O_4 , respectively. These peaks are characteristic of Co_3O_4 and can be readily indexed as those of cubic structure fcc Co_3O_4 in accordance with JCPDS card no. 42-1467 (Song et al., 2013; Wu et al., 2010). The peaks obtained for Co_3O_4 were very sharp and well defined which indicated the well-developed crystalline structure. PANI shows the characteristic diffraction peaks at 2θ values of 15.5, 20.77, and 25.27 which are distinctive of PANI and specify the polycrystalline structure of PANI (Rahy et al., 2008). The peaks appearing at angles of 2θ value of 20.77 and 25.27 represents the

periodic repetition of benzenoid and quinoid rings in PANI chains (Shi et al., 2009). XRD spectrum of PANI-Co₄ reveals that the broad and persistent peaks of PANI homopolymer, which specifies the polycrystalline nature of PANI, were retarded to a greater extent upon the incorporation of Co₃O₄ nanocubes into the polymer matrix. This weakening of PANI crystalline peaks with the doping of Co₃O₄ is possibly due to the fact that Co₃O₄ nanocubes are acting as impurities that retard the growth of the PANI crystallite. Characteristic Co₃O₄ diffraction peaks can be seen clearly in the XRD spectrum of PANI-Co₄ nanocomposite (marked by asterisk) which specify the uniform presence of Co₃O₄ nanocubes in nanocomposite. Hence, XRD investigation established effective synthesis of Co₃O₄ and formation of Co₃O₄ doped polyaniline nanocomposites.

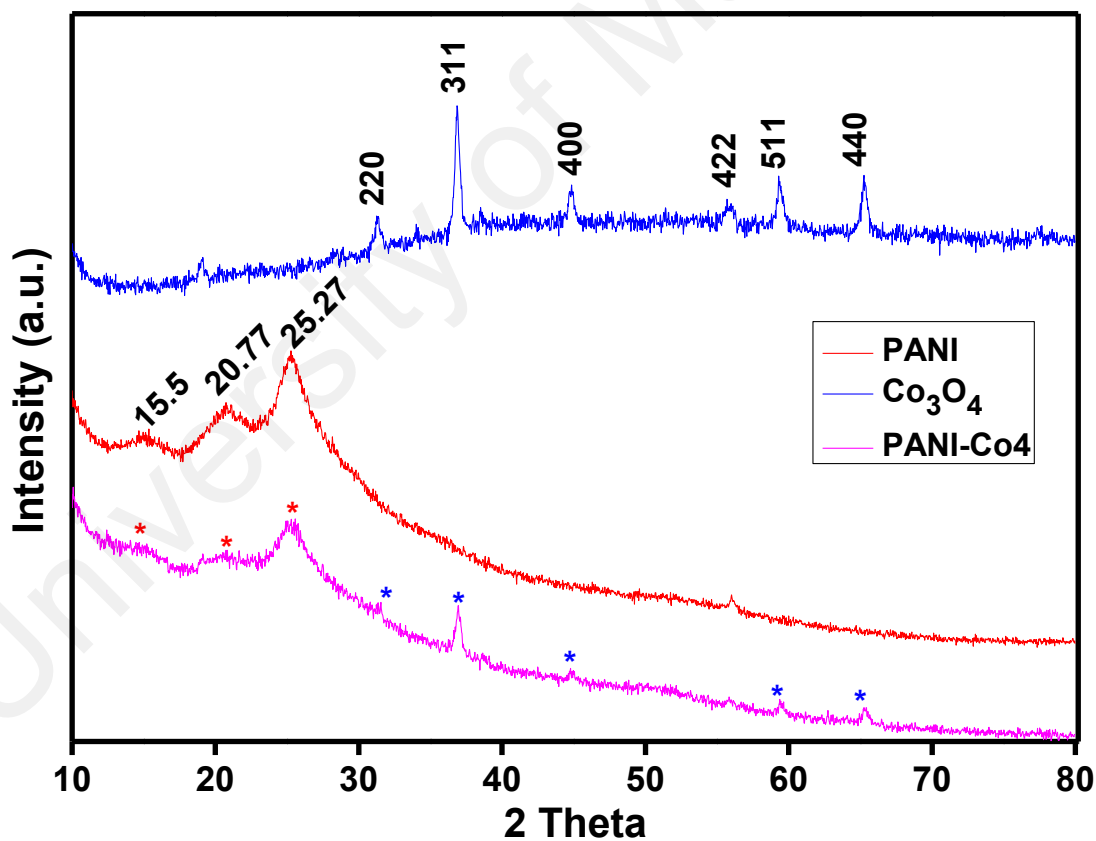


Figure 3.7: XRD patterns of Co₃O₄, PANI and PANI-Co₄

3.3.1.4 BET Analysis

To further investigate the effect of Co_3O_4 nanocube doping on the surface properties, Brunauer-Emmett-Teller (BET) analysis was employed for exploring the specific surface area and porosity of PANI and Co_3O_4 nanocubes-doped nanocomposites by measuring the nitrogen adsorption–desorption isotherms. As shown in Figure 3.8, the nitrogen adsorption–desorption isotherms for PANI and Co_3O_4 nanocube-doped PANI nanocomposites, namely PANI-Co4 and PANI-Co8, exhibited the characteristic type-IV isotherms according to the International Union of Pure and Applied Chemistry (IUPAC) classification which indicates their mesoporous nature (Shahabuddin et al., 2015b; Sing et al., 1985). The BET analyser measurements showed that the specific surface area for PANI homopolymer, PANI-Co4 and PANI-Co8 nanocomposites were found to be 9.42, 43.00 and 35.30 m^2g^{-1} respectively whereas the total volume of pores were in the range of 0.04, 0.17 and 0.13 $\text{cm}^3 \text{g}^{-1}$, respectively. Moreover, the average adsorption pore diameter for PANI, PANI-Co4 and PANI-Co8 were found to be 18.31, 15.57 and 15 nm respectively, which further justifies the mesoporous nature of the nanocomposites. The results revealed that doping of PANI with Co_3O_4 nanocubes enhanced the specific surface area of nanocomposites manifold as compared with bare PANI homopolymer. This increase in specific surface area suggests that Co_3O_4 nanocubes play important role in transforming the morphology of polymeric chains in nanocomposite thereby leading to tremendous increase in specific surface area. Specific surface area increases upon doping with Co_3O_4 nanocubes up to 4 wt% with respect to aniline but decreased upon further increasing of Co_3O_4 nanocubes concentration to 8 wt%. This might be due to the agglomeration of nanoparticles at higher doping percentage leading to the decrease in total effective surface area. Thus, PANI-Co4 nanocomposite displays the high BET specific surface area and large total volume of pores as compared to PANI homopolymer and PANI-Co8 nanocomposite.

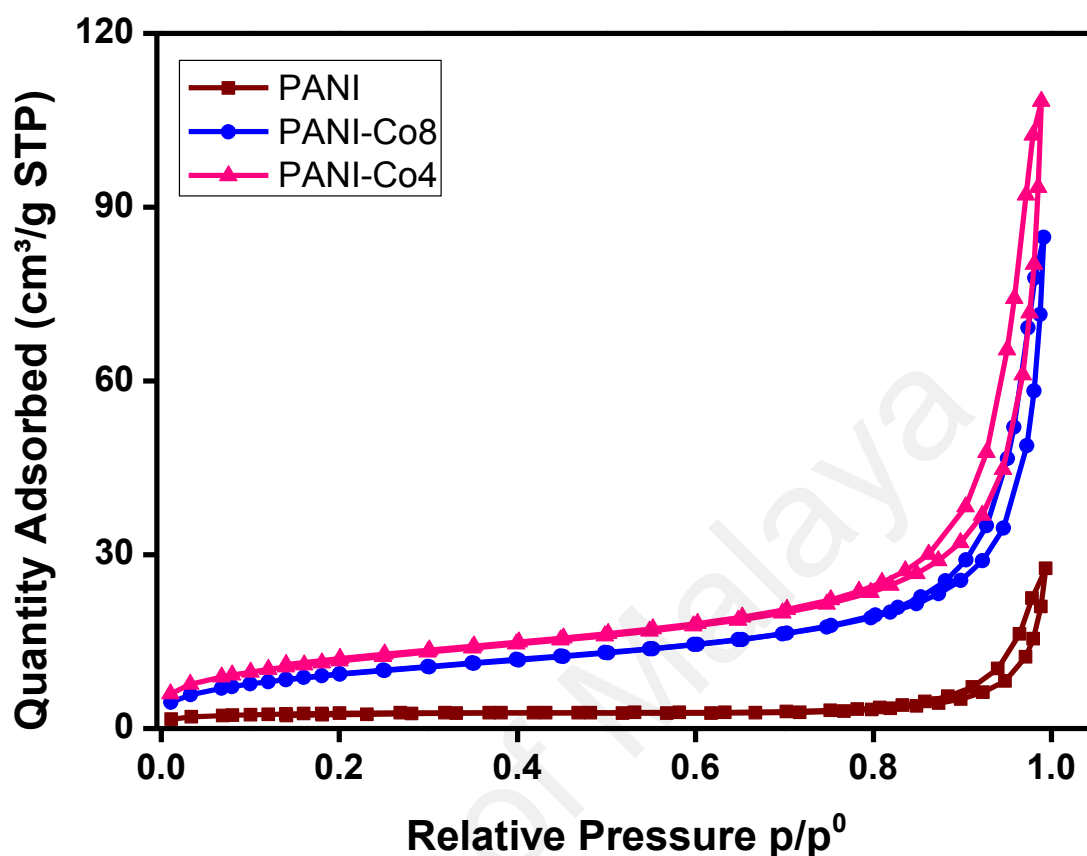


Figure 3.8: Nitrogen adsorption–desorption isotherms (BET) of PANI, PANI-Co4 and PANI-Co8 nanocomposites

3.3.1.5 FTIR Analysis

Figure 3.9 represents the FTIR spectra of cobalt oxide nanocubes, PANI and Co_3O_4 nanocube-doped polyaniline nanocomposite (PANI-Co4). As evident from the FTIR spectrum of the PANI homopolymer, characteristic IR bands appear around 1560 cm^{-1} and 1480 cm^{-1} which may be attributed to C-C stretching of quinoid and benzenoid rings in PANI respectively, which are characteristic peaks of conducting PANI (Yelil Arasi et al., 2009). The peak at 1285 cm^{-1} could be assigned to C-N and C=N stretching in PANI. IR peaks appearing at 807 cm^{-1} and 1127 cm^{-1} were allocated to out-of-plane C-H bending and in-plane C-H bending. The FTIR spectrum of Co_3O_4 nanocubes illustrated significant adsorption peaks at 1630 , 667 and 577 cm^{-1} . The peak at 577 cm^{-1} can be

attributed to Co-O stretching vibration mode (Estepa et al., 1997) whereas the peak at 667 cm^{-1} may be assigned to the bridging vibration of O-Co-O bond (Wu et al., 2003). A characteristic broad IR band at 1630 cm^{-1} can be attributed to H-O-H bending vibration mode which is due to the presence of adsorbed moisture which may be introduced during FTIR sample disks preparation in an open air atmosphere (Xing et al., 2004). Thus, FTIR spectrum of Co_3O_4 nanocubes confirm the formation of spinel Co_3O_4 . The FTIR spectrum of the Co_3O_4 nanocube-doped PANI nanocomposite depicts the characteristic bands of the PANI homopolymer but these bands are slightly shifted after the addition of Co_3O_4 nanoparticles. The characteristic peaks at 667 and 574 cm^{-1} in Co_3O_4 were detected at 647 and 580 cm^{-1} (marked by asterisk) in Co_3O_4 -doped polyaniline nanocomposite. This slight shifting of the band could be attributed to some amount of weak Van der Waals attraction between the polymer chain and Co_3O_4 .

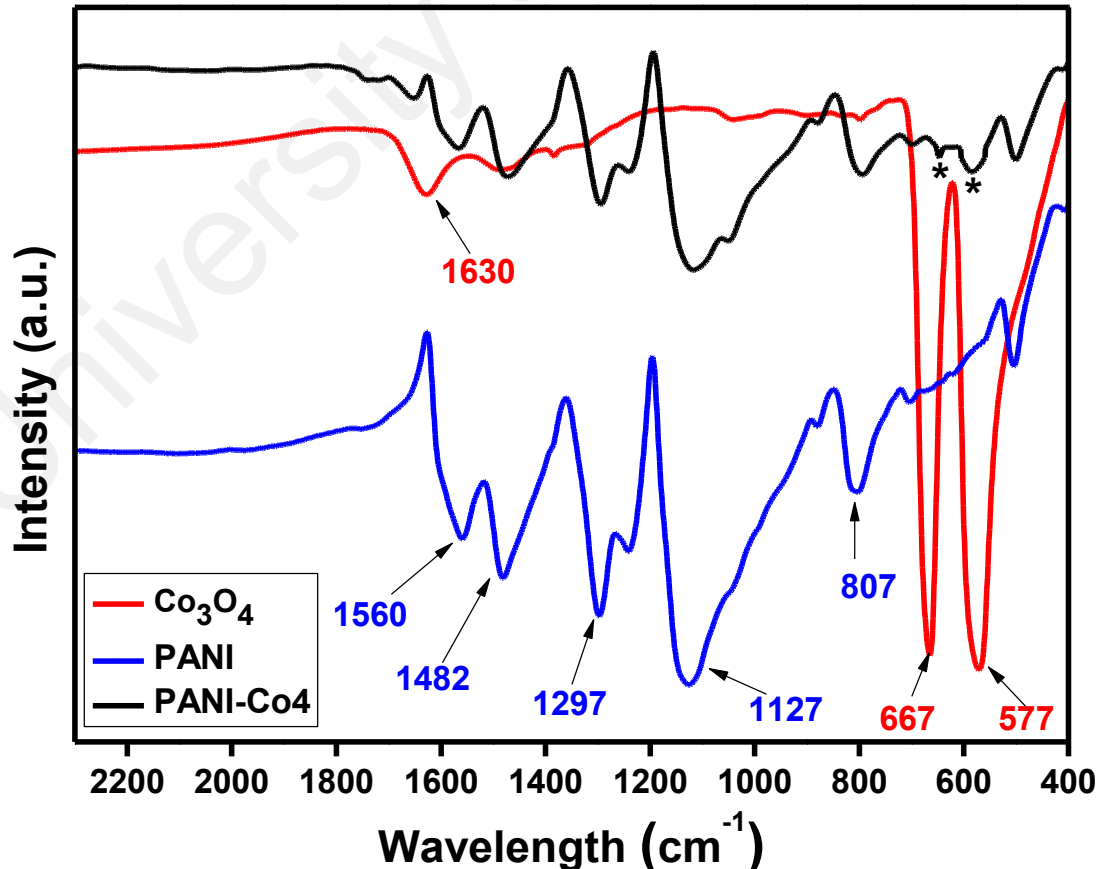


Figure 3.9: FTIR spectrum of Co_3O_4 , PANI and PANI- Co_4

3.3.2 Adsorption Studies

3.3.2.1 Adsorption of MO

The aqueous-phase adsorption behaviour of MO in the presence of Co_3O_4 nanocubes, PANI homopolymer, PANI-Co2, PANI-Co4 and PANI-Co8 nanocomposites were investigated in a set of Erlenmeyer flasks by batch process using a shaker with constant shaking of 180 rpm at ambient temperature. Figure 3.10 (a) and (b) demonstrate the rate of adsorption of MO at different time intervals and percentage adsorption of MO in the presence of various adsorbents, which indicates that adsorption of MO molecules on the surface of the adsorbent increased with time, and most of the adsorbent surface was saturated with MO within 120 minutes. As apparent from percentage adsorption studies, Co_3O_4 and PANI homopolymer exhibits low adsorption efficiencies as compared to the adsorption efficiencies of PANI-Co2, PANI-Co4 and PANI-Co8 nanocomposites. The percentage adsorption, as evident from Figure 3.10 (b), follows the following trend: PANI-Co4 > PANI-Co2 > PANI-Co8 > PANI > Co_3O_4 nanocubes. Figure 3.11 represents the UV-vis adsorption spectra of the MO in presence of PANI and Co_3O_4 nanocubes-doped nanocomposites at different time intervals which depicts the efficient adsorption of MO. As revealed from the figure, the reduction in the intensities of the adsorption band with the increasing irradiation time markedly specifies the effective removal of MO by adsorption phenomenon from the aqueous solution. Approximately 94% of MO was removed within an interval of 120 minutes, predicting an improved adsorption efficiency of PANI-Co4 nanocomposite over Co_3O_4 nanocubes, PANI homopolymer, PANI-Co2, and PANI-Co8, where the percentage removal was approximately 6%, 63%, 73% and 70%, respectively. In PANI homopolymer, adsorption was 63% after 120 minutes, as MO molecules can be adsorbed onto the surface of PANI due to electrostatic attraction between negatively charged MO and positively charged PANI backbone, which increases

the absorptivity of MO on PANI, a prime requisition for enhanced adsorption efficiency. The degree of adsorption of dye augments with the doping PANI homopolymer with of Co_3O_4 nanocubes which implies the synergistic association of PANI and Co_3O_4 nanocubes leading to the enhanced attraction of MO towards the nanocomposite material by increasing the effective surface area. The percentage removal of MO was enhanced greatly with increasing the concentration of Co_3O_4 from PANI-Co2 to PANI-Co4 and decreased from PANI-Co4 to PANI-Co8 which could be caused by the decrease in the effective surface area of adsorbent due to the agglomeration of Co_3O_4 nanocubes at a high doping percentage envisaging PANI-Co4 to be an optimum adsorbent composition.

University of Malaya

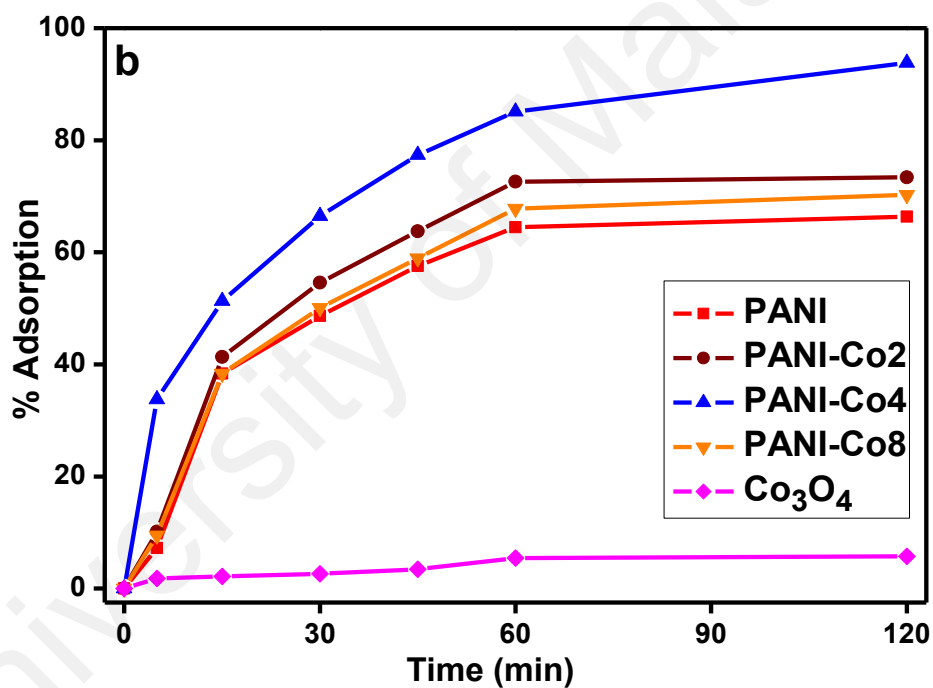
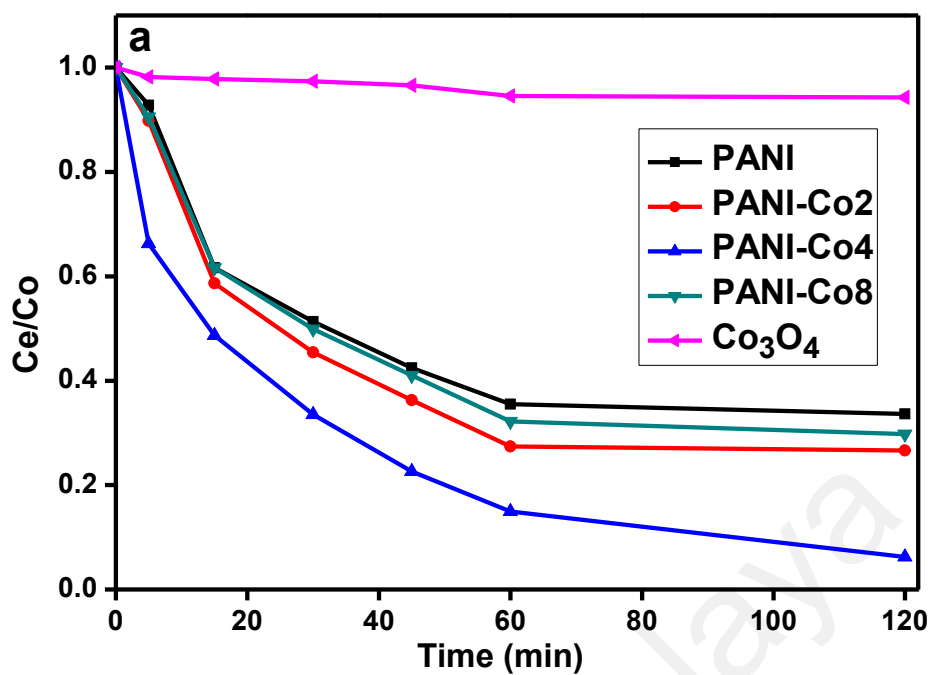


Figure 3.10: (a) Adsorption rate of MO at different time intervals and (b) Percentage removal of MO in the presence of various adsorbents. {initial MO concentration: 50 mg l⁻¹; amount of adsorbent: 0.5mg ml⁻¹; pH 7 at room temperature}

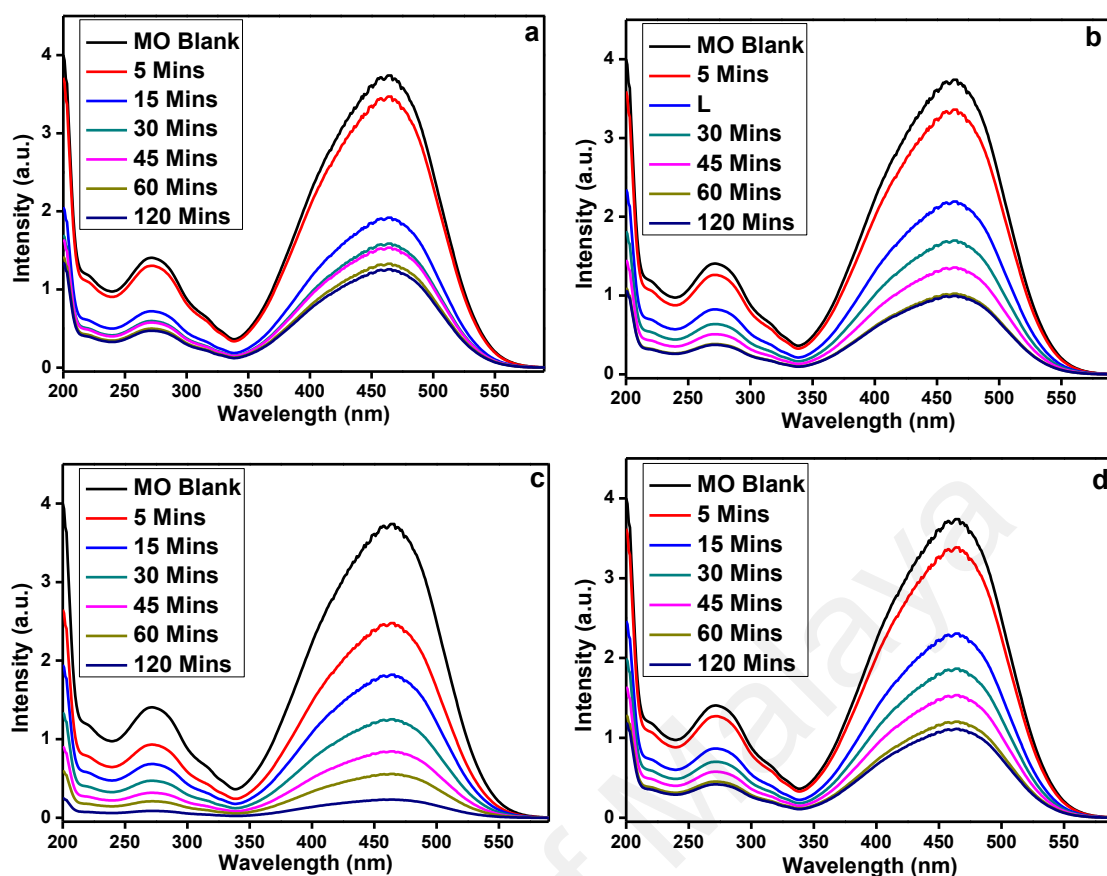


Figure 3.11: UV-vis absorption spectra of MO aqueous solution at different times in the presence of (a) PANI, (b) PANI-Co₂, (c) PANI-Co₄ and (d) PANI-Co₈. {initial MO concentration: 50 mg l⁻¹; amount of adsorbent: 0.5mg ml⁻¹; pH 7 at room temperature}

It is a well-established fact that polyaniline in its conductive emeraldine salt state possess large number of amine ($-N<$) and imine ($-N=$) functional groups which probably interact with metal ions (cobalt ions in present case) (Tang et al., 2009). There is a formation of metal oxide polyaniline complex since the nitrogen atom possess a lone pair of electrons which can be donated to the shared bond between N and the cobalt atom leading to considerable amount electrostatic interactions between PANI and Co₃O₄. During polymerization of PANI in presence of Co₃O₄, the latter act as impurity that retard the growth of the PANI crystallite leading to the formation of granular polyaniline nanocomposite with segregated flakes (as suggested by XRD and FESEM analysis) thereby increasing the effective surface area. Moreover, PANI emeraldine salt also carries substantial amounts of positive charges localized over its backbone which makes it a

suitable candidate for the removal of anionic dyes from aqueous solution. Methyl orange dye consist of a sulfonated group (-SO₃Na) which dissociates in aqueous solution and exists in anionic form as shown in Figure 3.12. Therefore, due to electrostatic attraction between the PANI nanocomposite and MO, it can be effectively removed from the waste water. Thus, in the present case Co₃O₄ nanocube dope polyaniline nanocomposite effectively interact with MO through electronic interactions and decolourises the dye solution proficiently.

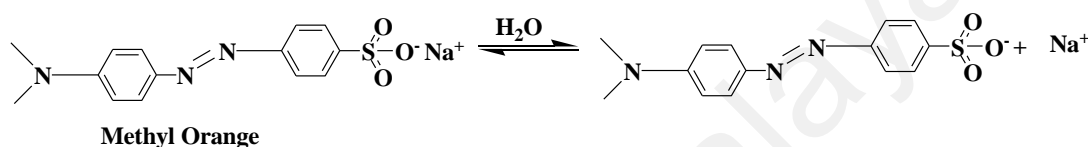


Figure 3.12: Dissociation of methyl orange dye in aqueous solution

Figure 3.13 and 3.14 illustrate the adsorption kinetics curves of MO with PANI homopolymer, PANI-Co₂, PANI-Co₄ and PANI-Co₈ nanocomposites which were conducted to determine various kinetic parameters and type of kinetic model, which fit these adsorption studies. It is well known that the dye adsorption procedure is governed by the contact time between the adsorbate and adsorbent in dispersion and diffusion processes. Throughout the adsorption process, the dye molecules migrate to the external surface of the adsorbent from where they further diffuse into the boundary layer and subsequently settle down into the vacant internal sites (Klett et al., 2014; Mahto et al., 2015). However, it is the electrostatic interaction between the positively charged backbone of PANI nanocomposites and the negatively charged MO dye which is responsible for the adsorption of dye. Therefore, the adsorption of MO on PANI homopolymer, PANI-Co₂, PANI-Co₄ and PANI-Co₈ nanocomposites with respect to time was studied in terms of, pseudo-first order, and pseudo-second order kinetics models. The kinetic models graphs are presented in Figure 3.13 and 3.14 which denote pseudo-first order, and pseudo-second order kinetics models respectively. The kinetic

parameters for the above models are briefed in Table 3.1. The linear form of the Lagergren pseudo-first-order kinetic model is expressed as per the following equation:

$$\ln (q_e - q_t) = \ln q_e - K_1 t \quad (3.4)$$

where q_e is the amount of dye ions adsorbed per unit weight of adsorbent at equilibrium, i.e. adsorption capacity in mg of dye/g of adsorbent, q_t is the adsorption capacity in mg of dye/g of adsorbent at time t and K_1 (min^{-1}) is the adsorption rate constant for a pseudo- first-order model. The kinetic parameters value such as K_1 , q_e and R^2 (correlation coefficient) were obtained from the slope and intercept of the graph plotted by $\ln (q_e - q_t)$ against time and are shown in Table 3.1. As evident from Table 3.1, the values obtained for correlation coefficient (R^2) varies from 0.875 to 0.944 whereas the experimental values of adsorption capacity (q_e , exp) varies significantly from the calculated values of adsorption capacity (q_e , cal) suggesting that the adsorption of MO on PANI homopolymer, PANI-Co2, PANI-Co4 and PANI-Co8 nanocomposites is not a diffusion-controlled phenomenon as they do not follow the pseudo-first-order kinetic model. Furthermore, the linear form of the pseudo-second-order model is given by the following equation:

$$t/q_t = (1 / K_2 q_e^2) + (t / q_e) \quad (3.5)$$

where K_2 ($\text{g mg}^{-1} \text{min}^{-1}$) is the adsorption rate constant for the pseudo-second-order, q_t is the adsorption capacity in mg of dye/g of adsorbent at time t and q_e is the adsorption capacity in mg of dye/g of adsorbent at equilibrium. The kinetic parameters value such as K_2 , q_e and R^2 (correlation coefficient) were obtained from the slope and intercept of the graph plotted by t/q_t against time and are illustrated in Table 3.1. The correlation coefficients (R^2) of linear plots for various adsorbent varies from 0.994-0.999 which suggest that the adsorption of MO onto PANI homopolymer, PANI-Co2, PANI-Co4 and

PANI-Co8 nanocomposites follows the pseudo-second-order kinetic model. Additionally, the experimental values of adsorption capacity (q_e, exp) are very close to the calculated values of adsorption capacity (q_e, cal).

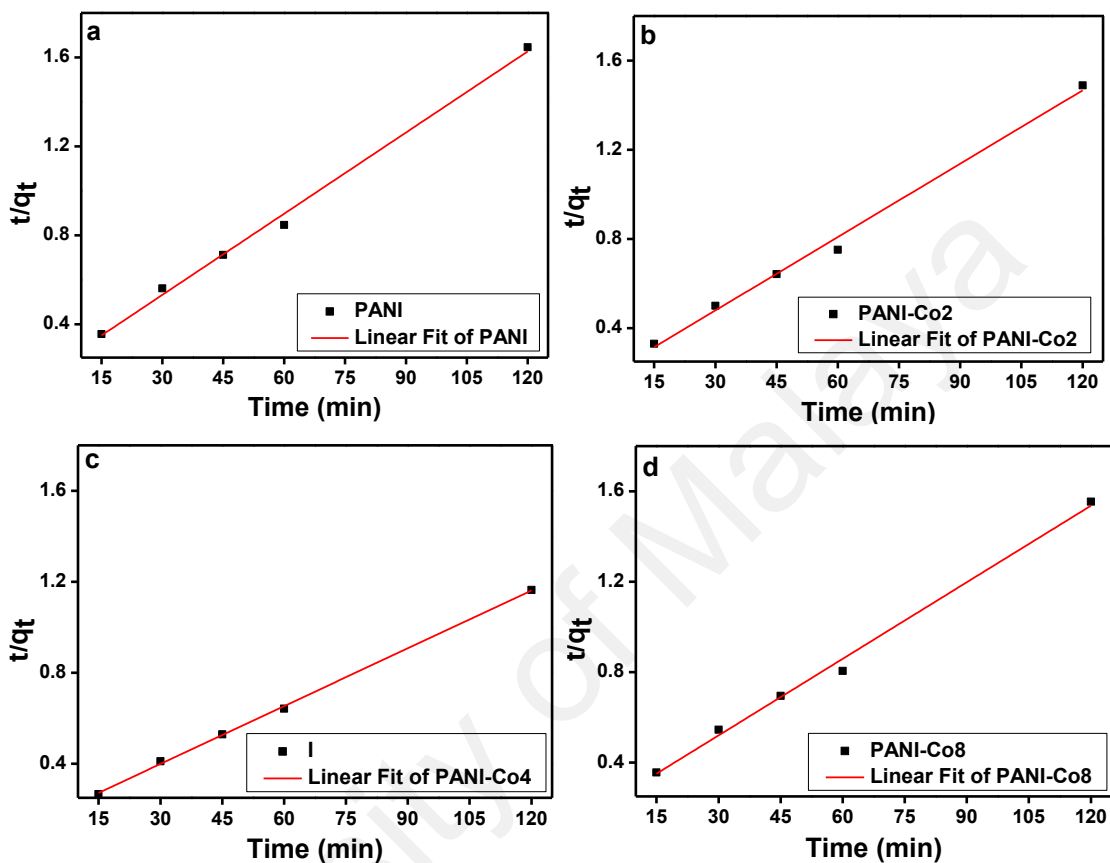


Figure 3.13: Pseudo-first-order kinetic plots for the removal of MO by (a) PANI, (b) PANI-Co2, (c) PANI-Co4 and (d) PANI-Co8. {initial MO concentration: 50 mg l^{-1} ; amount of adsorbent: 0.5 mg ml^{-1} ; pH 7 at room temperature}

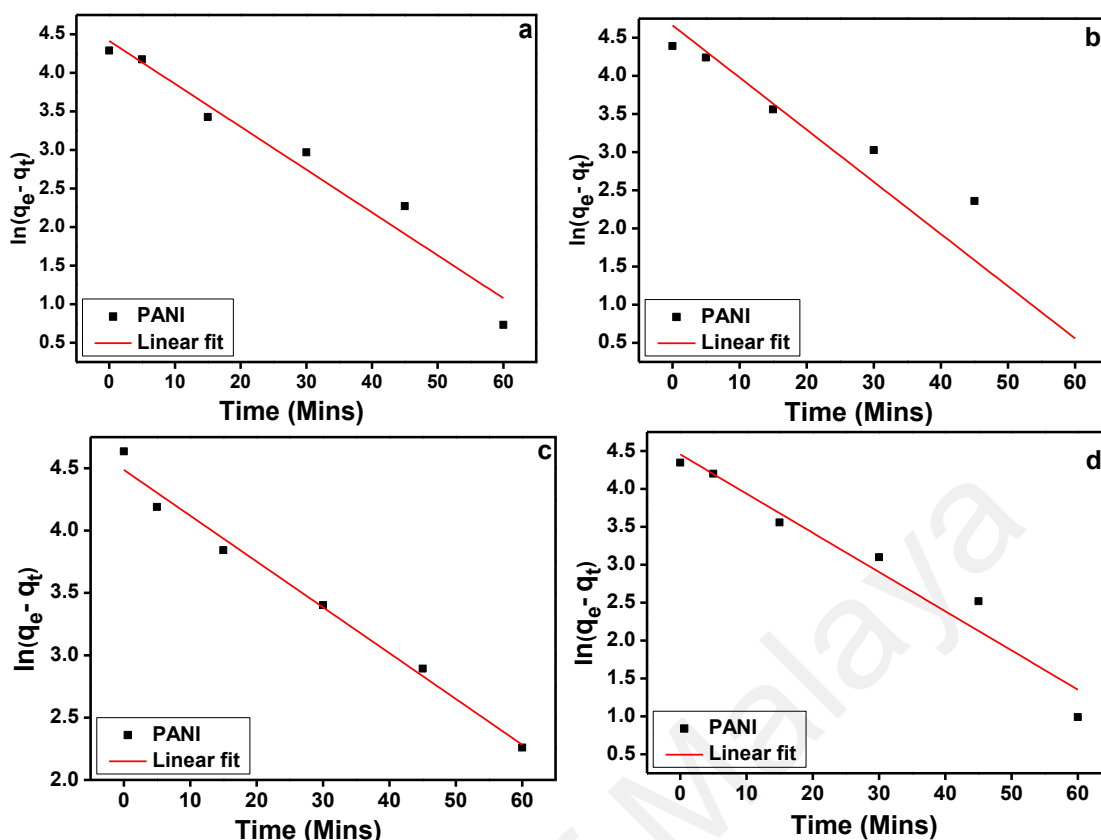


Figure 3.14: Pseudo-second-order kinetic plots for the removal of MO by (a) PANI, (b) PANI-Co2, (c) PANI-Co4 and (d) PANI-Co8. {initial MO concentration: 50 mg l⁻¹; amount of adsorbent: 0.5mg ml⁻¹; pH 7 at room temperature}

Table 3.2: Kinetic parameters for MO adsorption^a

Adsorbent	q _e , exp. (mg g ⁻¹)	Pseudo-first-order kinetic model			Pseudo-second-order kinetic model		
		R ²	K ₁ (min ⁻¹)	q _e , cal (mg g ⁻¹)	R ²	K ₂ (g mg ⁻¹ min ⁻¹)	q _e , cal (mg g ⁻¹)
PANI	72.93	0.952	0.0356	82.52	0.995	0.00105	75.24
PANI-Co2	80.62	0.875	0.0684	105.90	0.993	0.00097	80.62
PANI-Co4	103.07	0.984	0.0368	88.44	0.999	0.00062	103.07
PANI-Co8	77.20	0.944	0.0517	86.06	0.994	0.00087	77.20

^a cal: calculated; exp: experimental.

3.3.2.2 Effect of Adsorbent Dosage

In order to investigate the influence of adsorbent dosage on the percentage of MO removal, different quantities of PANI-Co4 nanocomposite adsorbent ranging from 0.25 to 2 mg ml⁻¹ were taken and adsorption of MO was examined with an initial concentration of 50 mg l⁻¹, pH 7 and ambient temperature. Figure 3.15 indicates the percentage removal of MO by nanocomposite which clearly specify that the percentage removal was sharply increased with increasing the amount of adsorbent from 0.25 to 2 mg ml⁻¹ with 99.50 percent of MO removal at an adsorbent dosage of 2 mg ml⁻¹. This increase in the percentage removal of MO could be attributed to increase in the available surface area and therefore availability of more adsorption sites at higher adsorbent dosage. Hence, 2 mg ml⁻¹ was used as a fixed adsorbent dosage for further experiments.

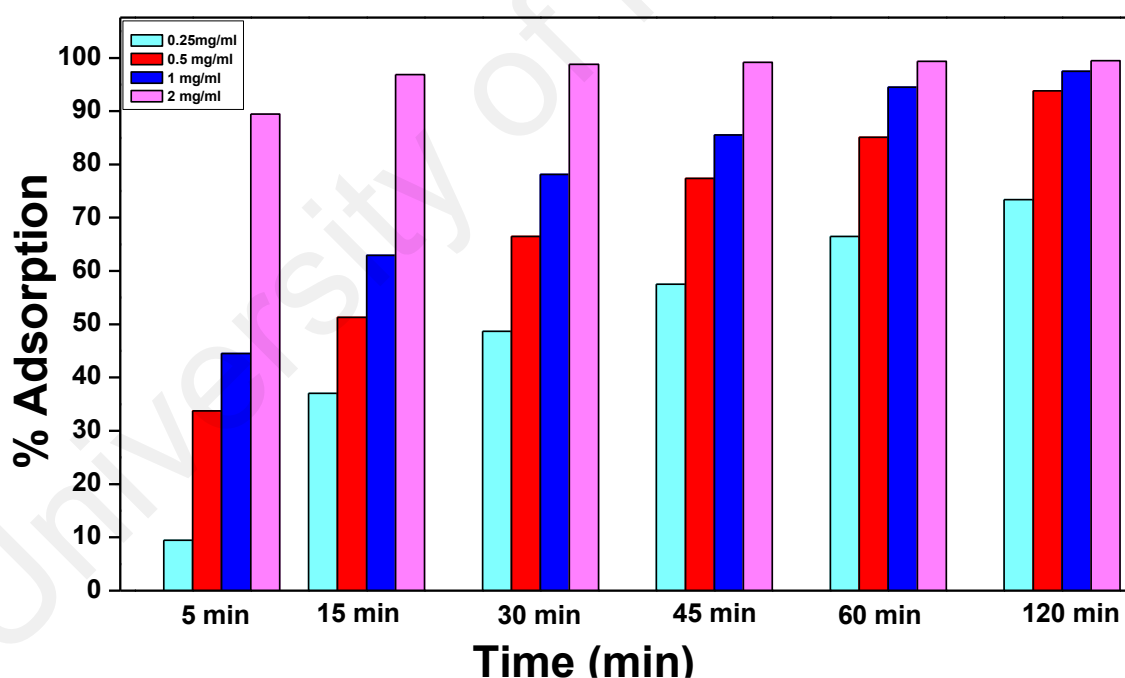


Figure 3.15: Effect of adsorbent dosage on percentage removal of MO in presence of PANI-Co4 at different time intervals {initial MO concentration: 50 mg l⁻¹; pH 7 at room temperature}

3.3.2.3 Effect of Time

The effect of contact time on MO adsorption on PANI-Co4 was determined at an initial MO concentration of 50 mg l^{-1} with an adsorbent dosage of 2 mg ml^{-1} , pH 7 and ambient temperature. The percentage adsorption was studied at the selected interval of time ranging from 5 to 120 minutes. As evident from Figure 3.16, the dye adsorption onto the nanocomposite reached upto 99 percent within 45 minutes. This rapid removal of MO is attributed to the availability of vacant adsorbent sites. On the basis of this experiment 45 minutes was selected as an optimum time for further studies.

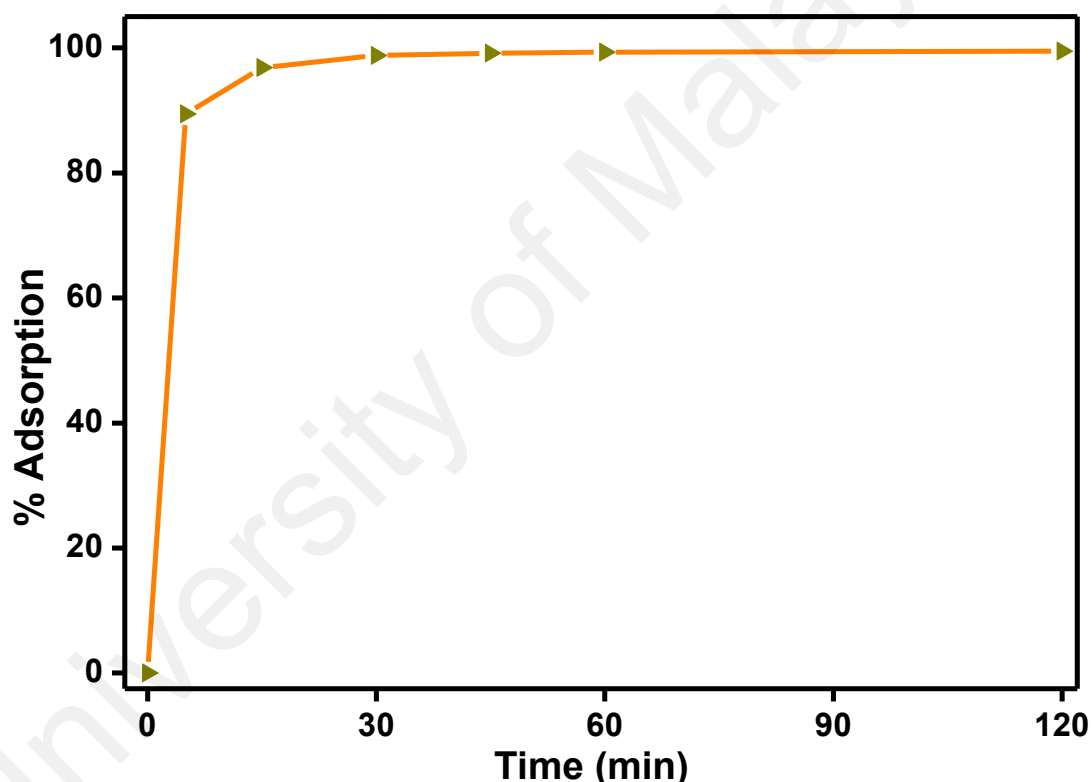


Figure 3.16: Effect of time on percentage removal of MO in presence of PANI-Co4 {initial MO concentration: 50 mg l^{-1} ; amount of adsorbent: 2 mg ml^{-1} ; pH 7 at room temperature}

3.3.2.4 Effect of pH

One of the utmost significant features in adsorption investigations, which have been reported by many researchers, is the substantial role of pH in adsorption efficiency. pH plays a significant role on the adsorption efficiency of the adsorbate molecule apparently

due to its influence on the surface charge of the adsorbent, the degree of ionization of the dye molecules present in the aqueous solution along with the ionization/dissociation of the functional groups on the active sites of adsorbate molecules (Ai et al., 2011; Anbia et al., 2010; Crini et al., 2008; Mahto et al., 2015). Therefore, to study the effect of initial pH on the percentage removal of MO dye using PANI-Co4, batch experiments were carried out from pH 2.0 to 10 by addition of the required amount of 0.1 N HCl or 0.1 N sodium hydroxide at ambient temperature. As represented by Figure 3.17, the adsorption of MO onto the surface of PANI-Co4 appears to be pH dependent with maximum efficiency being achieved at pH 7. Since the reported pKa value of MO is around 3.4, thus at pH values less than pKa value MO which exists in anionic form, gets protonated. On the other hand, due to the presence of imine and amine groups which are basic in nature, PANI develops positive charge in acidic environment. Therefore, at acidic pH there is considerable amount of electrostatic repulsion between protonated MO molecules and positively charged PANI-Co4 nanocomposites leading to the decrease in adsorption efficiency. Since at pH value greater than pKa value of MO, it persists predominantly in anionic form. It is a well-known fact that PANI emeraldine salt upon addition in aqueous solutions makes the solution acidic (pH 3.9) which do not change during the course of adsorption (Mahanta et al., 2008). Therefore, at neutral dye pH, due to the addition of conductive emeraldine form of PANI nanocomposite, the pH of the system becomes higher than pKa value of MO which leads to the intensive electrostatic attraction established between the positive backbone of nanocomposite and the anionic MO leading to maximum adsorption efficiency. At pH values above 7, adsorption behaviour shows a gradual regression up to pH 10 which could be due to the competitive adsorption of hydroxyl ion on imine and amine groups leading to decline in MO adsorption.

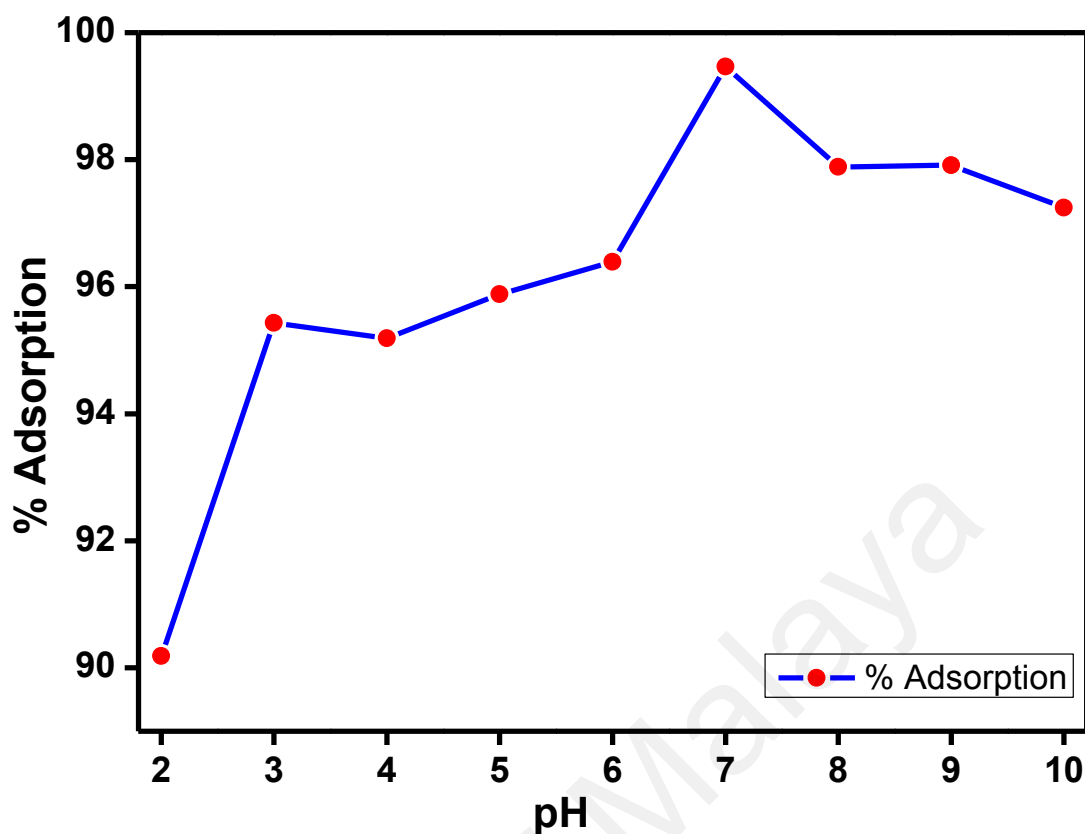


Figure 3.17: Effect of pH on percentage removal of MO in presence of PANI-Co4 {initial MO concentration: 50 mg l⁻¹; amount of adsorbent: 2mg ml⁻¹; time: 45 min; at room temperature}

3.3.2.5 Effect of NaCl Concentration

Industrial dye waste water usually comprises of high salt contents, therefore, it becomes essential to investigate the effect of salt concentration on the percentage removal of MO from aqueous solution using PANI-Co4. Figure 3.18 exhibits the effect of NaCl with variable concentrations ranging from 10 to 50 g l⁻¹ on MO removal percentage by PANI-Co4. As evident from Figure 3.18, the adsorption efficiency of nanocomposite is significantly influenced by the presence of inorganic ionic salts. The adsorption efficacy of the nanocomposite decrease with the increase in NaCl concentration from 10 to 50 g l⁻¹. The percentage removal decreases from 99.50 percent to 88.95 percent with increase in concentration of NaCl by 50 g l⁻¹. This decrease in adsorption efficiency may be ascribed to the neutralization of the surface charge of adsorbent by electrolyte ions which competes with MO molecules for the adsorption on the surface of electrolyte. However, this

decrease in adsorption capacity is not very high which indicates that PANI-Co4 can effectively remove MO from aqueous solution even in the presence of high salt concentration.

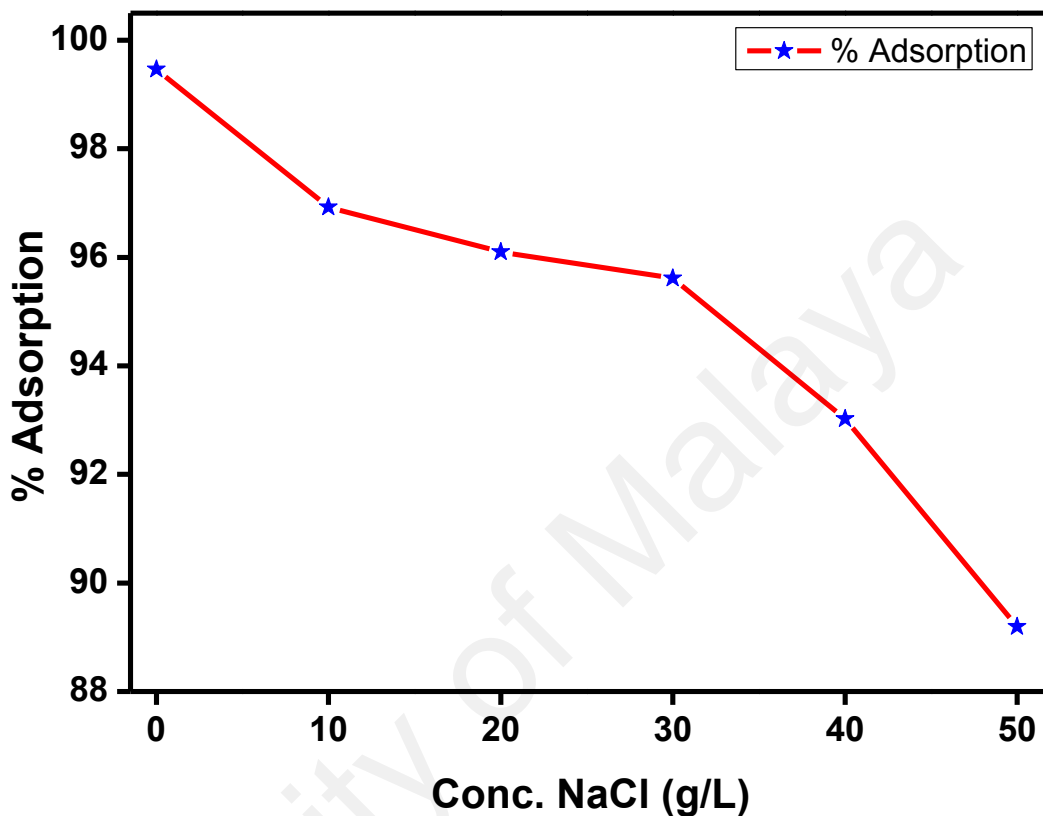


Figure 3.18: Effect of NaCl concentration on percentage removal of MO in presence of PANI-Co4 {initial MO concentration: 50 mg l⁻¹; amount of adsorbent: 2mg ml⁻¹; time: 45 min; pH: 7; at room temperature}

3.3.2.6 Reusability Studies

For the practical application of an adsorbent, stability and reusability are important parameters which need to be considered and thoroughly investigated. Thus, reproducibility of PANI-Co4 were investigated and illustrated in Figure 3.19. The adsorbent after initial cycle was recovered by centrifugation and filtration followed by thorough washing with deionised water, dried at 80° C in vacuum oven for two hours and subsequently employed as adsorbent for further cycles in order to examine their adsorptive efficiencies. As obvious from Figure 15, with each cycle there is marginal decrease in the adsorption efficiency of the adsorbent with percentage removal found out

to be 96.23%, 92.48%, 87.80%, and 81.95% for second, third, fourth and fifth cycle respectively. This investigation clearly reveals that approximately 82% of MO can be adsorbed even in the fifth cycle indicating high stability and reusability efficiency of PANI-Co₄ nanocomposite.

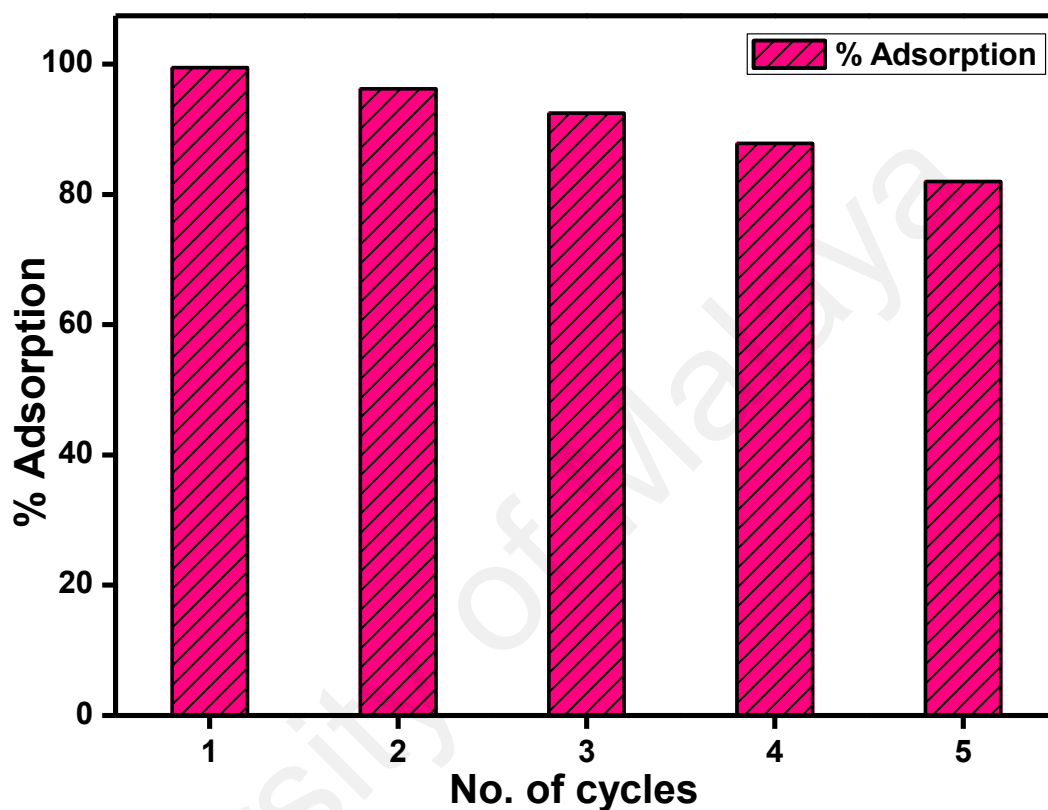


Figure 3.19: Reproducibility cycles of PANI-Co₄ {initial MO concentration: 50 mg l⁻¹; amount of adsorbent: 2 mg ml⁻¹; time: 45 min; pH: 7; at room temperature}

3.4 Conclusion

In this study, we demonstrated a simplistic and unique procedure for the synthesis of Co₃O₄ nanocube-doped polyaniline nanocomposites with enhanced adsorption efficiencies, through an in situ oxidative polymerization method. Co₃O₄ nanocubes incorporated into the matrix of PANI homopolymer revealed greater adsorption capacity of the nanocomposite, signifying the synergistic association between the conducting polymer and the semiconducting metal oxide. BET results showed the effective increase

in the surface area of nanocomposites doped with Co_3O_4 nanocubes whereas FESEM analysis indicated the transformation in surface morphology toward more segregated as compared to bare PANI. These changes in surface properties lead to the enhancement of adsorption capacity of the nanocomposites. The removal efficiency of MO was found to be pH dependent with maximum dye adsorption at pH 7 and no significant decrease in adsorption capacity was observed at high salt concentration. The kinetic parameters were explored to study the adsorption process and the kinetic data specified that the pseudo-second-order kinetic model is well fitted with the obtained experimental results. Moreover, the proposed synthetic approach may be used for the synthesis of numerous Co_3O_4 nanocube-doped nanocomposites materials utilising other conducting polymers which might address the existing concern of environmental pollution.

CHAPTER 4: SYNTHESIS OF CHITOSAN-GRAFTED-POLYANILINE/CO₃O₄ NANOCUBE NANOCOMPOSITE AND ITS PHOTOCATALYTIC ACTIVITY TOWARD METHYLENE BLUE DYE DEGRADATION²

4.1 Introduction

Hazardous wastes and toxic water pollutants are the cause of serious environmental problems and have attracted considerable attention. The textile and food industries use organic dyes that cause environmental contamination because these dyes are non-biodegradable and highly toxic to aquatic creatures and have oncogenic effects on humans (McCann et al., 1976). 3,7-bis(dimethylamino)-phenothiazin-5-ium chloride, commonly known as methylene blue (MB), is a heterocyclic aromatic chemical compound that appears as an odourless, dark-green solid powder yielding a navy blue solution upon dissolution in water. MB is used commercially for various applications, such as textiles, papers, leathers, additives, laser printing, etc., and is an extremely noxious chemical that is primarily used as a dye (Adams et al., 2007; Linz et al., 2006). Among the wide variety of strategies to degrade hazardous waste materials, especially organic compounds, to less toxic or less harmful materials, photocatalysis has emerged as one of the most encouraging techniques because it epitomises a tranquil method of exploiting the energy of either natural sunlight or artificial illumination, such as ultraviolet light, microwaves, etc. (Dai et al., 2014; Kuo et al., 2011; Riaz et al., 2014; Soltani et al., 2012).

² This chapter has been published in RSC Advances. *RSC Adv.*, 2015, **5**, 83857–83867 (Q1, Impact Factor: 3.84)

In recent years, much scientific interest has been attracted towards the synthesis of conductive-polymer-based organic-inorganic hybrid nanocomposite materials. Conducting polymers, including polythiophene, polyacetylene, polypyrrole, polyphenylene and polyaniline, have been used extensively in multidisciplinary scientific research areas, including sensors (Ogura et al., 1997; Ogura et al., 1998; Patil et al., 1999; Sukeerthi et al., 1994), batteries (MacDiarmid et al., 1987b; Mizumoto et al., 1989), electronics, thermoelectric, electromagnetic, electro-luminescence, and electromechanical applications (Angelopoulos, 2001; Bhadra et al., 2009; Gospodinova et al., 1998; Schoch, 1994; Unsworth et al., 1992). Among these electrically conductive polymers, polyaniline (PANI) continues to fascinate researchers due to its distinctive electrochemical performance, environmental constancy, easy preparation and wide variety of applications (Genies et al., 1990; Heeger et al., 1991; J Huang et al., 2003; Kong et al., 2000; Lux, 1994; MacDiarmid et al., 1989; Martin, 1994). As a consequence, PANI has been studied comprehensively and has appeared as the most promising candidate for viable commercial applications. However, poor mechanical properties and poor solubility limit the use of PANI in many environmental applications (Tiwari, 2007). Chemical stability towards dopants, thermal stability, and good processability, along with electrical conductivity, in PANI can be achieved by integrating PANI into a flexible matrix (Lu et al., 2003; Takahashi et al., 2002). Due to its enhanced mechanical strength, biocompatibility, excellent adhesion and absorption ability, chitosan has gained significant attention in preparing semi-interpenetrating chitosan/polyaniline composites (Peniche et al., 1999; Shin et al., 2005). Chitosan, which is obtained from the deacetylation of chitin, a natural biopolymer that is present in the exoskeleton of crustaceans, has an extensive array of applications in water treatment due to its non-toxicity and biodegradability (Gandhi et al., 2013; Kousalya et al., 2010). Due to the presence of hydroxyl (OH) and amine (NH₂) functional groups, chitosan acts as a

potential adsorbent that can bind to variety of chemical compounds through electrostatic attraction or hydrogen bonding. A wide variety of biopolymeric/conducting composite materials has been synthesized recently as adsorbent materials with potential environmental applications (Hena, 2010; Liu et al., 2013; Yavuz et al., 2011).

Non-biodegradable dyes have been degraded photocatalytically using inorganic metal sulphide and metal oxides nanoparticles, such as ZnS (Golsheikh et al., 2015), TiO₂ (Autin et al., 2013; Ray et al., 2000), ZnO (Singh, 2010), etc. Nanocomposites that are comprised of inorganic metal oxides and conducting polymers are potential photocatalysts that enhance the degradation rate of pollutants through synergetic effects between the metal oxide and the conducting polymer. PANI has been extensively used as conducting polymer, which acts as photo-sensitiser with a variety of inorganic metal oxides, such as TiO₂. PANI has high electron mobility, and its electrons get easily excited under UV-visible light. As reported by Zhang et al., the electrons that are generated in the excited π^* bonding orbital of the PANI molecule transfer into the conduction band of TiO₂, where they react with oxygen and water molecules to form superoxide radicals and OH radicals, increasing the degradation potential of TiO₂ (Zhang et al., 2006). The remarkable photochemical and electrochemical properties of spinel cobalt oxide (Co₃O₄) nanomaterials have attracted the attention of researchers because Co₃O₄ nanomaterials possess facile synthetic methodologies, excellent catalytic properties, and diverse morphologies (Jiao et al., 2010). Co₃O₄ is a promising candidate for multiple applications, including fuel cells, lithium ion batteries, photocatalysis, artificial photosynthesis, gas sensors, etc., due to its wide abundance and economic cost (Hu et al., 2008; Jiao et al., 2009; Li et al., 2005; Shahid et al., 2014).

The present investigation focuses on the degradation of methylene blue (MB) dye using chitosan-grafted-polyaniline doped with Co_3O_4 nanocubes synthesized via in situ oxidative polymerization. Co_3O_4 nanocubes were synthesized using the facile hydrothermal method and incorporated into the polymer matrix during polymerization. The selection of chitosan-grafted-polyaniline for photocatalytic activity is based on high electron mobility and the easy excitement of electrons for PANI under UV illumination, along with the high adsorbent capacity of chitosan for MB due to electrostatic attraction or hydrogen bonding and the stabilising polymer composite. In addition, Co_3O_4 doping helps to generate electrons and holes in PANI to enhance the degradability of MB. The photocatalytic activity for the degradation of MB under UV-light irradiation was investigated spectrophotometrically with different wt% of Co_3O_4 contents, and the optimised Co_3O_4 content for high degradation performance was 2 wt% with respect to aniline, with enhanced photocatalytic activity. Facile synthesis, cost-effectiveness and higher photocatalytic degradation performance make these Co_3O_4 nanocube-doped chitosan-grafted-polyaniline nanocomposites potential photocatalysts for MB dye degradation.

4.2 Experimental Section

4.2.1 Materials

Please refer to section 3.2.1

4.2.2 Synthesis Methodology

4.2.2.1 Synthesis of Co_3O_4 Nanocubes

Please refer to section 3.2.2.1

4.2.2.2 Preparation of Polyaniline (PANI)

Please refer to section 3.2.2.2

4.2.2.3 Preparation of Chitosan-Grafted Polyaniline (ChGP)

Chitosan-grafted-polyaniline (ChGP) composite was synthesized as previously reported by Tiwari et al. (Tiwari et al., 2007). Figure 4.1 illustrates synthetic route for the preparation of the chitosan-grafted-polyaniline copolymer. In a typical synthesis process, the required amount of chitosan was dissolved in 1% glacial acetic acid solution to make a 1 g/L concentration. To this solution, 1.5×10^{-2} M aniline in 0.5 M HCl was added under continuous stirring at room temperature. After 30 minutes, 12.5×10^{-2} M ammonium persulfate was added, and grafting was allowed to proceed for 2 hours. Subsequently, the solution was neutralised by 5% aqueous NaOH. The resulting ChGP was precipitated using absolute ethanol, filtered, washed with DI water until the filtrate became neutral and colourless, and dried in a vacuum oven. Finally, ChGP was ground to a fine powder, washed with acetone several times and dried at 50°C in a vacuum oven for 72 hours.

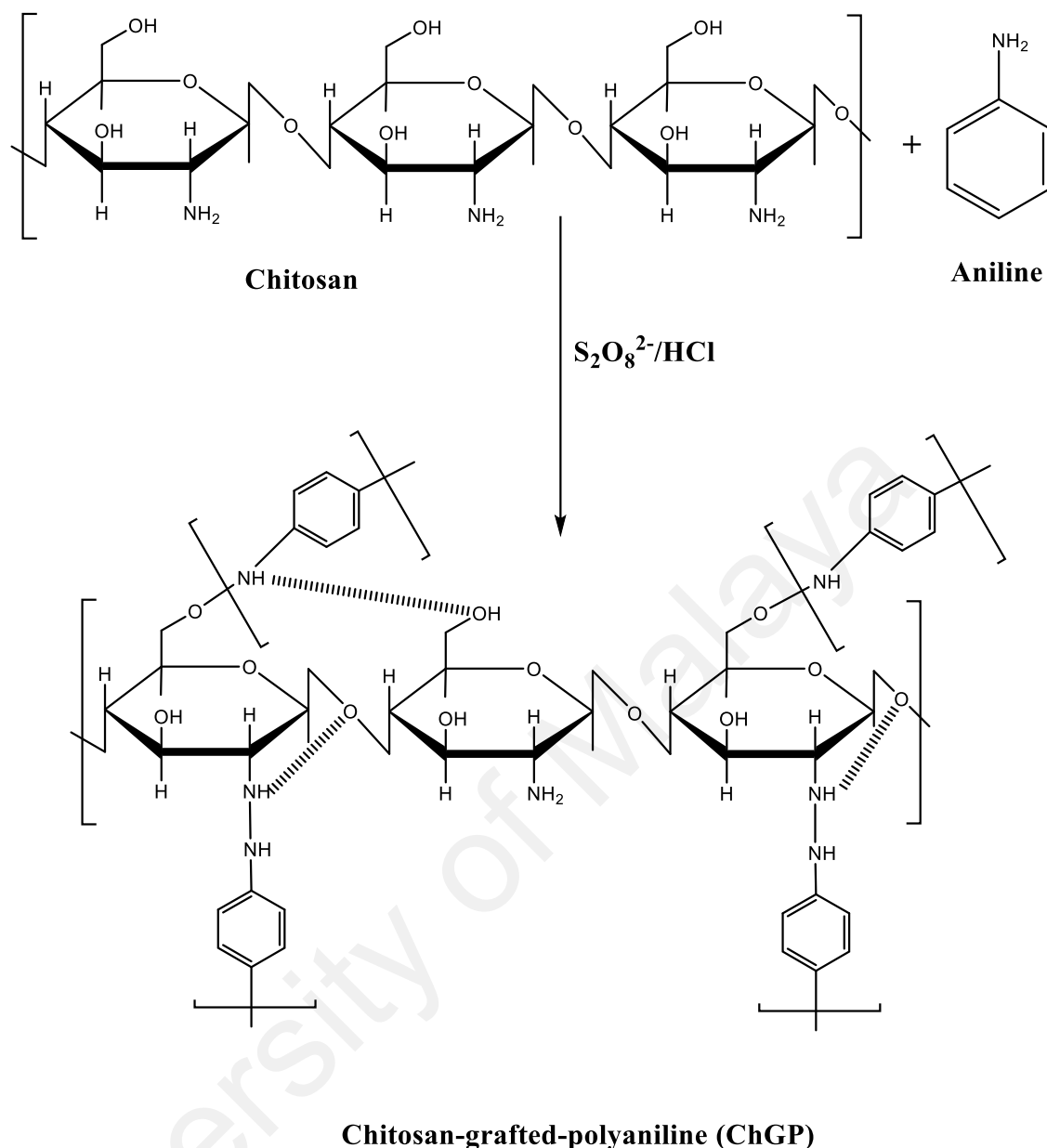


Figure 4.1: Reaction pathway for the synthesis of chitosan-grafted-polyaniline copolymer

4.2.2.4 Preparation of the ChGP- Co_3O_4 Nanocomposite

Cobalt oxide nanocube-doped ChGP- Co_3O_4 nanocomposites were prepared with different wt% of Co_3O_4 (1, 2, and 4 wt% w.r.t. aniline). Co_3O_4 nanocubes were dispersed in DI water by sonication and added dropwise to aniline solution in HCl with vigorous stirring. The resulting mixture was sonicated for a few minutes until it became uniform. The work-up procedure was the same as described in the previous section. The obtained

nanocomposites were labelled as ChGP, ChGPCo1, ChGPCo2, and ChGPCo4, indicating 0%, 1%, 2%, and 4% Co₃O₄ nanocubes, respectively.

4.2.3 Characterisation Techniques

The surface morphological and elemental analysis of the synthesized product was conducted using a JEOL JSM-7600F field emission scanning electron microscope operated at 10 kV. The size and shape of the obtained Co₃O₄ nanocubes were studied using a JEOL JEM-2100F high-resolution transmission electron microscope. Thermal stability investigations were carried out using Perkin Elmer TGA6 under N₂ atmosphere at a heating rate of 10°C/min. Then, 10 mg of dried sample was loaded inside the alumina crucible, and the weight changes were monitored from 35°C to 900°C. X-ray diffraction (XRD) patterns were recorded using an Empyrean X-ray diffractometer from $2\theta = 10^\circ$ to 80° using Cu K α radiations ($\lambda = 1.5418 \text{ \AA}$) at a scan rate of 0.02 sec^{-1} . X-ray photoelectron spectroscopy (XPS) was conducted using a Kratos analytical axis ultra-instrument with an Al K α radiation source of 253.6 eV. Diffuse reflectance spectra were recorded with UV-vis spectrophotometer, Shimadzu model UV-2550 against BaSO₄ white background. Fourier transform infrared (FT-IR) spectra of the powdered samples were recorded using a Perkin Elmer RX1 FT-IR ATR spectrometer in the range of 400–4000 cm⁻¹ in spectral-grade KBr pellets.

4.2.4 Measurement of Photocatalytic Activities

The prepared samples were evaluated for photocatalytic activities by monitoring the degradation of methylene blue (MB) dye in the aqueous phase. In a typical experiment, 15 mg of the prepared nanocomposite powder was dispersed in 50 mL of an aqueous

solution of MB with an initial concentration of 10 mgL^{-1} . The adsorption–desorption equilibrium was achieved by stirring the mixture in a dark environment for 80 minutes. The photocatalytic degradation was then conducted by irradiating the above mixture using a UV lamp (CL-1000 UV Crosslinkers; 5X8 W) that was placed nearly 10 cm above the solution. To maintain the uniform dispersion of photocatalyst particles, the mixture was stirred continuously using a magnetic bar. Then, 3 ml of the dye suspension was withdrawn at a regular time interval and centrifuged. The UV-visible absorption spectra of the supernatant solution were analysed using a UV-visible spectrometer (Thermo Scientific Evolution) in 1 cm quartz cuvettes to monitor the characteristic absorption peak of MB.

4.3 Results and Discussion

4.3.1 Characterization

4.3.1.1 Morphological Analysis of Nanocomposites

FESEM images were obtained to characterise the morphologies of cobalt oxide nanocubes, PANI, chitosan and the nanocomposite containing 2 wt% cobalt oxide (ChGPCo2). The morphology of the cobalt oxide nanocubes is shown in Figure 4.2 (a) and (b) at different magnifications. From these images, it is evident that cube-shaped cobalt oxide nanoparticles were formed with an approximately uniform particle size. To further confirm the formation of cobalt oxide nanocubes, TEM images were taken (Figure 4.2 (g)) and clearly demonstrate the presence of cube-shaped particles in the nano range, confirming the formation of cobalt oxide nanocubes. Figure 4.2 (c) and (d) illustrate the morphologies of PANI and chitosan, where PANI showed a flake-like structure as the characteristic structure of PANI, whereas chitosan exhibited an irregular shape with a cotton-like accumulation. Figure 4.2 (e) represents ChGP composite material, clearly

revealing the formation of cross-linked polymeric network with a high degree of porosity. This structure indicates the formation of a graft copolymer of chitosan and polyaniline, resulting in a highly porous material with cross-linked network. Figure 4.2 (f) shows the nanocomposite of chitosan-grafted-polyaniline with 2 wt% cobalt oxide nanocubes (ChGPCo2) that are embedded in the polymer matrix.

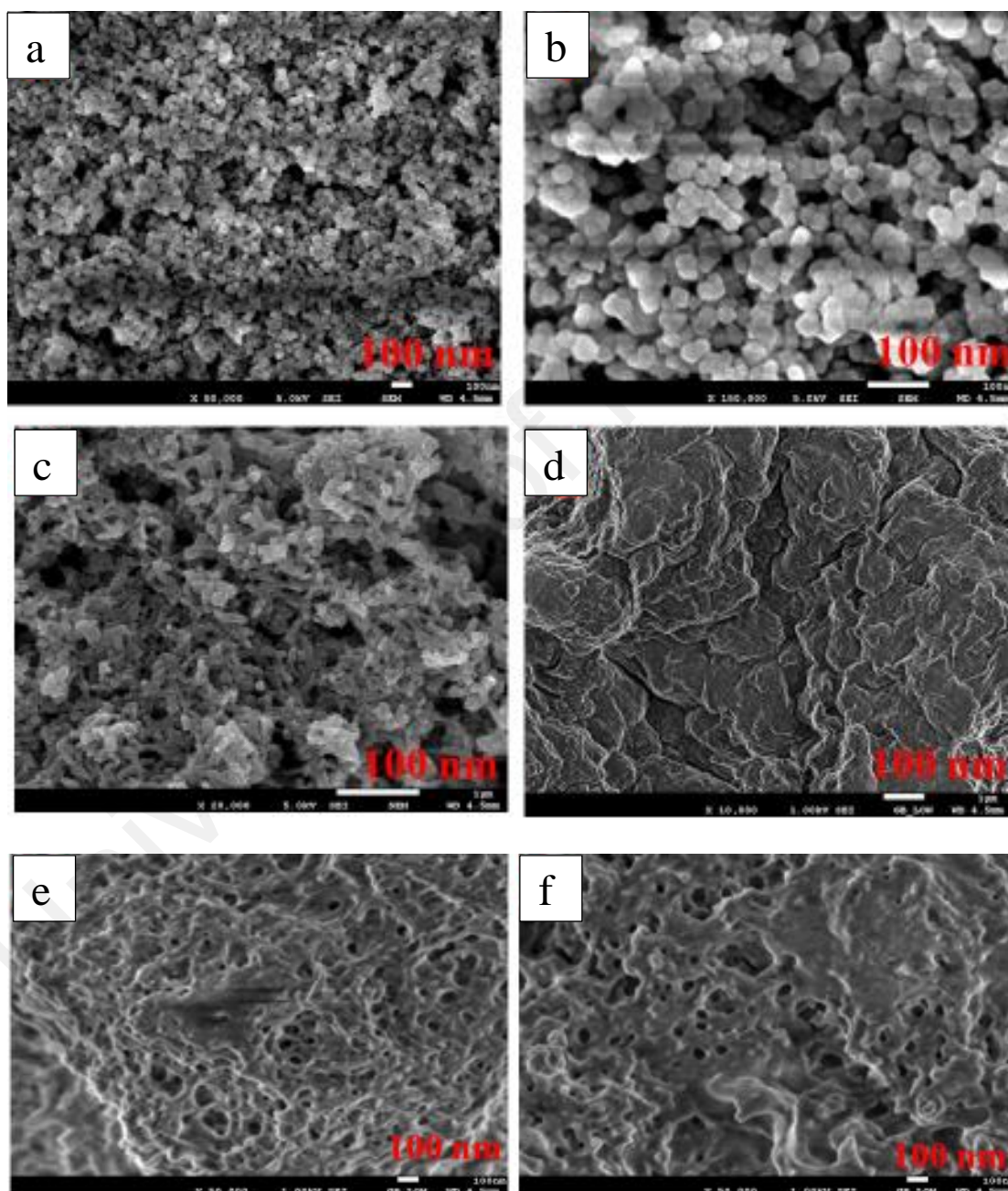


Figure 4.2: FESEM micrographs of (a and b) Co_3O_4 , (c) PANI, (d) chitosan, (e) ChGP (f) ChGPCo2 and continue..

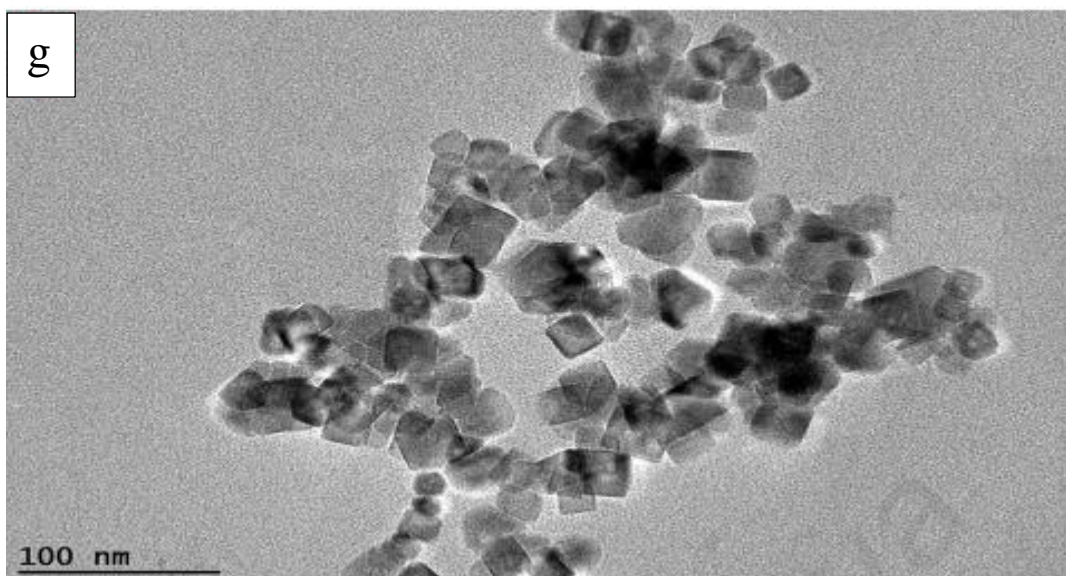


Figure 4.2: (g) TEM image of Co_3O_4 nanocubes

Because Co_3O_4 nanocubes were embedded in the polymeric matrix of the polymer, it was difficult to observe these cubes in the FESEM image of the nanocomposites, possibly due to their very low concentration (2 wt% w.r.t. aniline) as to the graft copolymer. Thus, an appropriate way to demonstrate the doping of cobalt oxide nanocubes in the polymeric matrix is FESEM-EDX and FESEM-mapping. Figure 4.3 shows the mapping result of nanocomposite with 2% cobalt oxide nanocubes. It can be clearly seen from the result that cobalt oxide is uniformly present in the nanocomposite (Figure 4.3 (e)) along with carbon, nitrogen and oxygen. An elemental analysis (Figure 4.4) shows the presence of cobalt, which further confirms the formation of cobalt oxide nanocube-doped chitosan-grafted-polyaniline nanocomposites.

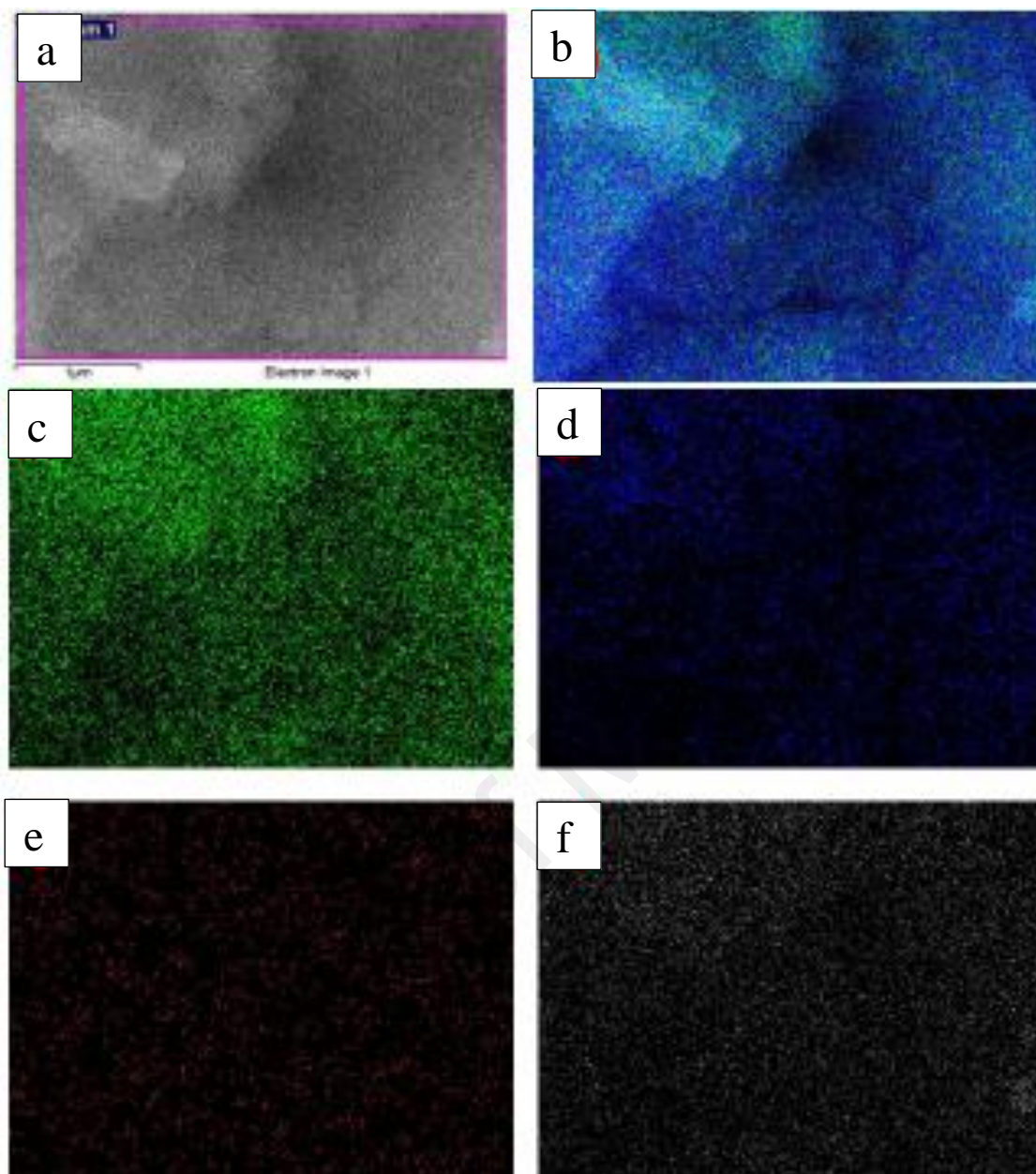


Figure 4.3: (a) FESEM image and (b) EDX elemental mapping of ChGPCo₂ nanocomposite on a Si wafer for the following elements: (c) C, (d) N, (e) Co and (f) O

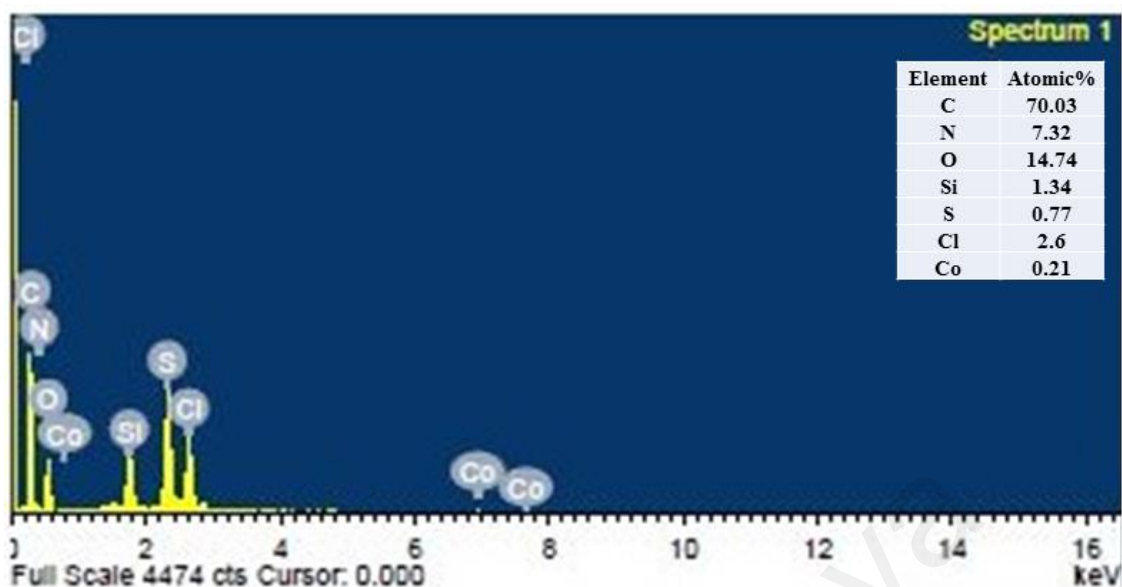
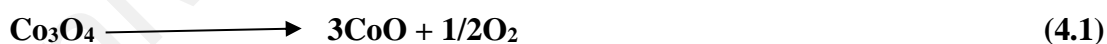


Figure 4.4: EDX spectrum of ChGPCo2 nanocomposite

4.3.1.2 Thermal Analysis

Figure 4.5 represents the TGA thermogram of cobalt oxide nanocubes, PANI, chitosan and chitosan-grafted-polyaniline nanocomposites as performed under a nitrogen atmosphere by heating samples from 35°C to 900°C with a ramp rate of 10°C/min. As is evident from the graph, in Co_3O_4 the first weight loss is observed from 50-145°C, which may be due to the dehydration of absorbed water. Co_3O_4 started to release oxygen as per the following equation:



and lost approximately 9% weight until 900°C. Chitosan shows the major weight loss at 50 to 130°C, 150 to 334°C and 340 to 900°C, which could be attributed to the loss of bound water, the decomposition of etheral groups and the decomposition of glucosamine residues, respectively. PANI shows three major weight losses from 40-120°C, which may be due to the loss of adsorbed moisture, the decomposition of unreacted monomers and the decomposition of impurities; 130-260°C is accredited to the loss of the dopant (HCl); and 260 to 900°C is possibly due to the decomposition of hydrocarbon chains. It is evident

from the graph that the thermal stability of ChGP, ChGPCo1, ChGPCo2 and ChGPCo4 improved compared to the thermal stabilities of chitosan and PANI. At the end of the experiment at 900°C, 2.8% of ChGP, 3.0% of ChGPCo1, 5.9% of ChGPCo2, and 7.7% of ChGPCo4 persisted as residue. The thermal analysis data presented above proposed the following trend of stabilities: ChGPCo4> ChGPCo2>ChGPCo1>ChGP, which can be accredited to the increase in the crosslinking of polymeric materials during grafting and to the presence of thermally stable pure Co₃O₄ at increased concentrations. The major thermal events are summarised in table 4.1.

Table 4.1: TGA summary of Co₃O₄, Chitosan, PANI, ChGP, ChGPCo1, ChGPCo2 and ChGPCo4.

Material	Initial Temp. (°C)	End Temp. (°C)	Percentage of Residue (%)	Major thermal events
Co ₃ O ₄	35	900	91%	a) 50-145 °C (dehydration of the absorbed moisture). b) 150-900 °C (Thermal decomposition of Co ₃ O ₄).
Chitosan	35	900	0.5%	a) 50-130°C (loss of bound water). b) 150- 334°C (decomposition of etheral groups). c) 340- 900°C (decomposition of glucosamine residues).
PANI	35	900	0.5%	a) 40-120°C (loss of adsorbed moisture, the decomposition of impurities and the unreacted monomer). b) 130-260°C (loss of dopant, HCl). c) 260 to 900°C (decomposition of polymeric chains).
ChGP	35	900	2.8%	a) Same as for PANI homopolymer and chitosan.
ChGPCo1	35	900	3.0%	
ChGPCo2	35	900	5.9%	
ChGPCo4	35	900	7.7%	

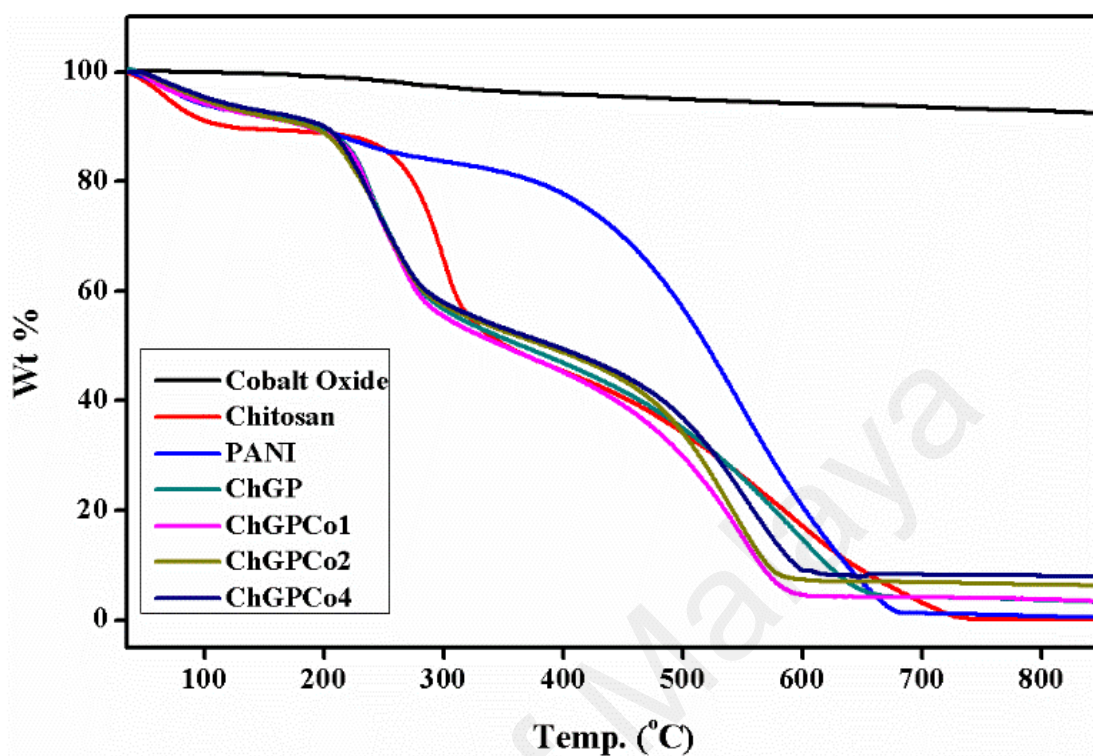


Figure 4.5: TGA thermogram analysis of PANI, chitosan, Co_3O_4 and nanocomposites

4.3.1.3 XRD Analysis

Figure 4.6 and Figure 4.7 show the typical XRD spectra of synthesized cobalt oxide nanocubes, PANI, chitosan and various chitosan-grafted-polyaniline nanocomposites. As apparent by the XRD pattern of Co_3O_4 nanocubes, diffraction peaks appeared at the 2θ value of 31.34, 36.87, 44.84, 55.82, 59.36 and 65.28, which correspond to 220, 311, 400, 422, 511 and 440 planes of cubic Co_3O_4 , respectively. These peaks are characteristic of Co_3O_4 and can be readily indexed as those of cubic structure fcc Co_3O_4 in accordance with JCPDS card no. 42-1467 (Song et al., 2013; Wu et al., 2010). For PANI, diffracted peaks appeared at $2\theta = 15.5$, 20.77, and 25.27, which are characteristic of PANI and indicate the polycrystalline structure of PANI (Rahy et al., 2008). The peaks at angles of $2\theta = 20.77$ and 25.27 correspond to the periodic repetition of benzenoid and quinoid rings in PANI chains (Shi et al., 2009). Chitosan shows characteristic peaks at $2\theta = 20.01$, 26.64

and 40.5 due to the presence of hydroxyl and amine groups in the chitosan structure (Yu et al., 2003). The XRD spectra of chitosan-grafted-polyaniline reveal a region of crystallinity from $2\theta = 18-24$, which suggests the grafting of PANI on a chitosan backbone (Tiwari et al., 2007). As evident from Figure 4.7, when Co_3O_4 nanocubes are incorporated into the polymer matrix, the broad peaks of PANI and chitosan disappear, possibly due to the nanocubes acting as impurities that retard the growth of the PANI crystallite and chitosan-grafted-polyaniline. The XRD patterns of PANI and chitosan-grafted-polyaniline composites have a diffracted peak at approximately $2\theta = 56$ with d-spacing = 1.60 \AA , which most likely originated from the divergent degree of protonation at all nitrogen atoms in emeraldine salt (Zong et al., 2002). Thus, the successful grafting of PANI onto chitosan and the formation of nanocomposites of Co_3O_4 and chitosan-grafted-polyaniline have been established by XRD analysis.

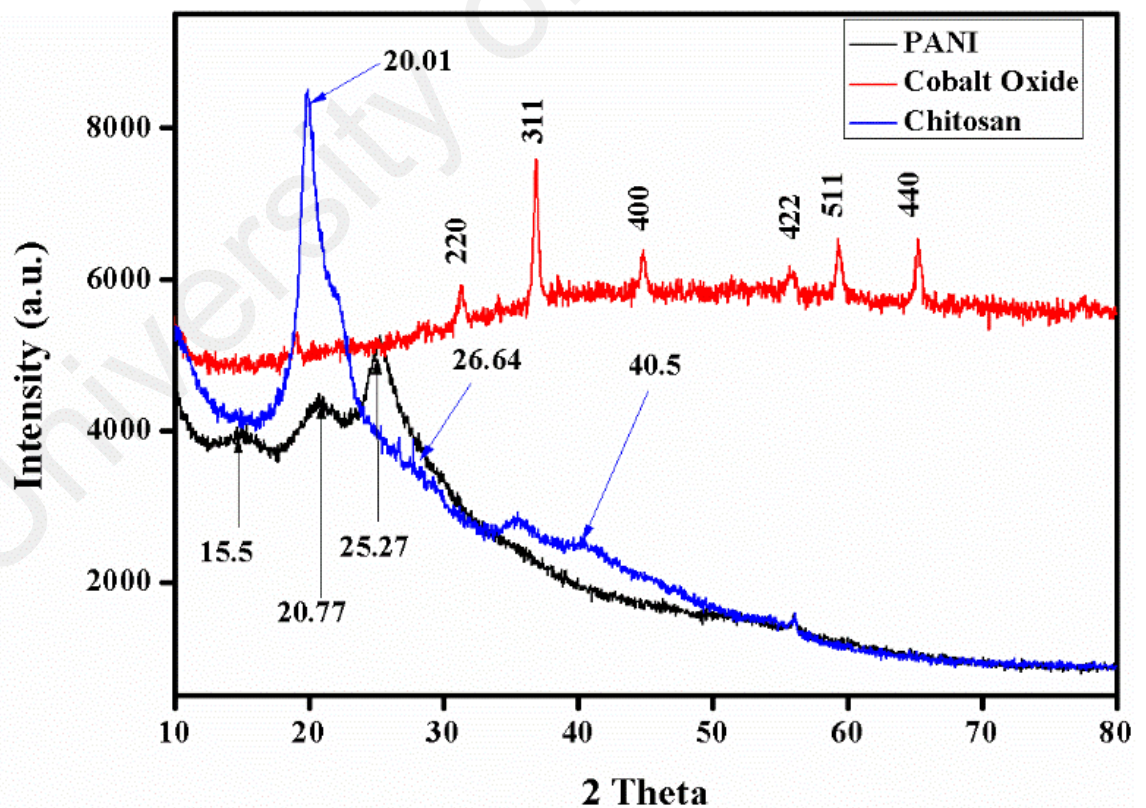


Figure 4.6: XRD patterns of Co_3O_4 , PANI and chitosan

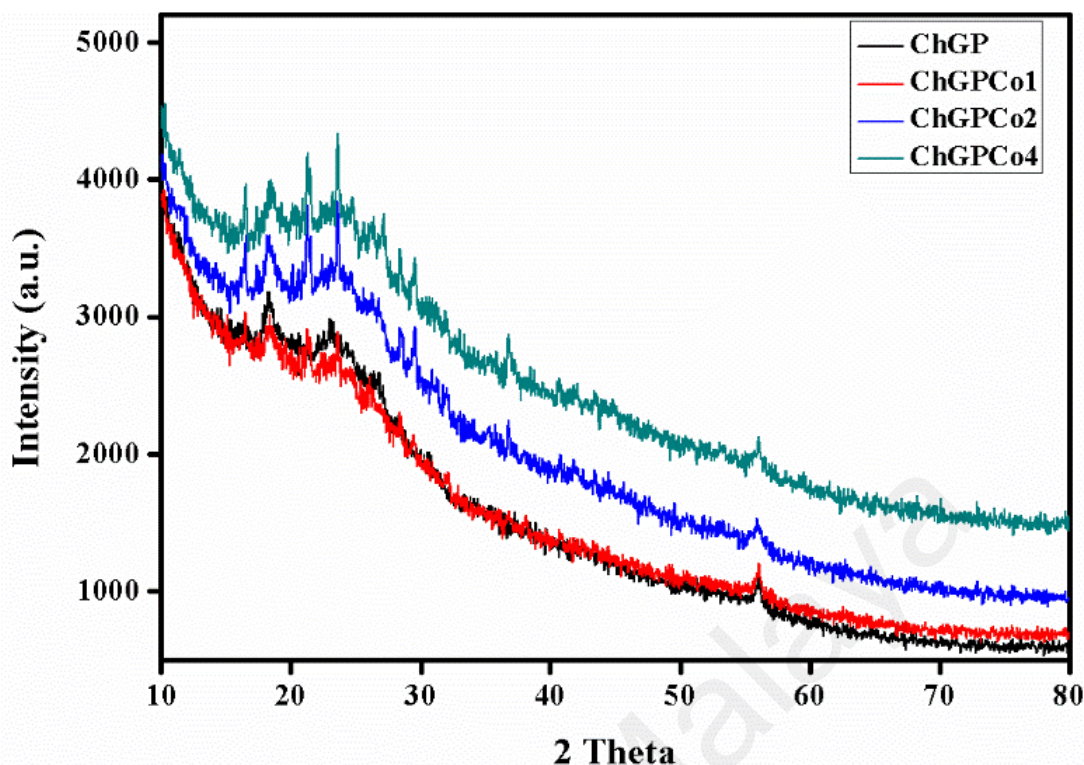


Figure 4.7: XRD patterns of ChGP, ChGPCo1, ChGPCo2 and ChGPCo4

4.3.1.4 XPS Analysis

X-ray photoelectron spectroscopy (XPS) analysis were employed for investigating the chemical nature of nanocomposite. Figure 4.8 (a) shows the survey spectra of ChGPCo2 illustrating the characteristic peaks of C, N, Cl, O and Co along with the Auger lines of Co(LMM), Co(LMV), O(KLL). The presence of chitosan in nanocomposite was confirmed by XPS spectra. Figure 4.8 (b) shows the high resolution C 1s core level spectra of ChGPCo2 which depicts three deconvoluted peaks at 284.77, 286.42 and 288.20 eV. The peak at 284.77 eV can be assigned to C-C bonding characteristic of polyaniline and chitosan (Aldissi et al., 1992). The peak at 286.42 eV can be assigned to C-N, C-O or C-O-C bonding that belongs to chitosan. The third peak at 288.20 eV may be assigned to C=O or C-O-C bonding characteristic of chitosan (Dambies et al., 2001) as it usually contains some acetamido groups that come from the original chitin. As shown in Figure 4.8 (c), the Co 2p core level spectrum for ChGPCo2 nanocomposites shows two peaks at 779.85 and 781.68 eV which are attributed to the Co 2p₁ and Co 2p₃ respectively. Hence

XPS studies clearly reveal the formation of the Co_3O_4 doped graft copolymer of chitosan and PANI.

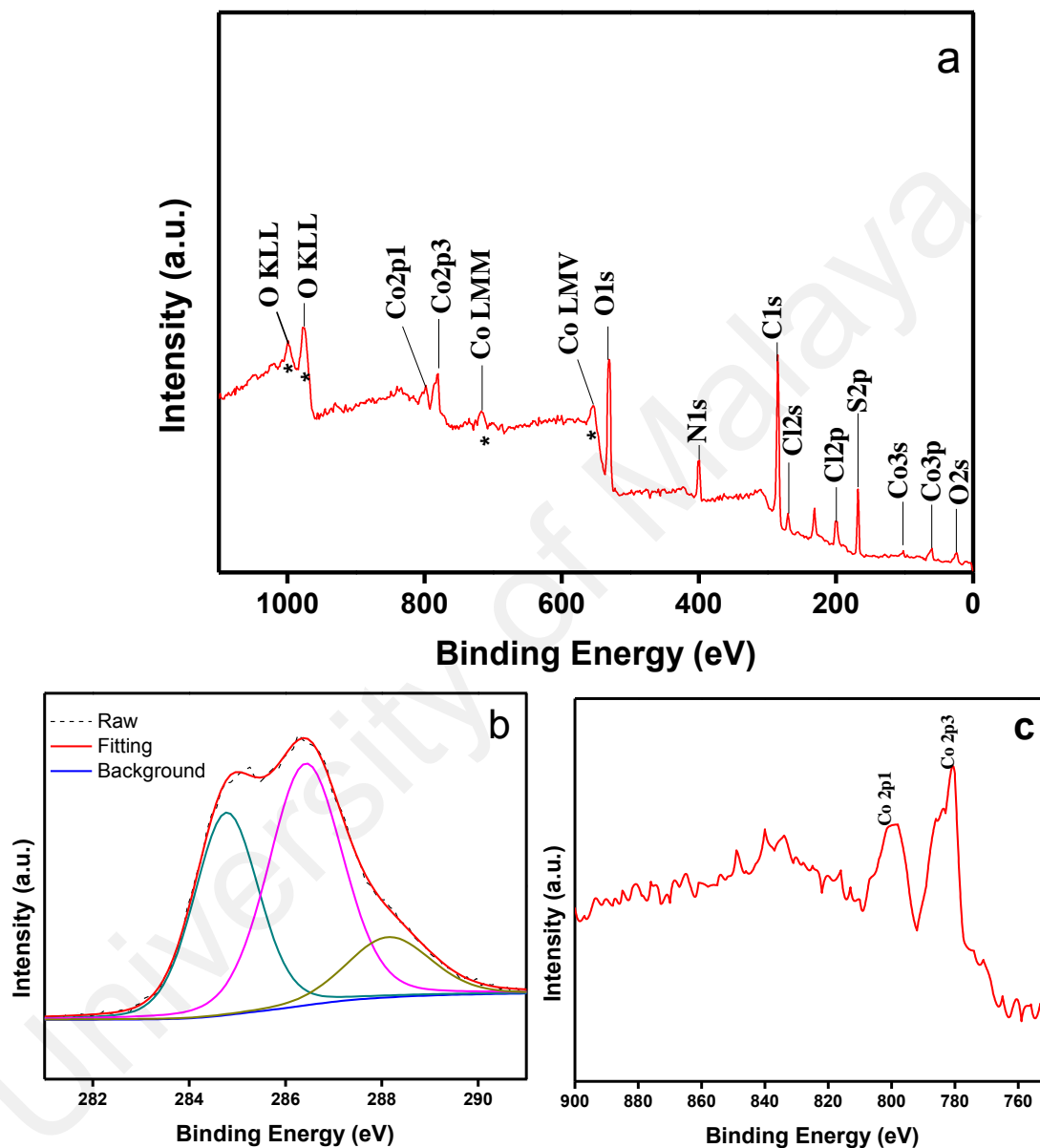


Figure 4.8: XP spectra of ChGPCo2 (a) Survey scan. The symbol * represents the Auger peaks; for Co(LMV), Co(LMM) and O(KLL) (b) C 1s core level and (c) Co 2p core level

4.3.1.5 UV-Vis Analysis

Figure 4.9 represents the UV-Visible spectra of chitosan, Co_3O_4 , PANI and ChGPCo2 respectively. As evident from Figure 4.9 (a) chitosan gives a flat absorption spectrum, showing no peaks in the range of 350 nm - 800 nm which is a characteristic of chitosan. Figure 4.9 (b) represents typical absorption spectrum of Co_3O_4 nanocubes where two distinct broad absorption bands in the range of 400 to 550 and 600 to 750 nm are observed which can be assigned to the $\text{O}^{2-} \rightarrow \text{Co}^{2+}$ and $\text{O}^{2-} \rightarrow \text{Co}^{3+}$ charge transfer process respectively (He et al., 2005). PANI shows two absorption bands in the range of 420 to 470 and 500 to 750 nm which are typical of the protonated form of PANI. The first absorption band can be assigned to the π - π^* transition of benzenoid rings, while second band can be assigned to the π - π^* transition of quinoid rings on the PANI chains. ChGPCo2 has optical absorption in the entire visible light region 400–800 nm as shown by its featureless diffuse spectrum. As ChGPCo2 exhibits absorption in the whole visible region, it is certain that it could function as effective light absorber and worthy photocatalysts. The band gap (E_g) of Co_3O_4 and PANI was further determined by using Perkin Elmer method of measuring the band gap energy (Dharma, 2015). The band gap of Co_3O_4 was calculated to be 1.6 eV which is close to the theoretical value of bulk Co_3O_4 (1.77eV). The band gap value for PANI was found to be 2.77 eV which is in well agreement with theoretical value of 2.8 eV.

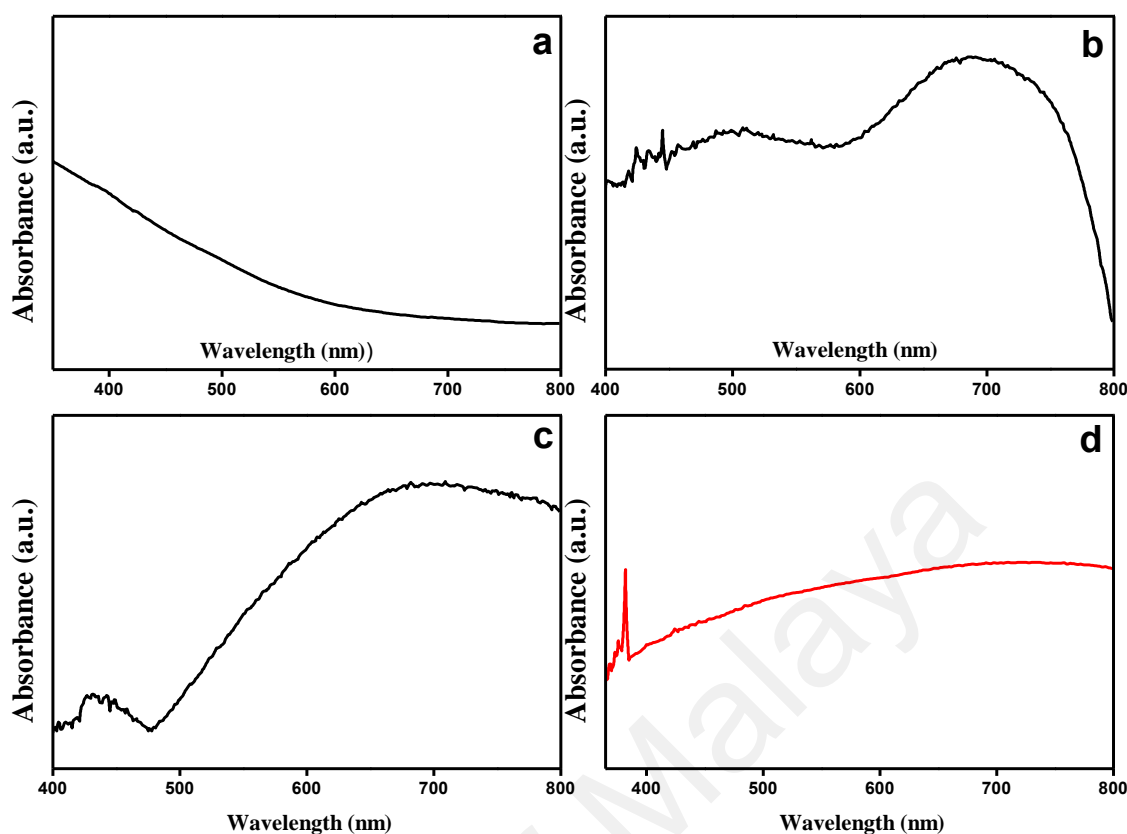


Figure 4.9: UV-Visible spectra of (a) chitosan, (b) Co_3O_4 , (c) PANI and (d) ChGPCo2

4.3.1.6 FTIR Analysis

The FTIR spectra of cobalt oxide nanocubes, chitosan, PANI and chitosan-grafted polyaniline composite are shown in Figure 4.10. The IR bands at 1560 cm^{-1} and 1480 cm^{-1} represent the characteristic C-C stretching of quinoid and benzenoid rings in PANI, respectively. The peak at 1297 cm^{-1} could be attributed to C-N and C=N stretching in PANI. The broad IR bands at $3400\text{--}3436\text{ cm}^{-1}$ can be attributed to the stretching mode of -OH and the primary amine group in chitosan. The IR peak at 1652 cm^{-1} corresponds to the C=O stretching in the amide groups of chitosan. The peaks at $2920\text{--}2877\text{ cm}^{-1}$ represent aliphatic -CH stretching vibrations. Two peaks at 667 cm^{-1} and 574 cm^{-1} in the spectrum of cobalt oxide are the characteristic peaks that confirm the spinel structure of Co_3O_4 . FTIR spectra of ChGPCo2 comprise peaks of chitosan and PANI. As a result of the overlapping of the -OH stretching of chitosan and the N-H stretching of PANI in graft copolymers, the IR band at approximately 3400 cm^{-1} became less intense and broad. These reduced intensities indicate that a considerable amount of O-H at chitosan has been

grafted with polyaniline chains (Hosseini et al., 2009). Peaks around 2920-2852 cm^{-1} can be attributed to N-H stretching with hydrogen-bonded amine groups and free -OH stretching. Peaks around 1514-1417 cm^{-1} are due to the quinoid and benzenoid stretching of PANI. IR peaks at 807 cm^{-1} and 1127 cm^{-1} were allocated to out-of-plane C-H bending and in-plane C-H bending. The characteristic peaks at 667 and 574 cm^{-1} in Co_3O_4 were detected at 647 and 559 cm^{-1} in Co_3O_4 -doped chitosan-grafted-polyaniline nanocomposites. The intensity of the peaks significantly enhances with an increased dopant concentration. This slight shifting of the band towards red could be attributed to some amount of weak Van der Waals attraction between the polymer chain and Co_3O_4 . Hence, the FTIR studies clearly indicate the formation of a graft copolymer of polyaniline on the chitosan backbone with some interaction between PANI and Co_3O_4 .

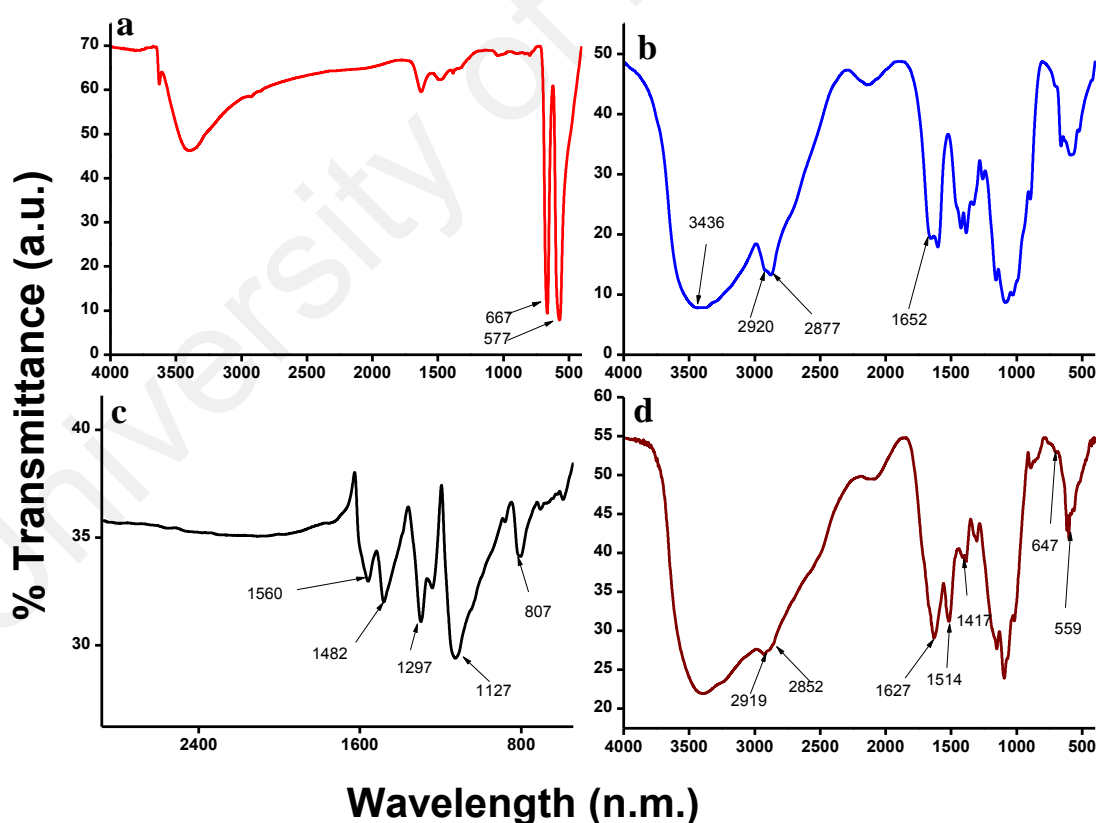


Figure 4.10: FTIR spectrum of (a) Co_3O_4 , (b) PANI, (c) chitosan and (d) ChGPCo2

4.3.2 Photodegradation Studies

4.3.2.1 Photocatalytic Degradation of MB Under UV Illumination

The photocatalytic aqueous-phase degradation of MB in the presence of chitosan, ChGP and Co_3O_4 nanocube-doped nanocomposites was investigated under UV-light illumination at ambient temperature. The adsorption of MB on the surface of the catalyst under dark conditions was monitored for 80 minutes via UV-vis absorption spectra as illustrated in Figure 4.11 (a) in order to attain adsorption-desorption equilibrium. It is apparent from Figure 4.11 (a) that the adsorption of MB molecules on the surface of the catalyst increased with time, and within 20 minutes, most of the catalyst surface was saturated with MB. After attaining equilibrium, approximately 9%, 12.5%, 18.4%, 19.8%, and 17.4% of MB was adsorbed on the surface of chitosan, ChGP, ChGPCo1, ChGPCo2 and ChGPCo4, respectively. The adsorption of MB increases gradually after the grafting of PANI onto chitosan, and this adsorption is further enhanced by doping with Co_3O_4 nanocubes, possibly due to some molecular interaction of nanoparticles with MB. As the percentage of Co_3O_4 increased from 2 wt% (w.r.t. aniline) to 4 wt%, there was a slight decrease in adsorption that could be caused by the reduction in the active surface area of catalyst due to the agglomeration of nanocubes at a high doping percentage.

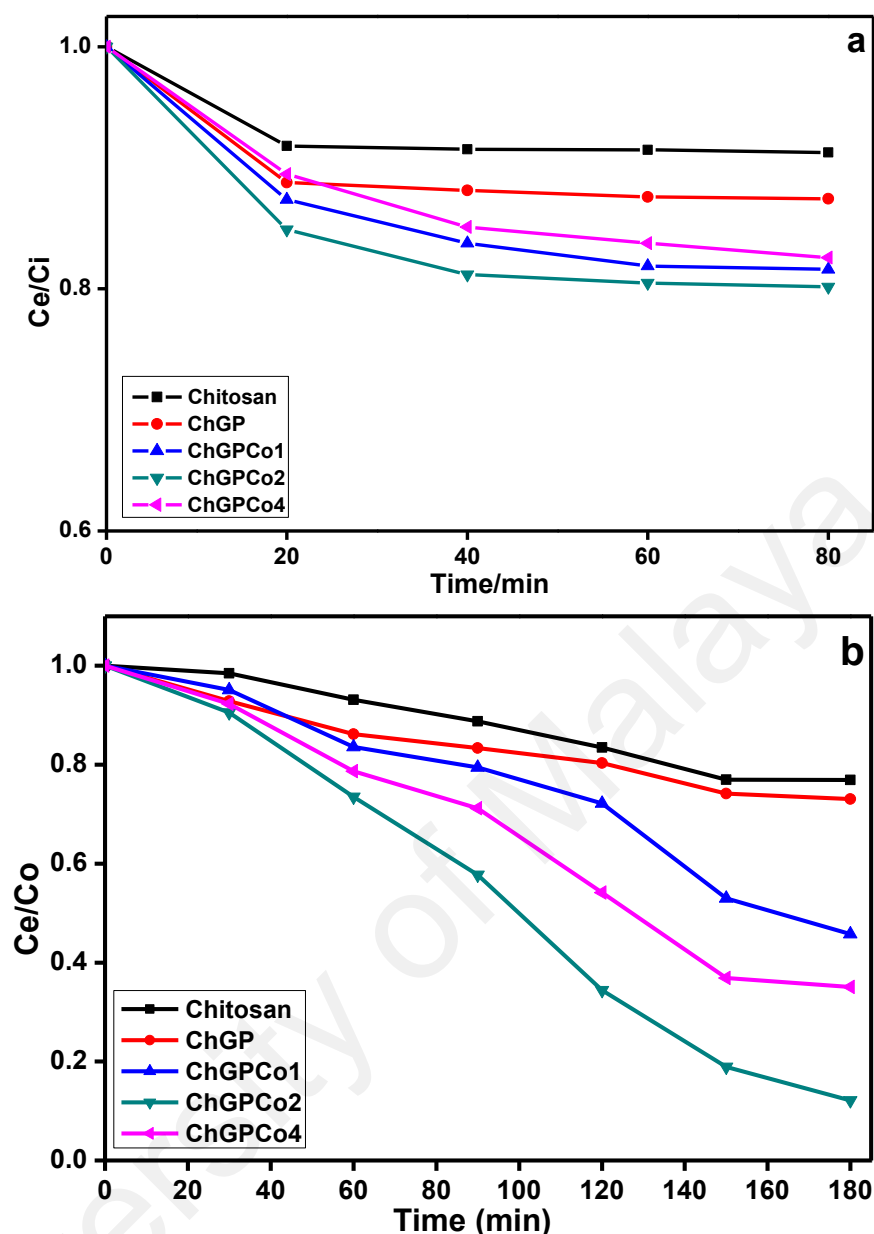


Figure 4.11: (a) Adsorption–desorption equilibrium rate of MB under dark conditions versus time in the presence of various photocatalysts (b) Photodegradation rate of MB at different time intervals in the presence of various photocatalysts

As seen from Figure 4.11 (b), chitosan and ChGP have low photocatalytic activities compared to the photocatalytic activities of ChGPCo1, ChGPCo2 and ChGPCo4. Figure 4.12 (a) illustrates the percentage decomposition of MB at different intervals of time, signifying the following degradation trend: ChGPCo2>ChGPCo4>ChGPCo1>ChGP>chitosan. Figure 4.12 (b) depicts the UV-vis adsorption spectra of the ChGPCo2 nanocomposite irradiated under UV illumination for different time intervals. As evident from the figure, the decrease in the intensities of the

adsorption band with the increasing irradiation time clearly indicates the efficient degradation of MB by a photocatalytic phenomenon. Nearly 88% of MB degraded within an interval of 180 minutes, predicting an enhanced photocatalytic activity of ChGPCo2 nanocomposite over chitosan, ChGP, ChGPCo1 and ChGPCo4, where the decompositions were approximately 23%, 27%, 54% and 65%, respectively. In the case of chitosan, the degradation is nearly 23% after 180 minutes, which could be due to the self-decomposition of MB because under UV light, MB can be self-decomposed to an extent of approximately 20% in a period of 2 hours (E. Subramanian et al., 2014). The extent of decomposition increases to 27% upon the grafting of PANI onto a chitosan backbone, which indicates some amount of photocatalytic phenomenon in ChGP due to the conducting chains of PANI. With nanocomposites doped by Co_3O_4 , the degradation was enhanced from ChGPCo1 to ChGPCo2 and decreased from ChGPCo2 to ChGPCo4. Thus, 2 wt% Co_3O_4 nanocubes (w.r.t. aniline) was predicted to be an optimum photocatalyst composition.

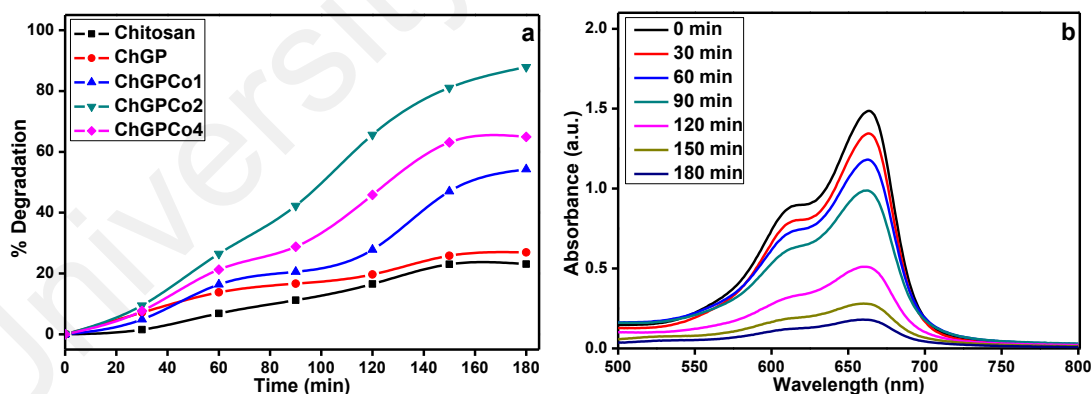


Figure 4.12: (a) Percentage degradation of MB in the presence of various photocatalysts (b) UV-vis absorption spectra of MB aqueous solution at different times in the presence of ChGPCo2 as a photocatalyst

MB itself can decompose in UV light to a certain extent by absorbing energy from UV irradiations forming singlet and triplet species. These singlets and triplets that are produced by MB molecules are extremely energetic and active, which immediately react

with the available oxygen to form advanced oxidation species (AOS) comprising superoxide, peroxide and hydroxyl radicals. These AOS are responsible for the degradation and mineralisation of MB. The possible mechanism of degradation of MB is illustrated in Figure 4.13. This decomposition, however, is insignificant because it can only degrade a very small percentage of MB in the absence of any photocatalyst. Chitosan is a biopolymer that has a tendency to form strong interactions with organic molecules through hydrogen bond formation due to the presence of amine and hydroxyl groups in its chain. This property of chitosan can be exploited to enhance the adsorption of MB on the surface of a catalyst, which is a prime requisition of efficient catalysis. Chitosan by itself does not enhance the degradation of MB under UV light but augments the adsorption of dye onto the surface of the catalyst. Chitosan-grafted PANI and its nanocomposites with Co_3O_4 nanocubes are capable of generating AOS under UV irradiation, leading to the degradation of MB. PANI in its conductive emeraldine salt form exhibits enhanced electron mobility, and these electrons can be excited by photoillumination. The electrons that are present in HOMO of PANI adsorb the energy from UV light and jump to LUMO through $\pi\text{-}\pi^*$ transitions, which are the characteristic transitions of PANI. These transitions in PANI are responsible for the generation of electrons and holes in the conduction band (LUMO) and valence band (HOMO) of PANI molecules, respectively, thereby leading to the formation of AOS and degradation of MB. Very few electron-hole pairs generated in PANI molecules migrate on the surface to initiate the series of photochemical reactions, while most of them recombine rapidly, thus reducing the efficiency of PANI to be used as an efficient photocatalyst alone. To enhance the photocatalytic efficiency of chitosan-grafted-polyaniline, semiconducting Co_3O_4 nanocubes were incorporated into the graft copolymer during the polymerization process. In Co_3O_4 nanocube-doped nanocomposites, the d-orbital conducting band of Co_3O_4 undergoes chemical bond interaction with LUMO of PANI upon UV irradiation. Due to

these electronic interactions, the LUMO of PANI came close to the d-orbital conducting band of Co_3O_4 , and electrons were injected from the conduction band of Co_3O_4 to LUMO of PANI. Thus, the electrons that were injected into the LUMO of PANI reached the surface and reacted with O_2 to form peroxides and superoxide radicals. The corresponding holes that were generated in the valence band of PANI and Co_3O_4 react with H_2O to form hydroxyl radicals, which again degrade MB as per Figure 4.13. Thus, Co_3O_4 enhances the charge separation in PANI to facilitate the formation of AOS, whereas chitosan aids in the adsorption of MB on the surface of the catalyst, thereby increasing the overall efficiency of the photocatalyst. Figure 4.14 provides the schematic illustration of the possible mechanism of MB degradation in the presence of Co_3O_4 -doped nanocomposites.

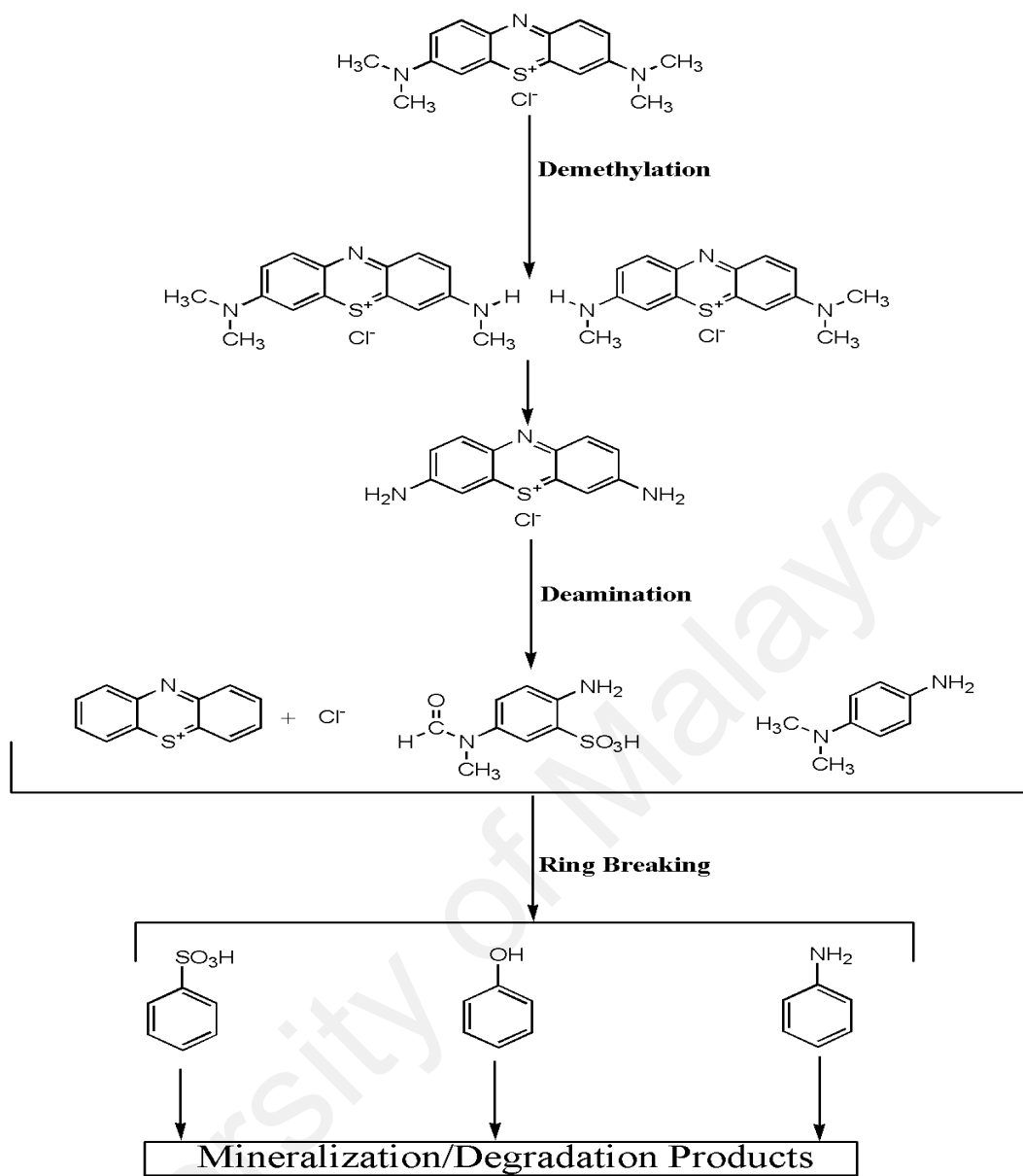


Figure 4.13: Proposed mechanism for the photocatalytic degradation of MB under UV irradiation

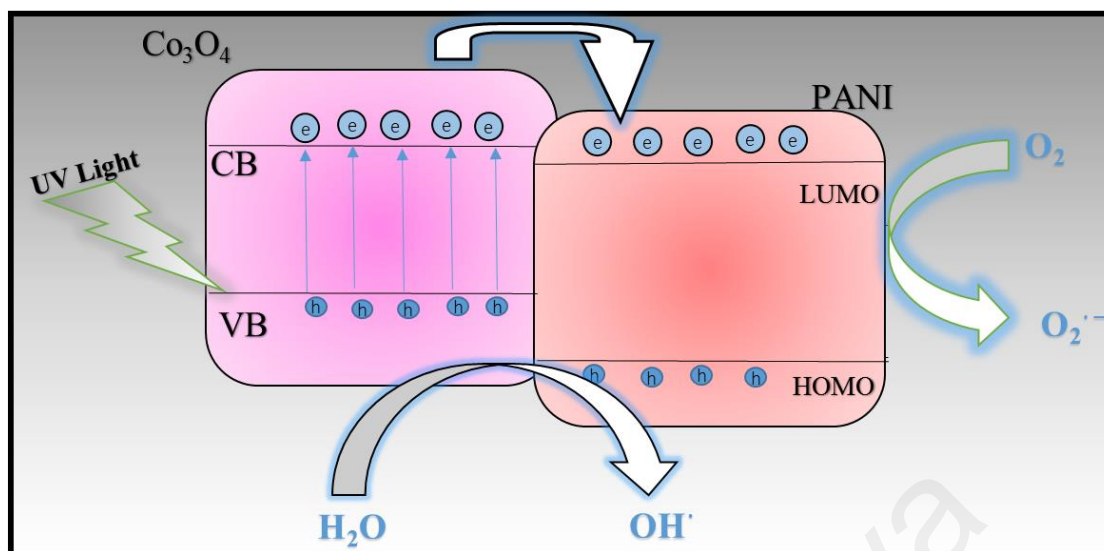


Figure 4.14: Schematic illustration for the formation of advanced oxidation species in Co_3O_4 -doped chitosan-grafted-polyaniline hybrid photocatalyst

4.3.2.2 Comparison of Photocatalytic Efficiencies

Table 4.1 shows the comparison of photocatalytic efficiencies of the present catalyst with those of others reported in literature. The prepared catalyst at an initial dye concentration of 10 mg/L with irradiation time of 180 minutes showed the photodecomposition efficiency of 88%. In earlier studies for the degradation of MB, Zhang et al.(Zhang et al., 2008) reported 88% degradation, Wang et al.(F Wang et al., 2010) reported 81.74% degradation, Kuo et al.(Kuo et al., 2011) reported 67% degradation, Soltani et al.(Soltani et al., 2012) reported 73% degradation, Autin et al.(Autin et al., 2013) reported 88% degradation, Dai et al.(Dai et al., 2014) reported 87% degradation, Subramanian et al.(E. Subramanian et al., 2014) reported 76.58% degradation with different time of irradiation as shown in Table 4.1. In a very recent work Xia et al.(Xia et al., 2015) have reported 95% photodecomposition of MB. In this perspective, it is well established that our catalyst renders enhanced efficiency.

Table 4.2: Comparison of photocatalytic efficiencies

Catalyst	Dye Degraded	% Degradation	Degradation time (min.)	Reference
PANI sensitized TiO ₂	MB	88	300	(Zhang et al., 2008)
PANI-TiO ₂	MB	81.74	120	(F Wang et al., 2010)
N ₂ modified TiO ₂	MB	67	240	(Kuo et al., 2011)
Zn/CdS	MB	73	360	(Soltani et al., 2012)
TiO ₂	MB	88	120	(Autin et al., 2013)
AgBr/ZnO	MB	87	240	(Dai et al., 2014)
PANI-TiO ₂	MB	76.58	120	(E Subramanian et al., 2014)
FeOOH-LDO	MB	95	180	(Xia et al., 2015)
Chitosan-grafted-PANI/Co ₃ O ₄	MB	88	180	This work

4.3.2.3 Reproducibility of the photocatalysts

Figure 4.15 shows the reproducibility of ChGPCo₂ as photocatalyst for MB degradation. The photocatalyst after first cycle was recovered by centrifugation and filtration followed by thorough washing with DI water, dried at 80 C in vacuum oven for two hours and subsequently employed as photocatalyst for second and third cycle in order to examine their photocatalytic efficiencies. ChGPCo₂, ChGPCo₂-R1 and ChGPCo₂-R2 (where R represents repeatedly used catalyst) denotes the photocatalyst for first, second and third cycle which shows the marginal decrease in their photocatalytic efficiencies with each repeated cycle. Table 4.2 represents the photocatalytic efficiencies of

photocatalyst which shows that the efficiency of the catalyst decreases in second and third run. This decrease in efficiency may be due to the fact that a considerable amount of unavoidable weight loss occurred during recovery and purification of photocatalyst. This weight loss contribute to the decrease in photocatlytic efficiency of catalyst in each repeated cycle (E. Subramanian et al., 2014). Moreover the decrease in photocatlytic activity can also be attributed to the adsorption of degradation by-products on the active sites of photocatalyst surface thereby decreasing the number of available photoactive sites (Silva et al., 2006).

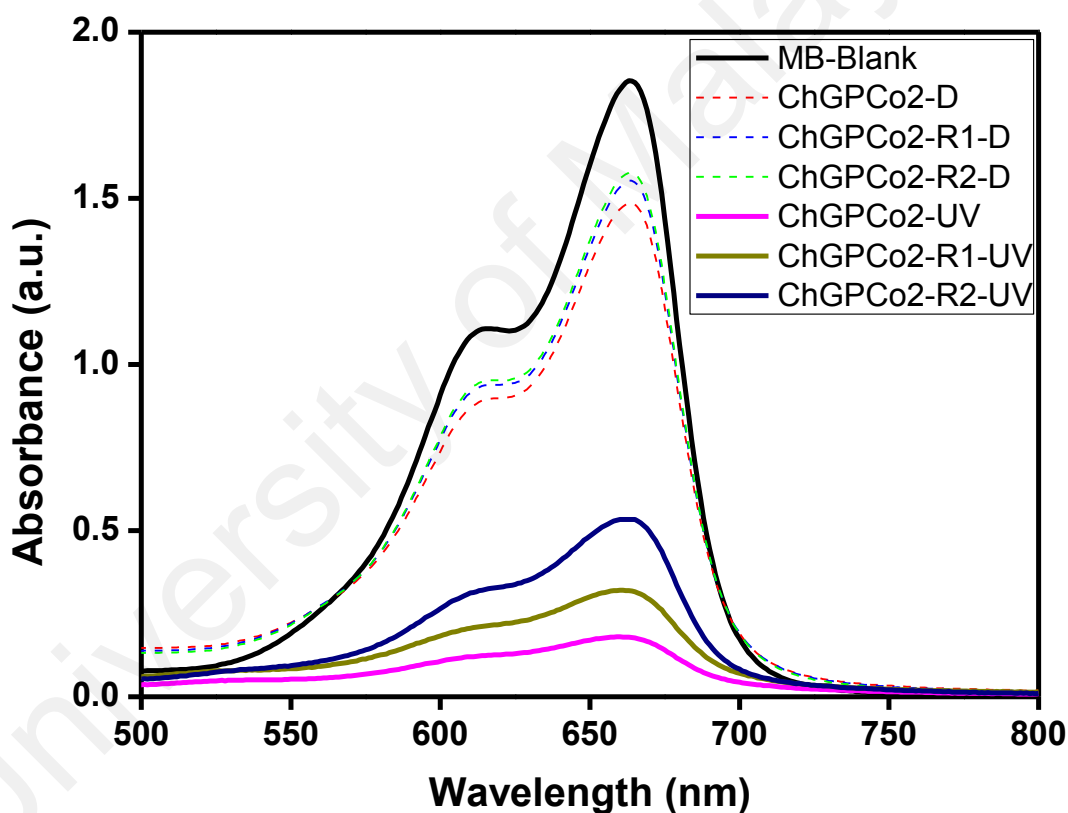


Figure 4.15: Reproducibility of ChGPCo2. (The symbol D represent dark adsorption whereas R represents repeated cycle)

Table 4.3: Percent of MB dye dark adsorption and photodecomposition

Catalyst	% of dark adsorption	% of photodecomposition
ChGPCo2	19.80%	88%
ChGPCo2-R1	16%	79.6%
ChGCo2-R2	14.88%	66.16%

4.4 Conclusions

Chitosan-grafted-polyaniline and Co_3O_4 nanocube-doped nanocomposites have been successfully synthesized through an in situ oxidative polymerization technique. Co_3O_4 nanocubes were successfully incorporated into the cross-linked network of the polymeric matrix. The present investigation highlights the synergistic effect of the conducting copolymer and the semiconducting metal oxide, which leads to the enhancement of the photocatalytic efficiency of the nanocomposite. The synthesized polymeric nanocomposite exhibits greater photocatalytic activity and degrades MB efficiently within a short duration of time. The synthetic methodology proposed here can be used to synthesise Co_3O_4 nanocomposites with other conducting polymers, which may address the present-day issue of environmental pollution.

**CHAPTER 5: SrTiO₃ NANOCUBE-DOPED POLYANILINE
NANOCOMPOSITES WITH ENHANCED PHOTOCATALYTIC
DEGRADATION OF METHYLENE BLUE UNDER VISIBLE LIGHT³**

5.1 Introduction

Presently one of the most essential issues in pollution control from an environmental and biological point of view is the removal of toxic chemicals from waste water. Due to the deliberate or unintentional discharge of dye effluents into aquatic bodies, the textile industry presents a worldwide pollution problem causing a major impact on the quality of available water resources. Textile treatment and dyeing contributes around 17-20% of the total industrial water pollution as per the World Bank estimate (Chan et al., 2011; Huang et al., 2014). 3,7-Bis(dimethylamino)-phenothiazin-5-ium chloride, generally known as methylene blue (MB), is a heterocyclic organic dye which is commercially used for various potential applications including food additives, plastic, paper, pharmaceutical, textile and leather industries (Bhattacharyya et al., 2005; Parida et al., 2010). It is an as an odourless, dark-green solid powder which produce a navy blue solution upon dissolution in water and is an extremely harmful chemical that is primarily used as a dye. The ample amount of dye effluents dumped into the environment may possibly result extreme oncogenic effects including vomiting, diarrhoea, cyanosis, jaundice, quadriplegia, tissue necrosis, distortion of ecosystem and discomposure in aquatic life, which oblige the effective and ample degradation of MB (Adams et al., 2007; Gouamid et al., 2013; Vinothkannan et al., 2015; Wu et al., 2006). Photocatalysis has appeared as one of the most promising techniques amongst the wide variety of approaches to degrade menacing waste materials, specifically organic compounds, to less noxious or less

³ This chapter has been published in *Polymers*. *Polymers* **2016**, 8, 27 (Q1, Impact Factor: 3.68)

harmful materials, because it provides a simple method of exploiting the energy of either natural sunlight or artificial illumination, such as ultraviolet light, microwaves, etc. (Riaz et al., 2014; Shahabuddin et al., 2015b; Zhou et al., 2015).

Due to the remarkable photochemical, physicochemical and electrochemical properties of inorganic semiconducting material, they have found wide variety of applications in the field of photoluminescence (Talpin et al., 2009), photovoltaics (Clifford et al., 2011; Gong et al., 2012), photochromism (Kazuma et al., 2012; Matsubara et al., 2007) and photo degradation (Huang et al., 2014; Shahabuddin et al., 2015b). The advanced oxidation process (AOP), an important property of semiconductors, have attracted the attention of researchers for the treatment of dye wastewater with enhanced degradation efficacy, physical and chemical properties and low toxicity. Owing to their filled valence band (VB) and empty conduction band (CB) in the ground state, semiconductors act as efficient photo- sensitizers in photocatalytic reactions. TiO_2 , one of the wide band gap inorganic semiconductor is often used for photoelectric conversion and photocatalytic treatment for degrading wide range of organic pollutants from water since it is non-toxic, photostable, reusable, and comparatively inexpensive (Fujishima et al., 2000; Tang et al., 2008; F Wang et al., 2010). Titanates, as compared to TiO_2 , demonstrate an enhanced intrinsic chemical reactivity which is advantageous for designing complex titanate-based composite materials. Improved photocatalytic activity and chemical stability have been demonstrated by various titanates namely CaTiO_3 (Demirors et al., 2009), SrTiO_3 (Huang et al., 2014; Nakashima et al., 2013; Shen et al., 2013), BaTiO_3 (Lee et al., 2013), and In_2TiO_5 (Liu et al., 2011). Since the conduction band edge of strontium titanate is 200 mV more negative than TiO_2 therefore it provides better energy assimilation for photocatalysis. SrTiO_3 has been exploited extensively for

degradation of organic pollutants and water splitting under UV illumination (Huang et al., 2014). However, the two foremost limiting aspects for the photocatalytic efficiency, namely low energy conversion due to rapid recombination of electron-hole (e^-h^+) pairs and wide band gaps of semiconductors, restricts photo-absorption only within the UV region. Thus numerous efforts have been made to enhance the photoresponse of semiconductors to the visible range to increase the photocatalytic properties (Riaz et al., 2015a; F Wang et al., 2010).

Recently conducting polymers with extend π -conjugated electron systems have been extensively explored for their electronic and optoelectronic properties. Due to their good environmental stability, high absorption coefficients in the visible spectrum and high electron-hole mobility, conducting polymers has attracted a considerable attention by researchers. Owing to their significant electron-hole mobility properties, conducting polymers have demonstrated to perform as stable photo-sensitizers for semiconductors such as TiO_2 , ZnO , WO_3 , ZnS etc. (Autin et al., 2013; Chen et al., 2012; Golsheikh et al., 2015; Sadek et al., 2008). In multidisciplinary scientific research areas, conducting polymers such as polypyrrole, polyaniline, polyphenylene, polythiophene, and polyacetylene have been exploited broadly including sensors (Sadek et al., 2006), batteries (Sengodu et al., 2015), electronics, thermoelectric, electromagnetic, electroluminescence, and electromechanical applications (Bhadra et al., 2009; Hu et al., 2015; Shih et al., 2015). Composite materials comprising of conjugated polymers and wide band gap inorganic semiconductors have been widely investigated for exploring optical, photocatalytic and photoelectric conversion applications (Gustafsson et al., 1992; Jang et al., 2000; Luzzati et al., 2002; Pron et al., 2002). Polyaniline (PANI), due to its notable physical and chemical properties such as thermal stability, high conductivity, easy

preparation procedure, better processability, low cost and wide variety of applications (Riaz et al., 2015a), is one of the vastly investigated conducting polymers amid all the conducting polymers. Additionally, PANI is an efficient electron donors and good hole transporter upon visible-light excitation. In combined state with a wide band gap semiconductors PANI can transfer the electrons generated upon visible-light irradiation to the conduction band of semiconductor such as TiO_2 since the lowest unoccupied molecular orbital (LUMO) level of PANI is energetically higher than the conduction band (CB) edge of TiO_2 (F Wang et al., 2010). As a consequence, substantial amount of interfacial charge transfer occurs and recombination of electron-hole pair is considerably reduced which could provide a significant photoresponse in solar light range of spectrum. This development will benefit the application of the photocatalysis under sunlight.

The present study centres on the degradation of methylene blue (MB) dye by polyaniline doped with SrTiO_3 nanocubes synthesized via in situ oxidative polymerization. SrTiO_3 nanocubes were synthesized using the simplistic hydrothermal technique and integrated into the polymer matrix during polymerization. PANI due to its high electron mobility, enhanced excitement of electrons under photo illumination and facile method of synthesis was chosen as a base conducting polymer for designing efficient photocatalyst. Furthermore, SrTiO_3 doping synergistically enhanced the generation of electrons and holes in combination with PANI to augment the degradability of MB. To evaluate the photocatalytic efficiency of synthesized polymeric composites, the photocatalytic treatment of MB in aqueous phase for its degradation under visible-light irradiation was chosen as a model reaction. Furthermore, the synthesized composite photocatalysts were characterized for morphological analysis, molecular structure and

photo-responsive properties and the effects of weight ratio of polyaniline to SrTiO₃ on the photocatalytic activities were studied.

5.2 Experimental Section

5.2.1 Materials

Aniline (Fluka, $\geq 99\%$) was distilled under reduced pressure and stored in the dark before use. Ammonium peroxydisulfate, APS (Merck, $\geq 99\%$), strontium hydroxide octahydrate (Sigma Aldrich, 95%), titanium(IV) oxide, anatase (Sigma Aldrich, 99.7%), sulfuric acid, H₂SO₄ (Sigma Aldrich, 98%), sodium hydroxide, NaOH (Sigma Aldrich, 98%), methanol (Merck, 99.9%) and acetone (Merck, 95%) were used as received without further purification. All of the reagents that were involved in the experiments were of analytical grade. Deionised water was used throughout the entire study.

5.2.2 Synthesis Methodology

5.2.2.1 Synthesis of SrTiO₃ Nanocubes

A typical hydrothermal technique was utilised for the synthesis of SrTiO₃ nanocubes. The calculated amount of Strontium hydroxide octahydrate (1.4 g) was dissolved in 20 ml NaOH (3 M) under constant stirring. To this solution, Titanium dioxide solution prepared by mixing 0.4 g of TiO₂ in 20 ml NaOH (3 M) was added dropwise at a rate of one drop per second with vigorous stirring. After 30 minutes of stirring, 40 ml of the reaction mixture was transferred to a 100 mL Teflon-lined stainless steel autoclave and subjected to hydrothermal treatment at 130°C for 72 hr. The obtained precipitate of SrTiO₃ nanocubes were then washed thoroughly with deionised water several times and dried in a vacuum oven at 100 millibar pressure and 60°C for 24 hours.

5.2.2.2 Preparation of Polyaniline (PANI)

Polyaniline was synthesized by the oxidative polymerization of distilled aniline that was dissolved in aqueous H_2SO_4 (0.5 M), using ammonium persulfate (APS) as an oxidant. Calculated amount of aniline (0.4 M, 40 mmol) was dissolved in 100 ml of an aqueous solution H_2SO_4 , and APS (0.4 M, 40 mmol) was dissolved in 100 ml H_2SO_4 (0.5 M). The oxidant solution was then added slowly to the aniline solution with continuous stirring at 0-5°C. The reaction mixture was stirred continuously for 3 hours and kept in refrigerator overnight to complete the reaction. The reaction mixture was then filtered and washed with H_2SO_4 (0.1 M) until the filtrate became colourless and subsequently with deionised water until the filtrate became neutral. It was then washed with mixture of acetone and methanol (1:1 ratio) to remove unreacted monomer and oligomers. The obtained polymer was dried in a vacuum oven at 100 millibar pressure and 60°C overnight. The green colour of the obtained polymer indicated the formation of conductive polyaniline emeraldine salt.

5.2.2.3 Preparation of PANI-SrTiO₃ Nanocomposite

SrTiO₃ nanocube-doped nanocomposites were prepared with different wt% of SrTiO₃ (250, 500, and 750 mg with respect to 0.4 M aniline, 40 mmol). Calculated amount of SrTiO₃ nanocubes were dispersed in 5 ml of deionised water by sonication and added dropwise to aniline solution (0.4 M, 40 mmol) in H_2SO_4 with vigorous stirring. The resulting mixture was sonicated for a few minutes until it became uniform. The work-up procedure was the same as described in the previous section. The obtained nanocomposites were labelled as P-Sr250, P-Sr500 and P-Sr750 indicating 250, 500, and 750 mg of SrTiO₃ nanocubes with respect to 0.4 M aniline, respectively. The dried

samples were measured to calculate yield and percentage of PANI loading in the nanocomposites (Table 5.1) according to the following equation:

$$\% \text{ PANI loading} = \{(W_1 - W_2) / W_0\} \times 100 \quad (5.1)$$

where W_1 is the yield (g), W_2 is the mass of SrTiO₃ nanocubes (g) and W_0 is the mass of aniline (g).

Table 5.1: Yield and % PANI loading in various nanocomposites.

Catalyst	Amount of SrTiO ₃ (g)	Yield (g)	% PANI loading
PANI	-	3.512	-
P-Sr250	0.250	3.6846	92.2
P-Sr500	0.500	3.6701	85.1
P-Sr750	0.750	3.6370	77.5

5.2.3 Characterisation Techniques

The surface morphological and elemental analysis of the synthesized product was conducted using a JEOL JSM-7600F field emission scanning electron microscope operated at 10 kV. The size and shape of the obtained SrTiO₃ nanocubes were studied using a JEOL JEM-2100F high-resolution transmission electron microscope. Thermal stability investigations were carried out using Perkin Elmer TGA6 under an N₂ atmosphere at a heating rate of 10°C/min. Then, 10 mg of dried sample was loaded inside the alumina crucible, and the weight changes were monitored from 35°C to 900°C. X-ray diffraction (XRD) patterns were recorded using an Empyrean X-ray diffractometer from $2\theta = 10^\circ$ to 90° using Cu K α radiations ($\lambda = 1.5418 \text{ \AA}$) at a scan rate of 0.02 sec^{-1} . Surface area analysis were carried out by nitrogen adsorption/desorption isotherms at 77 K using a Micromeritics Tristar II ASAP 2020 system. The thermodynamic based Barrett-Joyner-Halenda (BJH) method was used to determine the pore size data by using the desorption

branch of the isotherm whereas specific surface areas were measured using the Brunauer-Emmett-Teller (BET) method. Diffuse reflectance spectra were recorded with UV-vis spectrophotometer, Shimadzu model UV-2550 against BaSO₄ white background. Fourier transform infrared (FT-IR) spectra of the powdered samples were recorded using a Perkin Elmer RX1 FT-IR ATR spectrometer in the range of 400–4000 cm⁻¹ in spectral-grade KBr pellets.

5.2.4 Measurement of Photocatalytic Activities

The prepared samples were evaluated for photocatalytic activities by monitoring the degradation of methylene blue (MB) dye in the aqueous phase. In a typical experiment, 30 mg of the prepared nanocomposite powder was dispersed in 100 mL of an aqueous solution of MB with an initial concentration of 10 mgL⁻¹ in quartz vessel. The adsorption-desorption equilibrium was achieved by stirring the mixture in a dark environment for 60 minutes. The photocatalytic degradation was then conducted by irradiating the above mixture using a 150 W Xenon Arc Lamp emitting solar light mimicking 1 sun placed at a distance of 3 centimeters from solution. To maintain the uniform dispersion of photocatalyst particles, the mixture was stirred continuously. Then, 3 ml of the dye suspension was withdrawn at a regular time interval and centrifuged. The UV-visible absorption spectra of the supernatant solution were analysed using a UV-visible spectrometer (Thermo Scientific Evolution) in 1 cm quartz cuvettes to monitor the characteristic absorption peak of MB.

5.3 Result and Discussion

5.3.1 Characterization

5.3.1.1 Morphological Analysis of Nanocomposites

The structural characteristics and morphologies of PANI, SrTiO₃ and SrTiO₃ nanocubes-doped polyaniline were examined by using FESEM. Figure 5.1 (a) illustrates the morphology of PANI which showed a flake-like structure as the characteristic structure of PANI. Figure 5.1 (b) and Figure 1(c) show the morphology of the strontium titanate nanocubes at different magnifications. These images clearly reveal the formation of cube-shaped strontium titanate nanoparticles with an approximately uniform particle size. Additionally, to confirm the formation of strontium titanate nanocubes the synthesized nanoparticles were examined through TEM. Figure 5.2 demonstrates the TEM micrograph of strontium titanate with selected area electron diffraction (SAED) pattern (inset) which clearly exhibit the presence of cube-shaped crystalline particles in the nano range, confirming the formation of strontium titanate nanocubes. Figure 5.1(d) represents SrTiO₃ nanocube-doped polyaniline nanocomposite material P-Sr500 revealing the formation of granular polymeric network. As evident from the Figure A-1 (appendix A), the flakes like morphology of PANI was completely transformed into granular nanocrystalline polymeric nanocomposite material upon addition of SrTiO₃ into the polymeric matrix. Figure A-2 (appendix A) shows the TEM image of P-Sr500 which indicate the presence of SrTiO₃ nanoparticles into the polymer matrix of PANI.

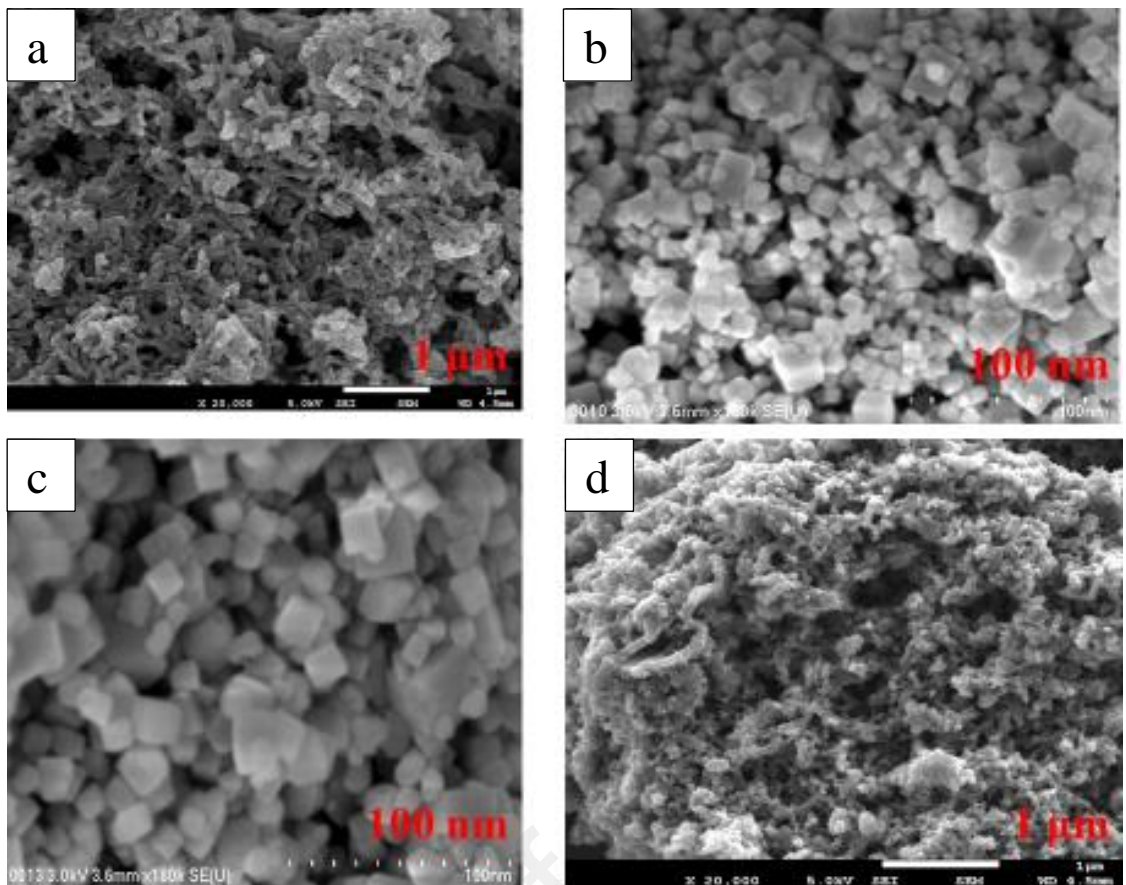


Figure 5.1: FESEM micrographs of (a) PANI, (b and c) SrTiO₃ and (d) P-Sr500

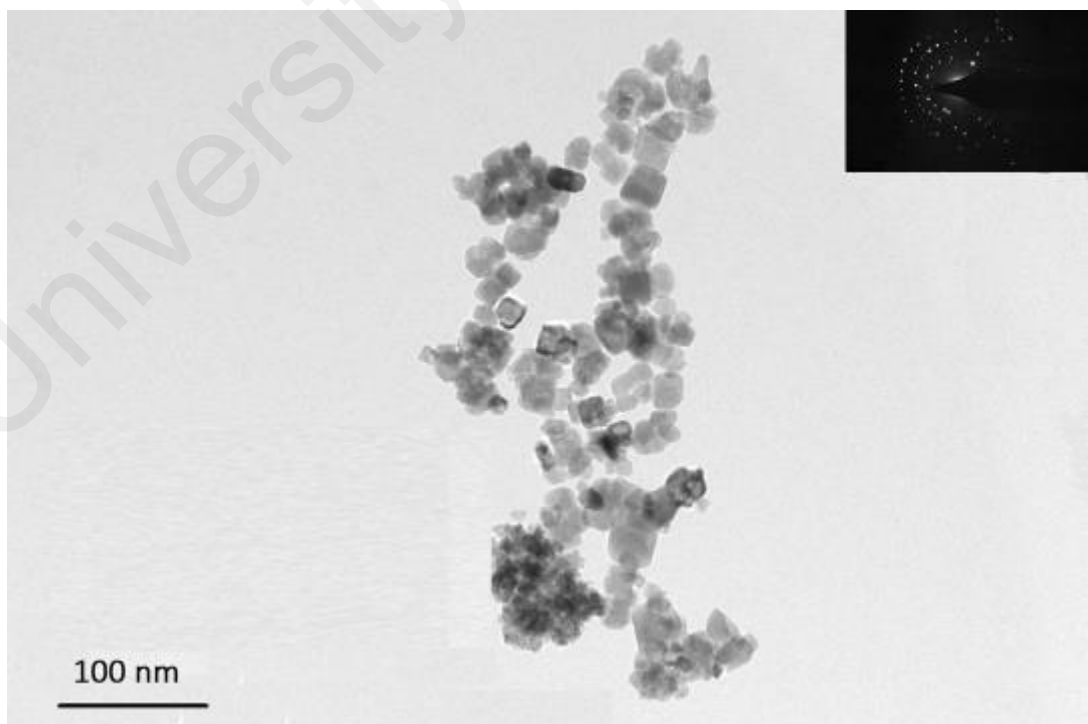


Figure 5.2: TEM image of SrTiO₃ nanocubes. The inset highlights the SAED pattern of SrTiO₃

Probably due to the low concentration of SrTiO₃ nanocubes in nanocomposites (500 mg with respect to 0.4 M aniline), it is difficult to observe these nanoparticles in the FESEM images of nanocomposite material as these particles are embedded in the polymer matrix of polyaniline. Therefore, FESEM-EDX and FESEM-mapping may possibly prove to be a suitable technique to validate the presence of strontium titanate nanoparticles in the matrix of polyaniline. Figure 5.3 illustrates the mapping result of nanocomposite with strontium titanate nanocubes (P-Sr500) which clearly reveals that strontium titanate (Figure 5.3 (f) and (g)) is uniformly present in the nanocomposites along with carbon, nitrogen and oxygen. An elemental analysis (Figure 5.4) shows the presence of strontium and titanium which further confirms the formation of strontium titanate nanocube-doped polyaniline nanocomposites.

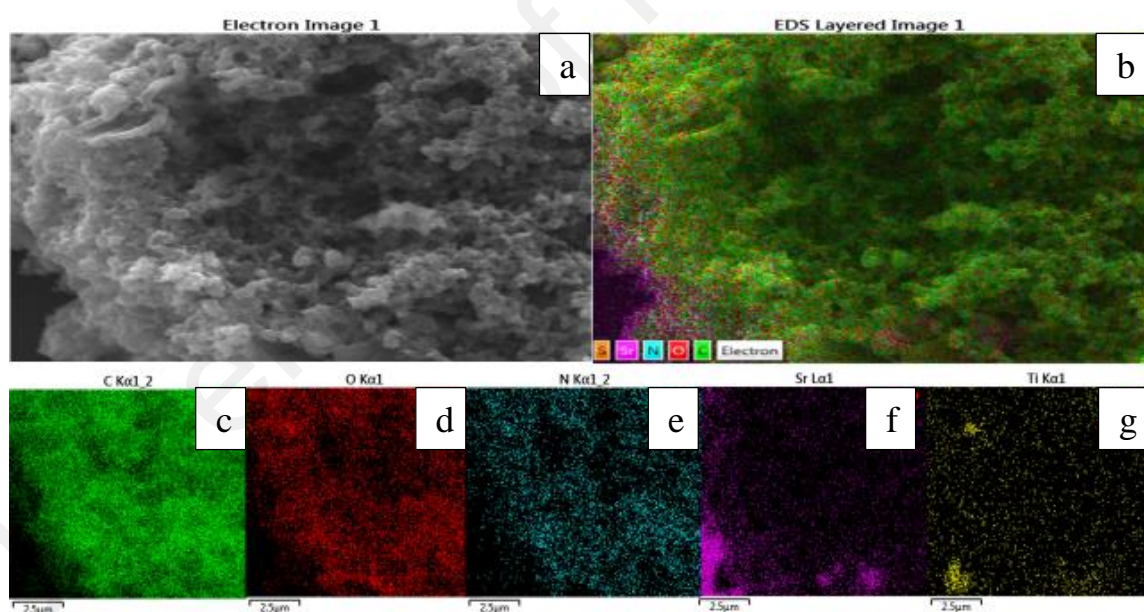


Figure 5.3: (a) FESEM image and (b) EDX elemental mapping of P-Sr500 nanocomposite on a Si wafer for the following elements: (c) C, (d) O, (e) N, (f) Sr and (g) Ti

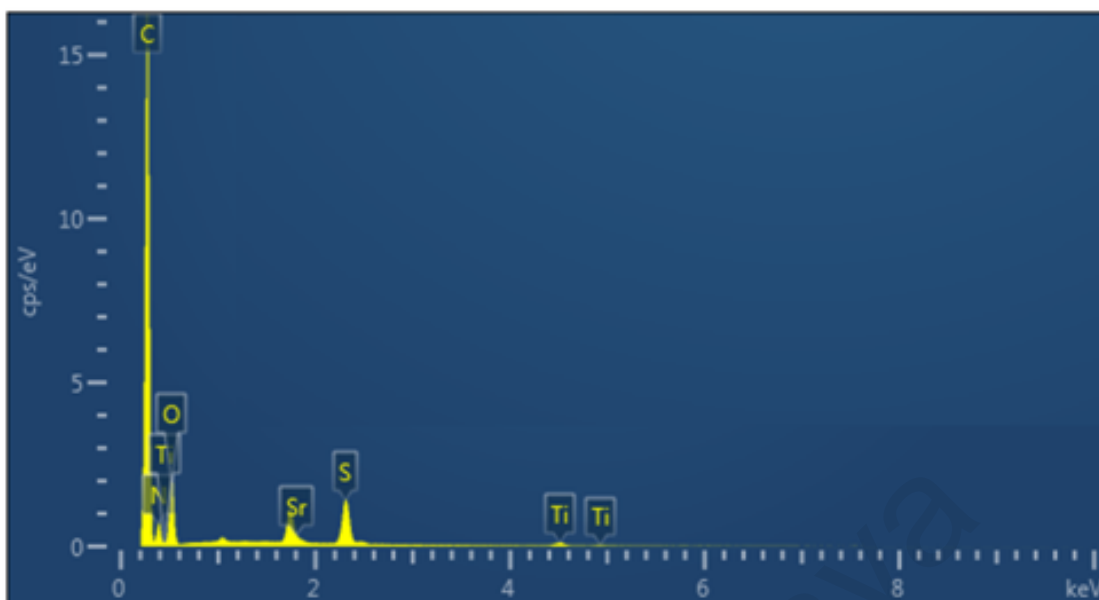


Figure 5.4: EDX spectrum of P-Sr500 nanocomposite

5.3.1.2 Thermal Analysis

The thermal analysis of SrTiO₃ nanocubes synthesized through hydrothermal technique, PANI homopolymer and SrTiO₃ nanocube-doped polyaniline nanocomposite, P-Sr500, was carried out using thermo gravimetric analysis performed under a nitrogen atmosphere by heating samples from 30°C to 900°C with a ramp rate of 10°C/min. Figure 5.5 shows the TGA thermogram of the SrTiO₃ nanocubes, PANI and P-Sr500. As obvious from the TGA curve of SrTiO₃, the first weight loss occurred between 50 and 150°C, which may be attributed to the dehydration of the absorbed moisture. No prominent changes were observed in the TGA curve of SrTiO₃ and total weight loss for a temperature range 35-900°C was found out to be < 10%. Three major weight losses were exhibited by the TGA thermogram of PANI homopolymer. The first weight loss occurred from 40-120°C, which may be due to the loss of adsorbed moisture, the decomposition of unreacted monomers and the decomposition of impurities. The second major weight loss is apparent from 120-260°C which may be accredited to the loss of the dopant (H₂SO₄) and final weight loss appeared from 260 to 900°C which is possibly due to the decomposition of polymeric chains. As evident from the graph the thermal stability of SrTiO₃ nanocube-doped polyaniline has improved to a greater extent

as compared to bare homopolymer. Approximately 40% of P-Sr500 persisted as residue at the end of thermal analysis at 900°C. Thus, the TGA analysis data clearly reveal that thermal stability of P-Sr500 has been greatly enhanced due to the presence of thermally stable pure SrTiO₃ nanocubes in the nanocomposite material. The major thermal events are summarised in table 5.2.

Table 5.2: TGA summary of SrTi₃, PANI and PSr-500.

Material	Initial Temp. (°C)	End Temp. (°C)	Percentage of Residue (%)	Major thermal events
SrTiO ₃	30	900	94%	a) 50-150°C (dehydration of the absorbed moisture).
PANI	30	900	7%	a) 40-120°C (loss of adsorbed moisture, the decomposition of impurities and the unreacted monomer). b) 120-265°C (loss of dopant, H ₂ SO ₄). c) 265-900°C (decomposition of polymeric chains).
PSr-500	30	900	40%	a) Same as for PANI homopolymer.

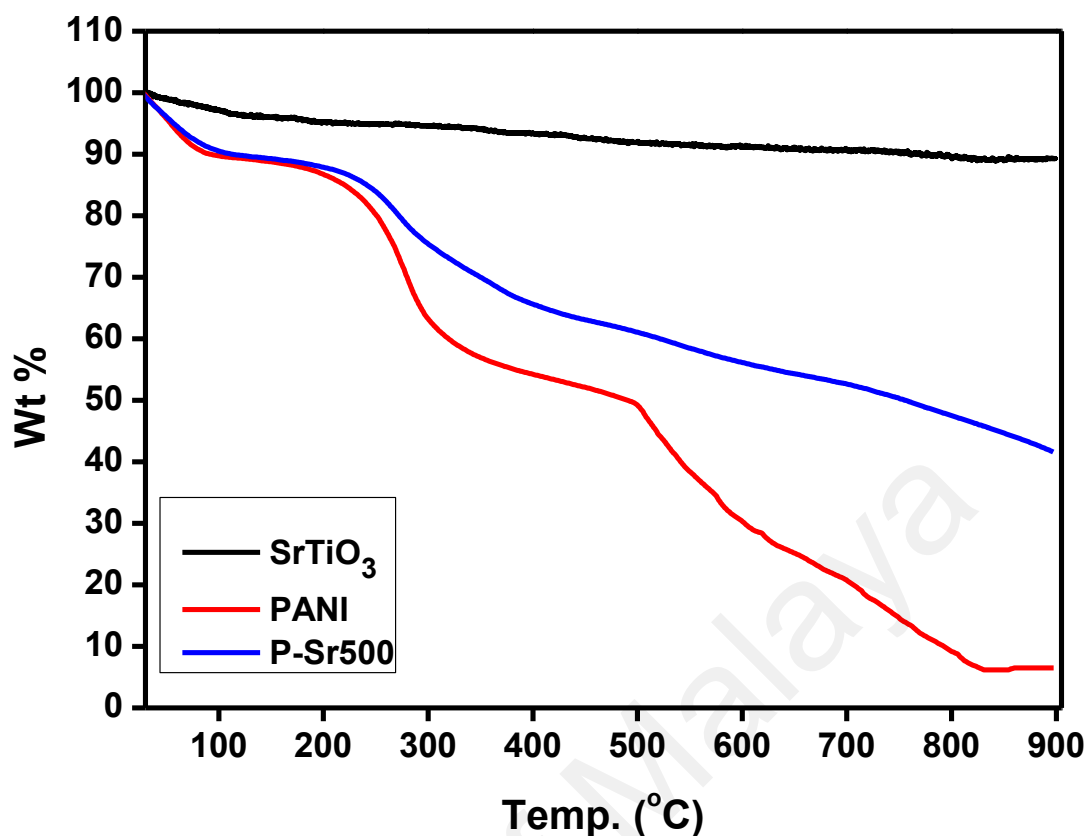


Figure 5.5: TGA thermogram analysis of PANI, SrTiO₃ and P-Sr500 nanocomposite

5.3.1.3 XRD Analysis

The typical room temperature XRD patterns of hydrothermally synthesized SrTiO₃ nanoparticles, PANI homopolymer, and SrTiO₃ nanocube-doped polyaniline nanocomposite are shown in Figure 5.6 and Figure A-3 (appendix A). The XRD patterns of SrTiO₃ nanocubes showed good crystallinity with diffraction peaks that correspond to 100, 110, 111, 200, 210, 211, 220, 310, 311, and 222 planes of cubic perovskite SrTiO₃ structure respectively. These peaks are characteristic of SrTiO₃ and can be readily indexed as those of cubic perovskite structure (space group: Pm3m) of SrTiO₃ in accordance with JCPDS card no. 35-0734. The peaks obtained for SrTiO₃ were very sharp and well defined which indicates the well-developed crystalline structure. The XRD patterns of SrTiO₃ illustrated the presence of weak peak at $2\theta = 25.25, 35.80$ and 43.90 (marked with asterisk) which may be due to the presence minute amount of SrCO₃ as a contamination. Formation of small quantity of SrCO₃ is quiet obvious in the hydrothermal processing

which is due to the presence of CO_2 from the air. CO_2 dissolve in reaction medium as CO_3^{2-} and react with Sr^{2+} ions leading to the formation of SrCO_3 during pretreatment and or the post treatment (Guo et al., 2006; Huang et al., 2014). The presence of SrCO_3 will not give any adverse effect on photocatalytic and thus it is negligible. For PANI homopolymer, the diffracted appeared at $2\theta = 15.6, 20.25,$ and 25.35 , which are characteristic of PANI and indicate the polycrystalline structure of PANI (Rahy et al., 2008). The peaks at angles of $2\theta = 20.25$ and 25.35 correspond to the periodic repetition of benzenoid and quinoid rings in PANI chains (Shi et al., 2009). As apparent from Figure 5.6 and Figure A-3 (appendix A), when strontium titanate nanocubes were doped into the polymer matrix of polyaniline, the broad and persistent peaks of PANI homopolymer were retarded to a greater extent. This diminishing of PANI crystalline peaks were enhanced with increasing the doping percentage of SrTiO_3 and is possibly due to the fact that SrTiO_3 nanocubes are acting as impurities that retard the growth of the PANI crystallite. Also, the diffraction peaks of SrTiO_3 in the nanocomposite become more sharp and apparent with increasing the doping percentage of SrTiO_3 nanocubes. Thus, XRD analysis established successful synthesis of SrTiO_3 and formation of SrTiO_3 doped polyaniline nanocomposites.

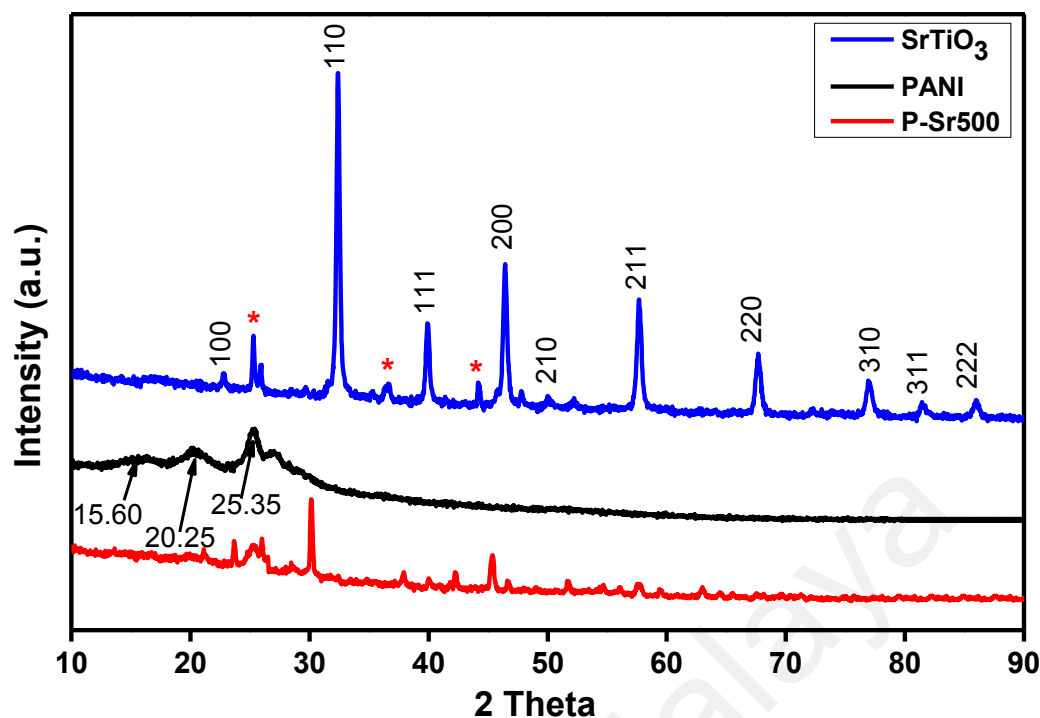


Figure 5.6: XRD patterns of PANI, SrTiO₃, and P-Sr500 nanocomposite

5.3.1.4 BET Analysis

Brunauer-Emmett-Teller (BET) analysis was employed for investigating the specific surface area and porosity of SrTiO₃ and SrTiO₃ nanocubes-doped nanocomposite by measuring the nitrogen adsorption-desorption isotherms. As shown in Figure 5.7 and Figure A-4 (appendix A), the nitrogen adsorption-desorption isotherms of P-Sr500 and SrTiO₃ demonstrated the characteristic of type-IV isotherms according to the International Union of Pure and Applied Chemistry (IUPAC) classification which specifies their mesoporous nature (Sing et al., 1985; Yu et al., 2013). The BET analyser measurements showed that the specific surface area for PANI homopolymer, SrTiO₃ nanocubes, P-Sr500 nanocomposite to be 9.42, 9.20 and 16.50 m²g⁻¹ respectively. Figure 5.8 represents the the Barrett-Joyner-Halenda (BJH) pore size distribution curve of P-Sr500 nanocomposite. As shown in Figure 5.8, the pore size distribution appears to be slightly inhomogeneous and particles with pore diameter of about 17 nm appear to be most abundant. The total volume of pores for PANI homopolymer, SrTiO₃ nanocubes

and P-Sr500 nanocomposite were found to be 0.042, 0.026 and 0.06 $\text{cm}^3 \text{g}^{-1}$, respectively. Thus, P-Sr500 nanocomposite exhibits the high BET specific surface area and large total volume of pores as compared to PANI homopolymer and SrTiO_3 nanocubes.

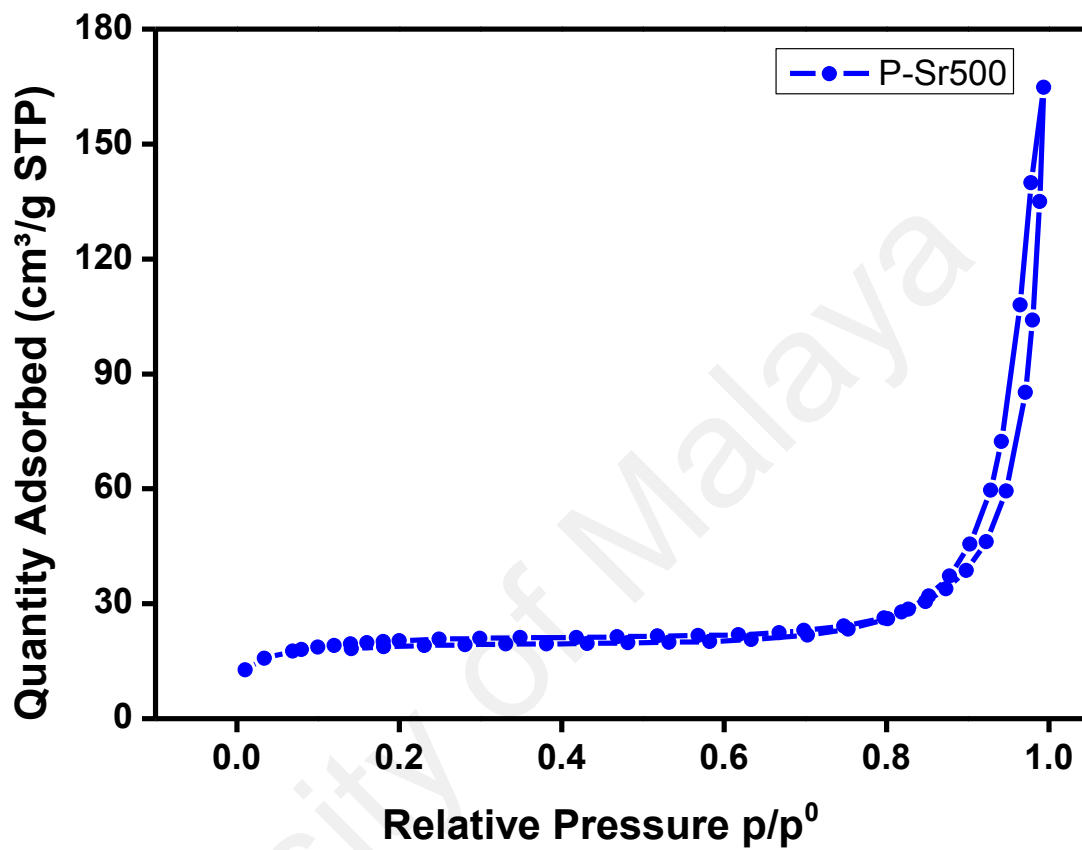


Figure 5.7: Nitrogen adsorption–desorption isotherms (BET) of P-Sr500 nanocomposite

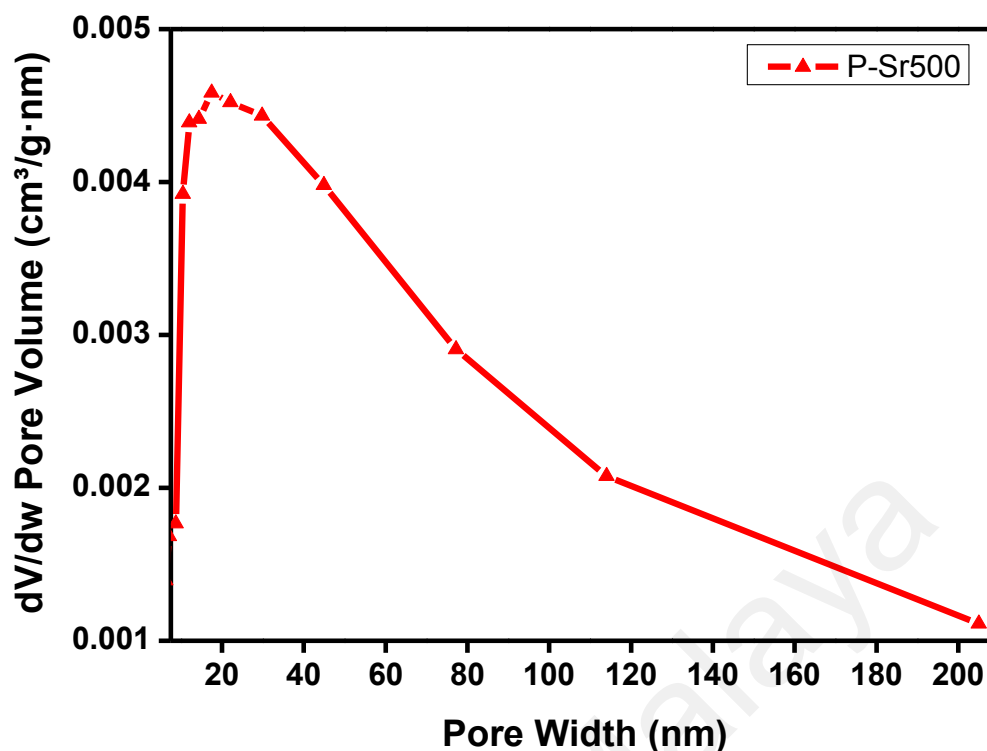


Figure 5.8: BJH pore-size distribution of P-Sr500 nanocomposite

5.3.1.5 UV-Vis Analysis

Figure 5.9 shows the UV-vis diffuses reflectance spectrum for the SrTiO₃ nanoparticles PANI homopolymer and SrTiO₃ nanocubes-doped polyaniline nanocomposites namely P-Sr250, P-Sr500 and P-Sr750 respectively. As evident from Figure 5.9 (a), SrTiO₃ exhibit a distinct broad absorption bands in the range of 200 to 398 nm, exhibiting the sharp absorption onset approximately at 398 nm which may be attributed to the electronic transition from valence band to conduction band and is in agreement with the band gap edge absorption of SrTiO₃ (3.2 eV) (Tan et al., 2014; Xian et al., 2014). PANI homopolymer shows three characteristic absorption bands at 380–460, 470–500, and 505–780 nm respectively which are typical of the protonated form of PANI homopolymer (X Wang et al., 2010). The first absorption band can be assigned to the π - π^* transition, the electron transition between the benzenoid segments. The second and third absorption bands can be assigned to the doping level and the π - π^* transition of quinoid rings on the PANI chains due to the the formation of polarons (Gülce et al., 2013;

Shahabuddin et al., 2015b). SrTiO₃ nanocubes-doped polyaniline nanocomposites shows the optical absorption in the entire visible light region ranging from 480–800 nm as shown by their diffuse adsorption spectrum. As these nanocomposites reveals absorption in the entire visible region, it is certain that they could function as effective light absorber with enhanced photocatalytic properties.

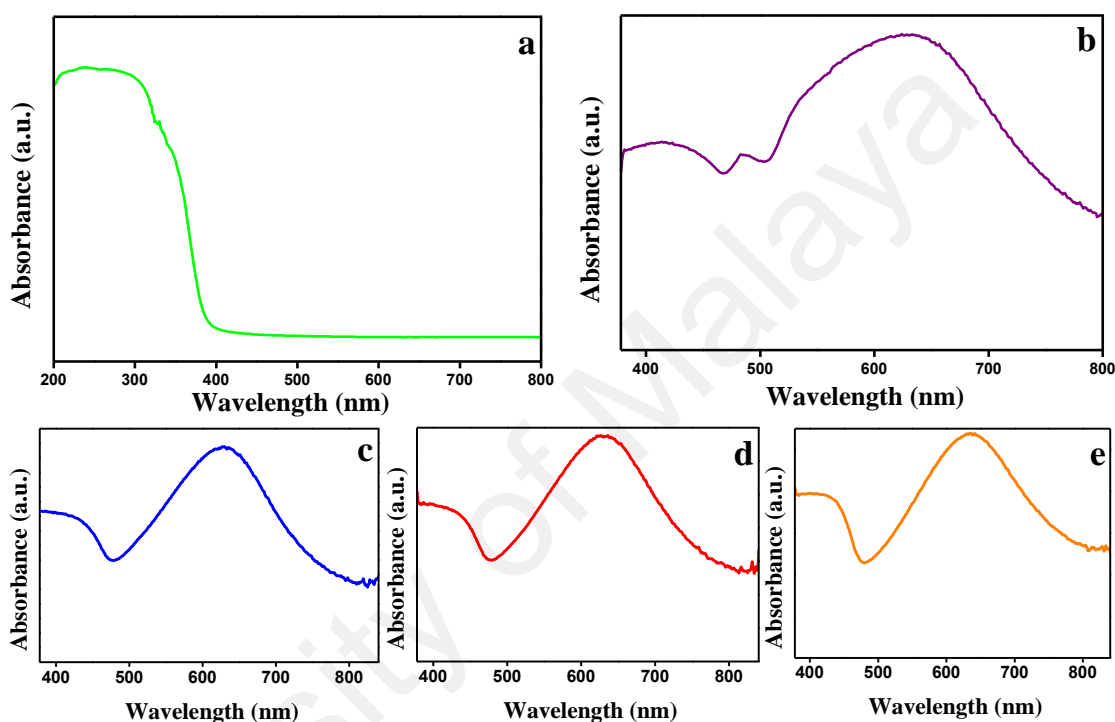


Figure 5.9: UV-Visible spectra of (a) SrTiO₃, (b) PANI (c) P-Sr250, (d) P-Sr500 and (e) P-Sr750 nanocomposite

5.3.1.6 FTIR Analysis

The FTIR spectra of PANI, strontium titanate nanocubes, and SrTiO₃ nanocube-doped- polyaniline nanocomposite are shown in Figure 5.10. The FTIR spectrum of the PANI homopolymer exhibits the characteristic IR bands at 1560 cm⁻¹ and 1430 cm⁻¹ which may be attributed to C-C stretching of quinoid and benzenoid rings in PANI, respectively. The peak at 1285 cm⁻¹ could be assigned to C-N and C=N stretching in PANI. A characteristic broad IR band at 3425 cm⁻¹ can be attributed to the N-H stretching mode in PANI. The occurrence of the benzenoid and quinoid units is the indication of the conductive emeraldine form of PANI. The IR spectrum of SrTiO₃ exhibits a band around

3120 cm^{-1} which may be assigned to the O–H stretching modes in crystallization water (Adireddy et al., 2010). The IR peak at 1480 cm^{-1} corresponds to carboxylate group stretching modes (Gopalakrishnamurthy et al., 1975) whereas the peak at 1135 cm^{-1} could be attributed to C=O stretching modes in COO–Sr. The absorption peak at around 855 cm^{-1} and 600 cm^{-1} are due to TiO_6 octahedron bending and stretching vibration (Last, 1957). The FTIR spectrum of the SrTiO_3 nanocube-doped PANI nanocomposites depicts the characteristic bands of the PANI homopolymer but these bands are slightly shifted after the addition of SrTiO_3 nanoparticles. The IR band at 1094 cm^{-1} in PANI was shifted to around 1040 cm^{-1} in SrTiO_3 doped nanocomposites while the intensity of band at 1430 cm^{-1} (as indicated by the arrows in Figure 5.10) increases with the increase in the concentration of SrTiO_3 . This slight shifting of the band towards red could be attributed to some amount of weak Van der Waals attraction between the polymer chain and SrTiO_3 . Hence, the FTIR studies are in good agreement with reported literature and clearly specify the formation of polyaniline, SrTiO_3 and SrTiO_3 doped polyaniline nanocomposites.

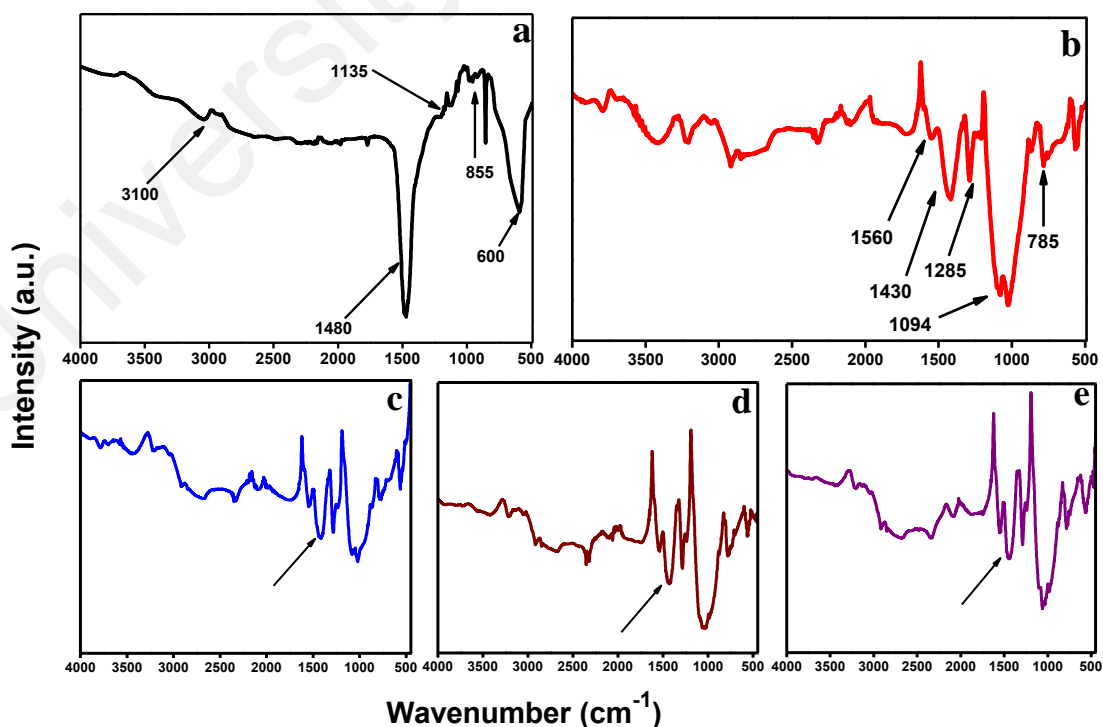


Figure 5.10 FTIR spectrum of (a) SrTiO_3 , (b) PANI, (c) P-Sr250, (d) P-Sr500 and (e) P-Sr750 nanocomposite

5.3.2 Photodegradation Studies

5.3.2.1 Photocatalytic Degradation of MB Under UV Illumination

The photocatalytic aqueous-phase decomposition of MB dye in the presence of the PANI homopolymer, P-Sr250, P-Sr500 and P-Sr750 nanocomposite catalysts were performed under natural sunlight irradiation at ambient temperature. In order to attain adsorption-desorption equilibrium, the adsorption of MB on the surface of the catalyst under dark conditions was monitored for 60 minutes via UV-vis absorption spectra as shown in Figure 5.11 (a) and 5.11 (b). It is evident from Figure 5.11 (a) that the adsorption of MB molecules on the surface of the catalyst augmented with time, and most of the catalyst surface was saturated with MB within 30 minutes. Approximately 18%, 26%, 31% and 29% of MB was adsorbed on the surface of PANI, P-Sr250, P-Sr500 and P-Sr750, respectively after adsorption-desorption equilibrium was achieved. MB molecules can be adsorbed onto the surface of PANI with face-to-face coordination via π - π conjugation between MB and the aromatic regions of PANI, which increases the adsorptivity of MB on PANI, a prime requisition for enhanced photocatalytic activity. The adsorption of MB on the surface of photocatalyst is further enhanced by doping PANI with SrTiO₃ nanocubes, which is probably owing to some molecular interaction of nanoparticles with MB. With increasing the percentage of SrTiO₃ in the nanocomposites, the adsorption decreases slightly which may be caused by the reduction in the effective surface area of catalyst due to the agglomeration of SrTiO₃ nanocubes at a high doping percentage.

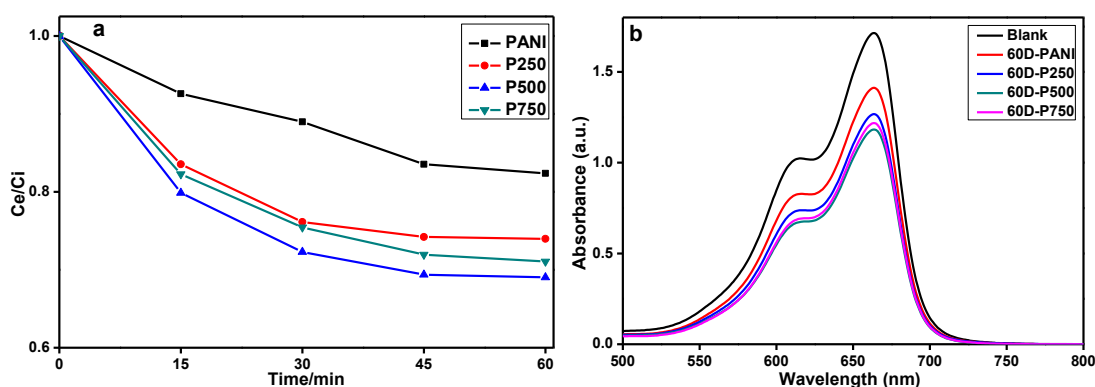


Figure 5.11 (a) Adsorption-desorption equilibrium rate of MB under dark conditions versus time in the presence of various photocatalysts (b) UV-vis absorption spectra of MB aqueous solution at 60-minute dark adsorption-desorption equilibrium

Figure 5.12 (a) and Figure 5.12 (b) illustrate rate of photodegradation of MB at different time intervals and percentage degradation of MB in the presence of various photocatalysts, which indicates that PANI exhibits low photocatalytic activity as compared to the photocatalytic activities of P-Sr250, P-Sr500 and P-Sr750 nanocomposite catalysts. The percentage degradation, as evident from Figure 5.12 (a) follows the following trend: P-Sr500 > P-Sr750 > P-Sr250 > PANI. The UV-vis adsorption spectra of the PANI and SrTiO₃ nanocubes-doped nanocomposites irradiated under solar light illumination for different time intervals are represented by Figure 5.13 which depicts the efficient degradation of MB by a photocatalytic phenomenon. As evident from the Figure 5.13 intensity of the adsorption band decreases with the increase in irradiation time and this decrease in intensity shows a different trend with each photocatalyst. The degradation percentage after 90 minutes of visible-light illumination for PANI, P-Sr250, P-Sr500 and P-Sr750 nanocomposite was found to be 63%, 68%, 97% and 84 % respectively which shows the enhanced photocatalytic activity of P-Sr500 over other photocatalysts. In PANI, degradation is 63% after 90 minutes which could be due to high electron mobility in PANI chains through π - π^* transitions under photoillumination. The degree of decomposition enhances with the doping of SrTiO₃ nanocubes in the conducting chains of PANI which signifies the synergistic

photocatalytic phenomenon. The photocatalytic degradation was enhanced greatly with increasing the concentration of SrTiO_3 from P-Sr250 to P-Sr500. However, the photocatalytic degradation gradually decreased from P-Sr500 to Sr750 which might be owing to the reduction in the effective surface area of catalyst due to the agglomeration of SrTiO_3 nanocubes at a high doping percentage, thereby predicting P-Sr500 to be an optimum photocatalyst composition.

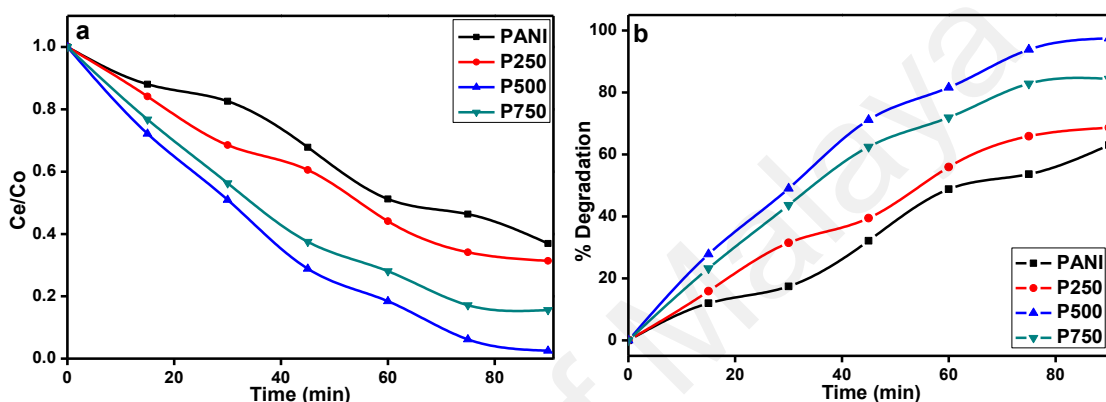


Figure 5.12: (a) Photodegradation rate of MB at different time intervals in the presence of various photocatalysts. (b) Percentage degradation of MB in the presence of various photocatalysts

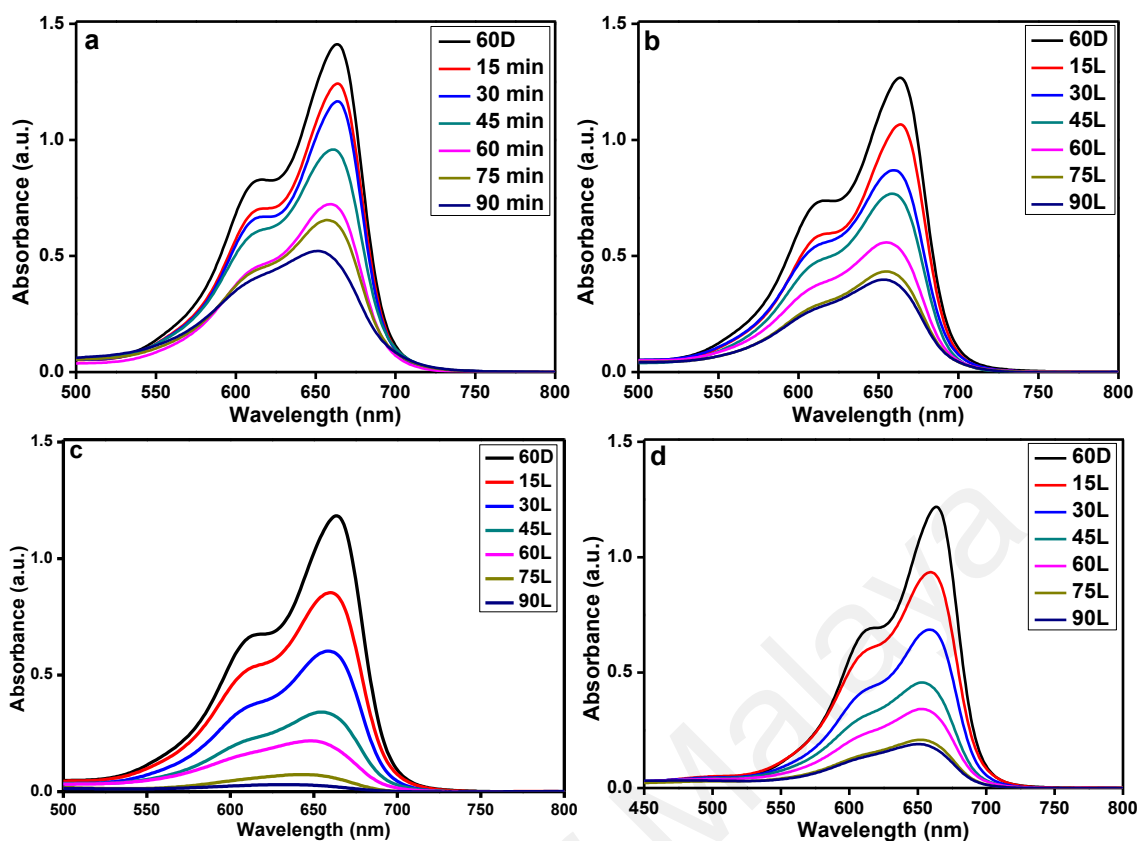


Figure 5.13: UV-vis absorption spectra of MB aqueous solution at different times in the presence of (a) PANI, (b) P-Sr250, (c) P-Sr500 and (d) P-Sr750 nanocomposite

MB dye can absorb light in the region 500-700 nm leading to the formation of singlet and triplet species by electronic transition and intersystem crossing and can undergo self-decomposition to a certain extent (E Subramanian et al., 2014). The singlets and triplets species owing to their higher energy and hyperactivity readily react with available oxygen leading to the formation of superoxide, peroxide and hydroxyl radicals also called as advanced oxidation species (AOS). These AOS are extremely reactive species which attack on dye thereby degrading and mineralizing it effectively. However, formation of AOS by MB alone is insignificant and need to be enhanced with the aid of photoactive catalysts. Analogous to MB PANI, SrTiO₃ and their hybrid nanocomposite photocatalysts can also generate AOS which can actively degrade MB. PANI is an efficient electron donors and good hole transporter upon visible-light excitation and exhibits enhanced electron mobility upon photo-illumination. Conjugated conductive polyaniline itself

possess valence band (Highest Occupied Molecular Orbital-HOMO) and conduction bands (Lowest Unoccupied Molecular Orbital-LUMO) similar to that of other conductors and semiconductors. Due to its characteristic π - π^* transitions, PANI can excite electrons from its HOMO to LUMO upon photo illumination by absorbing energy from photons. These characteristic transitions in PANI leads to the formation of electrons and holes in HOMO and LUMO of PANI, respectively, which are further responsible for the generation of AOS thereby degrading MB. However, the generation of AOS in PANI is low due to rapid electron-hole recombination, thus limiting the efficiency of PANI to be exploited as an effective photocatalyst. The photocatalytic efficiency of PANI was greatly improved via doping of SrTiO₃ nanocubes into the conducting chains of PANI through in-situ polymerization process. SrTiO₃, a wide band gap semiconductor ($E_g = 3.2$ eV), undergoes chemical bond interactions with LUMO of PANI through its d-orbital conduction band upon photo irradiation. These electronic interactions are responsible for the LUMO of PANI to come close to the conducting band of SrTiO₃ thus leading to the injection of electrons from LUMO of PANI to CB of SrTiO₃, thereby, increasing the charge separation and limiting the electron-hole recombination. These electrons and holes reaches to the surface of catalyst where they react rapidly with oxygen and water molecules to form peroxides, superoxide and hydroxyl radicals respectively, which effectively attack MB causing its decomposition and mineralization. Hence, SrTiO₃ works synergistically with PANI to greatly enhance the photocatalytic degradation of MB by expediting the formation of AOS. Figure A-5 (appendix A) provides the schematic representation of the probable mechanism of MB degradation in the presence of SrTiO₃ nanocubes-doped nanocomposites.

5.3.2.2 Comparison of Photocatalytic Efficiencies

Comparative study of the photocatalytic efficiencies of the photocatalysts reported in literature with the present catalyst is significant and is represented in Table 5.2. With catalyst loading of 30mg/100 ml at an initial dye concentration of 10 mg/L, the synthesized catalysts revealed the dye degradation efficiency of 97% with photo illumination for 90 minutes. As evident from Table 5.2, in previous studies for the degradation of MB with different time of photo illumination, Autin et al. reported 88% degradation (Autin et al., 2013), Eskizeybek et al reported 99% degradation (Eskizeybek et al., 2012), Kant et al. reported 99.47% degradation (Kant et al., 2013), Gülce et al. reported 97% degradation (Gülce et al., 2013), Dai et al. reported 87% degradation (Dai et al., 2014) and Olad et al. (Olad et al., 2012) reported 82% degradation using various photocatalysts. In the very latest investigations for the photocatalytic degradation of MB, the reported photodegradation was between 88 and 95% with concentration ranging from 3 to 10 mg/L (Golsheikh et al., 2015; Shahabuddin et al., 2015b; Xia et al., 2015). Thus, in this context it is very well established that our catalyst offers higher degradation efficiencies.

Table 5.3: Comparative study of the photocatalytic efficiencies of the different photocatalysts

Catalyst	Dye Degraded	Conc. (mg/L⁻¹)	Amt. of catalyst (mg/ml)	% Degradation	Degradation time (min.)	Source of light	Ref.
Chitosan/PANI /Co ₃ O ₄	MB	10	0.3	88	180	UV	(Shahabuddin et al., 2015b)
Graphene/ZnS	MB	10	0.2	95	180	UV	(Golsheikh et al., 2015)
PANI/CdO	MB	4.8	0.4	97	240	Sunlight	(Gülce et al., 2013)
TiO ₂	MB	5	-	88	120	LED	(Autin et al., 2013)
PANI/ZnO	MB	3.2	0.4	99	300	Sunlight	(Eskizeybek et al., 2012)
PANI/FZNPs	MB	3.2	0.25	99.47	300	Sunlight	(Kant et al., 2013)
AgBr/ZnO	MB	10	1	87	240	LED	(Dai et al., 2014)
PANI/ZnO	MB	10	300	82	60	Visible light	(Olad et al., 2012)

FeOOH-LDO	MB	3	35	95	180	Visible light	(Xia et al., 2015)
PANI/SrTiO ₃	MB	10	0.3	97	90	Visible light	(This work)

University of Malaysia

5.4 Conclusions

In summary, we present here a facile and distinctive route to synthesise nanostructured SrTiO₃ nanocube-doped polyaniline nanocomposite through an in situ oxidative polymerization procedure. The synthesized nanomaterial exhibited enhanced specific surface area as revealed by BET studies, uniform nanopore distribution as depicted by FESEM and TEM, and good photocatalytic performance. SrTiO₃ nanocubes incorporated into the matrix of PANI homopolymer demonstrated enhanced photocatalytic activity indicating the synergistic phenomenon between conducting polymer and the semiconducting metal oxide. The concentration of the MB decreased upto 97% after 90 min of visible light irradiation. The proposed technique may be used for the synthesis of numerous nanocomposites materials, with other conducting polymers addressing the present day issue of environmental pollution caused by various organic pollutants. Moreover, the enhanced photocatalytic activity in the visible light is more economical as compared to UV irradiation and may expedite generating industrial applications.

**CHAPTER 6: SYNTHESIS OF POLYANILINE COATED GRAPHENE OXIDE
@ SrTiO₃ NANOCUBE NANOCOMPOSITES FOR ENHANCED REMOVAL
OF CARCINOGENIC DYES FROM AQUEOUS SOLUTION⁴**

6.1 Introduction

Water pollution has possessed serious threat to environment thereby attracting much scientific attention towards the removal of organic waste and toxic water pollutants from aqueous bodies (Sen et al., 2011). Textiles industries, one of the major worldwide contributors for water pollution, causes major impact on the quality of available water resources through deliberate or inadvertent release of dye effluents into water bodies. Dyes are complex organic molecules which basically adhere to the surface of fabrics thereby imparting color to them. There are more than 100,000 commercially available dyes (Sen et al., 2011) which are used in wide varieties of application including textiles (Sokolowska-Gajda et al., 1996), paper (Ivanov et al., 1996), tanning industries (Kabdaşlı et al., 1999), plastics, printing food processing (Bensalah et al., 2009; Dawood et al., 2014; Yagub et al., 2014) and so on. Approximately 10,000 tonnes of synthetic dyes are used per year by textile industries alone, discharging nearly 100 tonnes of dyes in water bodies as effluents (Yagub et al., 2014). Most of the synthetic dyes evade conventional water treatment methods thereby accumulating in environment due to their high degree of stability towards biodegradation, temperature, light, detergents and soap (Chequer et al., 2013; Couto, 2009). Methylene blue (MB) and methyl orange (MO), commercial dyes used for various applications, such as textiles, papers, leathers, additives, laser

⁴ This chapter has been submitted in RSC Advances and under review (Q1, Impact factor 3.84)

printing, etc., are heterocyclic aromatic chemical compounds having complex chemical structures and synthetic origin owing to which they are resistant to biodegradation and very stable to light and oxidation (Aksu, 2005; Shahabuddin et al., 2016b; Shahabuddin et al., 2015b). These dyes are highly toxic, persistent, carcinogenic and mutagenic in nature. Hence, for safer environment, the removal of these noxious dyes from aqueous environment is extremely essential. Up to now considerable efforts such as coagulation (Papić et al., 2004), photocatalysis (Shahabuddin et al., 2016b; Shahabuddin et al., 2015b), biological treatment (Gonzalez - Gutierrez et al., 2009), chemical oxidation (Zou et al., 2015), membrane separation (Akbari et al., 2002) and adsorption (Haldorai et al., 2014; Mahto et al., 2015) have been performed to remediate noxious dyes from aqueous environment. Among all these techniques, adsorption continues to be fascinate the considerable attention due to its simplistic approach and numerous benefits such as greater efficiency and capability to remove dyes on large scale, ease of recovery and recyclability of adsorbents. Different classes of adsorbents such as activated carbon (Hosseini Koupale et al., 2013), polymeric materials (Hu et al., 2010), biomass (Valix et al., 2009), MWCNT (Ma et al., 2012) etc. have been employed to eliminate dyes from polluted water.

Conducting polymers such as polythiophene, polyacetylene, polypyrrole, polyphenylene and polyaniline have been widely studied in multidisciplinary research areas comprising electronics, electromagnetic, thermoelectric, sensors, batteries, electroluminescence, and electromechanical applications (Bairi et al., 2015; Bhadra et al., 2009; Hu et al., 2015; Sengodu et al., 2015; Shih et al., 2015). Among the conducting polymer family, polyaniline (PANI), owing to its unique electrochemical properties, higher environmental stability, easy synthetic methodologies, cost effectiveness, efficient

thermal stability and wide varieties of application, has been most intensively investigated conducting polymer by scientific community (Boeva et al., 2014). However, several drawbacks such as poor solubility, poor mechanical properties, lower effective surface area etc. restrict the use of PANI in many environmental applications (Tiwari, 2007). In order to overcome these limitations, PANI is often polymerised in the presence of variety of other organic and inorganic materials to enhance its properties. Morphology and active surface area are two major characteristics which play a significant role to increase the adsorption capacity of PANI based composite materials which can be manipulated by incorporating nanoscale materials in the matrix of polymer. PANI based nanocomposites have been extensively studied as adsorbent materials for the removal of dyes and other organic pollutants from waste waters and endures to be the favorable contender for various environmental applications (Zhao et al., 2011).

Graphene, a two dimensional one-atom-thick sheet of all sp^2 -hybridized carbon has received an emergent research interest due to its distinctive electronic, thermal, optical, mechanical, large surface-to volume ratio and excellent chemical tolerance capabilities (Golsheikh et al., 2015; Huang et al., 2012; Zhang et al., 2010; Zhu et al., 2010). One of the most attractive feature of graphene is its large theoretical specific surface area ($2630 \text{ m}^2 \text{ g}^{-1}$) which makes it a suitable candidate to be use as an adsorbent material (Stoller et al., 2008). Due to these distinctive properties, graphene is often used as a suitable matrix for designing nanocomposites with other substances such as polymers (Kuilla et al., 2010), metal-organic framework (Jahan et al., 2010; Petit et al., 2010), metal nanoparticles (Jasuja et al., 2009) and so on. PANI nanocomposites with graphene oxide (GO) have demonstrated enhanced physical and chemical properties compared with neat PANI or graphene oxide and have been exploited in numerous applications (Jasuja et al.,

2009; Kumar et al., 2012; Wang et al., 2009; Yong et al., 2012). Besides GO, inorganic metal oxides based nanocomposites had played a significant role in potential applications including photodegradation, waste water treatment through adsorption, photovoltaics, photochromism etc. owing to their low cost, facile synthesis, large surface area and physiochemical properties (Shahabuddin et al., 2016a). Various nanocomposite materials with inorganic metal oxides such as SrTiO₃ (Shahabuddin et al., 2016b), TiO₂ (Zhang et al., 2011), Fe₃O₄ (Nassar et al., 2012), Co₃O₄ (Jiao et al., 2010; Shahabuddin et al., 2015b) etc. have been employed for the effective treatment of dye waste water. Therefore, GO, PANI together with some metal oxide nanoparticles can be explored for the synthesis of nanocomposite materials to address the present day issue of water pollution.

In the present study we reported the facile synthesis of polyaniline coated graphene oxide doped with SrTiO₃ nanocube nanocomposites, synthesized through facile in situ oxidative polymerization technique for the adsorption of a cationic dye (MB) and an anionic dye (MO). Simultaneous removal of both cationic and anionic dyes by adsorbent is not achieved easily as the adsorbent must have ability to attract both negative and positively charged particles. Here graphene oxide due to the presence of oxygen-containing functionalities attains negative charge whereas polyaniline due to the presence of nitrogen containing functionalities (imine group –N= and amine group –N<) develops positively charged backbone thereby causing intensive electrostatic attraction between the nanocomposites and dye molecules. SrTiO₃ nanocubes act as spacers which help in segregation of GO sheets thereby increasing the overall effective surface area of the nanocomposites. Easy preparation, cheaper costs and superior adsorption capacity for anionic and cationic dyes projects these nanocomposites as the potential adsorbent material for waste water treatment.

6.2 Experimental Section

6.2.1 Materials

Aniline (Fluka, $\geq 99\%$) was distilled under reduced pressure and stored in the dark before use. Ammonium peroxydisulfate, APS (Merck, $\geq 99\%$); strontium hydroxide octahydrate (Sigma Aldrich, 95%); titanium(IV) oxide, anatase (Sigma Aldrich, 99.7%); Hydrochloric Acid, HCl (Merck, 37%); sulphuric acid, H₂SO₄ (Sigma Aldrich, 98%); Methanol (Merck, 99.9%); Potassium permanganate (Sigma Aldrich, $\geq 99\%$), hydrogen peroxide (Sigma Aldrich, 30%), Graphite powder (Sigma Aldrich, $\geq 99.99\%$,) and ammonia solution (R & M, 25%) were used as received without further purification. All of the reagents that were involved in the experiments were of analytical grade. Deionised water was used throughout the entire study.

6.2.2 Synthesis Methodology

6.2.2.1 Synthesis of Graphene oxide (GO)

GO was synthesized using a modified Hummer's method as reported elsewhere (Hummers Jr et al., 1958). Briefly, concentrated sulfuric acid (120 ml) was added into a three neck round bottom flask (500 ml) immersed in ice bath under continuous stirring at 500 rpm. 5.0 g graphite powder was added into ice-cooled concentrated sulfuric acid followed by subsequent addition of 2.5 g NaNO₃ and 15 g KMnO₄. After a while ice bath was removed and the reaction mixture was stirred overnight. When the colour of reaction mixture turned light grey and it converts into paste, 150 ml of deionised water was added gradually into the mixture to dilute the paste. At this point the temperature of the reaction vessel was raised to 98 °C under continuous stirring for 2 hours. Then 50 ml H₂O₂ was added and the reaction mixture was stirred for 30 minutes. The reaction mixture was then filtered and washed with 5% HCl until the filtrate became colourless. Later it was washed

with ethanol and subsequently with deionized water until the filtrate became neutral and dried in vacuum oven at 60 °C.

6.2.2.2 Synthesis of SrTiO₃ Nanocubes

Please refer to section 5.2.2.1.

6.2.2.3 Synthesis of Polyaniline (PANI)

Please refer to section 3.2.2.2.

6.2.2.4 Synthesis of PANI coated GO (GOPSr-0)

PANI coated GO nanocomposite was prepared by in situ oxidative polymerization of aniline by keeping the feed ratio of aniline to GO as 20:80. Calculated amount of aniline was dissolved in an aqueous solution of HCl (1 M). Then, calculated amount of GO was dispersed in this solution and sonicated for 1 hour. Later on, the oxidant solution (mole ratio with aniline 1:1.25) in 1M HCl was gradually added to the reaction mixture under vigorous stirring at room temperature. The reaction mixture was stirred continuously for two hours. The reaction mixture was then filtered and washed with HCl (0.5 M) until the filtrate became colourless and subsequently with DI water until the filtrate became neutral. The obtained composite was dried in a vacuum oven at 60°C overnight and labelled as GOPSr-0. Figure 6.1 represents the reaction pathway for the synthesis of GOPSr-0.

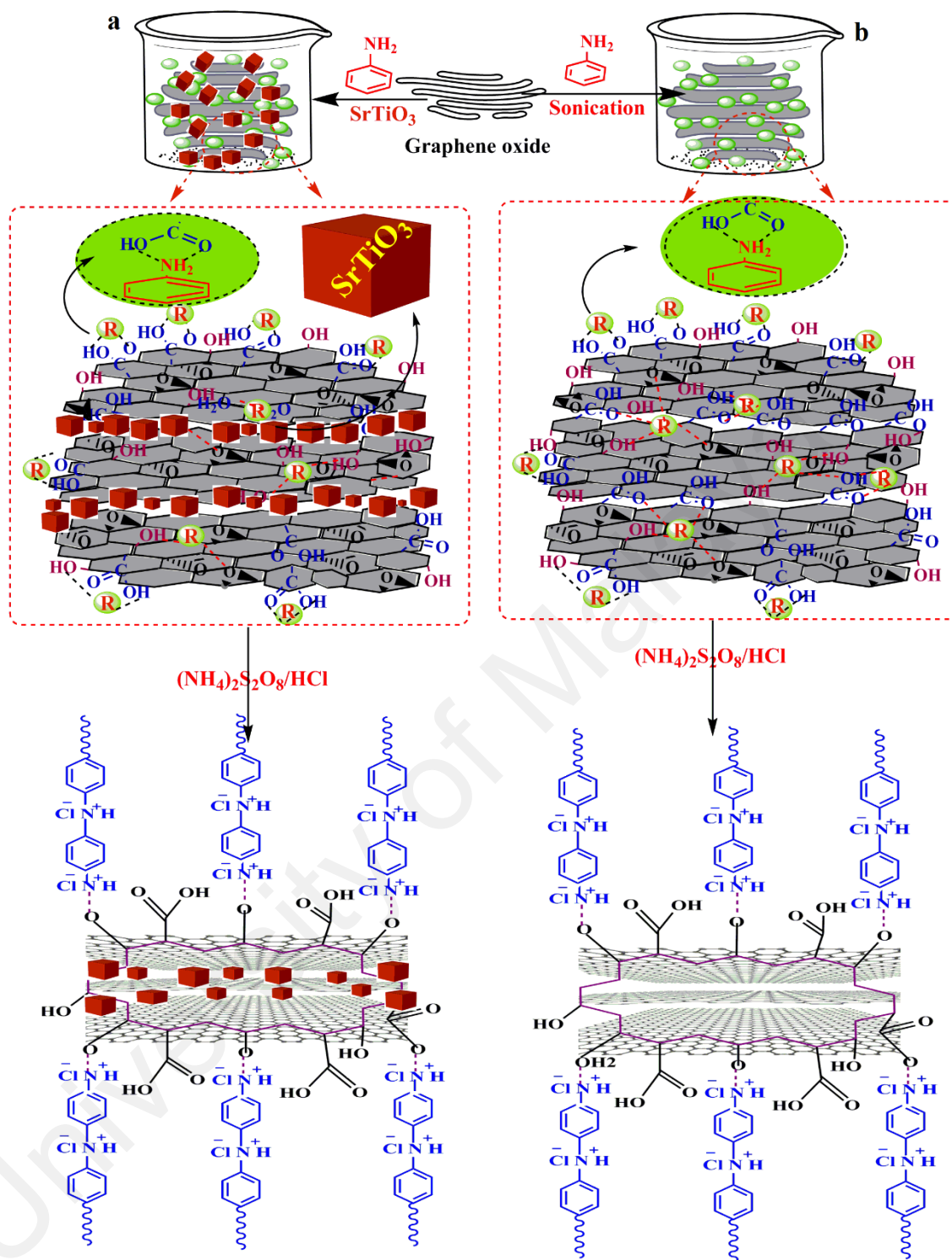


Figure 6.1: Reaction pathway for the synthesis of PANI coated GO nanocomposite (a) doped with SrTiO₃ and (b) without SrTiO₃

6.2.2.5 Synthesis of SrTiO₃ Nanocubes-doped PANI Coated GO (GOPSr)

SrTiO₃ nanocube-doped PANI coated GO nanocomposites were prepared with different wt% of SrTiO₃ (1, 2, and 5 wt% with respect to GO). Calculated amount of

SrTiO₃ nanocubes were dispersed in 5 ml of deionised water by sonication and added dropwise to aniline-GO suspension in HCl (as described in previous section) under vigorous stirring. The resulting mixture was sonicated for 1 hour until it became uniform. The work-up procedure was the same as described in the previous section. The obtained nanocomposites were labelled as GOPSr-1, GOPSr-2 and GOPSr-5 indicating 1, 2, and 5 wt% of SrTiO₃ nanocubes with respect to GO, respectively. Figure 6.1 represents the graphical illustration of the reaction pathway for the synthesis of SrTiO₃ nanocube-doped PANI coated GO nanocomposites.

6.2.3 Characterisation Techniques

The surface morphological and elemental analysis of the synthesized product was conducted using a JEOL JSM-7600F field emission scanning electron microscope operated at 10 kV. The size and shape of the obtained SrTiO₃ nanocubes were studied using a JEOL JEM-2100F high-resolution transmission electron microscope. X-ray diffraction (XRD) patterns were recorded using an Empyrean X-ray diffractometer from $2\theta = 10^\circ$ to 90° using Cu K α radiations ($\lambda = 1.5418 \text{ \AA}$) at a scan rate of 0.02 sec⁻¹. Fourier transform infrared (FT-IR) spectra of the powdered samples were recorded using a Perkin Elmer RX1 FT-IR ATR spectrometer in the range of 400–4000 cm⁻¹ in spectral-grade KBr pellets.

6.2.4 Dye adsorption study

The adsorption studies were carried out using MB and MO, as the model dyes in the water phase to investigate the adsorption ability of synthesized nanocomposites. The dye adsorption experiments were conducted at room temperature in a set of Erlenmeyer flasks

by batch process to study the outcome of different parameters such as type of adsorbent (SrTiO₃ nanocubes, GO, PANI, GOPSr-0, GOPSr-1, GOPSr-2 and GOPSr-5), time (0–60 min), initial pH (4.5–9.5) and effect of NaCl concentration (10–50 g/L). In general, 50 mg of the dye was dissolved in 1 L of distilled water and the solution pH was adjusted by adding HCl (0.1N) or NaOH (0.1N). Calculated amount of adsorbent was added in 100 ml dye solution and was kept on shaker with constant shaking of 180 rpm. Then, 3 ml of the dye suspension was withdrawn at a regular time interval and centrifuged. The UV-visible absorption spectra of the supernatant solution were analysed using a UV-visible spectrometer (Thermo Scientific Evolution) in 1 cm quartz cuvettes to monitor the characteristic absorption peak of MB and MO. The percentage dye removal from the aqueous solution was determined according to the following equation:

$$\text{Percentage of dye removal, \%R} = \{(C_0 - C_t)/C_0\} \times 100 \quad (6.1)$$

where C₀ is the initial concentration of the MO (mg/L) and C_t is the concentration of MO (mg/L) at time t.

6.3 Results and Discussion

6.3.1 Synthesis

The main goal of this study was to design a new highly segregated, PANI coated GO nanocomposite doped with SrTiO₃ nanocubes, bearing cationic as well as anionic functional sites for the enhanced removal of MB and MO dyes. To achieve the desired goal, aniline monomer containing amine functionality was introduced on the surface of GO which was subsequently polymerized in the presence of ammonium persulphate in acidic medium in order to obtain PANI coated GO nanocomposite as shown in Figure 6.1. PANI coated GO nanocomposites contain positively charged polymeric backbone

and sp^2 hybridized framework along with anionic functionalities. However, due to stacking of GO sheets, PANI coated GO nanocomposite possess substantial amount of agglomeration, which reduces the effective surface area of adsorbent. In order to enhanced the effective surface area SrTiO₃ nanocubes were incorporated into the matrix of PANI coated GO nanocomposite where these nancubes acts as spacer molecules to segregate the GO sheets thereby increasing the total effective surface area, a prime requisition for an efficient adsorbent (Figure 6.1).

6.3.2 Characterization

6.3.2.1 Morphological Analysis of Nanocomposites

The morphological and structural analysis of the synthesized graphene oxide, PANI, SrTiO₃ nanocubes and GOPSr-2 nanocomposite were studied through FESEM. Figure 6.2 (a) explicates the morphology of PANI which displayed specific flake-like structure as the characteristic structure of PANI. Figure 6.2 (b) reveals the surface morphology of GO clearly illustrating the disorderly stacked, folded sheet like accumulation which is representative structure of GO. Figure 6.2 (c) depicts the morphology of SrTiO₃ nanocube. As evident from the micrographs, SrTiO₃ nanoparticles have attained cube-shaped morphology with approximately uniform particle size. Moreover, to confirm the formation of SrTiO₃ nanocubes the synthesized nanoparticles were analysed via TEM. Figure 6.2 (d) represents the TEM image of SrTiO₃ nanocubes which visibly reveals the formation of cubic particles in nanoscale thereby confirming the formation of SrTiO₃ nanocubes. Figure 6.2 (e) exhibits PANI coated GO nanocomposite, GOPSr-0 which indicate the transformation in the surface morphology of GO upon coating by PANI. As obvious from the figure, the folded and stacked GO sheets becomes much segregated after being coated by PANI. This segregation was further enhanced by doping PANI coated

GO with SrTiO₃ as illustrated by Figure 6.2 (f). The SrTiO₃ can be seen on the surface of the nanocomposites embedded within the layers of GO and PANI as demonstrated by Figure A-6 (a) and (b) (appendix A). Figure A-7 exhibits the TEM images of GOPSr-2 at different magnifications. As evident from the TEM micrographs, folded sheets of GO are coated by PANI whereas SrTiO₃ nanoparticles can be seen embedded within the GO layers. Therefore, coating of GO with PANI and doping with SrTiO₃ nanocubes had completely transformed the surface morphology with much segregated composite material thereby leading to the higher surface area, a prime requisition for an ideal adsorbent material.

University of Malaya

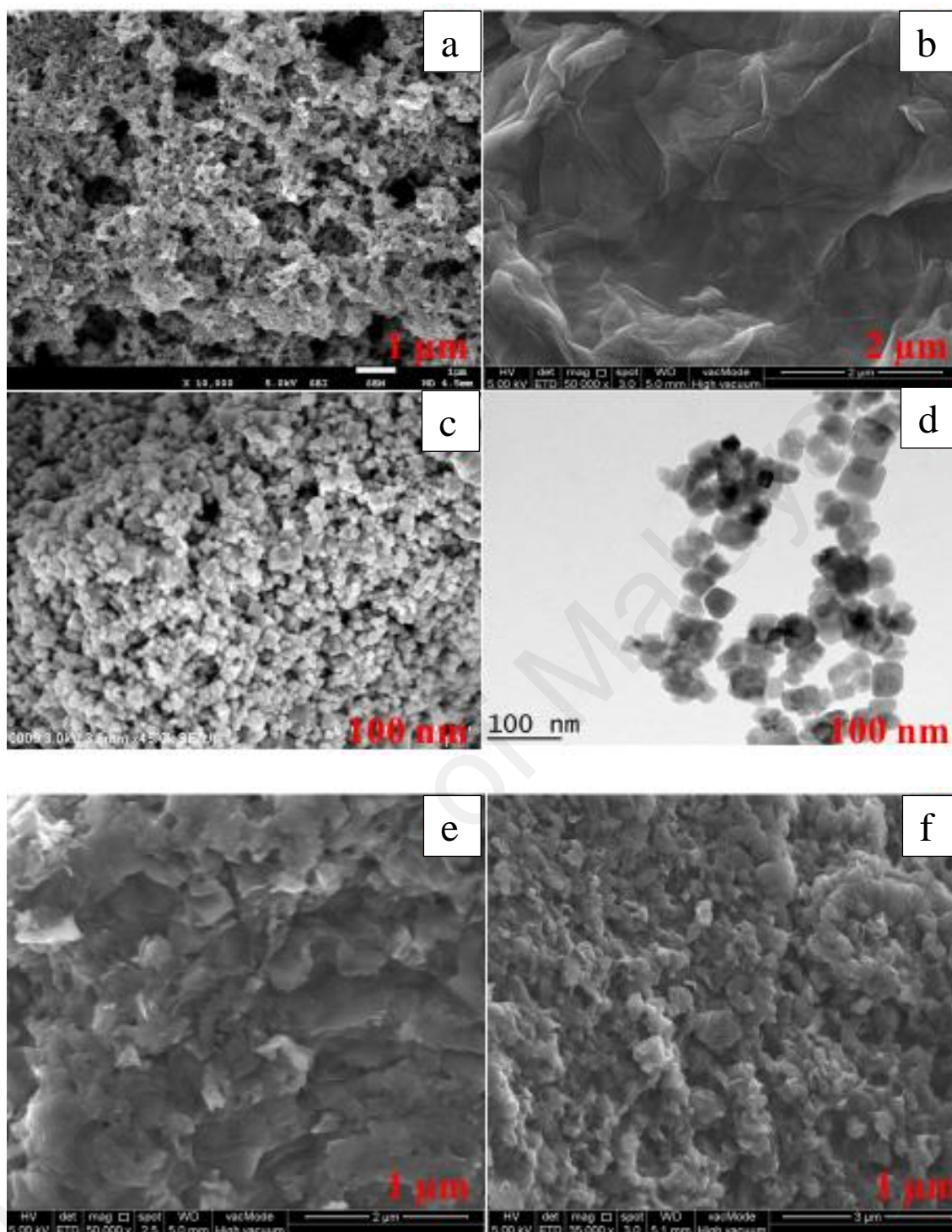


Figure 6.2: FESEM micrographs of (a) PANI, (b) GO, (c) SrTiO₃ nanocubes, (d) TEM of SrTiO₃ (e) GOPSr-0, (f) GOPSr-2 nanocomposite and (d) TEM image of SrTiO₃ nanocubes

Possibly owing to the lower concentration of SrTiO₃ nanocubes in nanocomposites (2 wt% with respect to GO), it is hard to observe SrTiO₃ nanoparticles uniformly in the

FESEM images of nanocomposites as these particles are embedded within the sheets of PANI coated GO. Hence, FESEM-mapping and FESEM-EDX might perhaps ascertain to be an appropriate method to validate the occurrence of SrTiO₃ nanoparticles in the matrix of PANI coated GO nanocomposite. Figure 6.3 demonstrates the elemental mapping analysis of GOPSr-2 which visibly reveals that SrTiO₃ nanocubes are uniformly present within the matrix of the composite material along with carbon, oxygen, nitrogen and chlorine. An elemental analysis {(Figure A-7) (appendix A)} displays the occurrence of strontium and titanium which additionally confirms the formation of SrTiO₃ nanocube-doped PANI coated GO nanocomposites.

University of Malaya

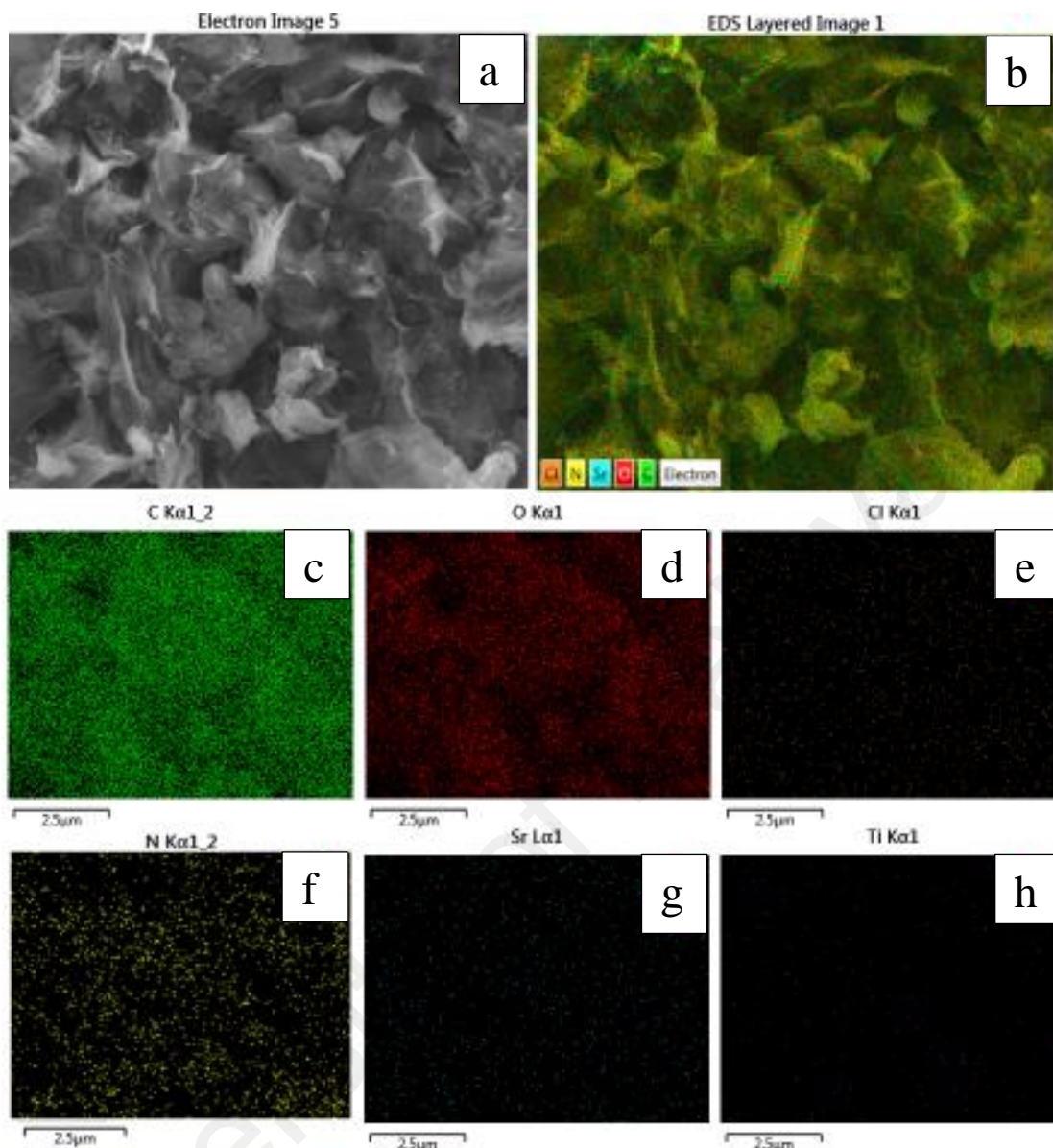


Figure 6.3: (a) FESEM image and (b) EDX elemental mapping of GOPSr-2 nanocomposite on a Si wafer for the following elements: (c) C, (d) O, (e) Cl, (f) N, (g) Sr and (h) Ti

6.3.2.2 FTIR Analysis

Figure 6.4 shows the FTIR spectra of PANI, GO, SrTiO₃, GOPSr-0 and GOPSr-2. The IR bands appearing at 1560 cm⁻¹ and 1480 cm⁻¹ signify the typical C-C stretching of quinoid and benzenoid rings in PANI, respectively. The peak at 1297 cm⁻¹ might be ascribed to C-N and C=N stretching modes in PANI. IR peaks at 807 cm⁻¹ and 1127 cm⁻¹ were allocated to out-of-plane C-H bending and in-plane C-H bending (Choudhury,

2009; Shahabuddin et al., 2016b). IR spectrum of GO reveals a broad peak around 3240 cm^{-1} which may be assigned to the O-H stretching vibrations. The IR peaks appearing at 1730, 1613, 1395 and 1219 cm^{-1} correspond to the C=O stretching mode, sp^2 -hybridized C=C stretching and O-H bending modes, C-OH stretching mode, and C-O-C stretching mode, respectively (Azarang et al., 2014). Additionally, the peak at 1044 cm^{-1} could be assigned to the C-O vibration due to the epoxy or alkoxy groups (Pham et al., 2011). The IR spectrum of SrTiO_3 exhibits a band around 3100 cm^{-1} which may be allocated to the O-H stretching modes in water of crystallization. The IR peaks around 1480, could be assigned to carboxylate group stretching modes, whereas the peaks at 855 and 600 cm^{-1} are attributed to TiO_6 octahedron bending and stretching vibration (Gopalakrishnamurthy et al., 1975; Shahabuddin et al., 2016b). The FTIR spectrum of PANI coated GO exhibits the characteristic GO band along with PANI peaks. The PANI peaks appear to be slightly shifted to 1568, 1482, 1257 and 801 cm^{-1} as revealed by the IR spectrum of PANI homopolymer. This slight shifting of peaks may be attributed to the change in chemical environment of PANI upon coating over GO indicating some chemical interaction between PANI chains and GO matrix. The IR spectrum of SrTiO_3 doped nanocomposite, GOPSr-2, exhibits characteristic peaks of both GO and PANI. The band at 1489 cm^{-1} represent the SrTiO_3 carboxylate group stretching modes which overlaps with C-C stretching of quinoid and benzenoid and is slightly shifted. The new peak also appears at 581 cm^{-1} slightly shifted towards red from its original position (600 cm^{-1}) which might be assigned to TiO_6 octahedron bending and stretching vibration mode. This slight shifting of the band towards red may perhaps be ascribed to some amount of weak Van der Waals attraction between the SrTiO_3 nanocubes with GO and PANI chains. Hence, the FTIR studies are in good agreement with reported literature and evidently stipulate the formation of PANI, GO, SrTiO_3 and SrTiO_3 doped PANI coated GO nanocomposites.

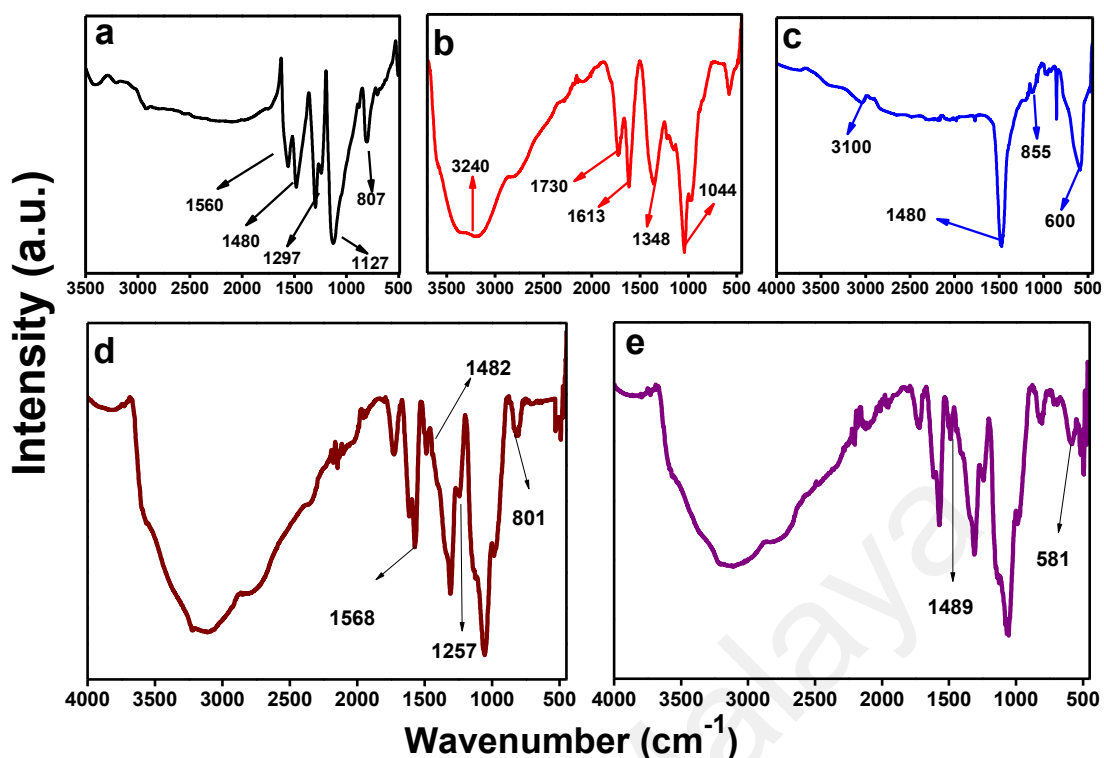


Figure 6.4: FTIR spectrum of (a) PANI, (b) GO, (c) SrTiO₃, (d) GOPSr-0 and (e) GOPSr-5

6.3.2.3 XRD Analysis

Figure 6.5 depicts the wide-angle X-ray diffraction (WAXD) pattern of the powder samples of hydrothermally synthesized SrTiO₃ nanocubes, GO, PANI homopolymer and GOPSr-2. SrTiO₃ nanocubes indicated good crystallinity with diffraction peaks corresponding to (100), (110), (111), (200), (210), (211), (220), (310), (311), and (222) planes of cubic perovskite SrTiO₃ structure respectively. These peaks are characteristic of SrTiO₃ and can be readily indexed as those of cubic perovskite structure (space group: Pm3m) of SrTiO₃ in accordance with JCPDS card no. 35-0734 (Shahabuddin et al., 2016b). The presence of well-defined and very sharp peaks in the XRD pattern of SrTiO₃ nanocubes indicate the well-developed crystalline structure. The XRD pattern of the GO illustrated an intense and sharp peak centered at $2\theta = 10.40$ which corresponds to the interplanar spacing of GO sheets. The observed 2θ for GO could be designated to the (001) reflection plane which is usually governed by the process of synthesis and number

of layers of water within the interplanar space of GO (Kumar et al., 2012; Zhang, 2010). As evident from Figure 6.5, PANI homopolymer exhibited the typical diffraction peaks at 2θ values of 15.60, 20.25, and 25.35 which are the characteristic peaks of conductive PANI. These peaks indicate the polycrystalline nature of PANI homopolymer (Rahy et al., 2008). The peaks appearing at angles of 2θ value of 20.77 and 25.27 epitomises the periodic repetition of benzenoid and quinoid rings in PANI chains (Shi et al., 2009). As apparent from the XRD pattern of GOPSr-2, the intense peak of GO has significantly reduced indicating that the aggregation of GO sheets had been considerably diminished and were abundantly utilized as the substrate by PANI homopolymer to produce a nanocomposite hybrid material (Kumar et al., 2012). Characteristic PANI and SrTiO₃ diffraction peaks can be seen clearly in the XRD spectrum of GOPSr-2 nanocomposite (marked by asterisk) which stipulate the uniform occurrence of PANI and SrTiO₃ nanocubes in nanocomposite. Therefore, XRD investigation established successful synthesis of SrTiO₃, GO, PANI and formation SrTiO₃ doped PANI coated GO nanocomposite.

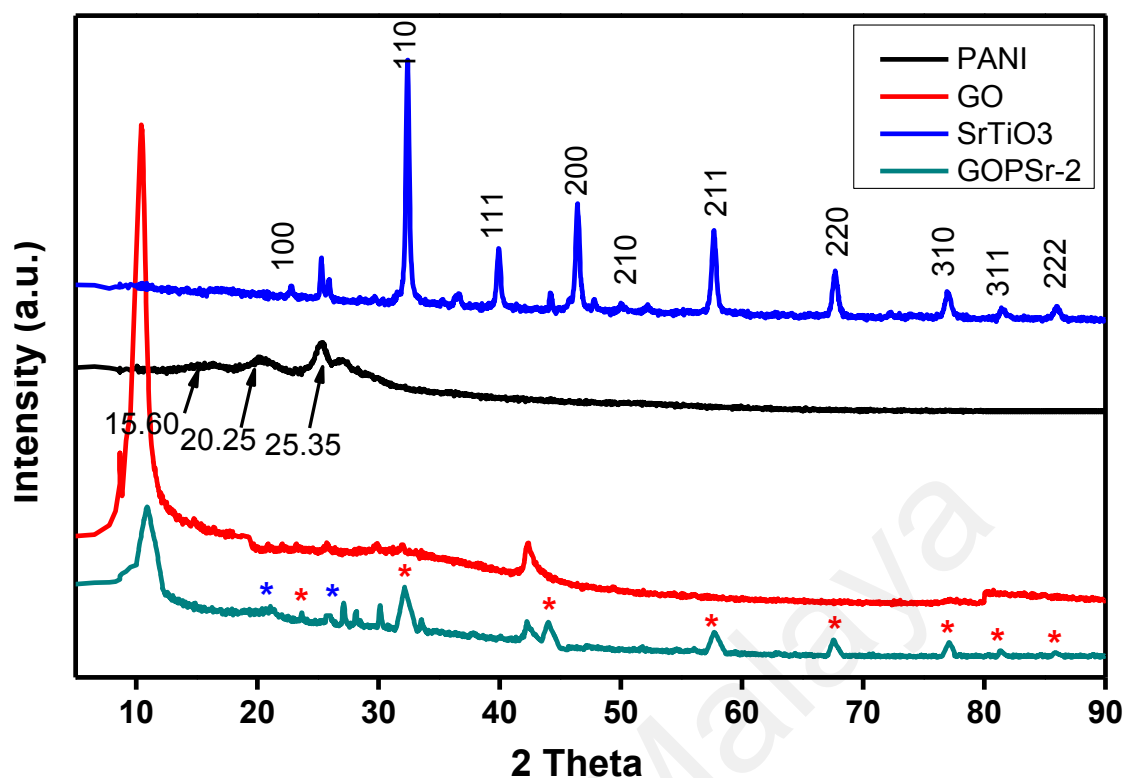


Figure 6.5: XRD pattern of PANI, GO, SrTiO₃, and GOPSr-2

6.3.3 Adsorption Studies

6.3.3.1 Adsorption Analysis of MB and MO

The aqueous-phase adsorption behaviour of MB and MO dyes was examined in a set of Erlenmeyer flasks, by batch process using a shaker with constant shaking of 180 rpm at ambient temperature, in the presence of SrTiO₃ nanocubes, GO, PANI homopolymer, GOPSr-0, GOPSr-1, GOPSr-2, and GOPSr-5 nanocomposites. Figure 6.6 and Figure 6.7 shows the adsorption behavior and percentage adsorption of MB and MO in the presence of various adsorbents, which clearly reveals the efficient adsorption phenomenon taking place between the dyes and adsorbents molecules. The adsorption data evidently demonstrated that SrTiO₃ nanocubes, GO and PANI homopolymer showed lower adsorption efficiencies as compared to the adsorption efficiencies of SrTiO₃ nanocubes-doped polyaniline coated GO nanocomposites, namely, GOPSr-1, GOPSr-2, and GOPSr-5. As apparent from Figure 6.6 (b) and 6.7 (b), the percentage adsorption for MB depicts

the following trend: GOPSr-2 > GOPSr-1 > GOPSr-5 > GOPSr-0 > GO > PANI > SrTiO₃ whereas percentage adsorption for MO illustrates the following trend: GOPSr-2 > GOPSr-5 > GOPSr-1 > GOPSr-0 > GO > PANI > SrTiO₃. Figure 6.6 (a) and 6.7 (a) exhibits the UV-vis adsorption spectra of the MB and MO in presence of different nanocomposites which indicate that the adsorption efficiency of nanocomposites is greatly enhanced in presence SrTiO₃ nanocubes as compared to bare GO, PANI and PANI coated GO thereby predicting a synergistic phenomenon between SrTiO₃ nanocubes GO and PANI. Approximately 99% of MB and 91% of MO were removed within a short duration of 30 minutes demonstrating enhanced adsorption efficiency of GOPSr-2 nanocomposite over SrTiO₃ nanocubes, GO, PANI homopolymer, GOPSr-0, GOPSr-1, and GOPSr-5 which exhibited nearly 8%, 57%, 18%, 78%, 87% and 84% adsorption for MB whereas 1.3%, 36%, 61%, 72% 84% and 89% adsorption for MO respectively. Therefore, the adsorption analysis of MB and MO dyes illustrates GOPSr-2 nanocomposite as an optimum adsorbent for efficient removal of carcinogenic MB and MO dyes from aqueous solutions.

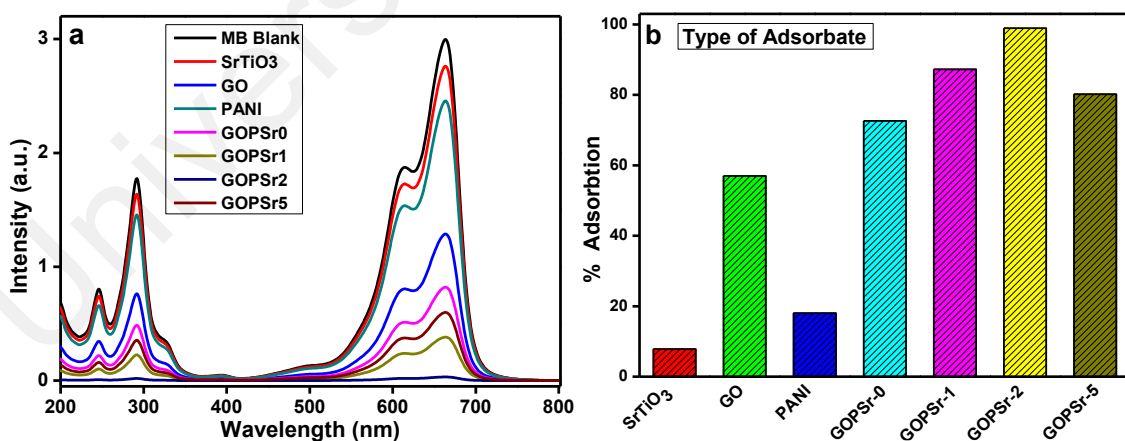


Figure 6.6: UV-vis absorption spectra of MB aqueous in the presence of various adsorbents and (b) Percentage removal of MB in the presence of various adsorbents. {initial MB concentration: 20 mg l⁻¹; amount of adsorbent: 0.5mg m⁻¹; pH 7; time: 30 minutes; at room temperature}

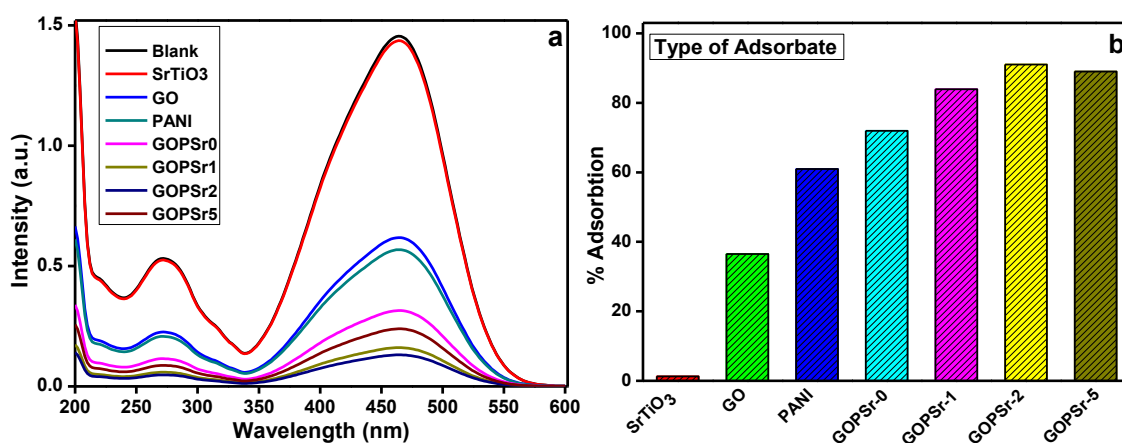


Figure 6.7: UV-vis absorption spectra of MO aqueous in the presence of various adsorbents and (b) Percentage removal of MO in the presence of various adsorbents. {initial MO concentration: 20 mg l⁻¹; amount of adsorbent: 0.5mg ml⁻¹; pH 7; time: 30 minutes; at room temperature}

Accumulation of a substance between liquid-solid interface or gas-solid interface due to physical or chemical associations is termed as adsorption process. With few exceptions, adsorption is usually controlled by physical parameters on most of the adsorbents such as polarity, van der Waals forces, hydrogen bonding, dipole-dipole interaction, π - π interaction, etc. (Choudhury, 2009). Therefore, the design of adsorbent usually depends on the type of substance to be adsorbed or removed where these physical parameters can be efficiently utilized. MB is a cationic dye which can be removed by adsorbent showing strong affinity towards positively charged species whereas MO is an anionic dye which required positively polar material for its efficient removal. GO, due to the presence of sp^2 hybridized framework and oxygen-containing functionalities such as hydroxyl and epoxy groups tend to show enhanced affinity towards cationic species. As evident from percentage adsorption data GO alone can adsorbed 57% of MB dye due to its cationic nature whereas it only removed 36% of MO which may be perhaps due to formation of hydrogen bonding or van der Waal's attraction between MO and GO. On the other hand, polyaniline in its conductive emeraldine salt state possess large number of amine ($-N<$) and imine ($-N=$) functional groups and possesses substantial amounts of positive charges localized over its backbone making it a suitable candidate for efficient adsorption of

negatively polarized substances. Thus, when PANI alone was used as adsorbent, it was capable of adsorbing 61% of MO while it only adsorbs 18% of MB. Thus, designing a nanocomposite material comprising of GO coated with conductive chains of PANI may offer an alternate material which can adsorb MB as well as MO simultaneously. As illustrated by percentage adsorption results in Figure 6.6 (b) and 6.7 (b), PANI coated GO (GOPSr-0) efficiently adsorbed MB and MO with 78% and 72% adsorption efficiency, respectively. However, although the efficiency of PANI coated GO has enhanced substantially, but still the overall performance of the nanocomposite was on lower side. This might be due to agglomeration of disorderly stacked GO sheets which reduces the effective surface area of the adsorbent and do not allow efficient adsorption of dye molecules on the surface of adsorbent. Therefore, in order to segregate the stacked GO layers, SrTiO₃ nanocubes were incorporated inside the nanocomposites during polymerization process (Figure 6.1). These SrTiO₃ nanocubes adhered to the sheets of GO through Sr³⁺ ions interactions with *sp*² hybridized framework of GO. Thus they act as spacers which help in segregation of GO sheets thereby enhancing the total effective surface area and increasing the thermal stability of the nanocomposite material as discussed in thermal analysis section. Hence, as revealed by adsorption results, SrTiO₃ nanocube-doped polyaniline coated GO nanocomposites showed highly enhanced adsorption capacity as compared to neat GO, PANI and GOPSr-0. The adsorption efficiency increased to 99% for MB and 91% for MO upon doping 2 wt.% of SrTiO₃ with respect to GO. The amount of doping percentage was optimized by varying the concentration of SrTiO₃ and it was found that when percentage of SrTiO₃ was increased to 5% there is slight decrease in adsorption efficiency which might be due to agglomeration of SrTiO₃ nanocubes at a high doping percentage predicting GOPSr-2 to be an optimum adsorbent composition.

6.3.3.2 Effect of Adsorbent Dosage

The effect of adsorbent dosage on percentage removal of MB and MO was examined by taking different quantities of GOPSr-2 nanocomposite ranging from 0.25 to 5 mg ml⁻¹ and investigating the dye adsorption efficiency with an initial concentration of 20 mg l⁻¹, pH 7 and ambient temperature for both dyes. Figure 6.8 depicts the percentage adsorption of MB and MO by GOPSr-2. As evident from the figure, the percentage adsorption of MB increases with increase in amount of adsorbent from 0.25 mg ml⁻¹ to 0.5 mg ml⁻¹ and become constant at higher dosage. Approximately 85% of MB was adsorbed on the surface of adsorbent when the dosage was 0.25 mg ml⁻¹ and increased to 99% on increasing the amount of adsorbent to 0.5 mg ml⁻¹. On the other hand, for MO, percentage removal increases gradually with the increase in adsorbent dosage from 0.25 mg ml⁻¹ to 0.5 mg ml⁻¹ with 19%, 39%, 74%, 91% and 95% adsorption at an adsorbent dosage of 0.25, 0.5, 1, 2 and 5 mg ml⁻¹ respectively. The increase in adsorption efficiency with increasing the amount of adsorbent could be ascribed to availability of more adsorption sites and increases in the available effective surface area increased adsorbent dosage. Moreover, the results reveal that GOPSr-2 have strong affinity toward MB as compared to MO as percentage removal was found to be 99% for MB and 39% for MO at adsorbent dosage of 0.5 mg ml⁻¹. Therefore, 0.5 mg ml⁻¹ and 2 mg ml⁻¹ were used as selected as the optimum dosage for MB and MO respectively, for subsequent experiments.

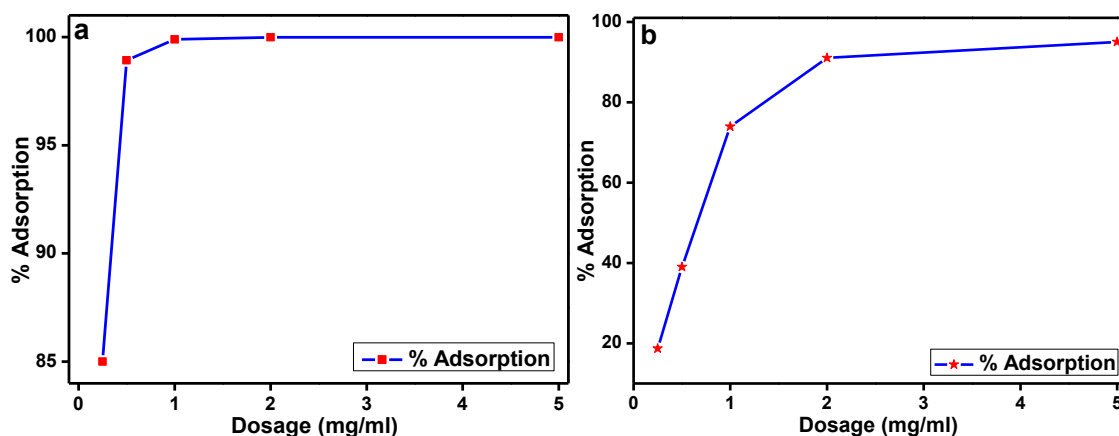


Figure 6.8: Effect of adsorbent dosage on percentage removal of (a) MB and (b) MO in presence of GOPSr-2. {initial MB and MO concentration: 20 mg l⁻¹; pH 7; time: 30 minutes at room temperature}

6.3.3.3 Effect of Contact Time

Contact time is an important parameter to determine the efficiency of adsorbent as rapid rate of adsorption indicates an efficient adsorbent. In order to determine the effect of contact time on percentage removal of dyes, adsorption was monitored at particular interval of time ranging from 10 to 60 minutes with an initial concentration of 20 mg l⁻¹, pH 7 and ambient temperature using an adsorbent dosage of 0.5 mg ml⁻¹ for MB and 2 mg ml⁻¹ for MO. Figure 6.9 illustrates the effect of contact time on percentage removal of MB and MO. As apparent from the figure, approximately 99% of MB was adsorbed on the surface of GOPSr-2 within 10 minutes indicating a rapid and efficient adsorption phenomenon. Alternatively, the adsorption of MO increases steadily with increase in time and reaches to an equilibrium at up to 40 minutes of contact time with approximately 94% of dye adsorption. Thus, based upon the following experiment 10 and 40 minutes were selected as an optimized contact time for further experiments.

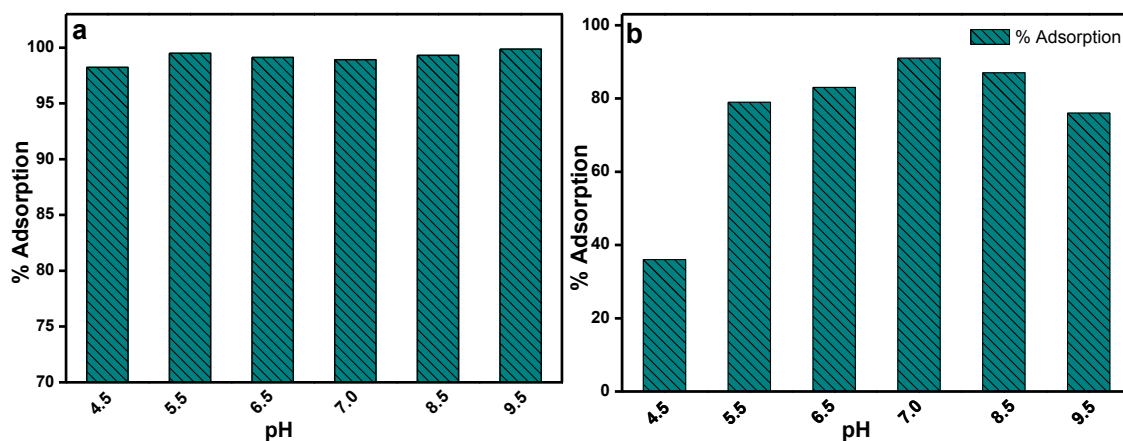


Figure 6.9: Effect of pH on percentage removal of (a) MB and (b) MO in presence of GOPSr-2. {initial MB and MO concentration: 20 mg l⁻¹; amount of adsorbent (MB): 0.5mg ml⁻¹, (MO) :2mg ml⁻¹; time: 30 minutes at room temperature}

6.3.3.4 Effect of pH

Amongst various physical parameters, the most significant factor influencing the efficiency of adsorbent in wastewater treatment is the pH of solution. The effectiveness of adsorption is reliant on the pH of medium, since diversity in pH prompts the variations in the surface properties of adsorbent and degree of ionization of the dyes molecules (Yagub et al., 2014). Hence, the effect of solution pH on the percentage removal of MB and MO dyes was investigated using GOPSr-2 as adsorbent at pH range from 4.5 to 9.5 adjusted by the addition of 0.1 N HCl or 0.1 N NaOH at ambient temperature. As depicted by figure 9, the adsorption of MB does not show any significant change from pH 4.5 until 9.5 thereby indicating GOPSr-2 to an excellent adsorbent material working on wide range of pH. However, MO adsorption on GOPSr-2 seems to be pH dependent with maximum adsorption attained at pH 7. This might be explained on the basis of pKa value of MO which is around 3.4. Therefore, if the pKa is more than the pH of MO which predominantly exists in anionic form, it gets protonated. Additionally, in acidic environment PANI tends to develop positive charge on its conductive backbone due to the presence basic (imine and amine) groups. Thus, at acidic pH significant amount of electrostatic repulsion occurred between positively charged PANI backbone and

protonated MO molecules which tends to decrease the adsorption efficiency of GOPSr-2 for MO adsorption. At pH values above 7, adsorption behaviour illustrates the gradual decrease up to pH 9.5 which might be owing to the competitive adsorption of hydroxyl ion on imine and amine groups resulting in the decline in MO adsorption. Thus, for both the dyes, the maximum adsorption was achieved at neutral pH (7) with approximately 98% adsorption for MB and 91% adsorption for MO.

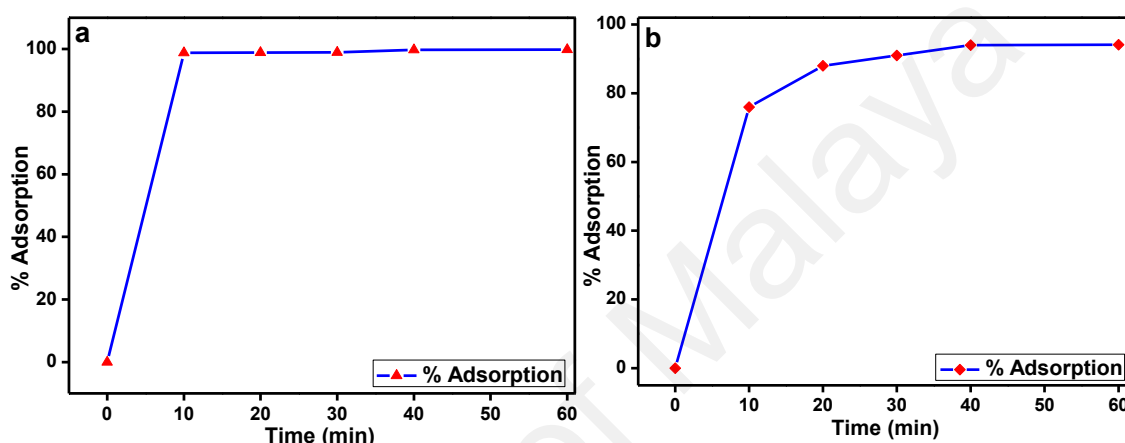


Figure 6.10: Effect of time on percentage removal of (a) MB and (b) MO in presence of GOPSr-2. {initial MB and MO concentration: 20 mg l⁻¹; amount of adsorbent (MB): 0.5mg ml⁻¹, (MO) :2mg ml⁻¹; pH(MB): 9.5 (MO): 7; at room temperature}

6.3.3.5 Effect of NaCl Concentration

One of the ultimate significant features in adsorption investigations, which have been reported by many researchers, is the effect of salt concentration on the percentage removal of dyes from Industrial dye waste water. Since commercial dye waste water generally contains high salt contents, thus, it becomes crucial to study the effect of salt concentration on the percentage removal of MB and MO from aqueous solution using GOPSr-2 nanocomposite. Figure 6.11 illustrates the effect of NaCl with variable concentrations ranging from 10 to 50 g l⁻¹ on MB and MO removal percentage by GOPSr-2. As apparent from Figure 6.11, the adsorption efficacy of nanocomposite is considerably influenced by the presence of NaCl. The adsorption capability of the nanocomposite decline with the increase in NaCl concentration from 10 to 50 g l⁻¹. The

percentage removal decreases from 99 percent to 89.60 percent and 95 percent to 81.75 percent with increase in concentration of NaCl by 50 g l⁻¹ for MB and MO respectively. This reduction in adsorption efficiency may be attributed to the neutralization of the surface charge of adsorbent by electrolyte ions which competes with dye molecules for the adsorption on the surface of nanocomposite. Nevertheless, this decline in adsorption efficiency is not very high which specifies that GOPSr-2 can effectively remove MB and MO from aqueous solution even in the presence of high concentration of salt.

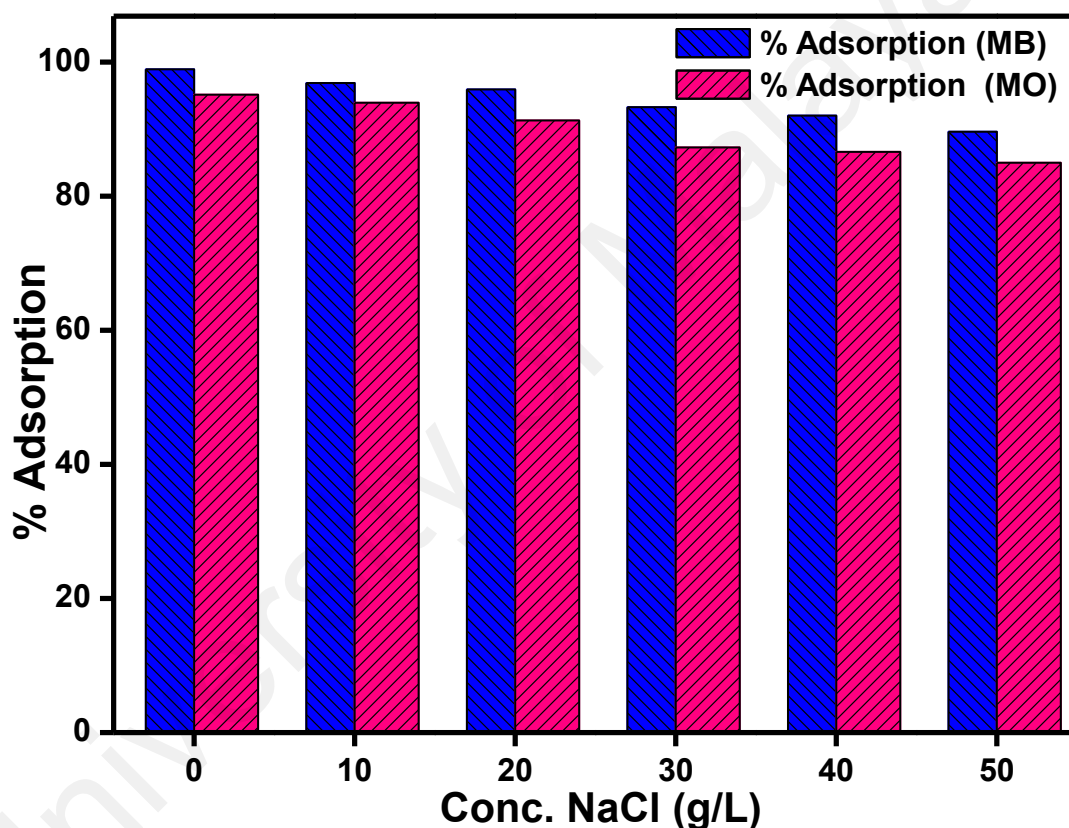


Figure 6.11: Effect of NaCl conc. on percentage removal of MB and MO in presence of GOPSr-2. {initial MB and MO concentration: 20 mg l⁻¹; amount of adsorbent (MB): 0.5mg ml⁻¹, (MO) :2mg ml⁻¹; pH(MB): 9.5 (MO): 7; at room temperature}

6.3.3.6 Reusability Studies

Stability and reusability of the adsorbent are considered to be the important factors for practical application and need to be thoroughly examined. Hence, reusability investigations of GOPSr-2 were conducted for examine the effect in adsorption capacity

of nanocomposite after repeated usage cycles. Figure 6.12 illustrated the reusability of GOPSr-2 for the adsorption of MB and MO up-to five cycles. The adsorbent after first cycle was recovered via centrifugation and filtration followed by thorough washing with deionised water, dried at 80° C in vacuum oven for two hours and successively employed as adsorbent for additional cycles so as to study their adsorptive efficiencies. As apparent from Figure 6.12, there is marginal decrease in the adsorption efficiency of the adsorbent after each repeated cycle. The percentage removal for MB was found to be 96.50%, 92.75%, 87.20% and 84.15% and for MO was found to be 94.20%, 91.35%, 85.90% and 81.75% for second, third, fourth and fifth cycle respectively. This decrease in efficiency could be owing to the fact that a substantial amount of unavoidable weight loss occurred during recovery and purification of adsorbent which contribute to the decrease in adsorption efficiency in each repeated cycle besides reduction in active available sites due to some adsorbed dye molecules. However, the investigation clearly reveals that approximately 84% of MB and 82% of MO can be removed even in the fifth cycle signifying high stability and reusability efficiency of GOPSr-2 nanocomposite.

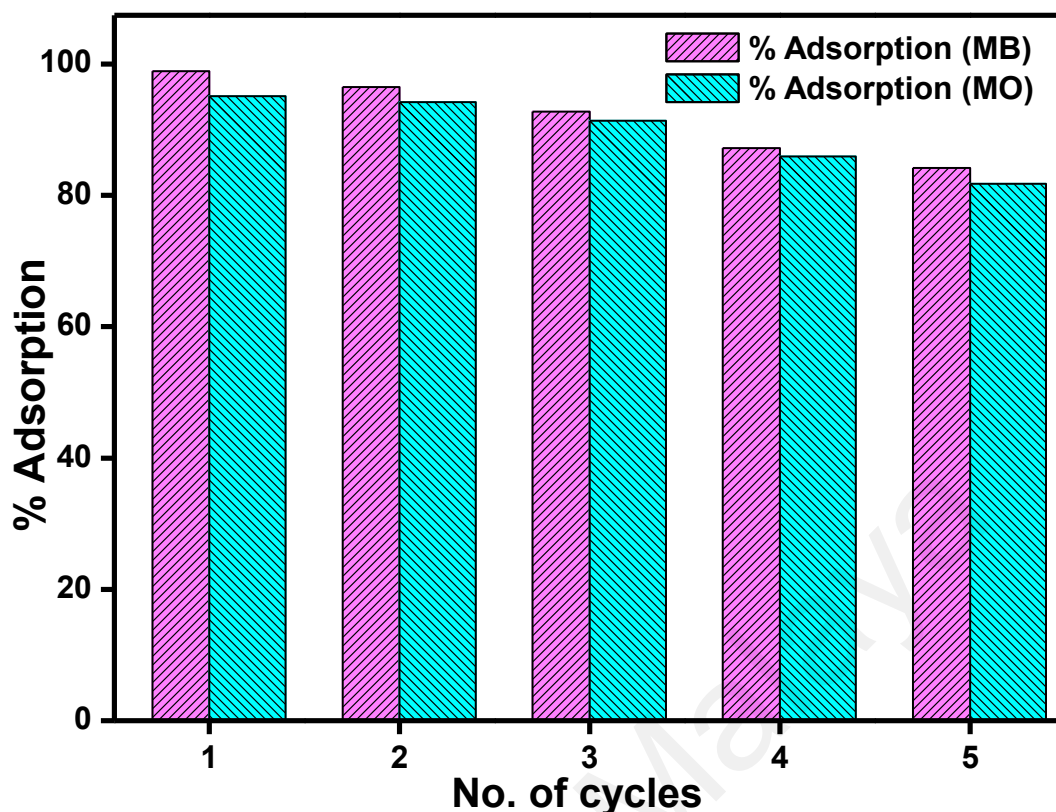


Figure 6.12: Reproducibility cycles of GOPSr-2 for MB and MO adsorption {initial MB and MO concentration: 20 mg l^{-1} ; amount of adsorbent (MB): 0.5 mg ml^{-1} , (MO) : 2 mg ml^{-1} ; pH(MB): 9.5 (MO): 7; at room temperature}

6.3.4 Proposed Mechanism

Figure 6.13 illustrates the schematic representation of the proposed adsorption mechanism of MB and MO by GOPSr-2. Adsorption mechanism can be explained as follows:

Since MB and MO are cationic and anionic in nature therefore, electrostatic attraction is one of the major factor which enhances the efficient removal of charged dyes. Since GO contains hydroxyl and epoxy groups along with sp^2 hybridized framework which makes it overall negatively polarised thereby forming strong electrostatic interaction with MB for its efficient removal. On the other hand, due to the presence of positively charged polymeric backbone, PANI contributes in the efficient removal of MO through electrostatic attraction. (This part has been comprehensively discussed in section 6.3.3.1).

Besides, since the surface of GOPSr-2 contains C=O and OH groups functional groups, whereas MB and MO contains CH₃ groups, so the lone pair of C=O and OH functional groups forms intermolecular H-bonding with CH₃ groups of MB & MO, thereby aiding in their efficient removal from the aqueous solution. Moreover, MB and MO dyes are ideally planar molecules which can be easily absorbed on the surface of GOPSr-2 via π - π interaction between the aromatic backbone of the dye and aromatic skeleton of the GOPSr-2 adsorbent. Therefore, all these physical forces, namely, electrostatic interaction, intermolecular H-bonding and π - π interaction works synergistically and leads in the efficient removal of dyes from aqueous solutions within a short duration of time.

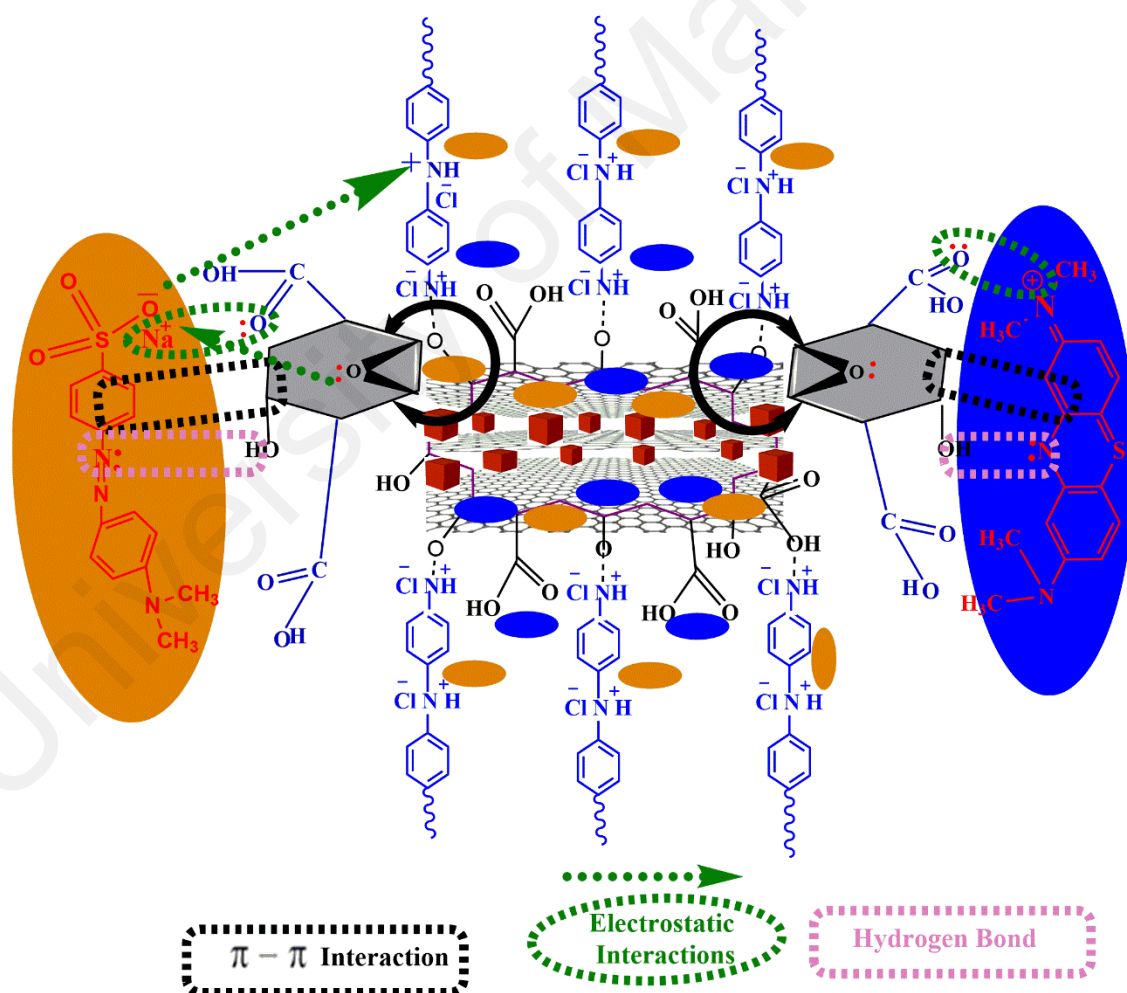


Figure 6.13: Proposed mechanism for the adsorption of MB and MO on the surface of GOPSr-2

6.4 Conclusion

Polyaniline coated graphene oxide doped with SrTiO₃ nanocube nanocomposites have been successfully synthesized via facile in situ oxidative polymerization technique. PANI was successfully coated on to the GO sheets and SrTiO₃ nanocubes were successfully incorporated within the matrix of nanocomposite. The surface morphology of GO completely transformed from aggregated sheets to much segregated one upon incorporation of PANI and SrTiO₃ nanocubes as depicted by FESEM analysis. The synthesized nanocomposites exhibited greater adsorption efficiencies as compared to bare GO and PANI homopolymer suggesting a synergistic phenomenon taking place between polymer chain, Graphene sheets and cubic nanoparticles. The removal efficiency of MB and MO was found to be pH dependent with maximum dye adsorption at pH 7 and no significant decrease in adsorption capacity was observed even at high salt concentration. Furthermore, synthetic methodology proposed here may be used for the synthesis of numerous SrTiO₃ nanocube-doped GO nanocomposites materials utilising other conducting polymers which may address the present concern of environmental pollution.

CHAPTER 7: CONCLUSION AND FUTURE WORK

The present research work highlights the synthesis and application of conducting polymer based nanocomposites for photocatalysis and adsorption applications. The nanocomposites were designed based upon the inherent properties such as nature of charge, band gap and adsorption capabilities of the materials. The synthesized nanocomposites were characterized comprehensively using various techniques including field emission scanning electron microscopy (FESEM), transmission electron microscopy (TEM), thermogravimetric analysis (TGA), X-ray diffraction (XRD), Fourier transform infrared spectroscopy (FTIR), UV-vis spectroscopy and X-ray photoelectron spectroscopy (XPS). These nanocomposites demonstrated enhanced physical and chemical properties, facile method of synthesis at room temperature, higher thermal stability, increased level of photocatalytic capabilities, enhanced adsorption efficiencies and reusability properties, which made them elegant materials for waste water treatment. These nanocomposites were successfully applied as photocatalysts and adsorbents for the degradation and removal of carcinogenic dyes from waste water.

Co_3O_4 nanocube-doped polyaniline based nanocomposite was synthesized via in-situ oxidative polymerization where the amount of nanocubes were optimised for obtaining maximum adsorption efficiency. The adsorption efficacies of PANI homopolymer and Co_3O_4 nanocube-doped nanocomposites were assessed by observing the adsorption of methyl orange as a model dye from aqueous solution. The results showed that the Co_3O_4 nanocubes-doped nanocomposites demonstrated higher degree of adsorption capacity as compared with the undoped PANI and the adsorption kinetics followed a pseudo second order kinetics. Furthermore, the nanocomposite with 4 wt% Co_3O_4 nanocubes with

respect to aniline exhibited a superior adsorption capacity (107 mg g^{-1}) as compared with other absorbents.

Since PANI can adsorb light energy and form active oxidation species (AOS) responsible for photodegradation of toxic pollutants, therefore its nanocomposite comprising Co_3O_4 nanocube and chitosan was designed to study photodegradation of methylene blue. PANI was grafted with chitosan (ChGP) and doped with various percentage of Co_3O_4 nanocube to obtain optimized photocatalyst with enhanced photocatalytic efficiency. The photocatalytic efficiencies of ChGP and Co_3O_4 nanocube-doped copolymers were estimated by monitoring the degradation of methylene blue dye under UV illumination. As per the obtained results, the degradation efficiency of Co_3O_4 nanocubes-doped copolymer photocatalysts was found to be higher than that of the undoped copolymer. Moreover, the nanocomposite with 2 wt% Co_3O_4 nanocubes with respect to aniline demonstrated maximum degradation efficiency and was found to be the optimum photocatalyst, with an 88% degradation efficiency after 180 minutes of irradiation under UV light.

As sunlight is green and easily available source of energy, therefore SrTiO_3 nanocubes-doped polyaniline nanocomposites were fabricated to be used as photocatalyst for degradation of harmful organic dye under solar irradiation. The photocatalytic proficiencies of the photocatalysts were studied by degrading methylene blue (MB) under visible-light irradiation. The results exhibited that the degradation efficiency of the SrTiO_3 nanocubes-doped nanocomposites possess higher photocatalytic efficiency than that of the undoped polyaniline. Additionally, the amount

of SrTiO₃ percentage in the nanocomposites was optimised and effects of weight ratio of polyaniline to SrTiO₃ on the photocatalytic activities were investigated. The results revealed that the nanocomposite P-Sr500, with a 97% degradation efficiency after 90 minutes of irradiation under solar light, was found to be an optimum photocatalyst.

Finally, to adsorb cationic as well as anionic dyes by same adsorbent, a new nanocomposite was designed comprising of PANI coated with graphene oxide and doped with SrTiO₃ nanocube through facile in-situ oxidative polymerization method. The presence of oxygenated functional groups comprising of hydroxyl and epoxy groups in GO and nitrogen containing functionalities such as imine groups and amine groups in polyaniline work synergistically to impart cationic and anionic nature to the synthesised nanocomposite whereas SrTiO₃ nanocubes act as spacers aiding in segregation of GO sheets thereby increasing the effective surface area of nanocomposite. These nanocomposites were employed as adsorbents for the efficient removal of carcinogenic dyes, namely, the cationic dye methylene blue and the anionic dye methyl orange. The adsorption efficiencies of graphene oxide (GO), PANI homopolymer and SrTiO₃ nanocubes-doped nanocomposites were assessed by monitoring the adsorption of methylene blue and methyl orange dyes from aqueous solution. The adsorption efficiency of nanocomposites doped with SrTiO₃ nanocubes were found to be of higher magnitude as compared with undoped nanocomposite. Moreover, the nanocomposite with 2 wt% SrTiO₃ with respect to graphene oxide demonstrated excellent adsorption behaviour with 99% and 91% removal of MB and MO respectively, in a very short duration of time.

Thus the whole research work can be summarized that by designing and developing conducting polymer based nanocomposites with suitable metal oxides nanoparticles for tuning the surface and physicochemical properties and by manipulating the band gap of nanocomposites, new class of photocatalysts and adsorbents materials can be fabricated for environmental applications.

Future Work

Further research work will be carried out towards synthesis of nanocomposites comprising various other conducting polymers such as polypyrrole, polythiophene etc. with different metal oxides nanoparticles. The fabrication of nanocomposite by optimising the various parameters will be then characterized and evaluated for their photocatalytic and adsorption applications.

University of Malaya

REFERENCES

- Abu-Zied, B., & Soliman, S. (2009). Nitrous oxide decomposition over $\text{MCO}_3\text{-Co}_3\text{O}_4$ (M= Ca, Sr, Ba) catalysts. *Catalysis Letters*, 132(3-4), 299-310.
- Adams, V., Marley, J., & McCarroll, C. (2007). Prilocaine induced methaemoglobinaemia in a medically compromised patient. *British Dental Journal*, 203(10), 585-587.
- Adireddy, S., Lin, C., Cao, B., Zhou, W., & Caruntu, G. (2010). Solution-based growth of monodisperse cube-like BaTiO_3 colloidal nanocrystals. *Chemistry of Materials*, 22(6), 1946-1948.
- Ahdulrazzaq, O., Bourdo, S. E., Woo, M., Saini, V., Berry, B. C., Ghosh, A., & Biris, A. S. (2015). Comparative aging study of organic solar cells utilizing polyaniline and PEDOT:PSS as hole transport layers. *ACS Applied Materials & Interfaces*, 7(50), 27667-27675.
- Ahmad, R., & Kumar, R. (2010). Conducting polyaniline/iron oxide composite: a novel adsorbent for the removal of amido black 10B. *Journal of Chemical & Engineering Data*, 55(9), 3489-3493.
- Ahmad Rafiqi, F., & Majid, K. (2015). Removal of copper from aqueous solution using polyaniline and polyaniline/ferricyanide composite. *Journal of Environmental Chemical Engineering*, 3(4, Part A), 2492-2501.
- Ai, L., Zhang, C., & Chen, Z. (2011). Removal of methylene blue from aqueous solution by a solvothermal-synthesized graphene/magnetite composite. *Journal of Hazardous Materials*, 192(3), 1515-1524.
- Akbari, A., Remigy, J., & Aptel, P. (2002). Treatment of textile dye effluent using a polyamide-based nanofiltration membrane. *Chemical Engineering and Processing: Process Intensification*, 41(7), 601-609.
- Aksu, Z. (2005). Application of biosorption for the removal of organic pollutants: a review. *Process Biochemistry*, 40(3), 997-1026.
- Aldissi, M., & Armes, S. (1992). X-ray photoelectron spectroscopy study of bulk and colloidal polyaniline. *Macromolecules*, 25(11), 2963-2968.
- Ali, I., & Gupta, V. (2006). Advances in water treatment by adsorption technology. *Nature protocols*, 1(6), 2661-2667.
- Amass, W., Amass, A., & Tighe, B. (1998). A review of biodegradable polymers: uses, current developments in the synthesis and characterization of biodegradable polyesters, blends of biodegradable polymers and recent advances in biodegradation studies. *Polymer International*, 47(2), 89-144.
- Ameen, S., Akhtar, M. S., Kim, Y. S., Yang, O. B., & Shin, H.-S. (2011). An effective nanocomposite of polyaniline and ZnO: preparation, characterizations, and its photocatalytic activity. *Colloid and Polymer Science*, 289(4), 415-421.

- Anand, J., Palaniappan, S., & Sathyanarayana, D. (1998). Conducting polyaniline blends and composites. *Progress in Polymer Science*, 23(6), 993-1018.
- Anbia, M., Hariri, S. A., & Ashrafizadeh, S. (2010). Adsorptive removal of anionic dyes by modified nanoporous silica SBA-3. *Applied Surface Science*, 256(10), 3228-3233.
- Angelopoulos, M. (2001). Conducting polymers in microelectronics. *IBM Journal of Research and Development*, 45(1), 57-75.
- Angelopoulos, M., Asturias, G., Ermer, S., Ray, A., Scherr, E., MacDiarmid, A., Epstein, A. (1988). Polyaniline: solutions, films and oxidation state. *Molecular Crystals and Liquid Crystals*, 160(1), 151-163.
- Angelopoulos, M., Ray, A., Macdiarmid, A. G., & Epstein, A. J. (1987). Polyaniline: processability from aqueous solutions and effect of water vapor on conductivity. *Synthetic Metals*, 21(1), 21-30.
- Armes, S., Aldissi, M., Agnew, S., & Gottesfeld, S. (1990). Synthesis and characterization of aqueous colloidal dispersions of poly (vinyl alcohol)/polyaniline particles. *Molecular Crystals and Liquid Crystals*, 190(1), 63-74.
- Armes, S., & Miller, J. (1988). Optimum reaction conditions for the polymerization of aniline in aqueous solution by ammonium persulphate. *Synthetic Metals*, 22(4), 385-393.
- Ateh, D., Navsaria, H., & Vadgama, P. (2006). Polypyrrole-based conducting polymers and interactions with biological tissues. *Journal of the Royal Society Interface*, 3(11), 741-752.
- Auta, M., & Hameed, B. (2014). Chitosan–clay composite as highly effective and low-cost adsorbent for batch and fixed-bed adsorption of methylene blue. *Chemical Engineering Journal*, 237, 352-361.
- Autin, O., Romelot, C., Rust, L., Hart, J., Jarvis, P., MacAdam, J., Jefferson, B. (2013). Evaluation of a UV-light emitting diodes unit for the removal of micropollutants in water for low energy advanced oxidation processes. *Chemosphere*, 92(6), 745-751.
- Ayad, M. M., & El-Nasr, A. A. (2010). Adsorption of cationic dye (methylene blue) from water using polyaniline nanotubes base. *The Journal of Physical Chemistry C*, 114(34), 14377-14383.
- Azarang, M., Shuhaimi, A., Yousefi, R., Moradi Golsheikh, A., & Sookhakian, M. (2014). Synthesis and characterization of ZnO NPs/reduced graphene oxide nanocomposite prepared in gelatin medium as highly efficient photo-degradation of MB. *Ceramics International*, 40(7), 10217-10221.
- Bairi, V. G., Bourdo, S. E., Sacre, N., Nair, D., Berry, B. C., Biris, A. S., & Viswanathan, T. (2015). Ammonia Gas Sensing Behavior of Tanninsulfonic Acid Doped Polyaniline-TiO₂ Composite. *Sensors*, 15(10), 26415-26429.

- Balint, R., Cassidy, N. J., & Cartmell, S. H. (2014). Conductive polymers: Towards a smart biomaterial for tissue engineering. *Acta Biomaterialia*, *10*(6), 2341-2353.
- Banerjee, P., Bhattacharyya, S. N., & Mandal, B. M. (1995). Poly (vinyl methyl ether) stabilized colloidal polyaniline dispersions. *Langmuir*, *11*(7), 2414-2418.
- Beier, R. C., & Nigg, H. N. (1992). Natural toxicants in foods. *Phytochemical Resources For Medicine and Agriculture* (pp. 247-367): Springer.
- Bensalah, N., Alfaro, M. Q., & Martínez-Huitle, C. (2009). Electrochemical treatment of synthetic wastewaters containing alphazurine A dye. *Chemical Engineering Journal*, *149*(1), 348-352.
- Bhadra, S., Chattopadhyay, S., Singha, N. K., & Khastgir, D. (2008a). Improvement of conductivity of electrochemically synthesized polyaniline. *Journal of Applied Polymer Science*, *108*(1), 57-64.
- Bhadra, S., & Khastgir, D. (2007a). Degradation and stability of polyaniline on exposure to electron beam irradiation (structure–property relationship). *Polymer Degradation and Stability*, *92*(10), 1824-1832.
- Bhadra, S., Khastgir, D., Singha, N. K., & Lee, J. H. (2009). Progress in preparation, processing and applications of polyaniline. *Progress in Polymer Science*, *34*(8), 783-810.
- Bhadra, S., Singha, N. K., Chattopadhyay, S., & Khastgir, D. (2007b). Effect of different reaction parameters on the conductivity and dielectric properties of polyaniline synthesized electrochemically and modeling of conductivity against reaction parameters through regression analysis. *Journal of Polymer Science Part B: Polymer Physics*, *45*(15), 2046-2059.
- Bhadra, S., Singha, N. K., & Khastgir, D. (2006). Polyaniline by new miniemulsion polymerization and the effect of reducing agent on conductivity. *Synthetic Metals*, *156*(16), 1148-1154.
- Bhadra, S., Singha, N. K., & Khastgir, D. (2008b). Effect of aromatic substitution in aniline on the properties of polyaniline. *European Polymer Journal*, *44*(6), 1763-1770.
- Bhattacharyya, K. G., & Sharma, A. (2005). Kinetics and thermodynamics of methylene blue adsorption on neem (*Azadirachta indica*) leaf powder. *Dyes and Pigments*, *65*(1), 51-59.
- Boeva, Z. A., & Sergeyev, V. (2014). Polyaniline: Synthesis, properties, and application. *Polymer Science Series C*, *56*(1), 144-153.
- Bredas, J. L., & Street, G. B. (1985). Polarons, bipolarons, and solitons in conducting polymers. *Accounts of Chemical Research*, *18*(10), 309-315.
- Camalet, J., Lacroix, J., Aeiya, S., Chane-Ching, K., & Lacaze, P. (1998). Electrosynthesis of adherent polyaniline films on iron and mild steel in aqueous oxalic acid medium. *Synthetic Metals*, *93*(2), 133-142.

- Cao, Y., Andreatta, A., Heeger, A. J., & Smith, P. (1989). Influence of chemical polymerization conditions on the properties of polyaniline. *Polymer*, 30(12), 2305-2311.
- Cao, Y., Smith, P., & Heeger, A. J. (1992). Counter-ion induced processibility of conducting polyaniline and of conducting polyblends of polyaniline in bulk polymers. *Synthetic Metals*, 48(1), 91-97.
- Chan, S. H. S., Yeong Wu, T., Juan, J. C., & Teh, C. Y. (2011). Recent developments of metal oxide semiconductors as photocatalysts in advanced oxidation processes (AOPs) for treatment of dye wastewater. *Journal of Chemical Technology and Biotechnology*, 86(9), 1130-1158.
- Chang, W., Skandan, G., Hahn, H., Danforth, S., & Kear, B. (1994). Chemical vapor condensation of nanostructured ceramic powders. *Nanostructured Materials*, 4(3), 345-351.
- Chen, J. F., Wang, Y. H., Guo, F., Wang, X. M., & Zheng, C. (2000). Synthesis of nanoparticles with novel technology: high-gravity reactive precipitation. *Industrial & Engineering Chemistry Research*, 39(4), 948-954.
- Chen, S., Wei, Z., Qi, X., Dong, L., Guo, Y.-G., Wan, L., Li, L. (2012). Nanostructured polyaniline-decorated Pt/C@ PANI core-shell catalyst with enhanced durability and activity. *Journal of the American Chemical Society*, 134(32), 13252-13255.
- Chen, S., Zhang, J., Zhang, C., Yue, Q., Li, Y., & Li, C. (2010). Equilibrium and kinetic studies of methyl orange and methyl violet adsorption on activated carbon derived from *Phragmites australis*. *Desalination*, 252(1), 149-156.
- Chequer, F. M. D., de Oliveira, D. P., Ferraz, E. R. A., de Oliveira, G. A. R., Cardoso, J. C., & Zanoni, M. V. B. (2013). *Textile dyes: dyeing process and environmental impact* (pp. 151-176). INTECH Open Access Publisher.
- Chevalier, J. W., Bergeron, J. Y., & Dao, L. H. (1992). Synthesis, characterization, and properties of poly (N-alkylanilines). *Macromolecules*, 25(13), 3325-3331.
- Chiang, C. K., Druy, M. A., Gau, S. C., Heeger, A. J., Louis, E. J., MacDiarmid, A. G., & Shirakawa, H. (1978). Synthesis of highly conducting films of derivatives of polyacetylene, (CH)_x. *Journal of the American Chemical Society*, 100(3), 1013-1015.
- Chiang, C. K., Fincher Jr, C., Park, Y. W., Heeger, A. J., Shirakawa, H., Louis, E. J., MacDiarmid, A. G. (1977). Electrical conductivity in doped polyacetylene. *Physical Review Letters*, 39(17), 1098.
- Choudhury, A. (2009). Polyaniline/silver nanocomposites: Dielectric properties and ethanol vapour sensitivity. *Sensors and Actuators B: Chemical*, 138(1), 318-325.
- Chowdhury, A.-N., Rahim, A., Ferdosi, Y. J., Azam, M. S., & Hossain, M. M. (2010). Cobalt-nickel mixed oxide surface: A promising adsorbent for the removal of PR dye from water. *Applied Surface Science*, 256(12), 3718-3724.

- Clifford, J. N., Martínez-Ferrero, E., Viterisi, A., & Palomares, E. (2011). Sensitizer molecular structure-device efficiency relationship in dye sensitized solar cells. *Chemical Society Reviews*, 40(3), 1635-1646.
- Couto, S. R. (2009). Dye removal by immobilised fungi. *Biotechnology Advances*, 27(3), 227-235.
- Crini, G., & Badot, P.-M. (2008). Application of chitosan, a natural aminopolysaccharide, for dye removal from aqueous solutions by adsorption processes using batch studies: A review of recent literature. *Progress in Polymer Science*, 33(4), 399-447.
- Dai, K., Lv, J., Lu, L., Liu, Q., Zhu, G., & Li, D. (2014). Synthesis of micro-nano heterostructure AgBr/ZnO composite for advanced visible light photocatalysis. *Materials Letters*, 130, 5-8.
- Dai, L. (2004). *Intelligent macromolecules for smart devices: from materials synthesis to device applications*. Springer Science & Business Media.
- Dambies, L., Guimon, C., Yiacoumi, S., & Guibal, E. (2001). Characterization of metal ion interactions with chitosan by X-ray photoelectron spectroscopy. *Colloids and Surfaces A: Physicochemical and Engineering Aspects*, 177(2), 203-214.
- Dawood, S., Sen, T. K., & Phan, C. (2014). Synthesis and characterisation of novel-activated carbon from waste biomass pine cone and its application in the removal of congo red dye from aqueous solution by adsorption. *Water, Air, & Soil Pollution*, 225(1), 1-16.
- DeBerry, D. W. (1985). Modification of the electrochemical and corrosion behavior of stainless steels with an electroactive coating. *Journal of The Electrochemical Society*, 132(5), 1022-1026.
- Demirors, A. F., & Imhof, A. (2009). BaTiO₃, SrTiO₃, CaTiO₃, and Ba_xSr_{1-x}TiO₃ Particles: A general approach for monodisperse colloidal perovskites. *Chemistry of Materials*, 21(13), 3002-3007.
- Dharma, J. (2015). Simple method of measuring the band gap energy value of TiO₂ in the powder form using a UV/Vis/NIR spectrometer. Retrieved from http://www.perkinelmer.com/CMSResources/Images/4474327APP_UVVISNIR_MeasureBandGapEnergyValue.pdf
- Diaz, A., & Logan, J. (1980). Electroactive polyaniline films. *Journal of Electroanalytical Chemistry and Interfacial Electrochemistry*, 111(1), 111-114.
- Dinadayalane, T. C., & Leszczynski, J. (2012). Fundamental structural, electronic, and chemical properties of carbon nanostructures: Graphene, fullerenes, carbon nanotubes, and their derivatives. *Handbook of Computational Chemistry* (pp. 793-867): Springer.
- Dinari, M., Momeni, M. M., & Goudarzirad, M. (2016). Dye-sensitized solar cells based on nanocomposite of polyaniline/graphene quantum dots. *Journal of Materials Science*, 51(6), 2964-2971.

- Dreyer, D. R., Park, S., Bielawski, C. W., & Ruoff, R. S. (2010). The chemistry of graphene oxide. *Chemical Society Reviews*, 39(1), 228-240.
- Dunsch, L. (1975). Zur anodischen oxydation des anilins in gesättigter nacl - lösung. v. potentiostatische elektrolyse von anilin und physikalisch - chemische eigenschaften des oxydationsproduktes. *Journal für Praktische Chemie*, 317(3), 409-419.
- Elwakeel, K. Z., El-Ghaffar, M. A., El-kousy, S. M., & El-Shorbagy, H. G. (2012). Synthesis of new ammonium chitosan derivatives and their application for dye removal from aqueous media. *Chemical Engineering Journal*, 203, 458-468.
- Epstein, A., Ginder, J., Zuo, F., Bigelow, R., Woo, H.-S., Tanner, D., MacDiarmid, A. (1987). Insulator-to-metal transition in polyaniline. *Synthetic Metals*, 18(1), 303-309.
- Eskizeybek, V., Sarı, F., Gülce, H., Gülce, A., & Avcı, A. (2012). Preparation of the new polyaniline/ZnO nanocomposite and its photocatalytic activity for degradation of methylene blue and malachite green dyes under UV and natural sun lights irradiations. *Applied Catalysis B: Environmental*, 119, 197-206.
- Estepa, L., & Daudon, M. (1997). Contribution of fourier transform infrared spectroscopy to the identification of urinary stones and kidney crystal deposits. *Biospectroscopy*, 3(5), 347-369.
- Fan, L., Zhang, Y., Luo, C., Lu, F., Qiu, H., & Sun, M. (2012). Synthesis and characterization of magnetic β -cyclodextrin-chitosan nanoparticles as nano-adsorbents for removal of methyl blue. *International Journal of Biological Macromolecules*, 50(2), 444-450.
- Feng, X. M., Mao, C. J., Yang, G., Hou, W. H., & Zhu, J. J. (2006). Polyaniline/Au composite hollow spheres: Synthesis, characterization, and application to the detection of dopamine. *Langmuir*, 22(9), 4384-4389.
- Fernández - García, M., & Rodriguez, J. A. (2011). Metal oxide nanoparticles. *Encyclopedia of Inorganic and Bioinorganic Chemistry*.
- Fiiipponi, L., & Sutherland, D. (2012). *Nanotechnologies: Principles, applications, implications and hands-on activities: a compendium for educators*. European Union, Directorate General for Research and Innovation.
- Fujishima, A., Rao, T. N., & Tryk, D. A. (2000). Titanium dioxide photocatalysis. *Journal of Photochemistry and Photobiology C: Photochemistry Reviews*, 1(1), 1-21.
- Fukushima, M., Tabei, E., Aramata, M., Hamada, Y., Mori, S., & Yamamoto, Y. (1998). Electrical conductivity of organosilicon polymers III: Carrier mobility analysis of iodine-doped polysilane by hall effect measurement. *Synthetic Metals*, 96(3), 245-248.

- Gandhi, M. R., & Meenakshi, S. (2013). Preparation of amino terminated polyamidoamine functionalized chitosan beads and its Cr (VI) uptake studies. *Carbohydrate Polymers*, 91(2), 631-637.
- Genies, E., Boyle, A., Lapkowski, M., & Tsintavis, C. (1990). Polyaniline: A historical survey. *Synthetic Metals*, 36(2), 139-182.
- Genies, E., Syed, A., & Tsintavis, C. (1985a). Electrochemical study of polyaniline in aqueous and organic medium. redox and kinetic properties. *Molecular Crystals and Liquid Crystals*, 121(1-4), 181-186.
- Genies, E., & Tsintavis, C. (1985b). Redox mechanism and electrochemical behaviour of polyaniline deposits. *Journal of Electroanalytical Chemistry and Interfacial Electrochemistry*, 195(1), 109-128.
- Gil, A., Assis, F., Albeniz, S., & Korili, S. (2011). Removal of dyes from wastewaters by adsorption on pillared clays. *Chemical Engineering Journal*, 168(3), 1032-1040.
- Golsheikh, A. M., Lim, H. N., Zakaria, R., & Huang, N. M. (2015). Sonochemical synthesis of reduced graphene oxide uniformly decorated with hierarchical ZnS nanospheres and its enhanced photocatalytic activities. *RSC Advances*, 5(17), 12726-12735.
- Gong, J., Liang, J., & Sumathy, K. (2012). Review on dye-sensitized solar cells (DSSCs): fundamental concepts and novel materials. *Renewable and Sustainable Energy Reviews*, 16(8), 5848-5860.
- Gonzalez - Gutierrez, L. V., & Escamill Silva, E. M. (2009). Reactive red azo dye degradation in a UASB bioreactor: Mechanism and kinetics. *Engineering in Life Sciences*, 9(4), 311-316.
- Gopalakrishnamurthy, H., Rao, M. S., & Kutty, T. N. (1975). Thermal decomposition of titanyle oxalates—I: Barium titanyle oxalate. *Journal of Inorganic and Nuclear Chemistry*, 37(4), 891-898.
- Gospodinova, N., & Terlemezyan, L. (1998). Conducting polymers prepared by oxidative polymerization: Polyaniline. *Progress in Polymer Science*, 23(8), 1443-1484.
- Gouamid, M., Ouahrani, M., & Bensaci, M. (2013). Adsorption equilibrium, kinetics and thermodynamics of methylene blue from aqueous solutions using date palm leaves. *Energy Procedia*, 36, 898-907.
- Green, A. G., & Woodhead, A. E. (1910). CCXLIII.—Aniline-black and allied compounds. Part I. *Journal of the Chemical Society, Transactions*, 97, 2388-2403.
- Gülce, H., Eskizeybek, V., Haspulat, B., Sarı, F., Gülce, A., & Avcı, A. (2013). Preparation of a new polyaniline/CdO nanocomposite and investigation of its photocatalytic activity: Comparative study under uv light and natural sunlight irradiation. *Industrial & Engineering Chemistry Research*, 52(32), 10924-10934.
- Guo, L., Luo, H., Gao, J., Guo, L., & Yang, J. (2006). Microwave hydrothermal synthesis of barium titanate powders. *Materials Letters*, 60(24), 3011-3014.

- Guo, X., Fei, G. T., Su, H., & De Zhang, L. (2011). Synthesis of polyaniline micro/nanospheres by a copper (II)-catalyzed self-assembly method with superior adsorption capacity of organic dye from aqueous solution. *Journal of Materials Chemistry*, 21(24), 8618-8625.
- Gupta, R., Singh, R., & Dubey, S. (2004). Removal of mercury ions from aqueous solutions by composite of polyaniline with polystyrene. *Separation and Purification Technology*, 38(3), 225-232.
- Gupta, V. (2009). Application of low-cost adsorbents for dye removal—A review. *Journal of Environmental Management*, 90(8), 2313-2342.
- Gustafsson, G., Cao, Y., Treacy, G., Klavetter, F., Colaneri, N., & Heeger, A. (1992). Flexible light-emitting diodes made from soluble conducting polymers. *Nature*, 357(6378), 477-479.
- Haldorai, Y., & Shim, J.-J. (2014). An efficient removal of methyl orange dye from aqueous solution by adsorption onto chitosan/MgO composite: A novel reusable adsorbent. *Applied Surface Science*, 292, 447-453.
- Han, M., Gong, Y., Zhou, J., Yin, C., Song, F., Muto, N., Iwata, Y. (2002). Plume dynamics during film and nanoparticles deposition by pulsed laser ablation. *Physics Letters A*, 302(4), 182-189.
- Hand, R. L., & Nelson, R. F. (1974). Anodic oxidation pathways of N-alkylanilines. *Journal of the American Chemical Society*, 96(3), 850-860.
- Hand, R. L., & Nelson, R. F. (1978). The anodic decomposition pathways of ortho - and meta - substituted anilines. *Journal of The Electrochemical Society*, 125(7), 1059-1069.
- Harrison, W. A. (1980). *Solid state theory*. Courier Corporation.
- He, T., Chen, D., Jiao, X., Wang, Y., & Duan, Y. (2005). Solubility-controlled synthesis of high-quality Co_3O_4 nanocrystals. *Chemistry of Materials*, 17(15), 4023-4030.
- Heeger, A. J., Smith, P., Fizazi, A., Moulton, J., Pakbaz, K., & Rughooputh, S. D. D. V. (1991). Recent progress in conducting polymers: Opportunities for science and opportunities for technology. *Synthetic Metals*, 41(3), 1027-1032.
- Heeger, A. J. (2001). Semiconducting and metallic polymers: The fourth generation of polymeric materials (Nobel lecture). *Angewandte Chemie International Edition*, 40(14), 2591-2611.
- Heeger, A. J., MacDiarmid, A. G., & Shirakawa, H. (2000). The nobel prize in chemistry. *The Royal Swedish Academy of Sciences*.
- Hena, S. (2010). Removal of chromium hexavalent ion from aqueous solutions using biopolymer chitosan coated with poly 3-methyl thiophene polymer. *Journal of Hazardous Materials*, 181(1), 474-479.

- Henrich, V., & Cox, P. (1994). *The surface chemistry of metal oxides*: Cambridge University Press.
- Hosseini Koupale, E., Alavi Moghaddam, M., & Hashemi, S. (2013). Successful treatment of high azo dye concentration wastewater using combined anaerobic/aerobic granular activated carbon-sequencing batch biofilm reactor (GAC-SBBR): Simultaneous adsorption and biodegradation processes. *Water Science & Technology*, 67(8).
- Hosseini, S. H., Simiari, J., & Farhadpour, B. (2009). Chemical and electrochemical grafting of polyaniline onto chitosan. *Iranian Polymer Journal*, 18, 3-13.
- Hu, J., Song, Z., Chen, L., Yang, H., Li, J., & Richards, R. (2010). Adsorption properties of MgO (111) nanoplates for the dye pollutants from wastewater. *Journal of Chemical & Engineering Data*, 55(9), 3742-3748.
- Hu, L., Peng, Q., & Li, Y. (2008). Selective synthesis of Co₃O₄ nanocrystal with different shape and crystal plane effect on catalytic property for methane combustion. *Journal of the American Chemical Society*, 130(48), 16136-16137.
- Hu, Z., Zu, L., Jiang, Y., Lian, H., Liu, Y., Li, Z., Cui, X. (2015). High specific capacitance of polyaniline/mesoporous manganese dioxide composite using KI-H₂SO₄ electrolyte. *Polymers*, 7(10), 1939-1953.
- Huang, J., Virji, S., Weiller, B. H., & Kaner, R. B. (2003). Polyaniline nanofibers: facile synthesis and chemical sensors. *Journal of the American Chemical Society*, 125(2), 314-315.
- Huang, J. X., Virji, S., Weiller, B. H., & Kaner, R. B. (2003). Polyaniline nanofibers: Facile synthesis and chemical sensors. *Journal of the American Chemical Society*, 125(2), 314-315.
- Huang, S.-T., Lee, W. W., Chang, J.-L., Huang, W.-S., Chou, S.-Y., & Chen, C.-C. (2014). Hydrothermal synthesis of SrTiO₃ nanocubes: Characterization, photocatalytic activities, and degradation pathway. *Journal of the Taiwan Institute of Chemical Engineers*, 45(4), 1927-1936.
- Huang, X., Qi, X., Boey, F., & Zhang, H. (2012). Graphene-based composites. *Chemical Society Reviews*, 41(2), 666-686.
- Hummers Jr, W. S., & Offeman, R. E. (1958). Preparation of graphitic oxide. *Journal of the American Chemical Society*, 80(6), 1339-1339.
- Hussain, A. P., & Kumar, A. (2003). Electrochemical synthesis and characterization of chloride doped polyaniline. *Bulletin of Materials Science*, 26(3), 329-334.
- Ilium, L. (1998). Chitosan and its use as a pharmaceutical excipient. *Pharmaceutical Research*, 15(9), 1326-1331.
- Interrante, L. V., & Hampden-Smith, M. J. (1997). *Chemistry of advanced materials: an overview*. Wiley-VCH

- Inzelt, G. (2011). Rise and rise of conducting polymers. *Journal of Solid State Electrochemistry*, 15(7-8), 1711-1718.
- Inzelt, G. (2012). *Conducting polymers: a new era in electrochemistry*: Springer Science & Business Media.
- Inzelt, G. (2012). Historical background (or: there is nothing new under the sun). *Conducting Polymers* (pp. 295-297). Springer Berlin Heidelberg.
- Iroh, J. O., Zhu, Y., Shah, K., Levine, K., Rajagopalan, R., Uyar, T., Voevodin, N. N. (2003). Electrochemical synthesis: A novel technique for processing multi-functional coatings. *Progress in Organic Coatings*, 47(3), 365-375.
- Ito, T., Shirakawa, H., & Ikeda, S. (1974). Simultaneous polymerization and formation of polyacetylene film on the surface of concentrated soluble Ziegler - type catalyst solution. *Journal of Polymer Science: Polymer Chemistry Edition*, 12(1), 11-20.
- Ivanov, K., Gruber, E., Schempp, W., & Kirov, D. (1996). Possibilities of using zeolite as filler and carrier for dyestuffs in paper. *Papier*, 50(7-8), 456-&.
- Jahan, M., Bao, Q., Yang, J.-X., & Loh, K. P. (2010). Structure-directing role of graphene in the synthesis of metal-organic framework nanowire. *Journal of the American Chemical Society*, 132(41), 14487-14495.
- Jang, S., Han, M., & Im, S. (2000). Preparation and characterization of conductive polyaniline/silica hybrid composites prepared by sol-gel process. *Synthetic Metals*, 110(1), 17-23.
- Jasuja, K., & Berry, V. (2009). Implantation and growth of dendritic gold nanostructures on graphene derivatives: Electrical property tailoring and raman enhancement. *ACS Nano*, 3(8), 2358-2366.
- Javadian, H., Angaji, M. T., & Naushad, M. (2014). Synthesis and characterization of polyaniline/gamma-alumina nanocomposite: A comparative study for the adsorption of three different anionic dyes. *Journal of Industrial and Engineering Chemistry*, 20(5), 3890-3900.
- Jiang, X., Sun, Y., Liu, L., Wang, S., & Tian, X. (2014). Adsorption of CI reactive blue 19 from aqueous solutions by porous particles of the grafted chitosan. *Chemical Engineering Journal*, 235, 151-157.
- Jiao, F., & Frei, H. (2009). Nanostructured cobalt oxide clusters in mesoporous silica as efficient oxygen evolving catalysts. *Angewandte Chemie International Edition*, 48(10), 1841-1844.
- Jiao, F., & Frei, H. (2010). Nanostructured cobalt and manganese oxide clusters as efficient water oxidation catalysts. *Energy & Environmental Science*, 3(8), 1018-1027.
- Kabdaşlı, I., Tünay, O., & Orhon, D. (1999). Wastewater control and management in a leather tanning district. *Water Science and Technology*, 40(1), 261-267.

- Kannusamy, P., & Sivalingam, T. (2013). Synthesis of porous chitosan–polyaniline/ZnO hybrid composite and application for removal of reactive orange 16 dye. *Colloids and Surfaces B: Biointerfaces*, 108, 229-238.
- Kant, S., Kalia, S., & Kumar, A. (2013). A novel nanocomposite of polyaniline and Fe 0.01 Ni 0.01 Zn 0.98 O: Photocatalytic, electrical and antibacterial properties. *Journal of Alloys and Compounds*, 578, 249-256.
- Karthik, R., & Meenakshi, S. (2014). Facile synthesis of cross linked–chitosan–grafted–polyaniline composite and its Cr (VI) uptake studies. *International Journal of Biological Macromolecules*, 67, 210-219.
- Kazuma, E., & Tatsuma, T. (2012). Photoinduced reversible changes in morphology of plasmonic Ag nanorods on TiO₂ and application to versatile photochromism. *Chemical Communications*, 48(12), 1733-1735.
- Khataee, A., & Kasiri, M. B. (2010). Photocatalytic degradation of organic dyes in the presence of nanostructured titanium dioxide: Influence of the chemical structure of dyes. *Journal of Molecular Catalysis A: Chemical*, 328(1), 8-26.
- Kirchmeyer, S., & Reuter, K. (2005). Scientific importance, properties and growing applications of poly (3, 4-ethylenedioxythiophene). *Journal of Materials Chemistry*, 15(21), 2077-2088.
- Klett, C., Barry, A., Balti, I., Lelli, P., Schoenstein, F., & Jouini, N. (2014). Nickel doped Zinc oxide as a potential sorbent for decolorization of specific dyes, methyloange and tartrazine by adsorption process. *Journal of Environmental Chemical Engineering*, 2(2), 914-926.
- Kong, J., Franklin, N. R., Zhou, C., Chapline, M. G., Peng, S., Cho, K., & Dai, H. (2000). Nanotube molecular wires as chemical sensors. *Science*, 287(5453), 622-625.
- Kousalya, G., Rajiv Gandhi, M., & Meenakshi, S. (2010). Removal of toxic Cr (VI) ions from aqueous solution using nano-hydroxyapatite-based chitin and chitosan hybrid composites. *Adsorption Science & Technology*, 28(1), 49-64.
- Krika, F., & Benlahbib, O. e. F. (2015). Removal of methyl orange from aqueous solution via adsorption on cork as a natural and low-coast adsorbent: Equilibrium, kinetic and thermodynamic study of removal process. *Desalination and Water Treatment*, 53(13), 3711-3723.
- Kuilla, T., Bhadra, S., Yao, D., Kim, N. H., Bose, S., & Lee, J. H. (2010). Recent advances in graphene based polymer composites. *Progress in Polymer Science*, 35(11), 1350-1375.
- Kumar, D., & Sharma, R. (1998). Advances in conductive polymers. *European Polymer Journal*, 34(8), 1053-1060.
- Kumar, N. A., Choi, H.-J., Shin, Y. R., Chang, D. W., Dai, L., & Baek, J.-B. (2012). Polyaniline-grafted reduced graphene oxide for efficient electrochemical supercapacitors. *ACS Nano*, 6(2), 1715-1723.

- Kuo, Y.-L., Su, T.-L., Kung, F.-C., & Wu, T.-J. (2011). A study of parameter setting and characterization of visible-light driven nitrogen-modified commercial TiO₂ photocatalysts. *Journal of Hazardous Materials*, 190(1), 938-944.
- Kyzas, G. Z., & Bikiaris, D. N. (2015). Recent modifications of chitosan for adsorption applications: A critical and systematic review. *Marine Drugs*, 13(1), 312-337.
- Last, J. T. (1957). Infrared-absorption studies on barium titanate and related materials. *Physical Review*, 105(6), 1740.
- Lee, W. W., Chung, W.-H., Huang, W.-S., Lin, W.-C., Lin, W.-Y., Jiang, Y.-R., & Chen, C.-C. (2013). Photocatalytic activity and mechanism of nano-cubic barium titanate prepared by a hydrothermal method. *Journal of the Taiwan Institute of Chemical Engineers*, 44(4), 660-669.
- Leng, J., McCall, R., Cromack, K., Ginder, J., Ye, H., Sun, Y., Epstein, A. (1992). Photoexcitations in pernigraniline: Ring-torsional polarons and bond-order solitons. *Physical Review Letters*, 68(8), 1184.
- Letheby, H. (1862). XXIX.—On the production of a blue substance by the electrolysis of sulphate of aniline. *Journal of the Chemical Society*, 15, 161-163.
- Li, J., Zeng, X., Ren, T., & van der Heide, E. (2014). The preparation of graphene oxide and its derivatives and their application in bio-tribological systems. *Lubricants*, 2(3), 137-161.
- Li, Q., Sun, L., Zhang, Y., Qian, Y., & Zhai, J. (2011). Characteristics of equilibrium, kinetics studies for adsorption of Hg (II) and Cr (VI) by polyaniline/humic acid composite. *Desalination*, 266(1), 188-194.
- Li, W.-Y., Xu, L.-N., & Chen, J. (2005). CO₃O₄ nanomaterials in lithium ion batteries and gas sensors. *Advanced Functional Materials*, 15(5), 851-857.
- Liang, L., Liu, J., Windisch Jr, C. F., Exarhos, G. J., & Lin, Y. (2002). Direct assembly of large arrays of oriented conducting polymer nanowires. *Angewandte Chemie International Edition*, 41(19), 3665-3668.
- Linz, A. J., Greenham, R. K., & Fallon Jr, L. F. (2006). Methemoglobinemia: An industrial outbreak among rubber molding workers. *Journal of Occupational and Environmental Medicine*, 48(5), 523-528.
- Liu, H. Q., Kameoka, J., Czaplewski, D. A., & Craighead, H. G. (2004). Polymeric nanowire chemical sensor. *Nano Letters*, 4(4), 671-675.
- Liu, X., Zhou, W., Qian, X., Shen, J., & An, X. (2013). Polyaniline/cellulose fiber composite prepared using persulfate as oxidant for Cr (VI)-detoxification. *Carbohydrate Polymers*, 92(1), 659-661.
- Liu, Y., Chen, G., Zhou, C., Hu, Y., Fu, D., Liu, J., & Wang, Q. (2011). Higher visible photocatalytic activities of nitrogen doped In₂TiO₅ sensitized by carbon nitride. *Journal of Hazardous Materials*, 190(1), 75-80.

- Lu, X., Tan, C. Y., Xu, J., & He, C. (2003). Thermal degradation of electrical conductivity of polyacrylic acid doped polyaniline: Effect of molecular weight of the dopants. *Synthetic Metals*, 138(3), 429-440.
- Lue, J. T. (2007). Physical properties of nanomaterials. *Encyclopedia of Nanoscience and Nanotechnology*, 10(1).
- Lux, F. (1994). Properties of electronically conductive polyaniline: A comparison between well-known literature data and some recent experimental findings. *Polymer*, 35(14), 2915-2936.
- Luzzati, S., Basso, M., Catellani, M., Brabec, C., Gebeyehu, D., & Sariciftci, N. (2002). Photo-induced electron transfer from a dithieno thiophene-based polymer to TiO₂. *Thin Solid Films*, 403, 52-56.
- Ma, J., Yu, F., Zhou, L., Jin, L., Yang, M., Luan, J., Chen, J. (2012). Enhanced adsorptive removal of methyl orange and methylene blue from aqueous solution by alkali-activated multiwalled carbon nanotubes. *ACS Applied Materials & Interfaces*, 4(11), 5749-5760.
- MacDiarmid, A., Chiang, J., Richter, A., Somasiri, N., & Epstein, A. (1987a). Polyaniline: Synthesis and characterization of the emeraldine oxidation state by elemental analysis. *Conducting Polymers* (pp. 105-120): Springer.
- MacDiarmid, A. G., & Epstein, A. J. (1991). "Synthetic metals": A novel role for organic polymers. In *Makromolekulare Chemie. Macromolecular Symposia* (Vol. 51, No. 1, pp. 11-28). Hüthig & Wepf Verlag.
- MacDiarmid, A., Manohar, S., Masters, J., Sun, Y., Weiss, H., & Epstein, A. (1991). Polyaniline: Synthesis and properties of pernigraniline base. *Synthetic Metals*, 41(1), 621-626.
- MacDiarmid, A., Yang, L., Huang, W., & Humphrey, B. (1987). Polyaniline: Electrochemistry and application to rechargeable batteries. *Synthetic Metals*, 18(1), 393-398.
- MacDiarmid, A. G. (2001). "Synthetic metals": A novel role for organic polymers (Nobel lecture). *Angewandte Chemie International Edition*, 40(14), 2581-2590.
- MacDiarmid, A. G., & Epstein, A. J. (1989). Polyanilines: A novel class of conducting polymers. *Faraday Discussions of the Chemical Society*, 88, 317-332.
- MacDiarmid, A. G., & Epstein, A. J. (1995). Secondary doping in polyaniline. *Synthetic Metals*, 69(1), 85-92.
- Mahanta, D., Madras, G., Radhakrishnan, S., & Patil, S. (2008). Adsorption of sulfonated dyes by polyaniline emeraldine salt and its kinetics. *The Journal of Physical Chemistry B*, 112(33), 10153-10157.
- Mahto, T. K., Chandra, S., Haldar, C., & Sahu, S. K. (2015). Kinetic and thermodynamic study of polyaniline functionalized magnetic mesoporous silica for magnetic field guided dye adsorption. *RSC Advances*, 5(59), 47909-47919.

- Makhlouf, M. T., Abu-Zied, B., & Mansoure, T. (2012). Direct fabrication of cobalt oxide nano-particles employing glycine as a combustion fuel. *Physical Chemistry*, 2(6), 86-93.
- Martin, C. R. (1994). *Nanomaterials--a membrane-based synthetic approach* (No. ONR-TR-96). Colorado State Univ Fort Collins Dept of Chemistry.
- Matsubara, K., & Tatsuma, T. (2007). Morphological changes and multicolor photochromism of Ag nanoparticles deposited on single crystalline TiO₂ surfaces. *Advanced Materials*, 19(19), 2802-2806.
- Mattoso, L. H., MacDiarmid, A. G., & Epstein, A. J. (1994). Controlled synthesis of high molecular weight polyaniline and poly (o-methoxyaniline). *Synthetic Metals*, 68(1), 1-11.
- McCann, J., & Ames, B. N. (1976). Detection of carcinogens as mutagens in the Salmonella/microsome test: Assay of 300 chemicals: Discussion. *Proceedings of the National Academy of Sciences*, 73(3), 950-954.
- McQuade, D. T., Pullen, A. E., & Swager, T. M. (2000). Conjugated polymer-based chemical sensors. *Chemical reviews*, 100(7), 2537-2574.
- Mengoli, G., Munari, M.-T., & Folonari, C. (1981). Anodic formation of polynitroanilide films onto copper. *Journal of Electroanalytical Chemistry and Interfacial Electrochemistry*, 124(1-2), 237-246.
- Min, S., Wang, F., & Han, Y. (2007). An investigation on synthesis and photocatalytic activity of polyaniline sensitized nanocrystalline TiO₂ composites. *Journal of Materials Science*, 42(24), 9966-9972.
- Mizumoto, M., Namba, M., Nishimura, S., Miyadera, H., Koseki, M., & Kobayashi, Y. (1989). Polyaniline as an electrode of rechargeable battery. *Synthetic Metals*, 28(1), 639-646.
- Mohilner, D. M., Adams, R. N., & Argersinger, W. J. (1962). Investigation of the kinetics and mechanism of the anodic oxidation of aniline in aqueous sulfuric acid solution at a platinum electrode. *Journal of the American Chemical Society*, 84(19), 3618-3622.
- Mostafa, T. B., & Darwish, A. S. (2014). An approach toward construction of tuned chitosan/polyaniline/metal hybrid nanocomposites for treatment of meat industry wastewater. *Chemical Engineering Journal*, 243, 326-339.
- Mostafaei, A., & Zolriasatein, A. (2012). Synthesis and characterization of conducting polyaniline nanocomposites containing ZnO nanorods. *Progress in Natural Science: Materials International*, 22(4), 273-280.
- Moussavi, G., & Mahmoudi, M. (2009). Removal of azo and anthraquinone reactive dyes from industrial wastewaters using MgO nanoparticles. *Journal of Hazardous Materials*, 168(2), 806-812.

- Muzzarelli, R. A. (1973). *Natural chelating polymers; alginic acid, chitin and chitosan*: Pergamon Press.
- Muzzarelli, R. A., & Tubertini, O. (1969). Chitin and chitosan as chromatographic supports and adsorbents for collection of metal ions from organic and aqueous solutions and sea-water. *Talanta*, 16(12), 1571-1577.
- Najim, T. S., & Salim, A. J. (2014). Polyaniline nanofibers and nanocomposites: Preparation, characterization, and application for Cr (VI) and phosphate ions removal from aqueous solution. *Arabian Journal of Chemistry*. In Press.
- Nakashima, K., Kera, M., Fujii, I., & Wada, S. (2013). A new approach for the preparation of SrTiO₃ nanocubes. *Ceramics International*, 39(3), 3231-3234.
- Nalwa, H. S. (1997). *Handbook of organic conductive molecules and polymers, volume 4, conductive polymers: transport, photophysics and applications*: Wiley
- Nassar, M. Y., & Ahmed, I. S. (2012). Template-free hydrothermal derived cobalt oxide nanopowders: Synthesis, characterization, and removal of organic dyes. *Materials Research Bulletin*, 47(9), 2638-2645.
- Nguyen, M. T., Kasai, P., Miller, J. L., & Diaz, A. F. (1994). Synthesis and properties of novel water-soluble conducting polyaniline copolymers. *Macromolecules*, 27(13), 3625-3631.
- Noguera, C. (1996). *Physics and chemistry at oxide surfaces*: Cambridge University Press.
- Ogura, K., Saino, T., Nakayama, M., & Shiigi, H. (1997). The humidity dependence of the electrical conductivity of a soluble polyaniline–poly (vinyl alcohol) composite film. *Journal of Material Chemistry*, 7(12), 2363-2366.
- Ogura, K., Shiigi, H., Nakayama, M., & Fujii, A. (1998). Thermogravimetric/mass and infrared spectroscopic properties and humidity sensitivity of polyaniline derivatives/polyvinyl alcohol composites. *Journal of The Electrochemical Society*, 145(10), 3351-3357.
- Oh, E., Min, Y., Wiesinger, J., Manohar, S., Scherr, E., Prest, P., Epstein, A. (1993). Polyaniline: dependency of selected properties on molecular weight. *Synthetic Metals*, 55(2), 977-982.
- Olad, A., & Nosrati, R. (2012). Preparation, characterization, and photocatalytic activity of polyaniline/ZnO nanocomposite. *Research on Chemical Intermediates*, 38(2), 323-336.
- Papić, S., Koprivanac, N., Božić, A. L., & Meteš, A. (2004). Removal of some reactive dyes from synthetic wastewater by combined Al (III) coagulation/carbon adsorption process. *Dyes and pigments*, 62(3), 291-298.
- Parida, K., Sahu, S., Reddy, K., & Sahoo, P. (2010). A kinetic, thermodynamic, and mechanistic approach toward adsorption of methylene blue over water-washed

manganese nodule leached residues. *Industrial & Engineering Chemistry Research*, 50(2), 843-848.

- Patil, R., Ahmed, S., Shiigi, H., Nakayama, M., & Ogura, K. (1999). Investigation of some physicochemical properties of camphor sulfonic acid (CSA)-doped poly (o anisidine)(PoAN) and CSA - doped PoAN/ABS composites. *Journal of Polymer Science Part A: Polymer Chemistry*, 37(24), 4596-4604.
- Paul, E. W., Ricco, A. J., & Wrighton, M. S. (1985). Resistance of polyaniline films as a function of electrochemical potential and the fabrication of polyaniline-based microelectronic devices. *The Journal of Physical Chemistry*, 89(8), 1441-1447.
- Peniche, C., Argüelles-Monal, W., Davidenko, N., Sastre, R., Gallardo, A., & San Román, J. (1999). Self-curing membranes of chitosan/PAA IPNs obtained by radical polymerization: preparation, characterization and interpolymer complexation. *Biomaterials*, 20(20), 1869-1878.
- Petit, C., & Badosz, T. J. (2010). Enhanced adsorption of ammonia on metal organic framework/graphite oxide composites: Analysis of surface interactions. *Advanced Functional Materials*, 20(1), 111-118.
- Pham, V. H., Cuong, T. V., Hur, S. H., Oh, E., Kim, E. J., Shin, E. W., & Chung, J. S. (2011). Chemical functionalization of graphene sheets by solvothermal reduction of a graphene oxide suspension in N-methyl-2-pyrrolidone. *Journal of Materials Chemistry*, 21(10), 3371-3377.
- Pron, A., Genoud, F., Menardo, C., & Nechtschein, M. (1988). The effect of the oxidation conditions on the chemical polymerization of polyaniline. *Synthetic Metals*, 24(3), 193-201.
- Pron, A., & Rannou, P. (2002). Processible conjugated polymers: from organic semiconductors to organic metals and superconductors. *Progress in Polymer Science*, 27(1), 135-190.
- Pud, A., Ogurtsov, N., Korzhenko, A., & Shapoval, G. (2003). Some aspects of preparation methods and properties of polyaniline blends and composites with organic polymers. *Progress in Polymer Science*, 28(12), 1701-1753.
- Raffainer, I. I., & Rudolf von Rohr, P. (2001). Promoted wet oxidation of the azo dye orange II under mild conditions. *Industrial & Engineering Chemistry Research*, 40(4), 1083-1089.
- Rahy, A., & Yang, D. J. (2008). Synthesis of highly conductive polyaniline nanofibers. *Materials Letters*, 62(28), 4311-4314.
- Rajput, N. (2015). Methods of preparation of nanoparticles-a review. *International Journal of Advances in Engineering & Technology*, 7(6), 1806.
- Ramadin, Y., Ahmad, M., Zihlif, A., Al-Haddad, R., Makadsi, M., Ragosta, G., & Martuscelli, E. (1998). Determination of the type of charge carriers in carbon fiber/polymer composite. *Polymer Testing*, 17(1), 35-42.

- Ray, S. S., & Biswas, M. (2000). Water-dispersible conducting nanocomposites of polyaniline and poly (N-vinylcarbazole) with nanodimensional zirconium dioxide. *Synthetic Metals*, 108(3), 231-236.
- Riaz, U., Ashraf, S., & Aqib, M. (2014). Microwave-assisted degradation of acid orange using a conjugated polymer, polyaniline, as catalyst. *Arabian Journal of Chemistry*, 7(1), 79-86.
- Riaz, U., Ashraf, S., & Kashyap, J. (2015a). Enhancement of photocatalytic properties of transitional metal oxides using conducting polymers: A mini review. *Materials Research Bulletin*, 71, 75-90.
- Riaz, U., Ashraf, S., & Kashyap, J. (2015b). Role of conducting polymers in enhancing TiO₂-based photocatalytic dye degradation: A short review. *Polymer-Plastics Technology and Engineering*, 54(17), 1850-1870.
- Rinaudo, M. (2006). Chitin and chitosan: Properties and applications. *Progress in Polymer Science*, 31(7), 603-632.
- Rodriguez, J. A., & Fernández-García, M. (2007). *Synthesis, properties, and applications of oxide nanomaterials*: John Wiley & Sons.
- Rupprecht, L. (1999). *Conductive polymers and plastics: in industrial applications*: William Andrew.
- Sadeghi - Kiakhani, M., Arami, M., & Gharanjig, K. (2013). Dye removal from colored - textile wastewater using chitosan - PPI dendrimer hybrid as a biopolymer: Optimization, kinetic, and isotherm studies. *Journal of Applied Polymer Science*, 127(4), 2607-2619.
- Sadek, A., Wlodarski, W., Shin, K., Kaner, R., & Kalantar-Zadeh, K. (2008). A polyaniline/WO₃ nanofiber composite-based ZnO/64 YX LiNbO₃ SAW hydrogen gas sensor. *Synthetic Metals*, 158(1), 29-32.
- Sadek, A., Wlodarski, W., Shin, K., Kaner, R. B., & Kalantar-Zadeh, K. (2006). A layered surface acoustic wave gas sensor based on a polyaniline/In₂O₃ nanofibre composite. *Nanotechnology*, 17(17), 4488.
- Schoch, K. (1994). Update on electrically conductive polymers and their applications. *Electrical Insulation Magazine, IEEE*, 10(3), 29-32.
- Scott, B. J., Wirnsberger, G., & Stucky, G. D. (2001). Mesoporous and mesostructured materials for optical applications. *Chemistry of Materials*, 13(10), 3140-3150.
- Sen, T. K., Afroze, S., & Ang, H. (2011). Equilibrium, kinetics and mechanism of removal of methylene blue from aqueous solution by adsorption onto pine cone biomass of *Pinus radiata*. *Water, Air, & Soil Pollution*, 218(1-4), 499-515.
- Sengodu, P., & Deshmukh, A. D. (2015). Conducting polymers and their inorganic composites for advanced Li-ion batteries: a review. *RSC Advances*, 5(52), 42109-42130.

- Shahabuddin, S., Sarih, N. M., Mohamad, S., & Baharin, S. N. A. (2016). Synthesis and characterization of Co₃O₄ nanocube-doped polyaniline nanocomposites with enhanced methyl orange adsorption from aqueous solution. *RSC Advances*, 6(49), 43388-43400.
- Shahabuddin, S., Muhamad Sarih, N., Mohamad, S., & Juan, J. C. (2016). SrTiO₃ nanocube-doped polyaniline nanocomposites with enhanced photocatalytic degradation of methylene blue under visible light. *Polymers*, 8(2), 27.
- Shahabuddin, S., Sarih, N. M., Ismail, F. H., Shahid, M. M., & Huang, N. M. (2015). Synthesis of chitosan grafted-polyaniline/Co₃O₄ nanocube nanocomposites and their photocatalytic activity toward methylene blue dye degradation. *RSC Advances*, 5(102), 83857-83867.
- Shahabuddin, S., Sarih, N. M., Ismail, F. H., Shahid, M. M., & Huang, N. M. (2015). Synthesis of chitosan grafted-polyaniline/Co₃O₄ nanocube nanocomposites and their photocatalytic activity toward methylene blue dye degradation. *RSC Advances*, 5(102), 83857-83867.
- Shahid, M. M., Pandikumar, A., Golsheikh, A. M., Huang, N. M., & Lim, H. N. (2014). Enhanced electrocatalytic performance of cobalt oxide nanocubes incorporating reduced graphene oxide as a modified platinum electrode for methanol oxidation. *RSC Advances*, 4(107), 62793-62801.
- Shao, D., Chen, C., & Wang, X. (2012). Application of polyaniline and multiwalled carbon nanotube magnetic composites for removal of Pb (II). *Chemical Engineering Journal*, 185, 144-150.
- Shen, P., Lofaro, J. C., Woerner, W. R., White, M. G., Su, D., & Orlov, A. (2013). Photocatalytic activity of hydrogen evolution over Rh doped SrTiO₃ prepared by polymerizable complex method. *Chemical Engineering Journal*, 223, 200-208.
- Shi, L., Wang, X., Lu, L., Yang, X., & Wu, X. (2009). Preparation of TiO₂/polyaniline nanocomposite from a lyotropic liquid crystalline solution. *Synthetic Metals*, 159(23), 2525-2529.
- Shih, H.-K., Chen, Y.-H., Chu, Y.-L., Cheng, C.-C., Chang, F.-C., Zhu, C.-Y., & Kuo, S.-W. (2015). Photo-crosslinking of pendent uracil units provides supramolecular hole injection/transport conducting polymers for highly efficient light-emitting diodes. *Polymers*, 7(5), 804-818.
- Shin, S. R., Park, S. J., Yoon, S. G., Spinks, G. M., Kim, S. I., & Kim, S. J. (2005). Synthesis of conducting polyaniline in semi-IPN based on chitosan. *Synthetic Metals*, 154(1), 213-216.
- Shirakawa, H. (2001). The discovery of polyacetylene film: the dawning of an era of conducting polymers (Nobel lecture). *Angewandte Chemie International Edition*, 40(14), 2574-2580.
- Shirakawa, H., Louis, E. J., MacDiarmid, A. G., Chiang, C. K., & Heeger, A. J. (1977). Synthesis of electrically conducting organic polymers: Halogen derivatives of

polyacetylene,(CH)_x. *Journal of The Chemical Society, Chemical Communications*(16), 578-580.

- Silva, C. G., Wang, W., & Faria, J. L. (2006). Photocatalytic and photochemical degradation of mono-, di- and tri-azo dyes in aqueous solution under UV irradiation. *Journal of Photochemistry and Photobiology A: Chemistry*, 181(2), 314-324.
- Sing, K., Everett, D., Haul, R., Moscou, L., Pierotti, R., Rouquerol, J., & Siemieniewska, T. (1985). Physical and biophysical chemistry division commission on colloid and surface chemistry including catalysis. *Pure and Applied Chemistry*, 57(4), 603-619.
- Singh, D. P. (2010). Synthesis and growth of ZnO nanowires. *Science of Advanced Materials*, 2(3), 245-272.
- Sokolowska-Gajda, J., Freeman, H. S., & Reife, A. (1996). Synthetic dyes based on environmental considerations. Part 2: Iron complexes formazan dyes. *Dyes and Pigments*, 30(1), 1-20.
- Soltani, N., Saion, E., Hussein, M. Z., Erfani, M., Abedini, A., Bahmanrokh, G., Vaziri, P. (2012). Visible light-induced degradation of methylene blue in the presence of photocatalytic ZnS and CdS nanoparticles. *International Journal of Molecular Sciences*, 13(10), 12242.
- Song, Z., Zhang, Y., Liu, W., Zhang, S., Liu, G., Chen, H., & Qiu, J. (2013). Hydrothermal synthesis and electrochemical performance of Co₃O₄/reduced graphene oxide nanosheet composites for supercapacitors. *Electrochimica Acta*, 112, 120-126.
- Stan, C. S., Popa, M., Olariu, M., & Secula, M. S. (2015). Synthesis and characterization of PSSA-polyaniline composite with an enhanced processability in thin films. *Open Chemistry*, 13(1).
- Stejskal, J., & Gilbert, R. (2002). Polyaniline. Preparation of a conducting polymer (IUPAC technical report). *Pure and Applied Chemistry*, 74(5), 857-867.
- Stoller, M. D., Park, S., Zhu, Y., An, J., & Ruoff, R. S. (2008). Graphene-based ultracapacitors. *Nano Letters*, 8(10), 3498-3502.
- Su, L., & Gan, Y. X. (2012). Experimental study on synthesizing TiO₂ nanotube/polyaniline (PANI) nanocomposites and their thermoelectric and photosensitive property characterization. *Composites Part B: Engineering*, 43(2), 170-182.
- Subramanian, E., Subbulakshmi, S., & Murugan, C. (2014). Inter-relationship between nanostructures of conducting polyaniline and the photocatalytic methylene blue dye degradation efficiencies of its hybrid composites with anatase TiO₂. *Materials Research Bulletin*, 51, 128-135.
- Subramanian, E., Subbulakshmi, S., & Murugan, C. (2014). Inter-relationship between nanostructures of conducting polyaniline and the photocatalytic methylene blue

dye degradation efficiencies of its hybrid composites with anatase TiO₂. *Materials Research Bulletin*, 51, 128-135.

- Sulimenko, T., Stejskal, J., Krivka, I., & Prokeš, J. (2001). Conductivity of colloidal polyaniline dispersions. *European Polymer Journal*, 37(2), 219-226.
- Tadjarodi, A., Imani, M., & Kerdari, H. (2013). Experimental design to optimize the synthesis of CdO cauliflower-like nanostructure and high performance in photodegradation of toxic azo dyes. *Materials Research Bulletin*, 48(3), 935-942.
- Takahashi, K., Nakamura, K., Yamaguchi, T., Komura, T., Ito, S., Aizawa, R., & Murata, K. (2002). Characterization of water-soluble externally HCl-doped conducting polyaniline. *Synthetic Metals*, 128(1), 27-33.
- Talopin, D. V., Lee, J.-S., Kovalenko, M. V., & Shevchenko, E. V. (2009). Prospects of colloidal nanocrystals for electronic and optoelectronic applications. *Chemical reviews*, 110(1), 389-458.
- Tan, H., Zhao, Z., Zhu, W.-b., Coker, E. N., Li, B., Zheng, M., Sun, Z. (2014). Oxygen vacancy enhanced photocatalytic activity of perovskite SrTiO₃. *ACS Applied Materials & Interfaces*, 6(21), 19184-19190.
- Tang, J., Durrant, J. R., & Klug, D. R. (2008). Mechanism of photocatalytic water splitting in TiO₂. Reaction of water with photoholes, importance of charge carrier dynamics, and evidence for four-hole chemistry. *Journal of The American Chemical Society*, 130(42), 13885-13891.
- Tang, L., Fang, Y., Pang, Y., Zeng, G., Wang, J., Zhou, Y., Chen, J. (2014). Synergistic adsorption and reduction of hexavalent chromium using highly uniform polyaniline-magnetic mesoporous silica composite. *Chemical Engineering Journal*, 254, 302-312.
- Tang, L., Wu, T., & Kan, J. (2009). Synthesis and properties of polyaniline-cobalt coordination polymer. *Synthetic Metals*, 159(15), 1644-1648.
- Tiwari, A. (2007). Gum Arabic graft polyaniline: an electrically active redox biomaterial for sensor applications. *Journal of Macromolecular Science, Part A: Pure and Applied Chemistry*, 44(7), 735-745.
- Tiwari, A., & Singh, V. (2007). Synthesis and characterization of electrical conducting chitosan-graft-polyaniline. *Express Polymer Letters*, 1(5), 308-317.
- Tourillon, G., & Skotheim, T. (1986). *Handbook of conducting polymers. Vol. 1*: Marcel Dekker.
- Unsworth, J., Lunn, B., Innis, P., Jin, Z., Kaynak, A., & Booth, N. (1992). Technical review: Conducting polymer electronics. *Journal of Intelligent Material Systems and Structures*, 3(3), 380-395.
- Uskoković, V., & Drogenik, M. (2005). Synthesis of materials within reverse micelles. *Surface Review and Letters*, 12(02), 239-277.

- Valix, M., Cheung, W. H., & McKay, G. (2009). Sulfur fixation on bagasse activated carbon by chemical treatment and its effect on acid dye adsorption. *Adsorption*, 15(5-6), 453-459.
- Vinothkannan, M., Karthikeyan, C., Kim, A. R., & Yoo, D. J. (2015). One-pot green synthesis of reduced graphene oxide (RGO)/Fe₃O₄ nanocomposites and its catalytic activity toward methylene blue dye degradation. *Spectrochimica Acta Part A: Molecular and Biomolecular Spectroscopy*, 136, 256-264.
- Virji, S., Huang, J. X., Kaner, R. B., & Weiller, B. H. (2004). Polyaniline nanofiber gas sensors: Examination of response mechanisms. *Nano Letters*, 4(3), 491-496.
- Wan, M. (2008). *Conducting polymers with micro or nanometer structure*: Springer.
- Wang, F., Min, S., Han, Y., & Feng, L. (2010). Visible-light-induced photocatalytic degradation of methylene blue with polyaniline-sensitized composite photocatalysts. *Superlattices and Microstructures*, 48(2), 170-180.
- Wang, F., & Min, S. X. (2007). TiO₂/polyaniline composites: An efficient photocatalyst for the degradation of methylene blue under natural light. *Chinese Chemical Letters*, 18(10), 1273-1277.
- Wang, H., Hao, Q., Yang, X., Lu, L., & Wang, X. (2009). Graphene oxide doped polyaniline for supercapacitors. *Electrochemistry Communications*, 11(6), 1158-1161.
- Wang, X., Li, Y., Zhao, Y., Liu, J., Tang, S., & Feng, W. (2010). Synthesis of PANI nanostructures with various morphologies from fibers to micromats to disks doped with salicylic acid. *Synthetic Metals*, 160(17), 2008-2014.
- Wei, Y., Hariharan, R., & Patel, S. A. (1990a). Chemical and electrochemical copolymerization of aniline with alkyl ring-substituted anilines. *Macromolecules*, 23(3), 758-764.
- Wei, Y., Hsueh, K. F., & Jang, G.-W. (1994). Monitoring the chemical polymerization of aniline by open-circuit-potential measurements. *Polymer*, 35(16), 3572-3575.
- Wei, Y., Jang, G. W., Chan, C. C., Hsueh, K. F., Hariharan, R., Patel, S. A., & Whitecar, C. K. (1990b). Polymerization of aniline and alkyl ring-substituted anilines in the presence of aromatic additives. *Journal of Physical Chemistry*, 94(19), 7716-7721.
- Wei, Y., Tang, X., Sun, Y., & Focke, W. W. (1989). A study of the mechanism of aniline polymerization. *Journal of Polymer Science Part A: Polymer Chemistry*, 27(7), 2385-2396.
- Wu, C.-H., & Chern, J.-M. (2006). Kinetics of photocatalytic decomposition of methylene blue. *Industrial & Engineering Chemistry Research*, 45(19), 6450-6457.

- Wu, S.-H., & Chen, D.-H. (2003). Synthesis and characterization of nickel nanoparticles by hydrazine reduction in ethylene glycol. *Journal of Colloid and Interface Science*, 259(2), 282-286.
- Wu, Z.-S., Ren, W., Wen, L., Gao, L., Zhao, J., Chen, Z., Cheng, H.-M. (2010). Graphene anchored with Co_3O_4 nanoparticles as anode of lithium ion batteries with enhanced reversible capacity and cyclic performance. *ACS Nano*, 4(6), 3187-3194.
- Wynne, K. J., & Street, G. B. (1982). Conducting polymers. A short review. *Industrial & Engineering Chemistry Product Research and Development*, 21(1), 23-28.
- Xia, S., Zhang, L., Pan, G., Qian, P., & Ni, Z. (2015). Photocatalytic degradation of methylene blue with a nanocomposite system: synthesis, photocatalysis and degradation pathways. *Physical Chemistry Chemical Physics*, 17(7), 5345-5351.
- Xian, T., Yang, H., Di, L., Ma, J., Zhang, H., & Dai, J. (2014). Photocatalytic reduction synthesis of SrTiO_3 -graphene nanocomposites and their enhanced photocatalytic activity. *Nanoscale Research Letters*, 9(1), 1-9.
- Xing, W., Li, F., Yan, Z.-f., & Lu, G. (2004). Synthesis and electrochemical properties of mesoporous nickel oxide. *Journal of Power Sources*, 134(2), 324-330.
- Xiong, P., Chen, Q., He, M., Sun, X., & Wang, X. (2012). Cobalt ferrite-polyaniline heteroarchitecture: A magnetically recyclable photocatalyst with highly enhanced performances. *Journal of Materials Chemistry*, 22(34), 17485-17493.
- Xiong, P., Wang, L., Sun, X., Xu, B., & Wang, X. (2013). Ternary titania-cobalt ferrite-polyaniline nanocomposite: A magnetically recyclable hybrid for adsorption and photodegradation of dyes under visible light. *Industrial & Engineering Chemistry Research*, 52(30), 10105-10113.
- Yagub, M. T., Sen, T. K., Afroze, S., & Ang, H. M. (2014). Dye and its removal from aqueous solution by adsorption: A review. *Advances in Colloid and Interface Science*, 209, 172-184.
- Yan, B., Chen, Z., Cai, L., Chen, Z., Fu, J., & Xu, Q. (2015). Fabrication of polyaniline hydrogel: Synthesis, characterization and adsorption of methylene blue. *Applied Surface Science*, 356, 39-47.
- Yang, P., Duan, J., & Tang, Q. (2015). Cobalt sulfide decorated polyaniline complex counter electrodes for efficient dye-sensitized solar cells. *Electrochimica Acta*, 184, 64-69. d
- Yasuda, A., & Shimidzu, T. (1993). Chemical and electrochemical analyses of polyaniline prepared with FeCl_3 . *Synthetic Metals*, 61(3), 239-245.
- Yasui, T. (1935). Electrolytic oxidation of aniline oil. *Bulletin of the Chemical Society of Japan*, 10(8), 305-311.

- Yavuz, A. G., Dincturk-Atalay, E., Uygun, A., Gode, F., & Aslan, E. (2011). A comparison study of adsorption of Cr (VI) from aqueous solutions onto alkyl-substituted polyaniline/chitosan composites. *Desalination*, 279(1), 325-331.
- Yelil Arasi, A., Juliet Latha Jeyakumari, J., Sundaresan, B., Dhanalakshmi, V., & Anbarasan, R. (2009). The structural properties of Poly(aniline) analysis via FTIR spectroscopy. *Spectrochimica Acta Part A: Molecular and Biomolecular Spectroscopy*, 74(5), 1229-1234.
- Yilmaz, F. (2007). *Polyaniline: Synthesis, Characterization, Solution Properties and Composites*. (Doctor of Philosophy), Middle East Technical University.
- Yong, Y.-C., Dong, X.-C., Chan-Park, M. B., Song, H., & Chen, P. (2012). Macroporous and monolithic anode based on polyaniline hybridized three-dimensional graphene for high-performance microbial fuel cells. *ACS nano*, 6(3), 2394-2400.
- Yu, L., He, Y., Bin, L., & Yue'e, F. (2003). Study of radiation induced graft copolymerization of butyl acrylate onto chitosan in acetic acid aqueous solution. *Journal of Applied Polymer Science*, 90(10), 2855-2860.
- Yu, L., Ruan, H., Zheng, Y., & Li, D. (2013). A facile solvothermal method to produce ZnS quantum dots-decorated graphene nanosheets with superior photoactivity. *Nanotechnology*, 24(37), 375601.
- Zhang, H., Wang, J., Wang, Z., Zhang, F., & Wang, S. (2009). A novel strategy for the synthesis of sheet - like polyaniline. *Macromolecular Rapid Communications*, 30(18), 1577-1582.
- Zhang, H., Zong, R., Zhao, J., & Zhu, Y. (2008). Dramatic visible photocatalytic degradation performances due to synergetic effect of TiO₂ with PANI. *Environmental Science & Technology*, 42(10), 3803-3807.
- Zhang, J. (2010). Graphene/polyaniline nanofiber composites as supercapacitor electrodes. *Chemistry of materials*, 22(4), 1392-1401.
- Zhang, K., Zhang, L. L., Zhao, X., & Wu, J. (2010). Graphene/polyaniline nanofiber composites as supercapacitor electrodes. *Chemistry of materials*, 22(4), 1392-1401.
- Zhang, L., Liu, P., & Su, Z. (2006). Preparation of PANI-TiO₂ nanocomposites and their solid-phase photocatalytic degradation. *Polymer Degradation and Stability*, 91(9), 2213-2219.
- Zhang, S., Chen, Q., Jing, D., Wang, Y., & Guo, L. (2012). Visible photoactivity and antiphotocorrosion performance of PdS-CdS photocatalysts modified by polyaniline. *International Journal of Hydrogen Energy*, 37(1), 791-796.
- Zhang, Z., & Kong, J. (2011). Novel magnetic Fe₃O₄@ C nanoparticles as adsorbents for removal of organic dyes from aqueous solution. *Journal of Hazardous Materials*, 193, 325-329.

- Zhao, X., Lv, L., Pan, B., Zhang, W., Zhang, S., & Zhang, Q. (2011). Polymer-supported nanocomposites for environmental application: A review. *Chemical Engineering Journal*, 170(2), 381-394.
- Zhou, C., Han, J., & Guo, R. (2008). Controllable synthesis of polyaniline multidimensional architectures: From plate-like structures to flower-like superstructures. *Macromolecules*, 41(17), 6473-6479.
- Zhou, D. D., Cui, X. T., Hines, A., & Greenberg, R. J. (2009). Conducting polymers in neural stimulation applications *Implantable Neural Prostheses 2* (pp. 217-252): Springer.
- Zhou, M., Han, D., Liu, X., Ma, C., Wang, H., Tang, Y., Yang, J. (2015). Enhanced visible light photocatalytic activity of alkaline earth metal ions-doped CdSe/rGO photocatalysts synthesized by hydrothermal method. *Applied Catalysis B: Environmental*, 172, 174-184.
- Zhu, H., Fu, Y., Jiang, R., Yao, J., Liu, L., Chen, Y., Zeng, G. (2013). Preparation, characterization and adsorption properties of chitosan modified magnetic graphitized multi-walled carbon nanotubes for highly effective removal of a carcinogenic dye from aqueous solution. *Applied Surface Science*, 285, 865-873.
- Zhu, Y., Murali, S., Cai, W., Li, X., Suk, J. W., Potts, J. R., & Ruoff, R. S. (2010). Graphene and graphene oxide: synthesis, properties, and applications. *Advanced Materials*, 22(35), 3906-3924.
- Zikakis, J. (2012). *Chitin, chitosan, and related enzymes*: Elsevier.
- Zong, X., Kim, K., Fang, D., Ran, S., Hsiao, B. S., & Chu, B. (2002). Structure and process relationship of electrospun bioabsorbable nanofiber membranes. *Polymer*, 43(16), 4403-4412.
- Zou, H., Ma, W., & Wang, Y. (2015). A novel process of dye wastewater treatment by linking advanced chemical oxidation with biological oxidation. *Archives of Environmental Protection*, 41(4), 33-39.

APPENDIX A
SUPPLEMENTARY DATA

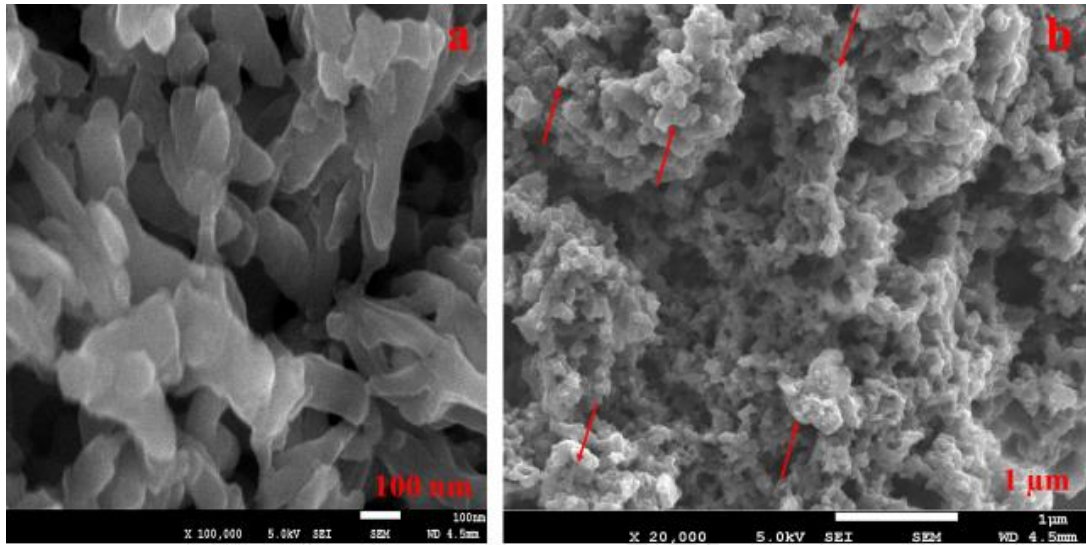


Figure A- 1 FESEM images of (a) PANI homopolymer and (b) P-Sr750

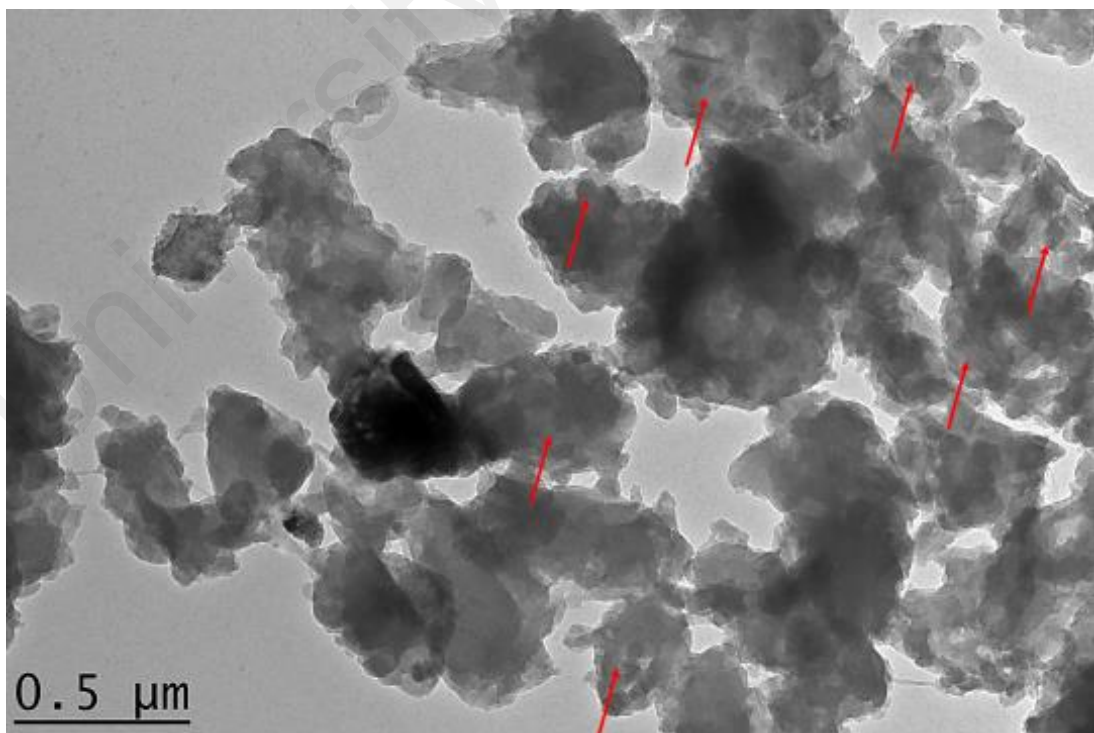


Figure A- 2 TEM image of P-Sr500

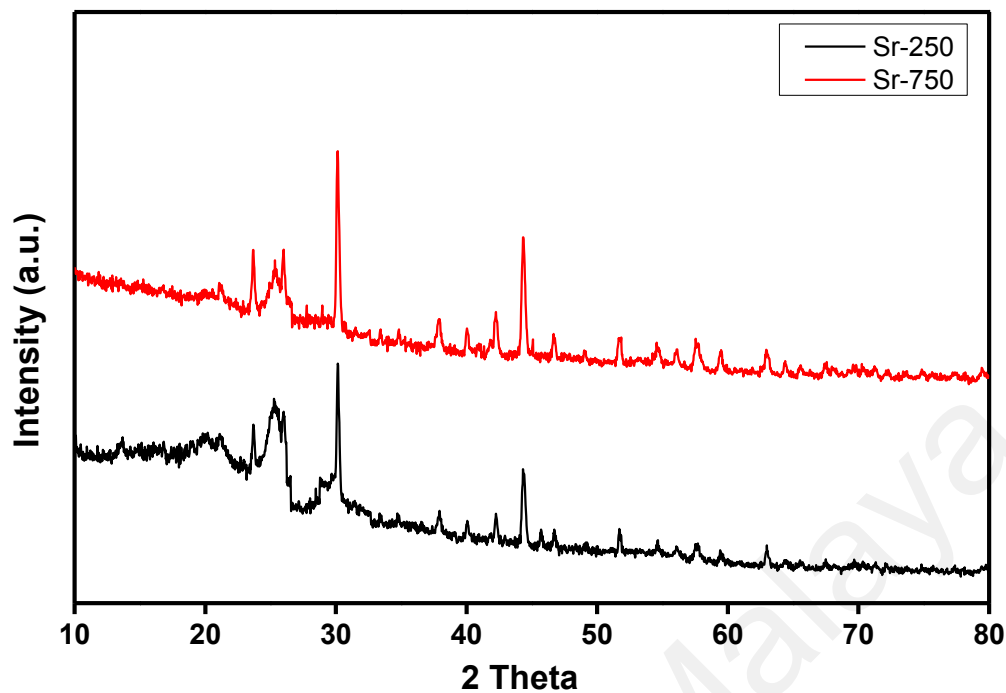


Figure A- 3 XRD patterns of P-Sr250 and P-Sr750

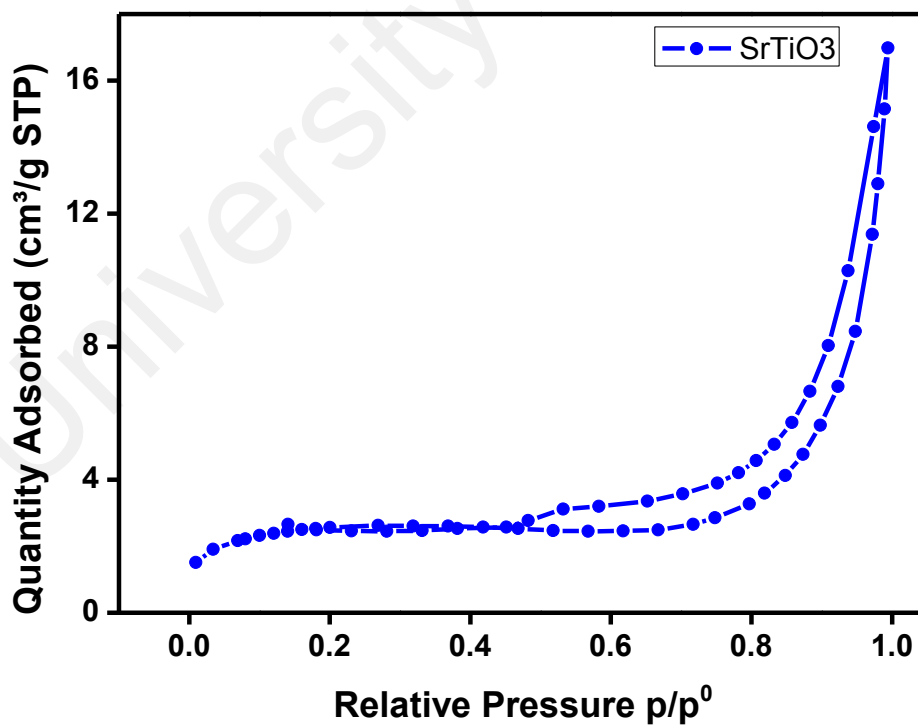


Figure A- 4 Nitrogen adsorption–desorption isotherms (BET) of SrTiO₃ nanocomposite

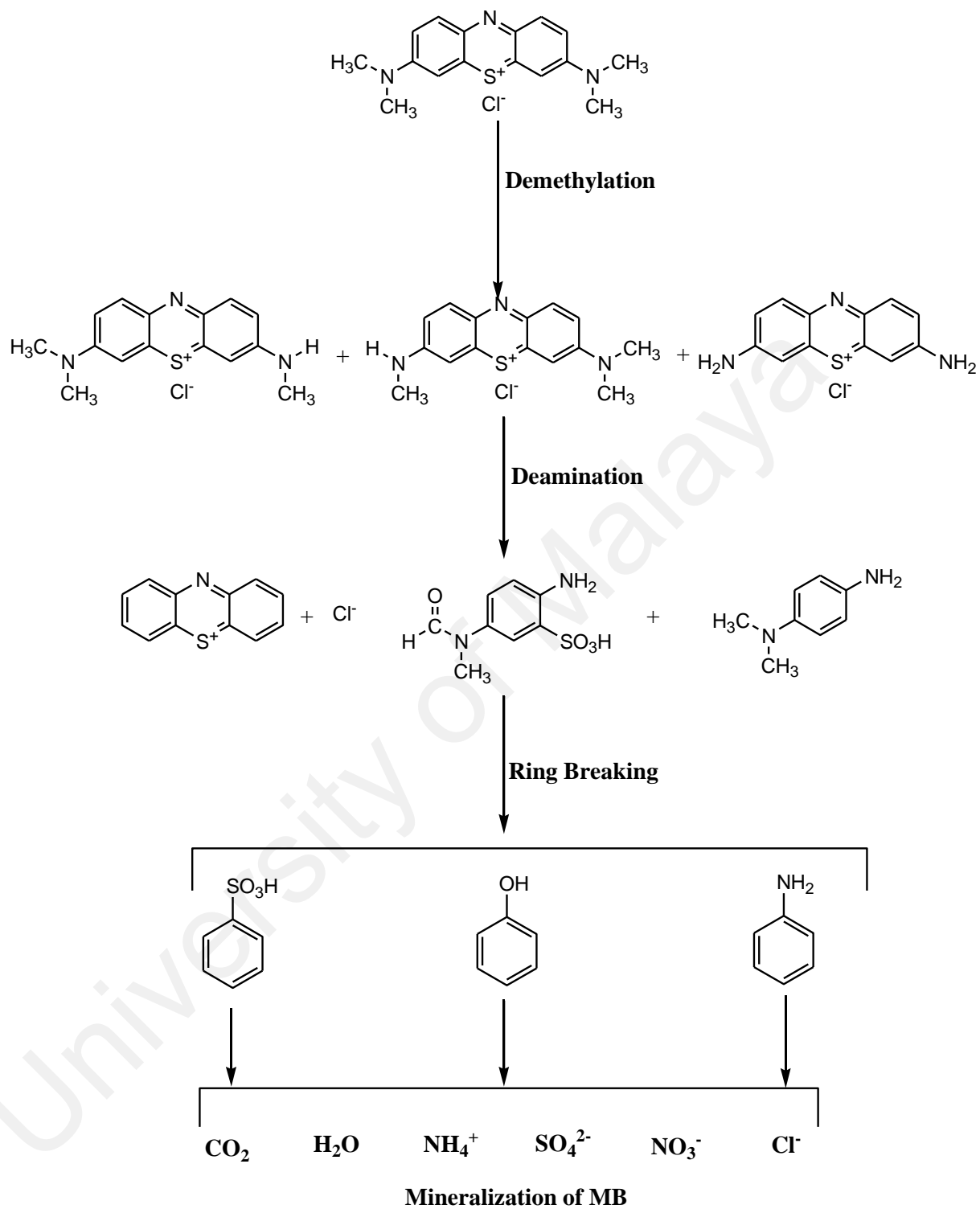


Figure A- 5 Proposed mechanism for the photocatalytic degradation of MB under UV irradiation

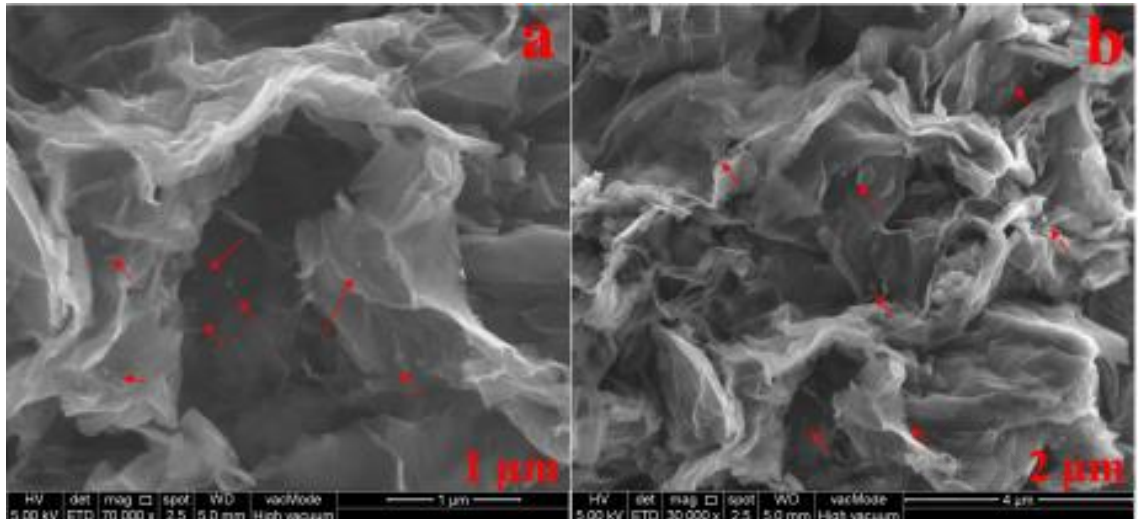


Figure A- 6 FESEM images of (a) and (b) GOPSr-2 nanocomposite at different magnifications

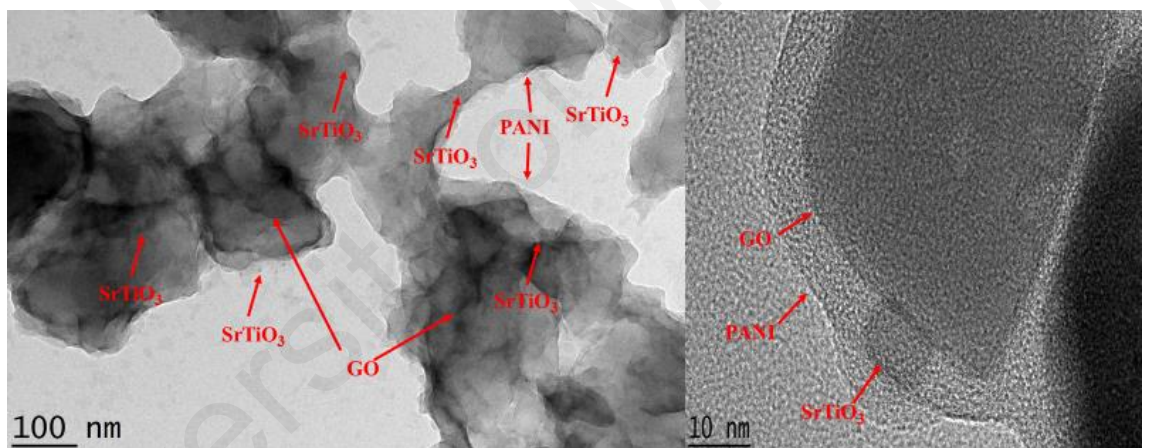


Figure A- 7 TEM images GOPSr-2 nanocomposite at different magnifications.

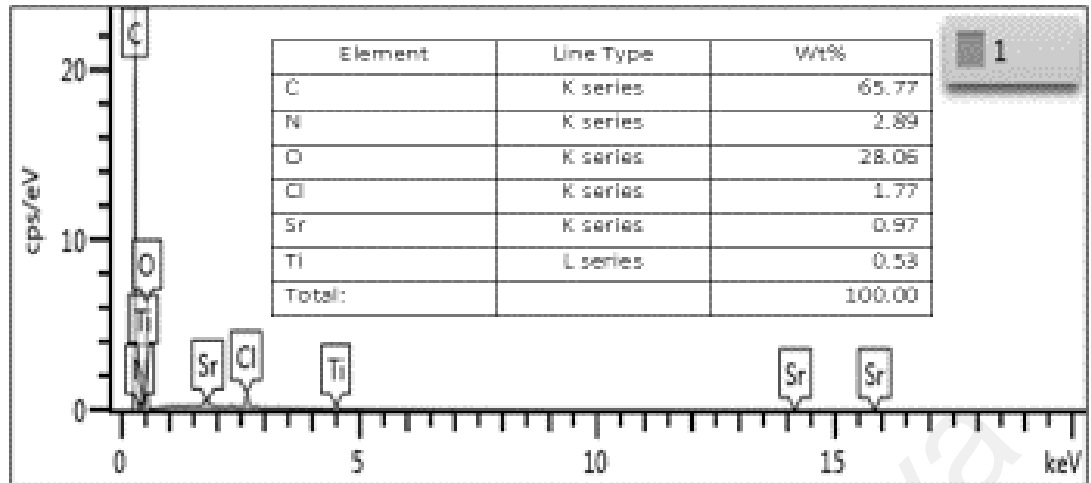


Figure A- 8 EDX spectrum of GOPSr-2 nanocomposite

LIST OF PUBLICATIONS AND PAPERS PRESENTED

Published Manuscripts

- 1) **Shahabuddin, S.**, Sarih, N. M., Mohamad, S., & Atika Baharin, S. N. (2016). *Synthesis and Characterization of Co_3O_4 Nanocube-Doped Polyaniline Nanocomposites with Enhanced Methyl Orange Adsorption from Aqueous Solution*. RSC Advances, 6(49), 43388-43400.
- 2) **Shahabuddin, S.**, Sarih, N. M., Ismail, F. H., Shahid, M. M., & Huang, N. M. (2015). *Synthesis of Chitosan Grafted-Polyaniline/ Co_3O_4 Nanocube Nanocomposites and Their Photocatalytic Activity Toward Methylene Blue Dye Degradation*. RSC Advances, 5(102), 83857-83867.
- 3) **Shahabuddin, S.**, Muhamad Sarih, N., Mohamad, S., & Joon Ching, J. (2016). *SrTiO_3 Nanocube-Doped Polyaniline Nanocomposites with Enhanced Photocatalytic Degradation of Methylene Blue under Visible Light*. Polymers, 8(2), 27.
- 4) **Shahabuddin, S.**, Sarih, N. M., Kamboh, M. A., Nodeh, H. R., & Mohamad, S. (2016). *Synthesis of Polyaniline Coated Graphene Oxide @ SrTiO_3 Nanocube Nanocomposites for Enhanced Removal of Carcinogenic Dyes from Aqueous Solution*. Polymers, 8(9), 305

Oral Presentation in International Conferences

- 1) **Shahabuddin, S.**, Muhamad Sarih, N., & Mohamad, S. (2015). *Chitosan Grafted Polyaniline/Co₃O₄ Nanocomposite and its Photocatalytic Activity for Degradation of Methylene Blue Dye Under UV Lights Irradiation*. Paper presented at the the 4th Federation of Asian Polymer Societies International Polymer Congress Secretariat, Kuala Lumpur, Malaysia.

- 2) **Shahabuddin, S.**, Muhamad Sarih, N., & Mohamad, S. (2016a). *Synthesis & Characterization of Conducting Polymer Based Nanocomposite and Their Photocatalytic Activity for Degradation of Methylene Blue Dye*. Paper presented at the International Conference on Emerging Research in Sciences & Humanities (ERSH-2016), Kuala Lumpur.

- 3) **Shahabuddin, S.**, Muhamad Sarih, N., & Mohamad, S. (2016b). *Synthesis and Characterization of Polyaniline/ SrTiO₃ Nanocomposite and Its Photocatalytic Activity for Degradation of Methylene Blue Dye Under Visible Light*. Paper presented at the International Symposium on Advanced Polymeric Materials 2016 (ISAPM), Kuala Lumpur, Malaysia.

Poster Presentation

- 1) **Shahabuddin, S.**, Muhamad Sarih, N., & Mohamad, S. (2016b). *SrTiO₃ Nanocube-doped Polyaniline for Effective Photocatalytic Degradation of Methylene Blue Dye Under Visible Light*. Poster presented at UM #111 Chemistry Symposium, Department of Chemistry, University of Malaya, Kuala Lumpur, Malaysia.

University of Malaya